



LUND UNIVERSITY

Air flows in building components

Kronvall, Johnny

1980

[Link to publication](#)

Citation for published version (APA):

Kronvall, J. (1980). *Air flows in building components*. Byggnadsfysik LTH, Lunds Tekniska Högskola.
<http://www.byfy.lth.se/fileadmin/byfy/files/TVBH-1000pdf/TVBH-1002kompr.pdf>

Total number of authors:

1

General rights

Unless other specific re-use rights are stated the following general rights apply:

Copyright and moral rights for the publications made accessible in the public portal are retained by the authors and/or other copyright owners and it is a condition of accessing publications that users recognise and abide by the legal requirements associated with these rights.

- Users may download and print one copy of any publication from the public portal for the purpose of private study or research.
- You may not further distribute the material or use it for any profit-making activity or commercial gain
- You may freely distribute the URL identifying the publication in the public portal

Read more about Creative commons licenses: <https://creativecommons.org/licenses/>

Take down policy

If you believe that this document breaches copyright please contact us providing details, and we will remove access to the work immediately and investigate your claim.

LUND UNIVERSITY

PO Box 117
221 00 Lund
+46 46-222 00 00

DIVISION OF BUILDING TECHNOLOGY
LUND INSTITUTE OF TECHNOLOGY

AIR FLOWS IN BUILDING COMPONENTS

JOHNNY KRONVALL

REPORT TVBH-1002
LUND , SWEDEN 1980

CODEN: LUTVDG / (TVBH-1002) / 1-194 / (1980)

AIR FLOWS IN BUILDING COMPONENTS

JOHNNY KRONVALL

Printed in Sweden
Studentlitteratur
Lund 1980

PREFACE

In Sweden, as well as in many other countries, the oil crisis of 1974 and several events in world politics since then have implied needs for energy saving purposes of different kinds. About 40 % of the energy for heating our buildings is used for ventilation. Since the ventilation rate, which should be settled from the physiological point of view primarily, cannot be fixed at a desired level unless the house envelope has a high degree of airtightness, different measures have to be undertaken to obtain the airtightness. A lack of knowledge within the discipline of Building Physics, concerning the physics of air flow in building components which makes proper calculations difficult to perform, was early identified. At the Division of Building Technology at Lund Institute of Technology, we considered such a research task to be interesting and profitable for the discipline as a whole. This made us start the research project which is reported in this work. The work was backed up by the "Airtightness group" of the National Swedish Council for Building Research. The research project has been sponsored mainly by the Council which is gratefully acknowledged.

There are a number of people to whom I owe considerable debts of gratitude for their efforts in supporting me in the work of preparing this thesis. Lars Erik Nevander, head of the Division and my supervisor, taught me a great deal about how scientific research should be carried out. He also gladly shared his great wealth of ideas with me during this work.

Claes Bankvall, my predecessor at the Division, now chief engineer at the Swedish Testing Institute has been a true discussion partner and has also contributed with a number of valuable ideas.

Ann-Charlotte Andersson, my dear colleague at the Division, assisted me to a considerable degree in the work with the computer calculations and at my request modified one of her many computer programs to make it capable of solving problems of air flows in both materials and ducts in materials.

Agneta Ohlsson, research engineer at the Division, carried out the laboratory work of the experimental investigations in a very careful and discerning way.

Ulf Leander, the Division's right hand man in electronics etc., contributed to the work with innumerable hints, ideas and solutions, not only within his own special field.

Lena Thorell, secretary at the Division, managed the financial administration of the research grant, thus for instance seeing to it that my salary arrived every month. Lena also typed the manuscript - rapidly, carefully and with great patience.

Lilian Johansson, technician and "art director" of the Division, performed the drawing of the numerous figures and handled the lay-out of the thesis with great accuracy and efficiency.

Also my other colleagues at the Division; Sven Strandberg, Lars Ohlsson, Gudni Johannesson, Alf Hansson and Carl Axel Hoppe have given their support in various ways.

Lisbeth, Maria and Cecilia, i.e. my family, have had to put up with my frequent absence from them, especially during the last six months. In spite of this, I think they have been my most devoted supporters.

Thank you very much, all of you!

Lund, October 1980

Johnny Kronvall

CONTENTS

SUMMARY	3
LIST OF SYMBOLS	4
1 INTRODUCTION AND BACKGROUND	7
2 APPLICABLE PARTS OF FLUID MECHANICS	9
2.1 Basic definitions and concept	9
2.2 The physics of flow through air-permeable materials	15
2.2.1 Permeability	15
2.2.2 Equations for flow through air-permeable materials	18
2.3 Flow through ducts, cracks, holes etc.	24
2.3.1 General concept	24
2.3.2 Flow in closed conduits	28
2.3.2.1 Laminar flow	28
2.3.2.2 Transitional and turbulent flow	32
2.3.2.3 Surface roughness	38
2.3.2.4 Pressure loss factors for abrupt changes in flow cross section and flow direction	45
2.3.3 Flow through holes and slots	58
3 EXPERIMENTAL INVESTIGATIONS	63
3.1 Surface roughness	63
3.1.1 Laboratory test equipment	64
3.1.2 Data processing and analysis	68
3.1.3 Measurement results	75
3.2 Duct flow	75
3.2.1 Experimental design	76
3.2.2 Data processing and analysis	77
3.2.3 Measurement results	79
4 CALCULATING PRESSURE DISTRIBUTION AND AIR FLOWS IN BUILDING COMPONENTS	85
4.1 General remarks on model design	85
4.2 The algorithms	88

4.3	Calculation procedures	91
4.3.1	Hand calculations	91
4.3.2	Computer calculations	96
4.3.2.1	Computerized analysis of flow resistance networks	96
4.3.2.2	Computer calculation by means of relaxation	103
4.4	Examples	105
4.4.1	Hand calculations	105
4.4.2	Computer calculations	115
4.4.2.1	Examples of computer calculations with flow resistance networks	115
4.4.2.2	Examples of computer calculations by means of relaxation	124
5	FLUCTUATING VS. STEADY STATE PRESSURE DIFFERENCES	133
5.1	The nature of the fluctuations	133
5.2	Pressure distribution under fluctuating pressure conditions	137
5.3	Air flow under fluctuating pressure conditions	146
6	LEAKAGE CHARACTERISTICS OF SINGLE BUILDING COMPONENTS AND BUILDING ENVELOPES	151
6.1	Building components	151
6.2	Building envelopes	157
7	APPENDICES	171
7.1	Surface roughness of some building materials	171
7.2	Permeability data	173
7.2.1	Fluid permeability coefficients of some building materials	173
7.2.2	Fluid permeance coefficients	177
7.3	Porosity of some building materials	178
7.4	Some properties of air	179
7.5	Input format for computer program JK-CIRCUS	180
	LIST OF REFERENCES	181

SUMMARY

This work deals with different aspects of air movements in building components. The investigation shows to what degree the concept of fluid mechanics can be applied to problems concerning air flows in building components. The applicable parts of fluid mechanics are presented as thoroughly as possible. Based on this concept, routines are outlined to make it possible to handle complex flow and pressure distribution problems. Both manual and computer calculation routines are described and the way they can be used is demonstrated in a number of examples.

Experimental investigations concerning determination of surface roughness of plates - instead of that of pipes which almost always has been investigated earlier - were carried out. A test device for this purpose was designed and tested on a number of building materials. Also magnitudes of contraction and bend loss factors were investigated experimentally.

Since, in practice, pressure differences acting across building components are seldom steady, the influence of fluctuating pressure differences was investigated theoretically. The analysis shows that rapid fluctuations influence the flow rate only a little. If the fluctuations are slow it is possible to calculate the flow rate as if the problem was a steady state one, using time averaged pressure difference values.

Leakage characteristics of different building components are reviewed and the air leakage behaviour of whole building envelopes is discussed. The great effect of entrance, bend, exit and orifice pressure losses is emphasized, and their influences on both leakage rate and flow characteristics are shown. An additional part of the so-called pressurization test, taking the form of the leakage rate - pressure difference curve into account, is suggested. Such a procedure could imply a new possibility of detecting large, and maybe hidden, flow paths giving rise to substantial contributions to the total leakage rate of a building.

Some tables are also included. They cover surface roughness, permeability and porosity data of different building materials. An extensive list of references is given.

LIST OF SYMBOLS

	quantity	unit
A	flow coefficient	$\text{m}^3/(\text{s} \cdot \text{Pa}^B)$
A	cross sectional area	m^2
A	admittance	$\text{m}^3/(\text{s} \cdot \text{Pa})$
a	air diffusivity	m^2/s
B	flow exponent	-
B	fluid permeance coefficient	m
B_f	dimensionless quantity (see eq. 2.3.2.4.d)	-
B_0	fluid permeability coefficient	m^2
b	crack/duct width	m
C	correction factor	-
C_d	coefficient of discharge	-
c	shape factor	-
d	diameter of a tube, distance	m
d	breadth of a crack,	running metre
d_H	hydraulic diameter	m
F	relative time	-
f	frequency	Hz
f_l	leakage function	
g	acceleration of free fall	m/s^2
h	gap width between rough surfaces	m
I	electrical current	A
K_c	contraction factor	-
K_e	expansion factor	-
k	factor (eq. 5.2.b)	-
L	(total) length	m
l	length (in flow direction)	m
m	mass	kg
n	number	-
\bar{n}	unit vector	-
P	porosity	-
p	pressure	Pa
q_v	volume flow rate	m^3/s
q_m	mass flow rate	kg/s

quantity	unit	
Re	Reynolds number	-
R	wetted perimeter	m
r	radius of a circle or sphere	m
s	estimated standard deviation	(any)
T	temperature	K
t	time	s
U	voltage	V
u	local velocity component in x-direction	m/s
u_m	average (bulk) velocity	m/s
v	local velocity component in y-direction	m/s
\vec{v}	velocity vector	-
W	relative pressure	-
w	local velocity component in z-direction	m/s
x	length coordinate	m
Y	electrical admittance	Ω^{-1}
y	length coordinate	m
z	length coordinate	m
α	flow rate coefficient,	$m^3/(s \cdot Pa^\beta)$
β	flow exponent	-
γ	surface direction characteristic	-
δ	roughness amplitudes	m
ϵ	surface roughness	m
ϵ	initial phase angle log	rad
ϵ	relative length	-
η	dynamic viscosity	Ns/m^2
θ	temperature	$^{\circ}C$
κ	compressibility	Pa^{-1}
λ	friction factor	-
ν	kinematic viscosity	m^2/s
ξ	loss factor	-
ξ_c	contraction loss factor	-
ξ_b	bend loss factor	-
ξ_e	expansion loss factor	-
π	ratio circumference/diameter of a circle	-

	quantity	unit
ρ	density	kg/m^3
ρ	correlation coefficient	-
σ	standard deviation	(any)
σ	ratio of constriction area to frontal area	-
ϕ	relative humidity	-
ϕ	potential (field)	
ϕ	pressure flow factor	-
ϕ	phase angle	rad
ϕ^*	geometrical function	-
ψ	stream function	-
ω	periphery velocity	rad/s

1 INTRODUCTION AND BACKGROUND

Heat transfer and moisture transfer are traditional parts of a knowledge complex sometimes denoted Building Physics. This discipline deals, in general terms, with the protection of buildings and maintenance of a good indoor climate under the influence of the outdoor climatic conditions. In addition to the parts of building physics mentioned above, knowledge of air tightness behaviour of buildings and building components is essential if a proper climate protection is to be achieved. Attempts to predict air infiltration rates and air flows in building components on the whole, and also intentional flows, have hitherto been difficult to perform. To a considerable degree this is actually due to a certain idleness on the building designers' and researchers' part, since considerable basic knowledge exists within other disciplines. In fact very rough methods of calculating air flow rates have been used. In this respect perhaps the Hagen-Poiseuille equation for flow between parallel planes is one of the most misused equations. Knowledge of surface roughness and the magnitude of the influence of this property for different flow cases has been poor. Permeability data concerning building materials have been - and still are - uncertain.

Quite a lot of effort has been spent on research concerning natural convection, both in building components and rooms. Apart from only a few early works, the concept of forced convection has been investigated just little until very recently, say the last five to ten years.

The aim of this work has been to:

- o investigate how, and to what degree the concept of fluid mechanics can be applied to problems concerning air flows in building components caused by forced convection
- o produce calculation routines capable of handling also large and complex flow and pressure distribution problems
- o investigate and interpret present knowledge of air leakage behaviour of buildings and building components

- o investigate the influence of non steady state pressure difference acting on a building component
- o design and test an experimental procedure for determination of surface roughness of plates
- o expand the knowledge of the magnitude of the surface roughness of building materials
- o study experimentally the magnitude of entrance and bend losses in duct flow.

If this aim has been fulfilled a powerful potential of making important and interesting applications and expansions exists. Thus if heat transfer is linked to the concept of this work, for example, interesting calculations concerning the effects of air movements in heat insulation materials can be done. A first attempt of tackling this is reported in Kronvall (1980 C).

Another important complex problem in building physics, namely that of moisture convection, could be investigated if heat, moisture and air flows, can be taken into consideration simultaneously. However, this is likely to be an extensive task and lies definitely out of the scope of this work.

2 APPLICABLE PARTS OF FLUID MECHANICS

2.1 BASIC DEFINITIONS AND CONCEPT

Fluid mechanics deals with fluids - their properties and the phenomena associated with the fluids at rest or in motion. A fluid may be either a liquid or a gas. Transport phenomena associated with fluid flow are also known as convection or convective mass transfer.

Convection may be either natural or forced. Natural convection is governed by forces acting upon any small part of the fluid while forced convection is governed by forces acting from outside the fluid. Fluid flow caused by density differences between different parts of a fluid under influence of the gravitation is an example of natural convection while gas flow caused by a fan or liquid flow caused by a pump are examples of forced convection.

There are two possible aspects of the mechanics of fluids; a macroscopic and a microscopic. The macroscopic aspect involves what may be called "a continuous matter theory" meaning that the fluid is treated as a continuous medium, its motion being determined if the motion of every material point of the fluid is given by mathematical equations. The microscopic aspect is obtained if the molecule structure of the fluid is taken into account. Usually the microscopic aspect results only in minor corrections to the equations of the continuous matter theory. For most cases of practical interest the macroscopic aspect holds very well.

The motion of a fluid, regarded as a continuum, is geometrically described if the position of every material point of the fluid is known at every time. There are three basic equations which form the basis of the mathematical description of fluids in motion. They are

- o the continuity equation
- o the momentum equation
- o the energy equation

They are normally expressed mathematically as a system of differential equations. An additional set of initial and/or boundary conditions is needed to make the problem fully determined.

The continuity equation states that mass inflow to a control volume equals the mass outflow from it. This is mathematically described as:

$$\frac{\partial}{\partial x} (\rho u) + \frac{\partial}{\partial y} (\rho v) + \frac{\partial}{\partial z} (\rho w) = - \frac{\partial \rho}{\partial t} \quad (2.1.a)$$

where x , y and z are coordinates in a Cartesian coordinate system, ρ is the density of the fluid and u , v and w are the local velocity components in the x , y and z directions respectively. With a vector notation where $\bar{v} = (u, v, w)$, (the local velocity vector), the continuity equation can be written:

$$\text{div} (\rho \bar{v}) = \nabla \cdot (\rho \bar{v}) = - \frac{\partial \rho}{\partial t} \quad (2.1.b)$$

where ∇ denotes the nabla operator. This is the general form of the continuity equation. Various simplifications are possible in particular problems, however. These are summarized in table 2.1.a.

TABLE 2.1.a. Different forms of the continuity equation.

Form of continuity equation	Applicable conditions
$\nabla \cdot (\rho \cdot \bar{v}) = - \frac{\partial \rho}{\partial t}$	Any, except where fluid is supplied or withdrawn
$\nabla \cdot (\rho \bar{v}) = 0$	Steady flow, local values independent of time
$\nabla \cdot \bar{v} = 0$	Steady flow of incompressible fluid
$\frac{\partial}{\partial x} (\rho u) = - \frac{\partial \rho}{\partial t}$	One-dimensional flow
$\frac{\partial}{\partial x} (\rho u) = 0 \Rightarrow$	Steady, one-dimensional flow
$\Rightarrow \rho u = \text{constant and}$ $q_v = A \cdot u = \text{constant}$	Steady volume flow (incompressible fluid)
$q_m = \rho \cdot A \cdot u = \text{constant}$	Steady mass flow

The momentum equation is based on Newton's second law of motion. It states that the change in momentum as the fluid flows through a control volume is equal to all external forces acting on the control surface or volume. If the fluid is incompressible ($\rho = \text{constant}$) and has constant viscosity ($\eta = \text{constant}$) it is stated:

$$\rho \cdot \left(\underbrace{\frac{\partial \bar{v}}{\partial t}}_{\text{Local acceleration}} + \underbrace{\bar{v} \cdot \nabla \bar{v}}_{\text{Convective acceleration}} \right) = -\nabla \bar{p} + \underbrace{\rho \cdot \bar{g}}_{\text{Body force per unit volume}} + \underbrace{\eta \nabla^2 \bar{v}}_{\text{Viscous force per unit volume}} \quad (2.1.c)$$

The equation (2.1.c) is often referred to as the Navier-Stokes equation.

In the x-direction of a Cartesian system eq. (2.1.c) can be written:

$$\begin{aligned} \rho \left(\frac{\partial u}{\partial t} + u \frac{\partial u}{\partial x} + v \frac{\partial u}{\partial y} + w \frac{\partial u}{\partial z} \right) &= \\ &= - \frac{\partial p}{\partial x} + \rho g_x + \eta \left(\frac{\partial^2 u}{\partial x^2} + \frac{\partial^2 u}{\partial y^2} + \frac{\partial^2 u}{\partial z^2} \right) \end{aligned} \quad (2.1.d)$$

In eq. (2.1.c) and (2.1.d) η denotes the dynamic viscosity (Ns/m^2). If the viscosity is zero, eq. (2.1.c) reduces to:

$$\rho \left(\frac{\partial \bar{v}}{\partial t} + \bar{v} \cdot \nabla \bar{v} \right) = - \nabla \bar{p} + \rho \cdot \bar{g} \quad (2.1.e)$$

commonly known as Euler flow.

Only for very simple cases is it possible to solve either of the equations (2.1.b) to (2.1.e) in these forms. Further use of them is possible by introducing a stream function ψ or a velocity potential ϕ . In the general 3-dimensional form the use of ϕ facilitates integration of the equations rather than the stream function. The potential ϕ is defined by the following relationships:

$$u = \frac{\partial \phi}{\partial x}, \quad v = \frac{\partial \phi}{\partial y}, \quad w = \frac{\partial \phi}{\partial z} \quad (2.1.f)$$

As the continuity equation states that

$$\nabla \cdot (\rho \bar{\mathbf{v}}) = - \frac{\partial \rho}{\partial t}$$

and if the fluid is assumed to be incompressible $(\frac{\partial \rho}{\partial t}) = 0$ this leads to:

$$\nabla^2 \phi = 0 \quad (2.1.g)$$

or

$$\frac{\partial^2 \phi}{\partial x^2} + \frac{\partial^2 \phi}{\partial y^2} + \frac{\partial^2 \phi}{\partial z^2} = 0 \quad (2.1.h)$$

commonly known as the Laplace equation.

The energy equation is perhaps one of the most widely used equation in fluid mechanics. It can be formulated in many different ways depending on what kind of energy is concerned but it generally states that the energy content of a control volume is constant.

The energy equation is used in the form of the Bernoulli equation for the majority of fluid mechanics problems either in the form

$$\frac{p}{\rho \cdot g} + z + \frac{u^2}{2g} = \text{constant} \quad (2.1.j)$$

for incompressible flows, or

$$\frac{dp}{\rho \cdot g} + dz + \frac{u \, du}{g} = 0 \quad (2.1.k)$$

for compressible fluids.

(2.1.j) may also be written:

$$p + z \cdot \rho \cdot g + \rho \, u^2/2 = \text{constant} \quad (2.1.l)$$

where the three terms represent different kinds of energy; pressure, potential and kinetic energy.

A fluid flow may be characterized as laminar, transitional or turbulent. The characterization is based on the nature of the flow at a certain point of a flow field and at a certain time. These natures of fluid flow were investigated in the classical experiments of Reynolds (1883). A sketch of the apparatus used by him is illustrated in figure 2.1.a.

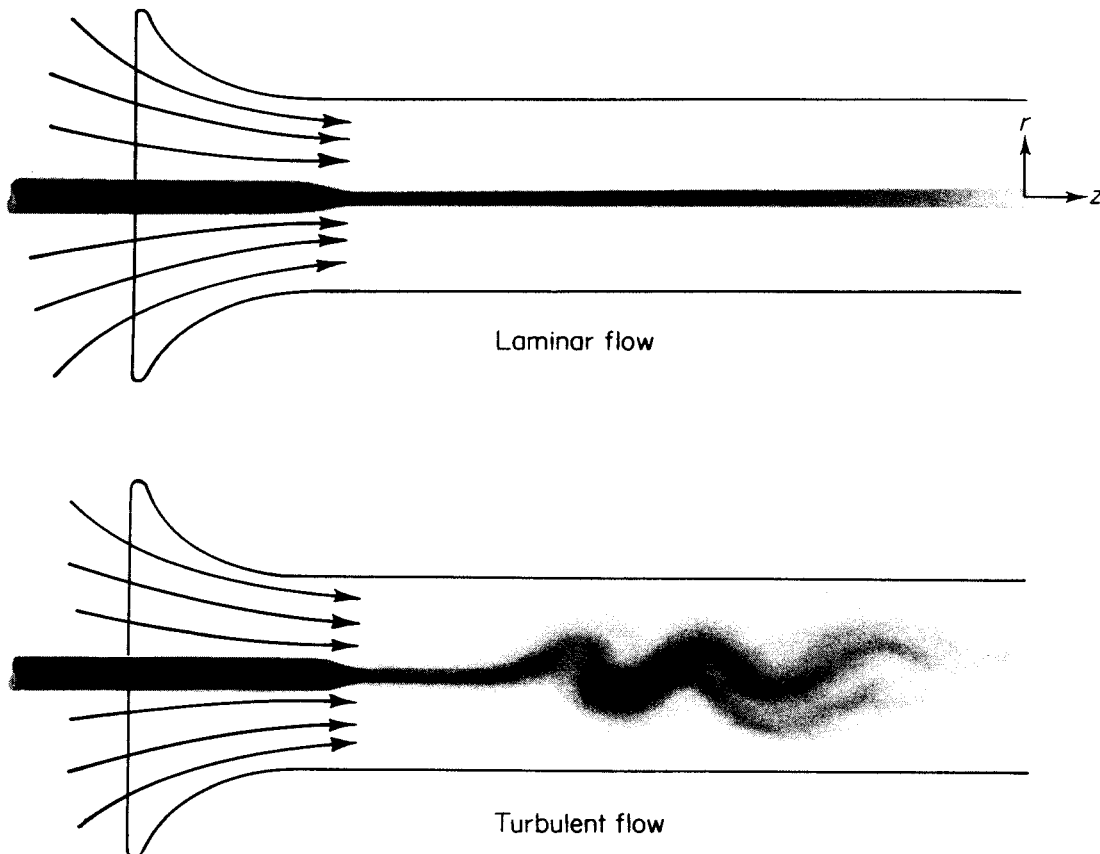


FIG. 2.1.a. Reynolds experimental investigation of the transition to turbulence.

A dye streak was injected into the water that entered the tube from a reservoir. Reynolds observed two distinct types of flow. In the first the dye streak maintained its identity and remained in the centre of the tube. This laminar flow is characterized by smooth motion of one lamina of fluid past another. In the second flow the dye streak was soon dispersed throughout the tube when the laminar flow that existed at the entrance underwent the transition to turbulent flow. This flow is characterized

by an irregular and (nearly) random motion superimposed on the main motion of the fluid. The mixing causes a momentum exchange in the transverse direction. The longitudinal pressure gradient is proportional to the square of the velocity.

Reynolds also found that the transition from laminar to turbulent flow in a pipe could be correlated by a dimensionless group which is now known as the Reynolds number (Re), defined as:

$$\text{Re} = \frac{u_m \cdot d}{\nu} \quad (2.1.m)$$

where:

u_m = average velocity in the flow direction (m/s)

d = the diameter of the tube (m)

ν = the kinematic viscosity (m^2/s)

In fact Re describes the ratio between viscous force and inertia force of a small fluid element.

In the case of a pipe the critical value of Re, sometimes denoted Re_{cr} , often given lies between 2000 and 2500 but it has been found that laminar (streamline) flow may exist up to $\text{Re} = 40\,000$ using an exceptionally smooth inlet. For $\text{Re} > 4000$ in pipe flow the flow is normally turbulent. The region between Re_{cr} and 4000 is called the transition region within which the flow alternates between laminar and turbulent with respect to time.

It should be emphasized that the dynamic similarity at the same Re of two systems, which is explained above, is valid only if $\bar{v} \cdot \nabla \bar{v}$ is equal to zero, i.e. for pipe flow the case with a straight tube.

2.2 THE PHYSICS OF FLOW THROUGH AIR PERMEABLE MATERIALS

2.2.1 Permeability

An air permeable material permits air to flow through it when a pressure difference acts across it. In its macro structure an air-permeable material must contain air flow paths going all the way through the material sample. In porous materials which are the most common when building materials are concerned the flow paths often consist of interconnected pores. Air flow is possible only if at least part of the pore space is interconnected. The interconnected part of the pore system is called the effective pore space of the porous medium. Scheidegger (1963).

The permeability of a material is a property which states the degree of easiness for a fluid to pass through the material under the influence of a pressure gradient. The permeability is in other words the fluid flow conductivity of a permeable material. The permeability is determined by the structure of the material.

The fluid permeability coefficient is defined by

$$B_0 = - \frac{q_v}{A} \cdot \frac{\eta}{\text{grad } p} \quad (2.2.1.a)$$

where:

B_0 = the fluid permeability coefficient, m^2

q_v = the volume flow rate across A, m^3/s

A = the cross-sectional area, m^2

η = the dynamic viscosity, Ns/m^2

p = the total pressure, Pa

B_0 has the dimension of length squared (m^2) and it is roughly a measure of the mean square pore diameter of the material. Bankvall (1972). This coefficient has the advantage, compared to other permeability coefficients sometimes used, of being dependent only of the medium and not the fluid. The fluid property that describes the specific fluid is the dynamic viscosity.

A permeable medium is normally assumed to be homogenous which means that its bulk properties do not vary (much). However, a homogenous

material does not have to be isotropic but may be anisotropic. Such a material does not have the same permeability in all directions. Mineral- and glassfibre wool are examples of such materials.

For an anisotropic material the permeability equation will be written

$$\bar{q}_V = - (\bar{B}_0 / \eta) \text{grad } p \quad (2.2.1.b)$$

where \bar{B}_0 is a symmetric tensor. The tensor may be properly referred to as the "permeability tensor" of the porous medium and it is written:

$$\bar{B}_0 = \begin{pmatrix} B_{0x} & 0 & 0 \\ 0 & B_{0y} & 0 \\ 0 & 0 & B_{0z} \end{pmatrix} \quad (2.2.1.c)$$

The directional permeability coefficient B'_0 , may be written as:

$$B'_0 = \bar{n} \cdot \bar{B}_0 \cdot \bar{n} \quad (2.2.1.d)$$

where \bar{n} is a unit vector along the flow direction. $\bar{n} = (n_x, n_y, n_z)$.

If this is written out, one obtains:

$$B'_0 = n_x^2 \cdot B_{0x} + n_y^2 \cdot B_{0y} + n_z^2 \cdot B_{0z} \quad (2.2.1.e)$$

This is the general equation of an ellipsoid and therefore it is sometimes called the permeability ellipsoid. Its axes have the lengths equal to the inverse square root of the principal permeabilities.

The fact that the tensor is symmetric leads to the following conclusions.

- o Generally, the force potential gradient $\text{grad } p$ and the flow \bar{q}_V are not parallel.
- o There exist three orthogonal "principal axes" in space of the permeability tensor, along which the pressure gradient and the flow have the same direction.

The task remains to relate the components of \overline{B}_0 to directional permeability measurements. Scheidegger (1973) gives the following theorem:

"If the inverse of the square root of the directional permeability, $B_0^{-1/2}$, is measured on all of the corresponding directions in a point of an anisotropic porous medium, then one obtains an ellipsoid. The axes of the latter are in the directions of the principal axes of permeability, their length being equal to the inverse square roots of the principal permeabilities."

This is demonstrated in figure 2.2.a.

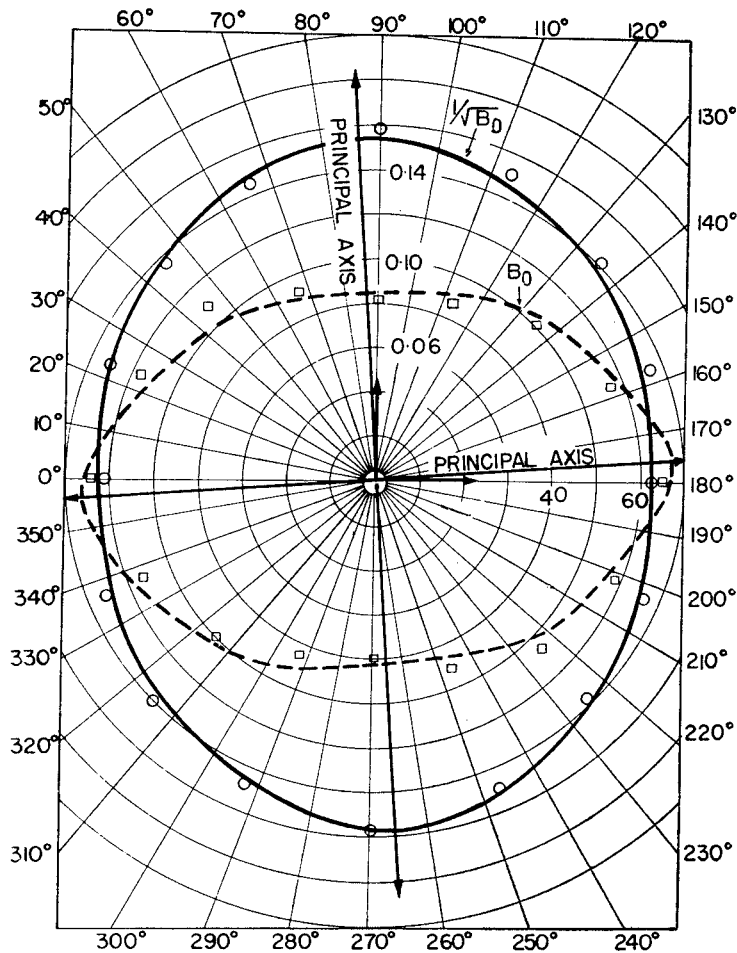


FIG. 2.2.1.a. Polar permeability diagram. The actually measured values (squares) fit on a complicated curve (broken line) which corresponds to an ellipse (solid) if $B_0^{-1/2}$ were drawn instead of B_0 . The circles correspond to the values of $B_0^{-1/2}$ as measured. (After Scheidegger (1954) and Johnson and Hughes (1948)).

2.2.2 Equations for flow through air-permeable materials

Equation (2.2.1.a)

$$\bar{u} = - \frac{B_0}{\eta} \cdot \text{grad } p \quad (2.2.2.a)$$

is based on the experiments of Darcy (1856) and therefore called Darcy's Law. In this form the law has been proved to be valid for non-compressible steady state flow through porous media of homogeneous permeability. It is valid for anisotropic media if the permeability tensor \overline{B}_0 is used instead of B_0 .

Darcy's Law represents a solution of Laplace's equation, eq (2.1.g - h) i.e.

$$\nabla^2 \phi = 0$$

ϕ is a scalar (potential) field. The potential in these cases is the total pressure p . For other applications it may be for example temperature, (K) or electric potential (V). This makes it possible to use solutions from other fields of physics such as the theory of conduction of heat in solids and electrical potential theory.

If the fluid in motion is compressible Laplace's equation is not applicable. However, Leibenzon (1947) pointed out that

$$\nabla^2 \int_{p_0}^p \rho dp = 0 \quad (2.2.2.b)$$

gives the solutions for this case. For example in the one-dimensional case for an ideal gas.

$$u_0 = - \frac{B_0}{\eta} \cdot \left(\frac{dp}{dx} \right)_0 = - \frac{B_0}{\eta} (p_L^2 - p_0^2) / (2 p_0 L) \quad (2.2.2.c)$$

where

$$p(x = 0) = p_0$$

$$p(x = L) = p_L$$

Below a number of solutions for steady state flow of specific geometrical configurations are given. Most of them are based on transformations before solving the Laplace equation.

For two-dimensional steady flow in a region bounded by a polygon it is theoretically possible to find the proper transformation for solution of Laplace's equation by the use of the so-called "Schwarz-Christoffel theorem", Christoffel (1867) and Schwarz (1869). Solutions obtained by use of that theorem are given by, for example, Carslaw & Jaeger (1959), Welty (1974) and Kutateladze & Borishanskii (1966). The solutions are all worked out for temperature fields but the results are of course quite applicable on fluid flow fields too.

1. Two-dimensional radial flow of an incompressible fluid into (from) a well which completely penetrates the fluid-bearing medium. See figure 2.2.2.a!

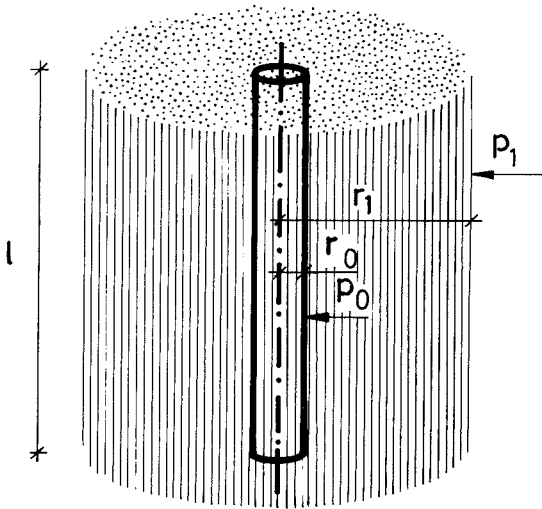


FIG. 2.2.2.a.

For this case:

$$\frac{q_v}{l} = \frac{B_0}{\eta} \cdot \frac{2\pi}{\ln \frac{r_1}{r_0}} (p_1 - p_0) \quad (2.2.2.d)$$

2. Three dimensional radial flow of an incompressible fluid from a point source into an infinite half sphere.

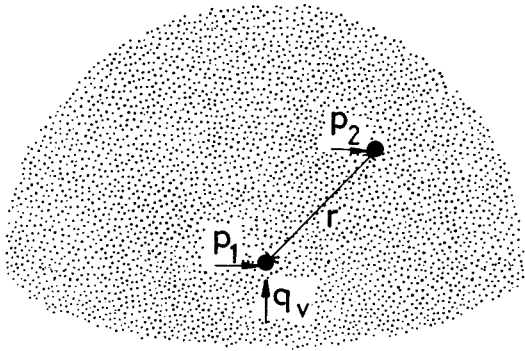


FIG. 2.2.2.b.

$$q_v = \frac{B_0}{\eta} \cdot (p_1 - p_2) \cdot 2 \pi r \quad (2.2.2.e)$$

3. A cylinder at a certain distance from a plane; the cylinder and the plane being isothermals. (Cf. the steady loss of heat from a buried cable, Melsom & Booth (1915))

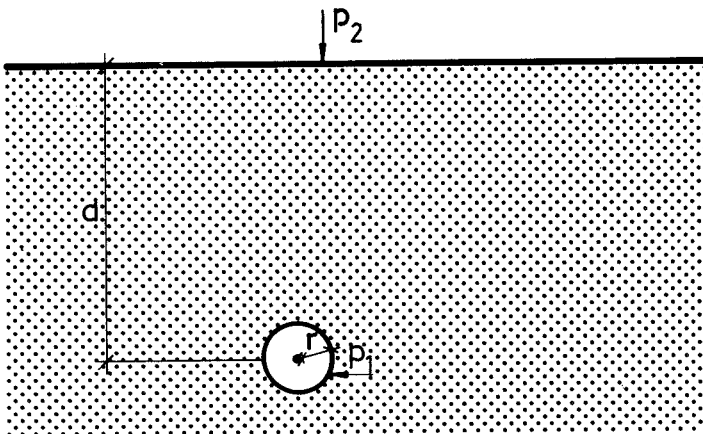


FIG. 2.2.2.c.

$$\frac{q_v}{l} = (p_1 - p_2) / \left(\frac{\eta}{2\pi B_0} \cosh^{-1} \frac{d}{r} \right) \quad (2.2.2.f)$$

if $r \ll d$ and $d > 3r$.

4. A thin disc at a certain distance from a plane; the disc and the plane being isothermals.

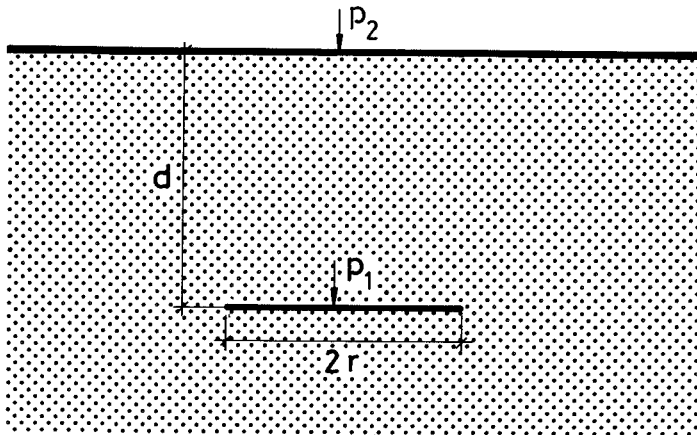


FIG. 2.2.2.d.

$$q_v \approx \frac{B_0}{\eta} (p_1 - p_2) \cdot \frac{2.22 r}{1 - r / 2.83 d} \quad (2.2.2.g)$$

5. A sphere at a certain distance from a plane; the sphere and the plane being isothermals.

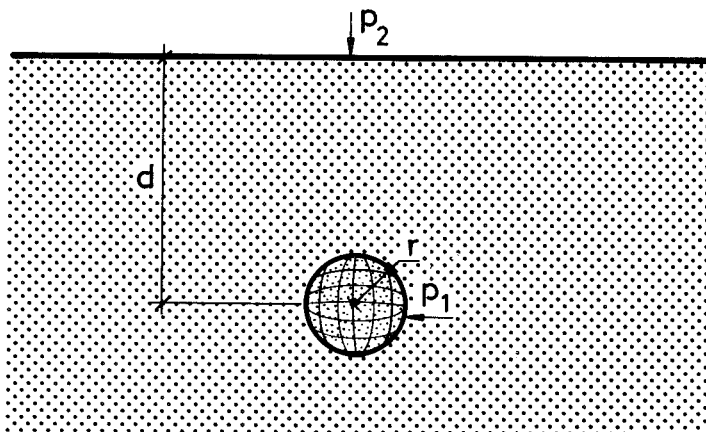


FIG. 2.2.2.e.

$$q_v = \frac{B_0}{\eta} \cdot (p_1 - p_2) \cdot \frac{4\pi r}{1 - r/20} \quad (2.2.2.h)$$

6. Two cylinders in an infinite homogeneous medium.

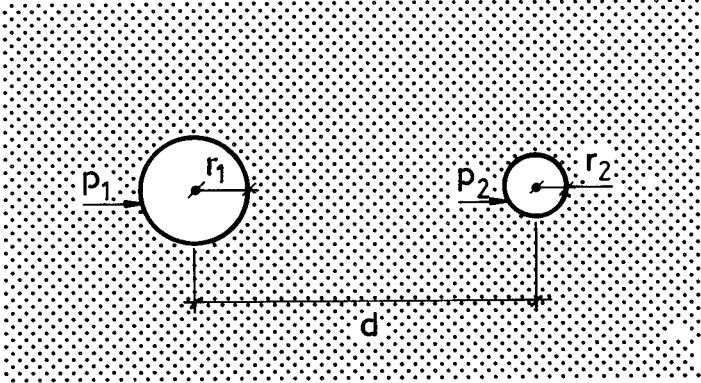


FIG. 2.2.2.f.

$$\frac{q_v}{l} = \frac{B_0}{\eta} \cdot (p_1 - p_2) \frac{2\pi}{\cosh^{-1} \left((d^2 - r_1^2 - r_2^2) / 2r_1 r_2 \right)} \quad (2.2.2.i)$$

7. Long thin slab at a certain distance from a plane; the slab and the plane being isothermals.

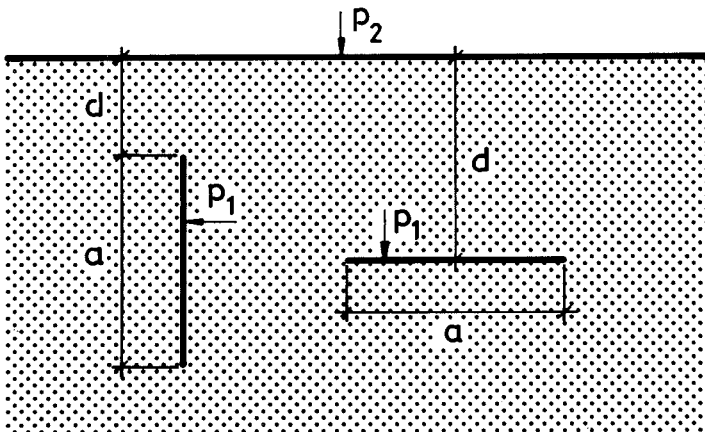


FIG. 2.2.2.g.

Vertical slab:

$$\frac{q_v}{l} \cong \frac{B_0}{\eta} \cdot (p_1 - p_2) / 0.42 \left(\frac{d}{a}\right)^{0.24} \quad (2.2.2.k)$$

Horizontal slab:

$$\frac{q_v}{l} \cong \frac{B_0}{\eta} \cdot (p_1 - p_2) / 0.34 \left(\frac{d}{a}\right)^{0.32} \quad (2.2.2.l)$$

These relationships are valid only if $0.5 \leq \frac{d}{a} \leq 12$.

8. Circular ring at a certain distance from a plane; the ring and the plane being isothermals.

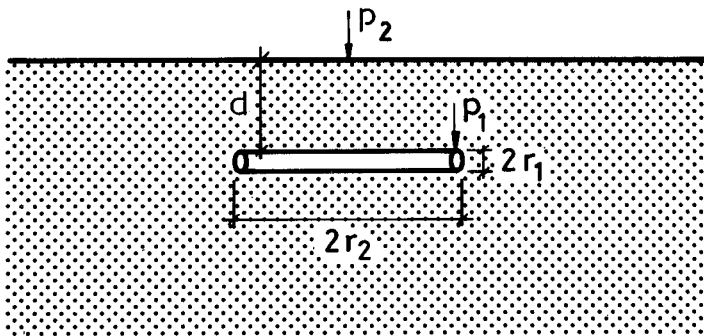


FIG. 2.2.2.h.

FIG. 2.2.2.h.

$$q_v = \frac{B_0}{\eta} \cdot (p_1 - p_2) / R \quad (2.2.2.m)$$

where

$$R = \frac{1}{4\pi r_2} \ln \frac{8 \cdot r_2}{r_1} \left(1 + \frac{\ln \frac{4 r_2}{d}}{\ln \frac{8 r_2}{r_1}} \right) \quad (2.2.2.n)$$

Valid if $r_1 \ll d \ll r_2$

2.3 FLOW THROUGH DUCTS, CRACKS, HOLES ETC

2.3.1 General concept

The aim is - generally speaking - to establish relationships between pressure difference between the openings of a flow path, a geometrical description of the flow path and the resulting flow rate. An example of a flow path is shown in figure 2.3.a.

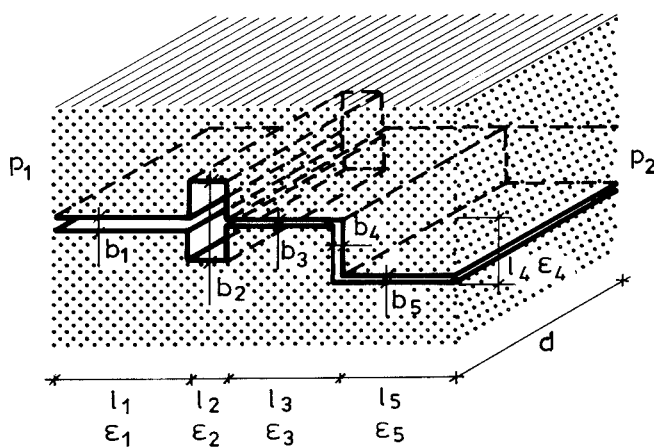


FIG. 2.3.1.a. Example of a flow path. b = crack (duct) width (m), l = length in flow direction (m), ϵ = surface roughness (m), p = total pressure (Pa), d = breadth of crack (duct) (running metre).

Other complications may occur such as converging or diverging sides of the crack (duct) or part(s) of the duct being filled with some permeable medium.

It is quite obvious that the solving of such problems arising in practice is almost always impossible by use of basic equations, i.e. Navier - Stokes equations, because of the relative complexity of the problems. This leads into a need for simplifications and the most relevant one, if complicated numerical solutions are excluded for the moment, is the concept of pipe flow. This originates from the 19th and 20th century. Especially in the 1930's and 1940's much effort was spent on the work of

getting a concept well adapted to practical needs. This is mainly ascribed to Nikuradse, Colebrook and Moody. (Specific references are given below). Few problems in building physics, however, deal with pure pipe flow. Fortunately flow through conduits of other shapes may be handled by use of a so called hydraulic diameter making it possible to use the concept of pipe flow for duct flow etc. too.

In this work the hydraulic diameter, d_H , is defined as:

$$d_H = \frac{4 A}{R} \quad (2.3.1.a)$$

where A is the area of the cross section of the conduit and R is the so-called wetted perimeter i.e. in the cases of gas flow equal to the circumference of the cross section.

Examples:

Circle (diameter = d):

$$d_H = \frac{4 \cdot \pi \left(\frac{d}{2}\right)^2}{2 \pi \left(\frac{d}{2}\right)} = d$$

Ellipse (axes a and b):

$$d_H = \frac{4 \cdot \pi \cdot a \cdot b}{2 \pi \sqrt{\frac{a^2 + b^2}{2}}} = \frac{2 \sqrt{2} a b}{\sqrt{a^2 + b^2}}$$

Rectangular duct (sides a and b):

$$d_H = \frac{4 \cdot a \cdot b}{2(a + b)} = \frac{2 a b}{a + b}$$

Parallel planes (distance = b):

Let $a \gg b$ in the expression above.

$$d_H = 2 b$$

For rectangular channels it might be interesting to see at what aspect ratio (a/b) the hydraulic diameter can with reasonable accuracy be put to $2b$. d_H vs. a/b is plotted in figure 2.3.1.b. The choice of degree of "reasonable accuracy" is left to the reader.

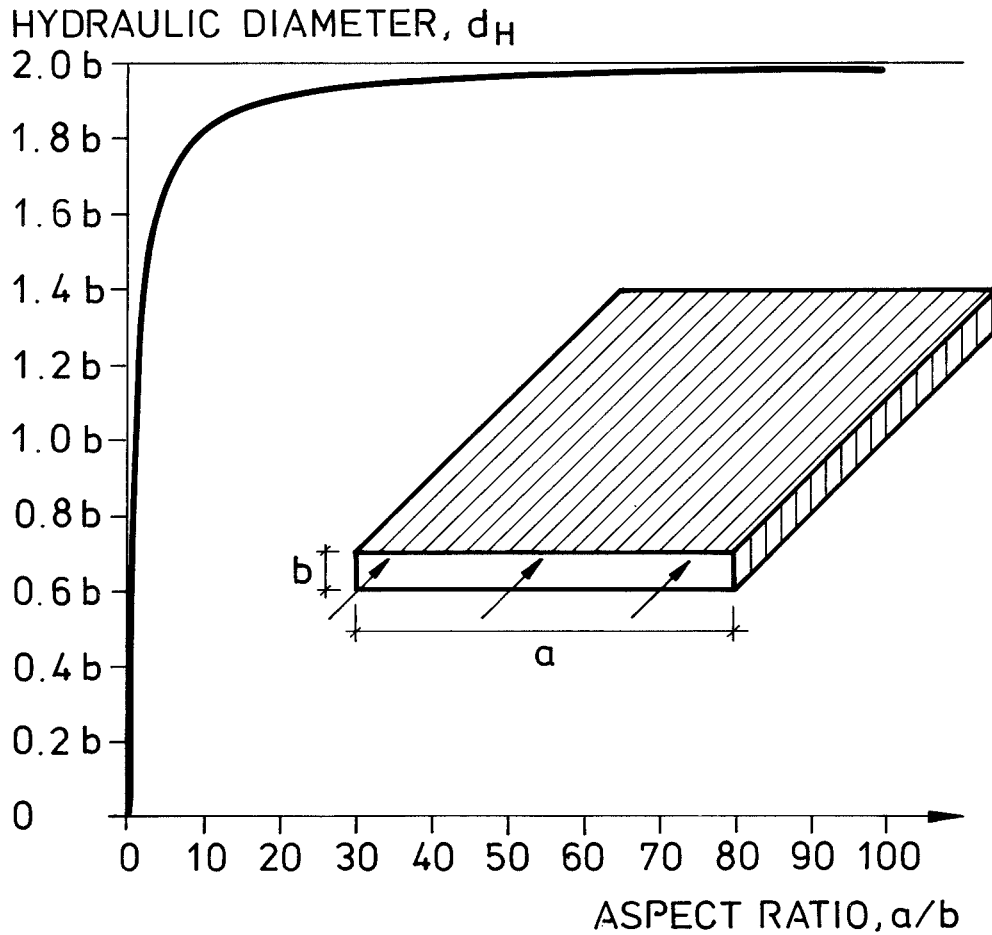


FIG. 2.3.1.b. The hydraulic diameter, d_H , for different values of the aspect ratio, a/b for a rectangular channel.

The use of the hydraulic diameter concept is based on an assumption of evenly distributed wall shear stresses over the circumference of the conduit. Many experiments have proved that in practice this is the case too. Evenly distributed wall shear stresses are equivalent to an even distribution of the local velocity near the walls. Figure 2.3.1.c.

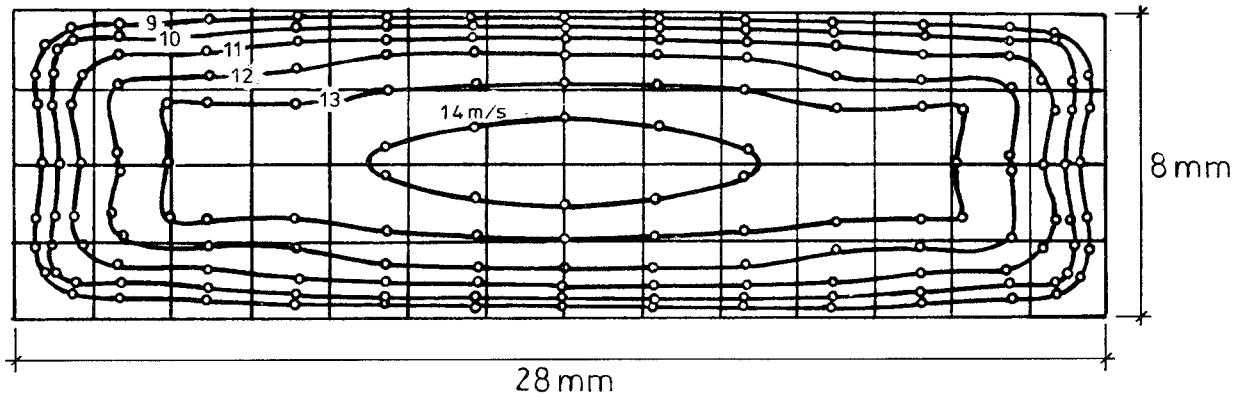


FIG. 2.3.1.c. Velocity distribution in a rectangular channel. After Goldstein (1965).

These conditions can be explained by the existence of secondary flows (first done by Prandtl (1926)). See figure 2.3.1.d.

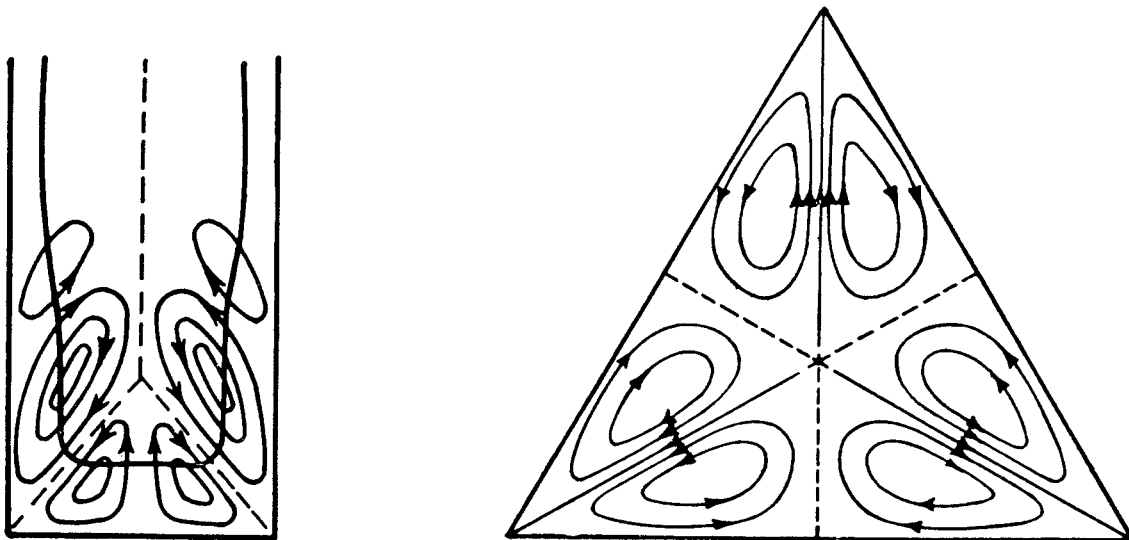


FIG. 2.3.1.d. Secondary flows. After Goldstein (1965).

Having a property, d_H , describing the geometry of the cross section of the conduit the pressure loss along the flow in the conduit is expressed by the general friction formula - sometimes denoted the Darcy - Weisbach formula:

$$\Delta p = \lambda \cdot \frac{l}{d_H} \cdot \frac{\rho u_m^2}{2} \quad (2.3.1.b)$$

where

Δp = pressure loss, Pa

λ = friction factor, (-)

l = length in flow direction, (m)

d_H = hydraulic diameter, (m)

ρ = density of the fluid, (kg/m³)

u_m = average (bulk) velocity, (m/s)

The magnitude of the friction factor will be evaluated in the forthcoming parts for laminar and turbulent flow.

Gas flow in pipes, ducts, cracks etc is dependent on geometry and surface roughness and in a rigorous analysis heat transfer too. In many cases it is possible, however, to assume isothermal conditions; see for example Chivers & Mitchell (1971), without great differences from the more exact thermodynamic approach. This assumption simplifies the analyses considerably.

2.3.2 Flow in closed conduits

2.3.2.1 Laminar flow

For one-dimensional, laminar, stationary flow between two infinite walls at a certain distance from each other it is possible to obtain a direct solution of the Navier - Stokes equation. The equation will take the form

$$-\frac{\partial p}{\partial x} = \eta \frac{\partial^2 u}{\partial y^2} \quad (2.3.2.1.a)$$

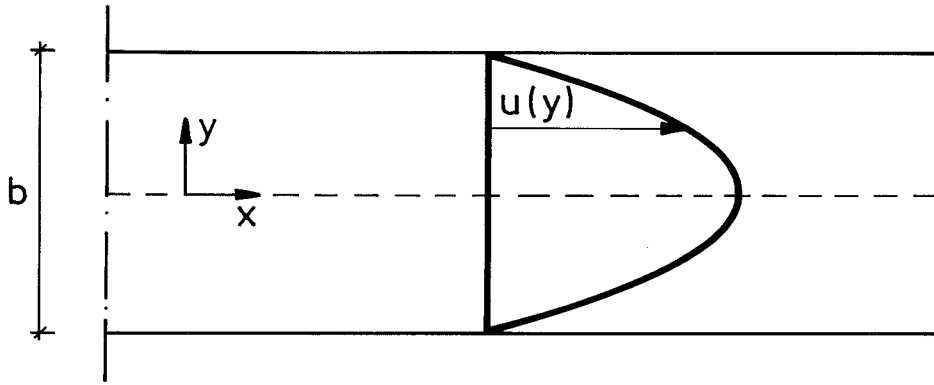


FIG. 2.3.2.1.a.

$$\frac{\partial^2 u}{\partial y^2} = -\frac{\partial p}{\partial x} \cdot \frac{1}{\eta} \quad (2.3.2.1.b)$$

$$\frac{\partial u}{\partial y} = -\frac{\partial p}{\partial x} \cdot \frac{1}{\eta} (y + c_1)$$

$$u(y) = -\frac{\partial p}{\partial x} \cdot \frac{1}{\eta} \left(\frac{y^2}{2} + c_1 y + c_2 \right)$$

$u = u_{\max}$ when $y = 0$ so

$\left(\frac{\partial u}{\partial y} \right)_{y=0}$ should be equal to 0 and

$\left(\frac{\partial^2 u}{\partial y^2} \right)_{y=0}$ should be less than 0

This yields

$$c_1 = 0:$$

$$u = 0 \text{ when } y = \pm \frac{b}{2}$$

$$0 = -\frac{\partial p}{\partial x} \cdot \frac{1}{\eta} \left(\left(\frac{b}{2} \right)^2 / 2 + c_2 \right)$$

So:

$$u(y) = \frac{1}{2\eta} \cdot \frac{\partial p}{\partial x} \left(\left(\frac{b}{2}\right)^2 - y^2 \right) \quad (2.3.2.1.c)$$

$$u_m = \frac{1}{b} \int_{-b/2}^{+b/2} u(y) dy = \frac{\Delta p \cdot b^2}{12 \cdot l \cdot \eta} \quad (2.3.2.1.d)$$

Equation (2.3.2.1.d) is commonly referred to as the Hagen-Poiseuille equation, first published by Poiseuille (1841) and Hagen (1839). The pressure drop along the flow is:

$$\Delta p = \frac{12 u_m \cdot \eta \cdot l}{b^2} \quad (2.3.2.1.e)$$

Since

$$Re = \frac{u_m \cdot d_H}{\nu} = \frac{u_m \cdot 2b \cdot \rho}{\eta}$$

(2.3.2.1.e) can be written

$$\Delta p = \frac{96}{Re} \cdot \frac{l}{d_H} \cdot \frac{\rho u_m^2}{2} \quad (2.3.2.1.f)$$

This is a form of the common hydraulic resistance formula where the friction factor, λ

$$\lambda = \frac{96}{Re} \quad (2.3.2.1.g)$$

Note, however, that rough walls close to each other influence the flow rate - see part 2.3.2.3.p.

It should be mentioned that for a circular cross section:

$$\lambda = \frac{64}{Re} \quad (2.3.2.1.h)$$

Jones (1976) gives a geometrical function, based on a work by Cornisch (1928) to make calculations for any rectangular cross-section possible. The appropriate dimensional factor in question, $\phi^*(b/d)$, is taken to produce the following equation for the friction factor:

$$\lambda = \frac{64}{\phi^*(b/d) \cdot \text{Re}} \quad (2.3.2.1.i)$$

where Re is the standard Reynolds number based on the hydraulic diameter. The quantity $\phi^*(b/d) \cdot \text{Re}$ is denoted Re^* and according to Jones (1976) happens to be valid instead of Re for turbulent flow too.

$$\phi^*\left(\frac{b}{d}\right) = \frac{2}{3} \left(1 + \frac{d}{b}\right)^2 \cdot \left(1 - \frac{192}{\pi^5} \frac{d}{b} \cdot \sum_{n=0}^{\infty} \frac{1}{(2n+1)^5} \cdot \tanh\left(\frac{(2n+1)\pi \cdot b}{2d}\right)\right) \quad (2.3.2.1.j)$$

The function $\phi^*\left(\frac{b}{d}\right)$, designed actual, is shown graphically in figure 2.3.2.1.b.

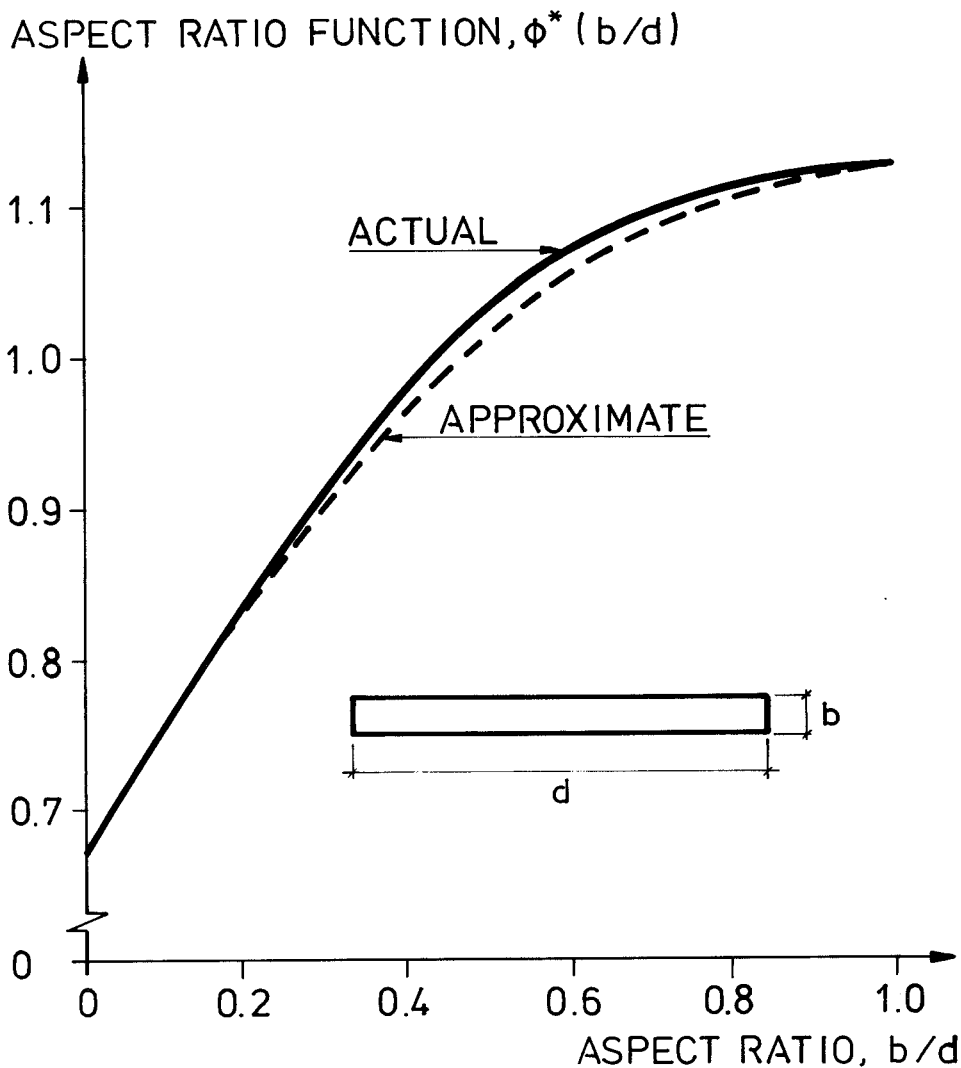


FIG. 2.3.2.1.b. Geometrical function $\phi^*\left(\frac{b}{d}\right)$.

An approximate relationship which will give ϕ^* within about 2 percent is

$$\phi^* \left(\frac{b}{d}\right) \cong \frac{2}{3} + \frac{11}{24} \frac{d}{b} \left(2 - \frac{d}{b}\right) \quad (2.3.2.1.k)$$

which has the correct limits and slope at $d/b \rightarrow 1$, cf. figure 2.3.2.1.b.

The velocity profile in a pipe with rectangular cross section with sides a and b in the directions of y and z respectively could be solved from the following differential equation (Happel & Brenner (1965):

$$u = -\frac{\Delta p}{2\eta} y(y-a) + \sum_{m=1}^{\infty} \sin\left(\frac{m\pi y}{a}\right) \cdot \left(A_m \cosh \frac{m\pi z}{a} + B_m \sinh \frac{m\pi z}{a}\right) \quad (2.3.2.1.1)$$

The coefficients A_m and B_m are evaluated by means of Fourier transformation and the side length b enters as a boundary condition.

By integration we obtain the flow rate q_v :

$$q_v = \frac{\Delta p}{24\eta} a \cdot b(a^2 + b^2) - \frac{8}{\pi^5} \frac{\Delta p}{\eta} \cdot \sum_{n=1}^{\infty} \left[\frac{1}{(2n-1)^5} a^4 \tanh\left(\frac{2n-1}{2a} \pi \cdot b\right) + b^4 \tanh\left(\frac{2n-1}{2b} \pi a\right) \right] \quad (2.3.2.1.m)$$

An exact solution for a pipe having a cross section of an equilateral triangle with sides of length b yields:

$$q_v = \frac{\sqrt{3} \cdot \Delta p \cdot b^4}{320 \eta} \quad (2.3.2.1.n)$$

2.3.2.2 Transitional & turbulent flow

When the flow characteristic turns over from laminar flow in a closed conduit matters turn out to be a bit more complicated than was the case for laminar flow. The friction factor, λ , for laminar flow is depending on Re only. However, the surface roughness has an influence in cases when the sides of the channel are very rough - see part 2.3.2.3. λ depends on

both Re and the surface roughness of the walls relative to the hydraulic diameter in the transitional and turbulent case. Some authors, Hopf (1923) and Fromm (1923) have claimed that λ in these cases is dependent on the planeness of the walls too but this has not, as far as is known, been commented upon later in the literature with exception of Nikuradse (1933) and Bretting (1960) who both in passing mention the phenomenon.

Surface roughness is discussed further in part 2.3.2.3 and the authors experiments on this subject are presented in part 3.1.

The flow resistance for transitional and turbulent flow was investigated extensively by, among others, Nikuradse (1926 - 1933), Drew et al. (1932) Colebrook (1938) and Moody (1944). One of the most frequently used work of reference for determining flow resistance since then is the so called Moody diagram for pipe flow. Figure 2.3.2.2.a. The analytical relationships on which the diagram is based originates from the earlier investigations referred to above.

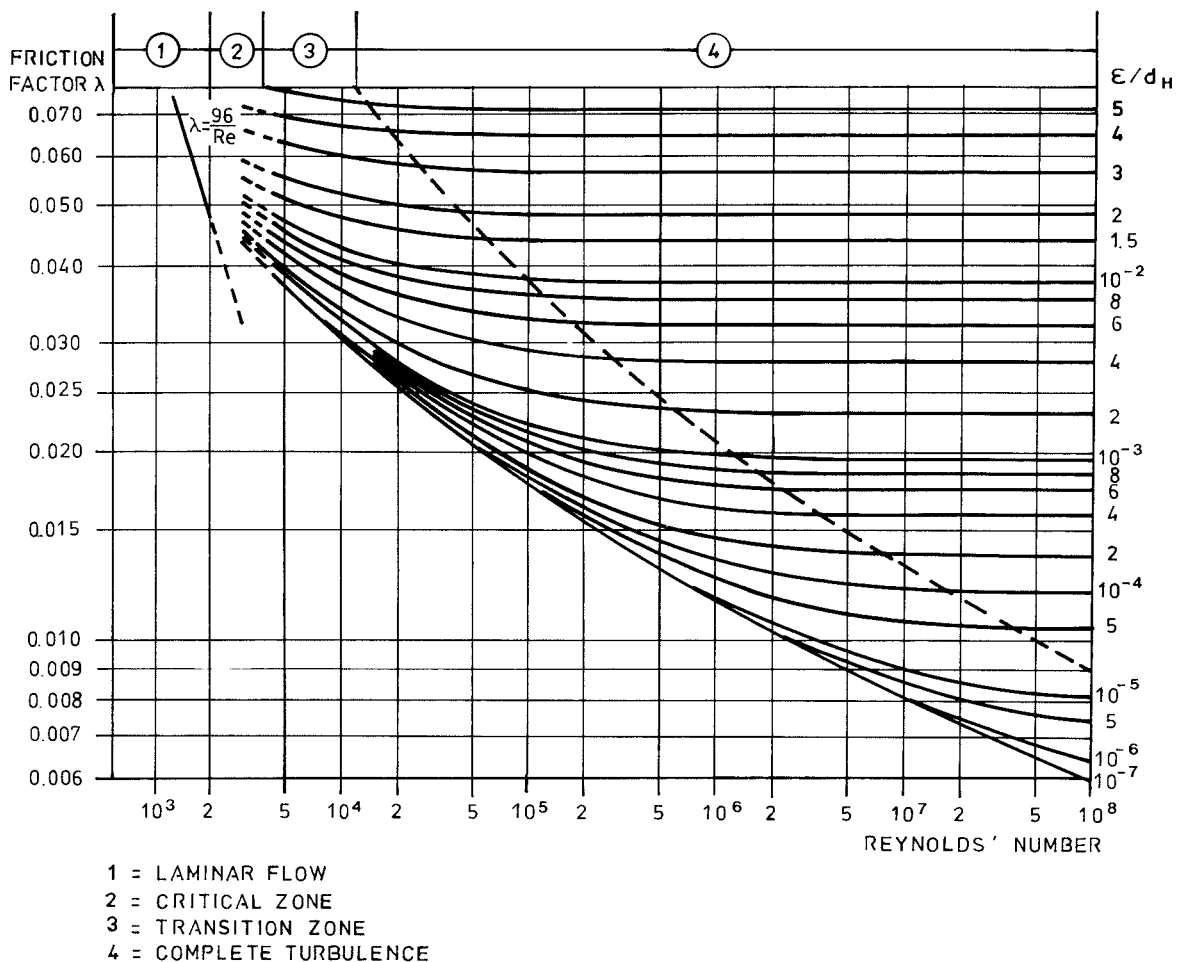


FIG. 2.3.3. a. Moody diagram.

As mentioned, the Moody diagram is made for flow in pipes with circular cross section. However, with some modifications, it will be applicable for flow in conduits with other cross sections such as rectangular and triangular ones. In the diagram, curves for the friction factor λ versus Re are plotted to logarithmic scales for various constant values of the relative roughness ϵ/d .

The field covered by the Moody-diagram can be divided into four areas, each of them representing specific flow characteristics.

1. The first is the region of laminar flow up to a critical number, Re_{cr} (= 2000 in the diagram). Here the flow is fully stabilized under the control of viscous forces which damp out turbulence. A steady turbulent flow is impossible in any round pipe below a certain value. The most commonly reported value is that of Schiller (1925) who found $Re_{LC} = 2320$ where Re_{LC} stands for "lower Reynolds criterion". For ducts, however, the critical Reynolds number is not known to that degree of certainty. Lin (1955), for example, obtained by means of a stability-analysis

$$Re_{crit, Lin} = 5300 \quad (2.3.2.2.a)$$

while Hahnemann & Ehret (1941), (1942) report from their extensive measurements

$$Re_{crit} \cong 3000 \quad (2.3.2.2.b)$$

The values of λ in this region are given by a single curve, $\lambda = 64/Re$, independent of roughness, representing the Hagen-Poiseuille Law. As mentioned above this law states that $\lambda = 96/Re$ for flow between infinite parallel plates.

2. Between $Re = Re_{cr}$ and $Re \cong 3000$ to 4000 the flow conditions depend upon the initial turbulence due to such extraneous factors as sudden section-changes, obstructions or a sharp-edged entrance corner prior to the reach of pipe considered, and the conditions are probably also affected by pressure waves initiating instability. This region is called the critical zone. The minimum value of λ in the critical zone is the dotted continuation of the laminar flow-line. However, the flow is likely to be pulsating rather than steady. Prandtl (1965). Attempts to connect the laminar flow-line

with the curves to the right of the critical zone have been suggested but the procedure seems to be somewhat dubious for it may result in a rise of λ with increasing Re. If λ is represented by a straight line increasing with Re,

$$\lambda = c_1 \cdot \text{Re} = c_2 \cdot u_m \quad (2.3.2.2.c)$$

and

$$\frac{\Delta p}{l} = \lambda \cdot d_H \cdot \frac{\rho u_m^2}{2} = c_3 \cdot u_m^3 \quad (2.3.2.2.d)$$

which is obviously not correct since the exponent operating on u_m must be between 1.0 (laminar case) and 2.0 (turbulent case).

Despite the incorrectness, a relationship of the type:

$$\lambda = \frac{(3500 - \text{Re}) \frac{64}{2000} + \lambda_T (\text{Re} - 2000)}{1500} \quad (2.3.2.2.e)$$

where λ_T is in accordance to 2.3.2.2.f, is often used for calculations.

3. Above a Reynolds number of 3000 to 4000 conditions again become reasonably determinate. First we find the transition zone. In this zone the turbulence is "incomplete" - the flow is still influenced by viscous forces but starts to be influenced also by the roughness. These two conditions are represented in the two terms in the Colebrook-White function:

$$\frac{1}{\sqrt{\lambda}} = -2 \log \left(\frac{\varepsilon/d}{3.71} + \frac{2.51}{\text{Re} \sqrt{\lambda}} \right) \quad (2.3.2.2.f)$$

which determines the friction factor in the transition zone.

The end of the transition zone is a Re-value specific for each ε/d -value. This curve - dotted in the diagram - is called the partition line and Moody gives the following equation for it:

$$\frac{1}{\sqrt{\lambda}} = \frac{\text{Re}}{200} \cdot \frac{\varepsilon}{d} \quad (2.3.2.2.g)$$

4. The zone to the right of the partition line is called the rough-pipe zone or the zone of complete turbulence. Here the friction factor is independent of viscosity i.e. Re and ϵ/d only influence the value of λ .

$$\frac{1}{\sqrt{\lambda}} = -2 \log \left(\frac{\epsilon/d}{3.71} \right) \quad (2.3.2.2.h)$$

Several authors have proposed explicit formulations of the equation for the transition zone eq. (2.3.2.2.f) and some of them have given one single equation for the zone $Re >$ say 4000, Wood (1966), Churchill (1977), Wadmark (1978), Selander (1978), Verma (1979) and Chen (1979). Chen made comparisons between his formula, eq. 2.3.2.2.i, and others and found excellent agreement with the Colebrook equation (mean deviation for 36 comparison points = 0.1%) Chen's equation is:

$$\frac{1}{\sqrt{\lambda}} = -2 \log \left[\frac{\epsilon/d}{3.71} - \frac{5.045}{Re} \log \left(\frac{(\epsilon/d)^{1.110}}{2.826} + \frac{5.851}{Re^{0.898}} \right) \right] \quad (2.3.2.2.i)$$

for $Re > 3000$

Selander (1978) gives the following equation where an accuracy of only a few percent ($\leq 5\%$) is required:

$$\lambda = \left[1.9 \log (10/Re + 0.2 \epsilon/d) \right]^{-2} \quad (2.3.2.2.k)$$

and the following if more accuracy is required ($\leq 0.5\%$)

$$\lambda = \left[2 \log \left(\frac{-4.793}{Re} \log (10/Re + 0.2 \epsilon/d) + 0.2698 \frac{\epsilon}{d} \right) \right]^{-2} \quad (2.3.2.2.l)$$

Alternative formulations of the equation for the partition line have also been given. Moody based his formula for the partition line on a paper by Rouse (1942) who had plotted eq. (2.3.2.2.f) to a scale of $1/\sqrt{\lambda}$ against $Re \sqrt{\lambda}$ on semi-logarithmic paper and introduced the partition line, eq. (2.3.2.2.g) based solely upon optical inspection. Pigott, in his discussion to Moody's paper (p.680) suggests another equation, also based on optical inspection.

$$Re = 3500/(\epsilon/d) \quad (2.3.2.2.m)$$

There were further discussion about the number which should be divided by (ϵ/d) . See figure 2.3.2.2.b!

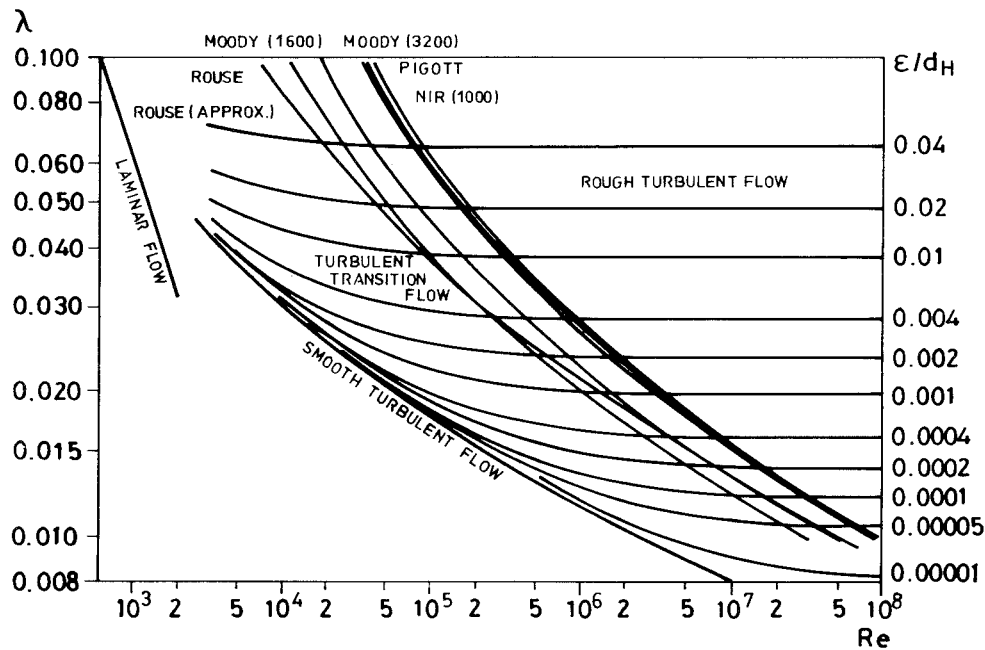


FIG. 2.3.2.2.b. Moody diagram with partition lines.

Nir (1979) developed an equation for the partition line by choosing an angle between the lines $\lambda = \lambda(Re, \epsilon/d_H)$ and horizontal lines in the Moody diagram. He shows that the equation

$$Re = 10^{3/2 \sqrt{\lambda}} \quad (2.3.2.2.n)$$

defines a transition line where the angle mentioned above is 0.83° .

Hitherto the description of the Moody diagram has been linked up with flow in circular pipes. It has been suggested, however, that the diagram could be used for flow in other pipes e.g. pipes with rectangular cross section. This implies the use of the hydraulic diameter, d_H , discussed in 2.3.1. Until quite recently the Moody diagram was used without any further alterations than replacing $\lambda = Re/64$ with $Re/96$ (Poiseuille) and the diameter d with d_H . Investigations by Jones (1976), part 2.3.1, and later by Brundrett (1978) suggest alternative formulations for the hydraulic diameter. In the discussion of Jones' paper Brundrett criticizes the use of ϕ^* (b/d) for turbulent flow and in

Brundrett (1978) he presents an alternative hydraulic diameter, d_H^* , to be used for the calculation of the Reynolds number to be inserted in (2.3.2.2.f) instead of d_H .

$$d_H^* = c \cdot d_H \quad (2.3.2.2.o)$$

where

c is a factor with values according to table 2.3.2.2.a.

Brundrett's method is a simplification of an earlier procedure of Deissler & Taylor (1958) and is based on analysis of the velocity profile and resulting wall shear stress.

Duct	c
Round	1
Square	1.156
Squares with 0.28 B corner radius	1.092
2:1 ellipse	1.166
Eq. Triangle	1.332
$n:1$ Rectangle	$\frac{1.156 + (n - 1)}{n}$

Table 2.3.2.2.a. The factor c in $d_H^* = c \cdot d_H$ for different duct shapes. From Brundrett (1978).

2.3.2.3 Surface roughness

Surface roughness of a wall in a pipe or duct is a property of the wall on which the flow behaviour in the transition and turbulent zone depends to a considerable degree. The surface roughness is caused by irregularities in the profile of the surface. The depth of these are quite large compared to the distance between them. Pioneer work on the subject was done by Nikuradse who made experiments with pipes in which the inner walls were covered with uniform sand particles glued to the walls. Figure 2.3.2.3.a shows his results in a logarithmic $Re - \lambda$ diagram.

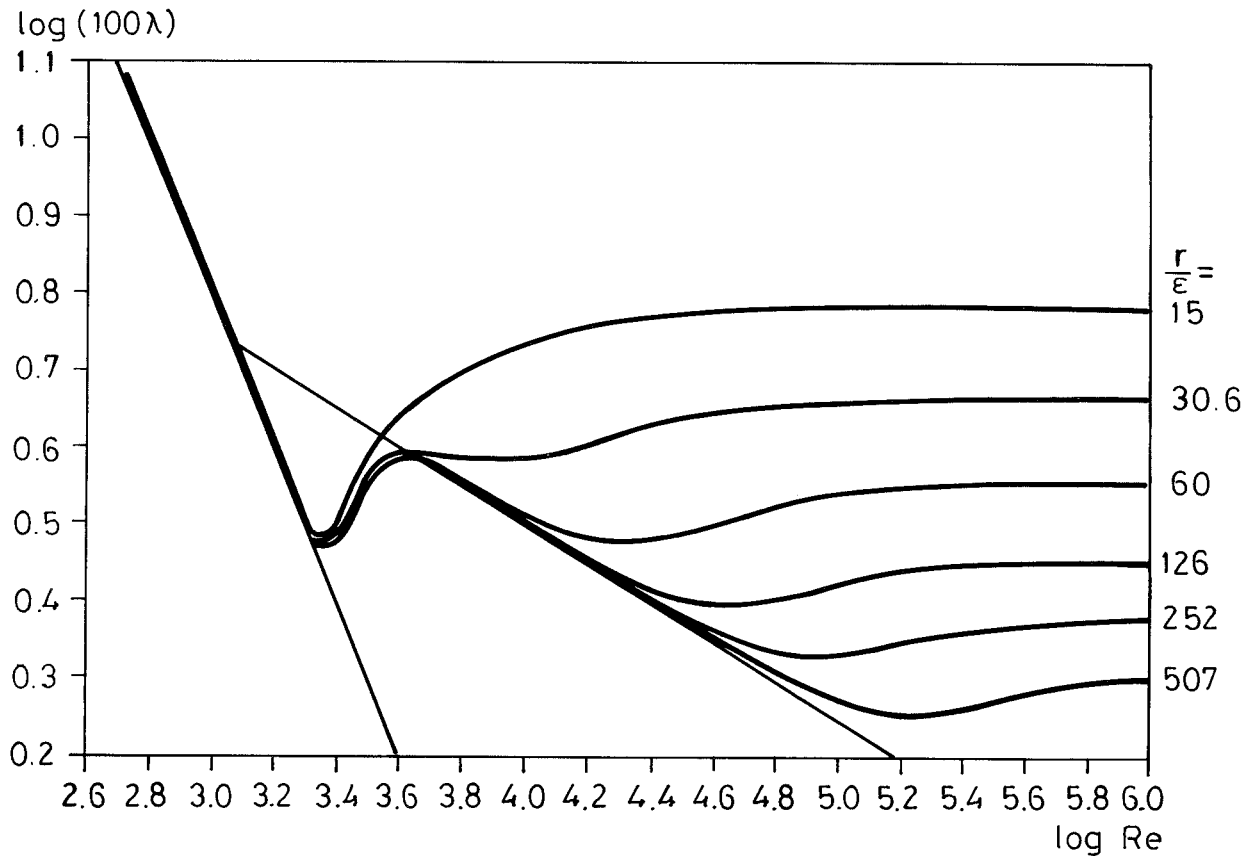


FIG. 2.3.2.3.a. Nikuradse's experiments with uniform sand roughness.
 $\log Re$ vs. $\log(100\lambda)$ for different r/ϵ . After
 Nikuradse (1933).

It was Colebrook some years later who made similar experiments using "real" pipe wall materials, such as iron, wood, concrete. Figure 2.3.2.3.b originates from Colebrook (1938). It shows a principal discrepancy between uniform sand roughness and "real" materials roughness as far as the resulting friction is concerned.

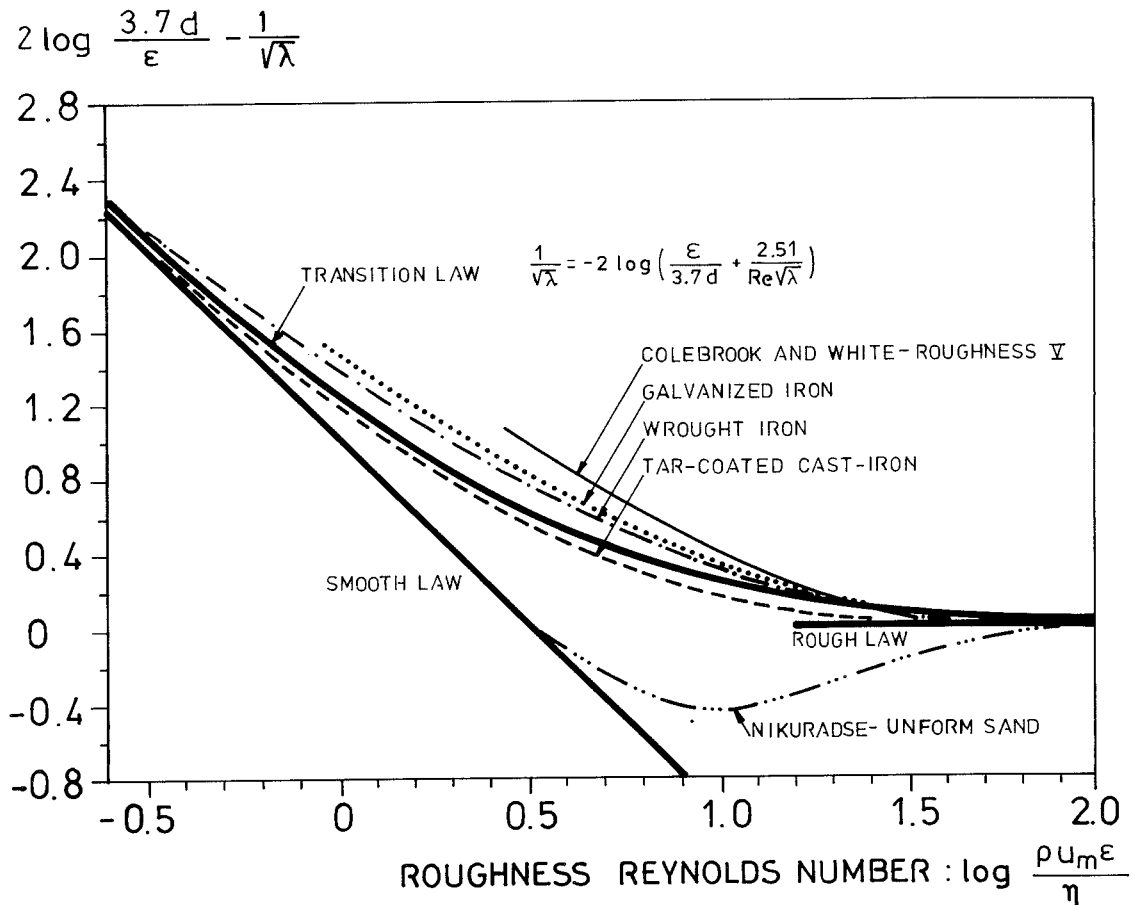


FIG. 2.3.2.3.b. Theoretical and experimentally determined "transition" laws for various rough surfaces. After Colebrook (1938).

The transition starts at higher Re-values in the case of sand roughness. This is due to the circumstance that there is a lack of turbulence producing isolated eddies when the roughness is based on uniform sand.

In the experiments of Nikuradse the absolute roughness ϵ had a physical meaning. It was the radius of the sand particles used. As the layer was thin (no double layers of sand) the size was also taken to represent the mean depth of the irregularities.

When real surfaces are concerned the absolute roughness ϵ must be determined from pipe flow experiments like Colebrooks. Much hope has been based upon the possibilities of predicting the surface roughness from some kind of geometrical measurement of the surface finish. Only a little effort has been spent on the problem, but some years ago Warburton (1974) reported,

relationships for such a prediction for graphite surfaces of various surface finishes. Though his results are quite encouraging for this material it is not possible to extend the analyses directly to other materials. Different ways of measuring surface finishes are reported by Künzli (1964). Another concise work in the field of surface finish measurements is Rau & Leonhardt (1979). Waschull (1979) and Chetwynd (1979) may be mentioned too. A special device - the so-called Bendtsen hard-board tester is commonly used for hardboard. In fact there is a Scandinavian standard for the test, SCAN-P 21:67, (1967) and the testing procedure, is also described in Lundgren (1959).

One problem is to determine the flow rate of fluid flow between rough surfaces. Valuable contributions to the knowledge of these matters come from lubrication technology. Thus Patir & Cheng (1978) suggest an "average flow model" relying on surface roughness statistics - either simulated or measured - with special flow factors which are applied as correction terms to ordinary equations for crack flow in the laminar region. A gap between two rough surfaces is illustrated in figure 2.3.2.3.c.

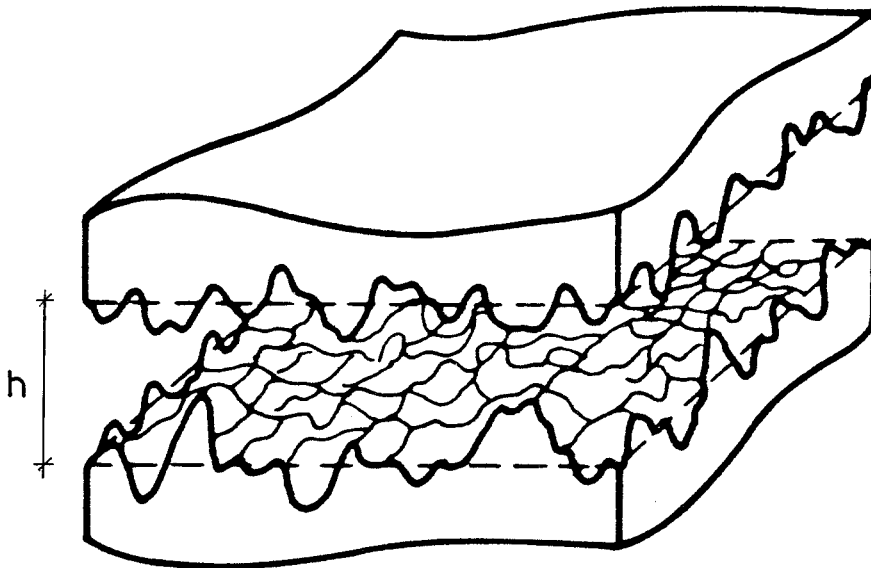


FIG. 2.3.2.3.c. Gap between two rough surfaces. After Patir & Cheng (1978).

The quantity h stands for the distance between the mean levels of the two surfaces and h_T is the local distance in any point. See figure 2.3.2.3.d.

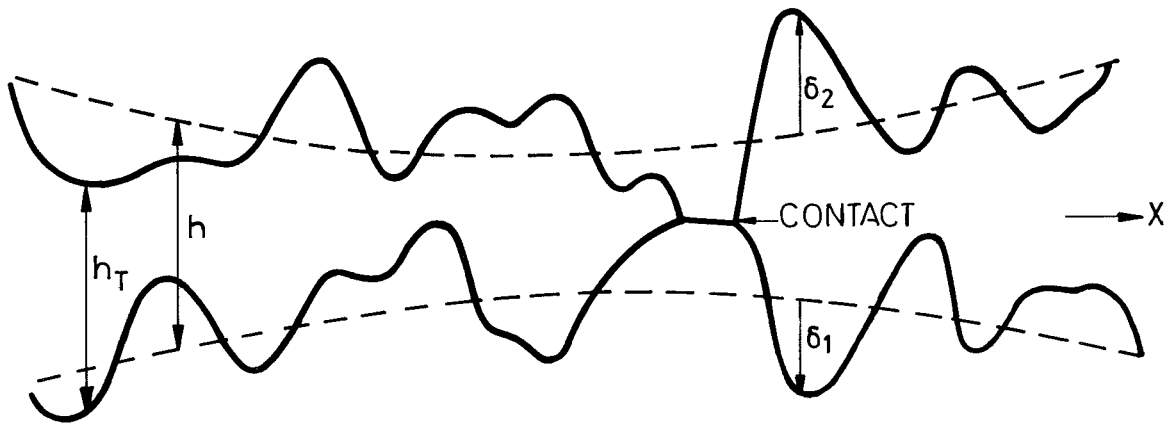


FIG. 2.3.2.3.d. Explanation of the notation used. After Patir & Cheng (1978).

Any local distance can be written:

$$h_T = h + \delta_1 + \delta_2 \quad (2.3.2.3.c)$$

where δ_1 and δ_2 are the roughness amplitudes of the two surfaces measured from their mean levels. Let δ_1 and δ_2 have a Gaussian distribution with standard deviations σ_1 and σ_2 respectively. The combined roughness has a standard deviation

$$\sigma = \sqrt{\sigma_1^2 + \sigma_2^2} \quad (2.3.2.3.d)$$

This is strictly valid only if δ_1 and δ_2 are statistically independent, which in some cases may be a somewhat dubious assumption, especially when real cracks - for example shrinkage cracks - are concerned.

The ratio h/σ is an important parameter showing the effect of surface roughness. This can be seen in figure 2.3.2.3.e where the flow factor, ϕ , is plotted against h/σ for different surface direction characteristics γ . (See definition below!)

PRESSURE FLOW FACTOR

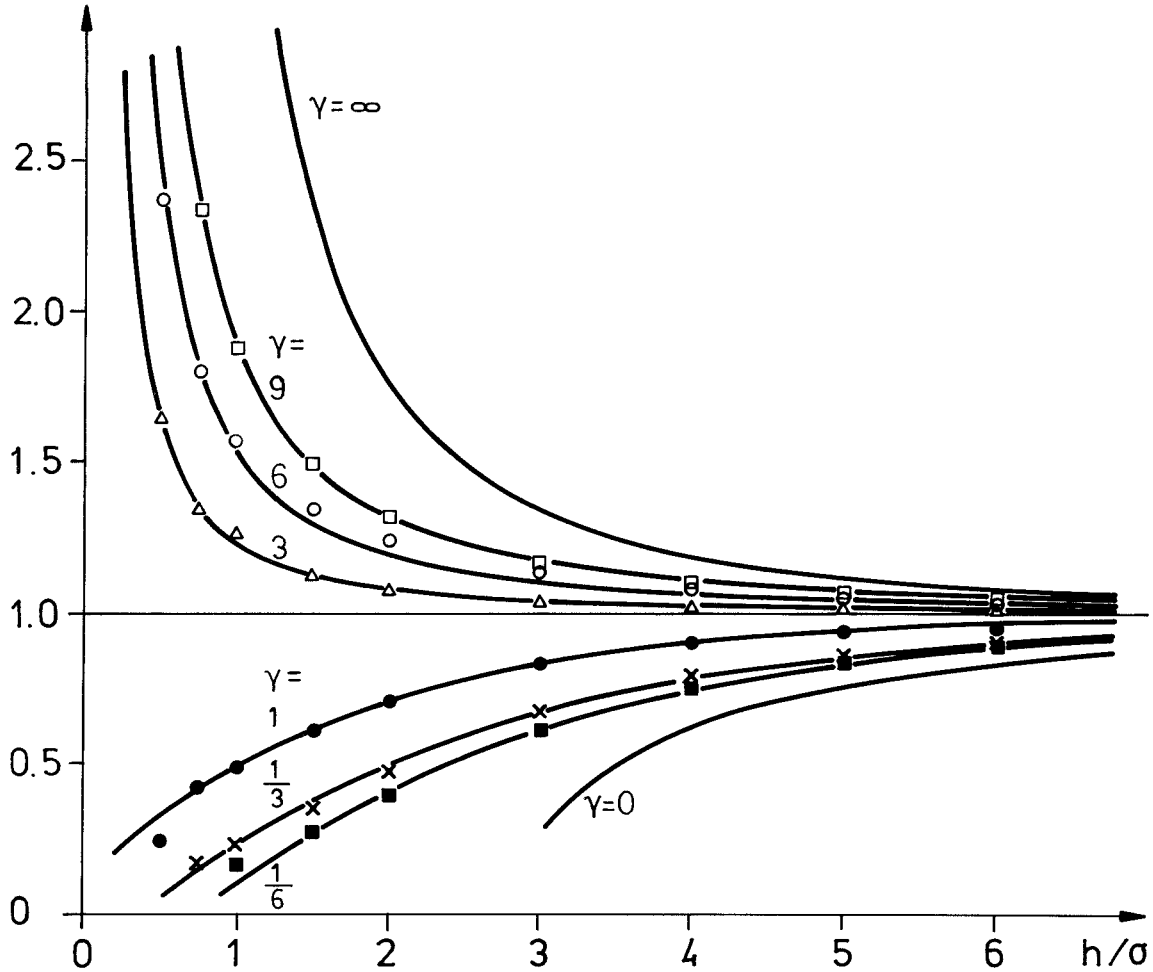


FIG. 2.3.2.3.e. Effects of directional properties of roughness on the flow factor ϕ . After Patir & Cheng (1978).

The flow factor is simply a multiple factor in the ordinary Hagen-Poiseuille equation (loc.cit. eq. (2.3.2.1.e)).

$$q_m = \phi \frac{h^3 \cdot \Delta p}{12 \eta l} \quad (2.3.2.3.e)$$

The surface direction characteristic, γ , is according to Peklenik (1967 - 1968):

$$\gamma = \frac{\lambda_{0.5x}}{\lambda_{0.5y}} \quad (2.3.2.3.f)$$

where $\lambda_{0.5}$ is the length at which the auto-correlation function of a profile reduces to 50% of its initial value. Suffix x = in x-direction, y = in y-direction. Purely transverse, isotropic and longitudinal roughness patterns correspond to $\gamma = 0, 1$ and ∞ , respectively. Figure 2.3.2.3.f.

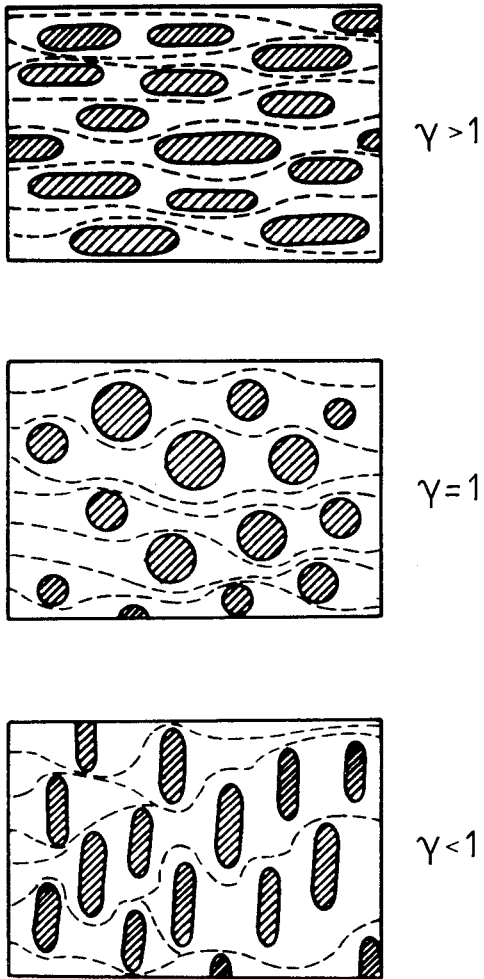


FIG. 2.3.2.3.f. Longitudinally oriented ($\gamma > 1$), isotropic ($\gamma = 1$) and transversely oriented ($\gamma < 1$) surfaces. After Patir & Cheng (1978).

The data shown in figure 2.3.2.3.f can be fitted into relations of the form

$$\phi = 1 - Ce^{-r \frac{h}{\sigma}} ; \gamma \leq 1 \quad (2.3.2.3.g)$$

$$\phi = 1 + Ce^{-r} ; \gamma > 1 \quad (2.3.2.3.h)$$

with empirical coefficients given in Patir & Cheng (1978). As an example, for $\gamma = 1$, $C = 0.90$ and $r = 0.56$.

2.3.2.4 Pressure loss factors for abrupt changes in flow cross section and flow direction

When the velocity profile in a pipe or duct flow has developed its final form the pressure drop per length unit in the flow direction is described by the general friction law.

$$\frac{\Delta p}{l} = \frac{\lambda}{d_H} \cdot \frac{\rho u_m^2}{2} \quad (2.3.2.4.a)$$

If abrupt changes in flow cross section or flow direction are introduced, extra pressure losses caused by the changes will arise. We are first going to look at pressure drop due to changes in cross section.

Several authors from the middle of the 19th century and later have devoted quite a lot of work to these matters. The sign ϕ denotes works on flow in pipes with circular cross section and = parallel plane flow or flow in ducts with rectangular cross section. Early works are Poiseuille (1846) ϕ , Boussinesq (1890, 1891) ϕ and Knibbs (1897) ϕ . The greatest effort has been spent on the constriction case, and a variety of methods for approximative solution of the equations of motion has been used. Hence linearization of the inertia terms was used by for example Han (1960) =, Langhaar (1942) ϕ , Sparrow & Lin (1964) ϕ , patching of a boundary layer and a perturbation about developed flow analysis Boussinesq (1891) ϕ , Collins & Schowalter (1962) ϕ , Stephan (1959), integral analysis Campbell & Slattery (1963) ϕ , Mohanty & Asthana (1978) ϕ , Paivanas (1962) ϕ and =, Roidt & Cess (1962) =, Schiller (1922) ϕ , Schlichting (1934) =, numerical methods Bodoia & Osterle (1961) =, Christiansen et al (1972) ϕ , Lundgren et al (1964) ϕ and =.

Experimental results are reported by eq. Benedict et al (1966) ϕ , Kreith & Eisenstadt (1957) ϕ , Astarita & Greco (1968) ϕ , ESDU (1978) ϕ , Kaye & Rosen (1971) ϕ , Idelchik (1960) ϕ and Karev (1953) ϕ .

Kays (1948, 1950) ϕ and =, used a momentum-force analysis and experiments of both the contraction and the expansion case and derived useful loss-values for engineering purposes. Bunditkul & Yang (1977) made later a more detailed examination using numerical methods and the same authors, Bunditkul & Yang (1979), have recently expanded the use of the loss factors

of Kays to channels with a short flow construction.

The principal behaviour of the flow of a closed conduit when the cross section is abruptly contracted and then abruptly expanded again is shown in figure 2.3.2.4.a.

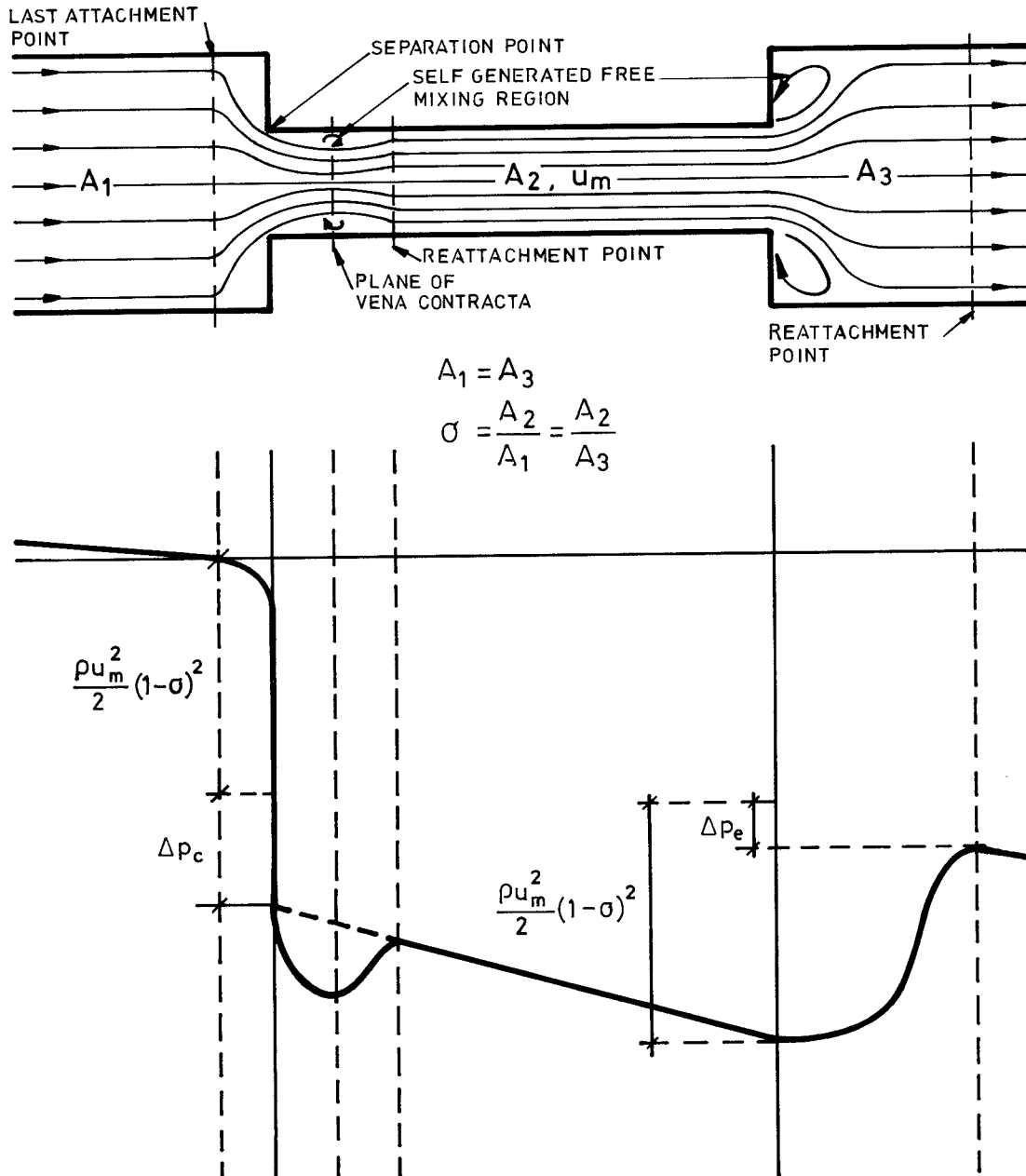


FIG. 2.3.2.4.a. Abrupt contraction and abrupt expansion of a closed conduit flow. Streamlines and pressure variations.

The figure shows the entrance pressure drops and the exit pressure rise characteristics of the flow.

The entrance pressure drop is made up of two parts, separated as follows: The first is the pressure drop due to flow-area change only, without friction. The second one is the pressure loss due to the irreversible free expansion that follows the abrupt contraction, which arises from boundary-layer separation (as characterized by the vena contracta), and the consequent pressure change due to change of momentum rate associated with changes in velocity profile downstream from the vena contracta. For our applications density changes are so small that a constant density treatment is satisfactory. The entrance pressure drop, Δp_c , can then be expressed as

$$\Delta p_c = \frac{\rho u_m^2}{2} (1 - \sigma)^2 + K_c \frac{\rho u_m^2}{2} = \xi_c \cdot \frac{\rho u_m^2}{2} \quad (2.3.2.4.b)$$

where

ρ = density of the air, kg/m³

u_m = average velocity in the constricted flow area, m/s

σ = ratio of constriction area to frontal area

K_c = contraction factor

$\xi_c = (1 - \sigma)^2 + K_c$ = contraction loss factor

The exit pressure rise, Δp_e , is similarly subdivided into two parts. The first is the pressure rise which would occur due to area change alone, without friction. The second is the pressure loss associated with the irreversible free expansion and momentum changes following an abrupt expansion and this term subtracts from the other. Thus

$$\Delta p_e = \frac{\rho u_m^2}{2} (1 - \sigma)^2 - K_e \frac{\rho u_m^2}{2} = -\xi_e \frac{\rho u_m^2}{2} \quad (2.3.2.4.c)$$

where K_e is the expansion or exit factor and $\xi_e = K_e - (1 - \sigma)^2$ = the expansion or exit loss factor.

K_c and K_e are functions of the contraction and expansion geometry and of the Reynolds number in the constricted conduit. The latter dependence arises from the influence of the velocity profiles on the momentum rates and the resulting effect on the change of momentum at the entrance and exit.

In figure 2.3.2.4.b K_c and K_e are presented for duct flow and multiple tube flow.

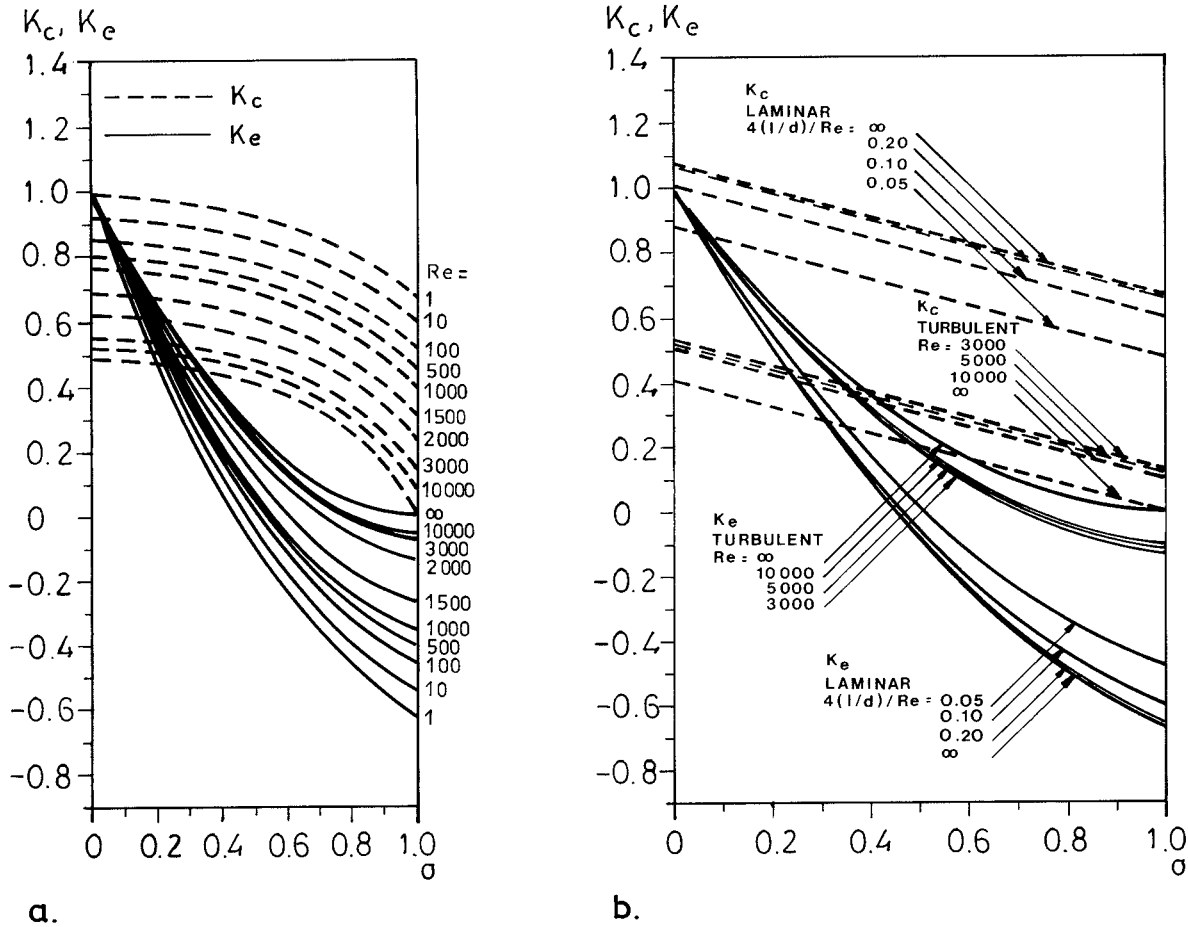


FIG. 2.3.2.4.b. Entrance, K_c and exit, K_e , factors for (a) duct flow and (b) multiple tube flow. After (a) Bunditkul & Yang (1977) and Kays (1950) (b).

Note that the loss factors, ξ_c and ξ_e , include all excess pressure loss superposed on the normal duct friction over the total length of the pipe, so the total pressure loss, Δp_{tot} , along the pipe is written

$$\Delta p_{tot} = \xi_c \cdot \frac{\rho u_m^2}{2} + \lambda \frac{l}{d_H} \cdot \frac{\rho u_m^2}{2} + \xi_e \frac{\rho u_m^2}{2} \quad (2.3.2.4.d)$$

where l is the total length in the flow direction of the constricted cross section of the pipe.

The concept of the note is essential to bring to the reader's attention because other factors, with which it is necessary to reduce l for the inlet length (to developed velocity profile), exist in the literature. This way of treating the problem, however, is time-consuming and laborious and therefore the procedure presented above is chosen for this study.

To make it possible to use the loss factors from figure 2.3.2.4.b for (computerized) calculations it is necessary to produce analytical expressions for K_c and K_e as functions of Re and σ . This was done by plotting K_c and K_e versus Re for different σ . Figure 2.3.2.4.c and 2.3.2.4.d.

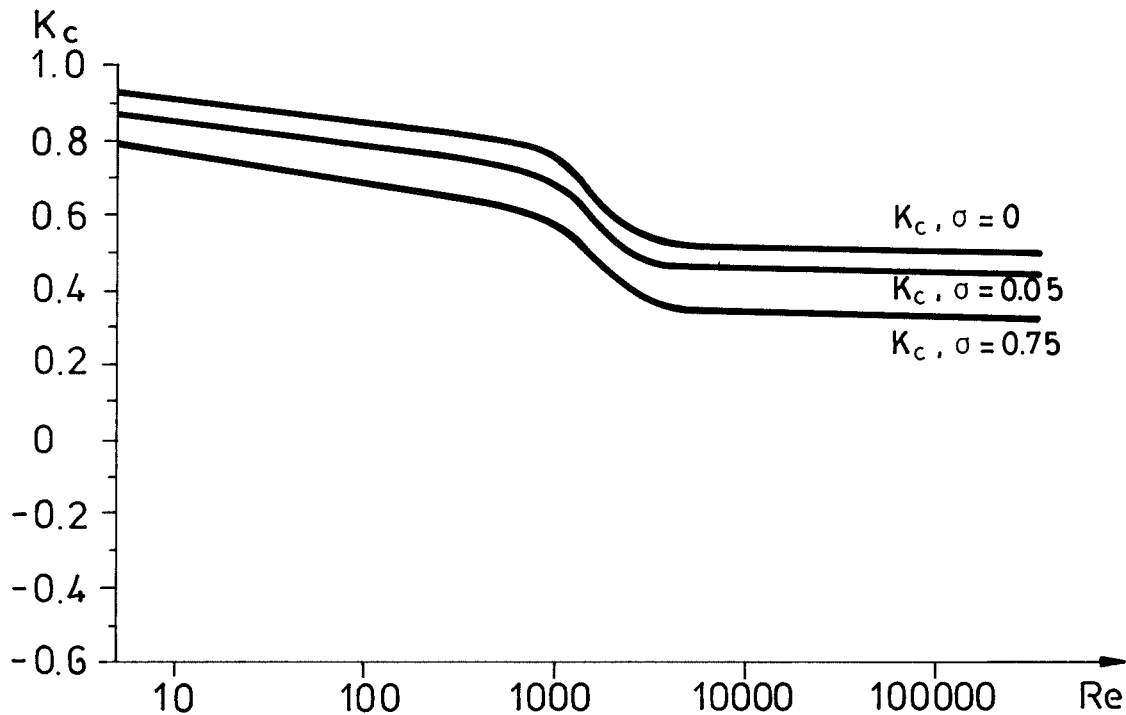


FIG. 2.3.2.4.c. Contraction factors versus Re for different σ .

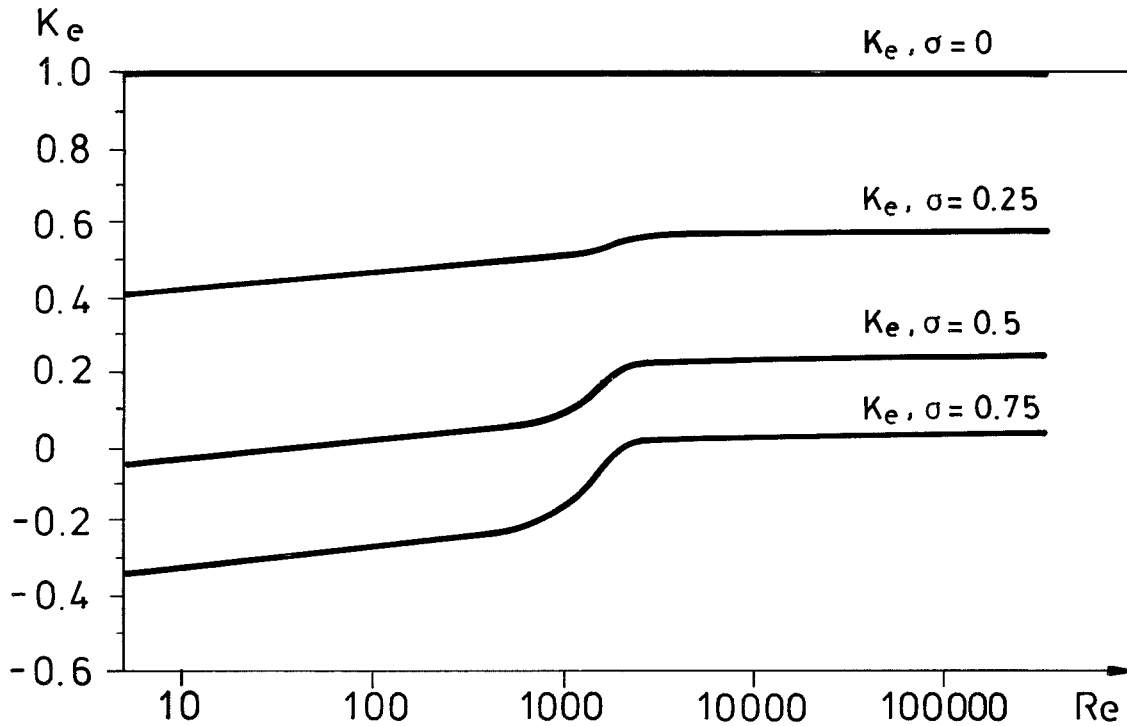


FIG. 2.3.2.4.d. Expansion factors versus Re for different σ .

Approximate relationships between contraction and expansion factors, Re and σ were obtained with curve-fitting technique. The results are summarized below and plotted in figure 2.3.2.4.e and 2.3.2.4.f.

Reynolds number, Contraction factor K_C :

- 1000	$0.98 \cdot Re^{-0.03} - 0.067\sigma + 0.373\sigma^2$
1000 - 3000	$10.59 \cdot Re^{-0.374} - 0.067\sigma + 0.373\sigma^2$
3000 -	$0.57 \cdot Re^{-0.01} - 0.067\sigma + 0.373\sigma^2$

Reynolds number, Expansion factor K_e :

- 1000	$-0.036 + 9.60 \cdot 10^{-5} Re + \Delta K_e$
1000 - 3000	$1.28 \cdot 10^{-5} Re^{1.223} + \Delta K_e$
3000 -	$0.21 \cdot Re^{0.012} + \Delta K_e$

$$\Delta K_e = 0.78 - 1.56\sigma \quad \text{if } \sigma \text{ is less than } 0.5$$

$$\Delta K_e = 0.48 - 0.96\sigma \quad \text{if } \sigma \text{ is greater than } 0.5$$

$$\text{if } \sigma < 0.05 \text{ then } K_e = 1.00$$

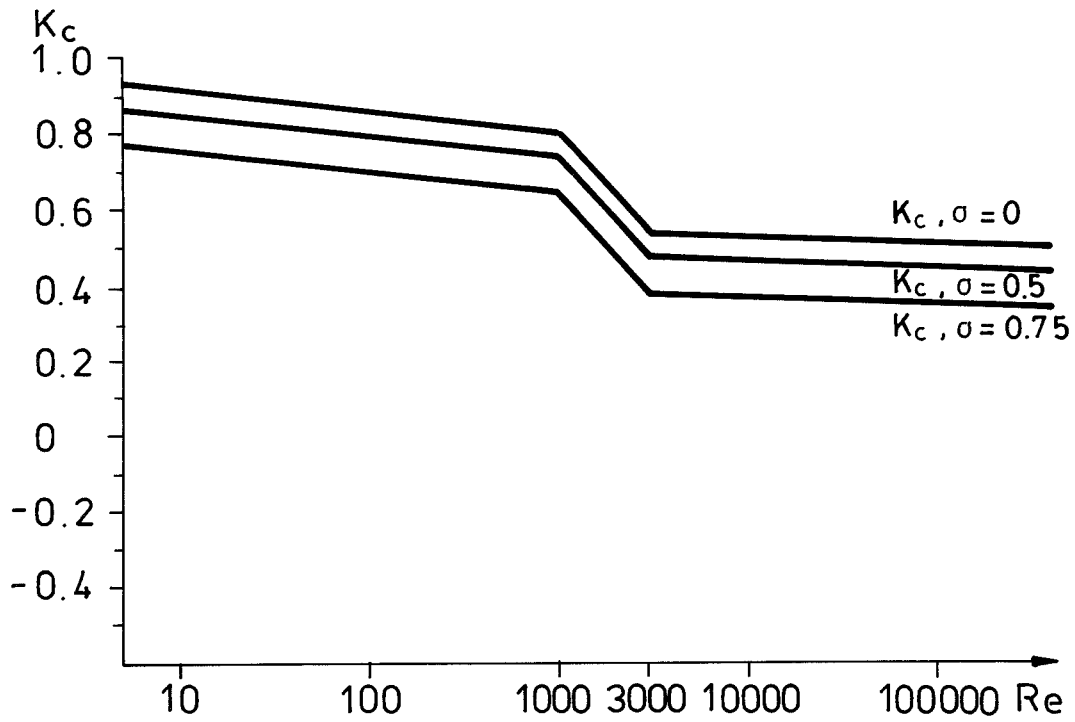


FIG. 2.3.2.4.e. Approximate values of contraction factors.

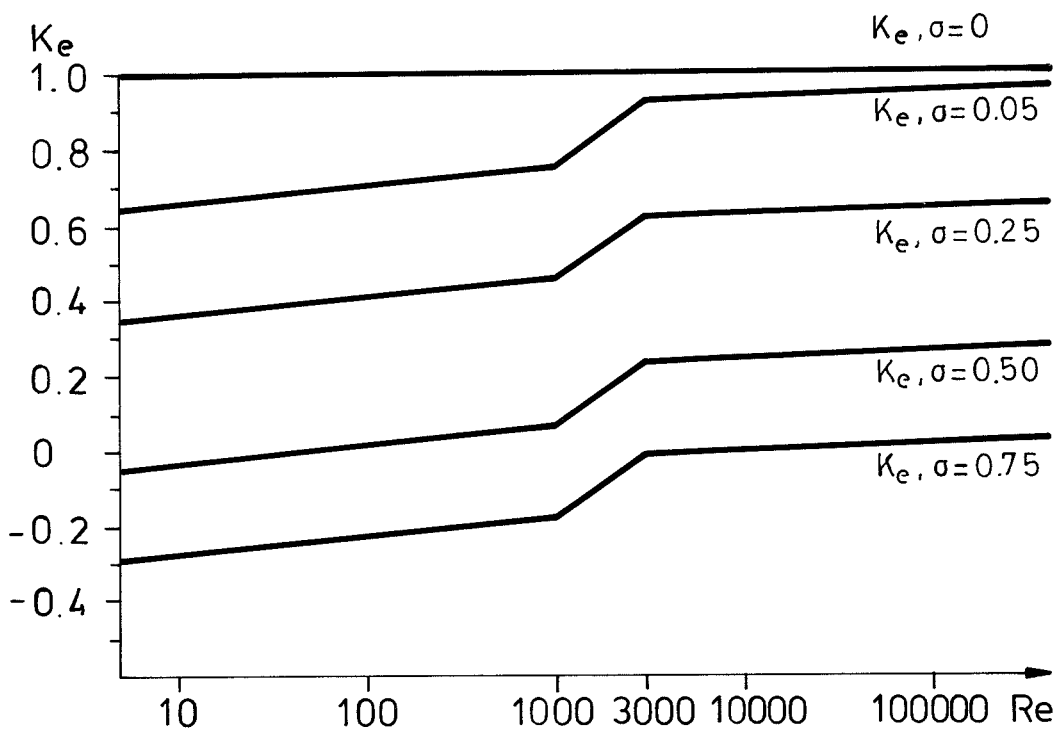


FIG. 2.3.2.4.f. Approximate values of expansion factors.

However, Kay's and Bunditkul & Yang's (1977) work were based on tube lengths hydrodynamically long enough for the velocity profile to be completely developed downstream of the contraction. As mentioned briefly above, Bunditkul & Yang (1979) expanded the feasibility of the factors for tubes being so short in the flow direction that the flow is still developing at the exit. Their results are worked out for the laminar flow region and obtained by numerically integrating the full Navier-Stokes and energy equations using finite-difference technique. An example from their results is shown in figure 2.3.2.4.g.

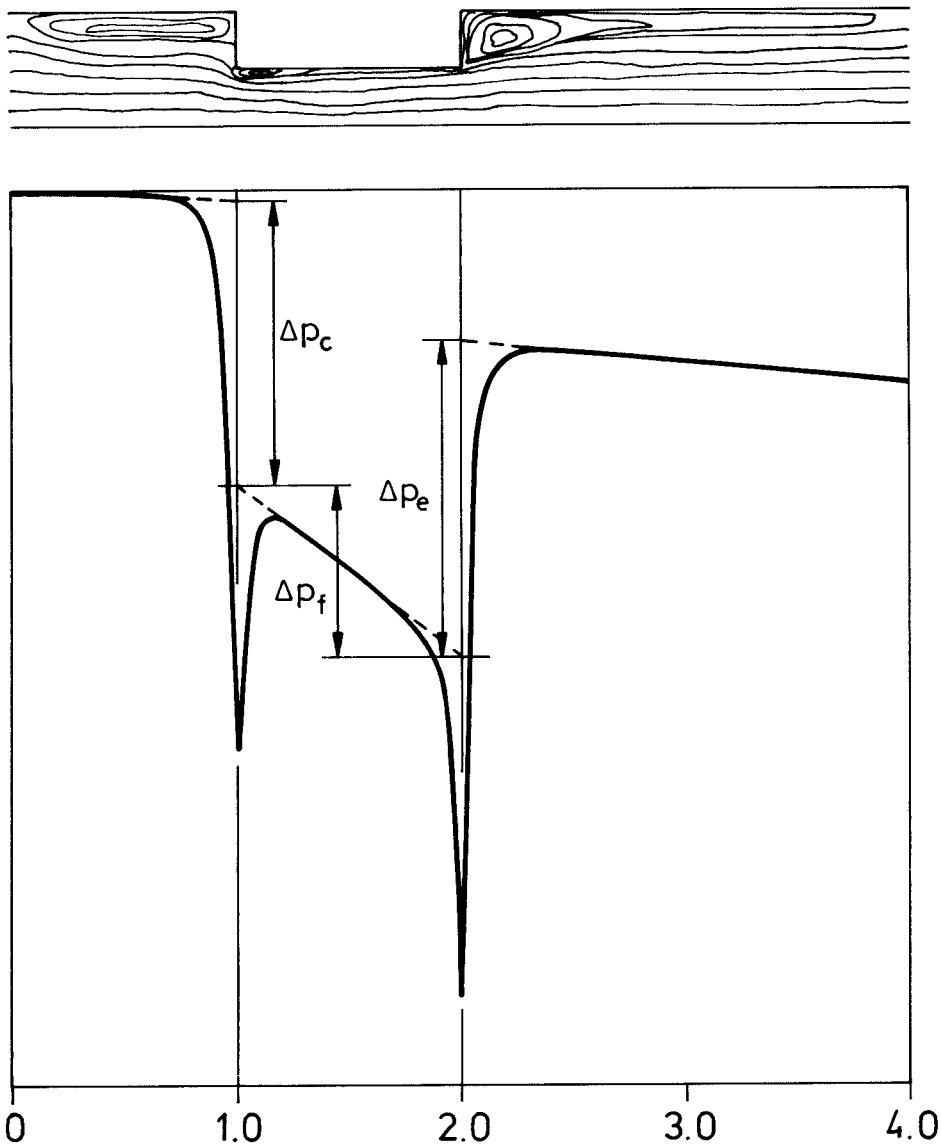


FIG. 2.3.2.4.g. Streamlines and pressure drop for $Re = 500$, $1/d_H = 1.0$, $\sigma = 0.5$ ($B_f = 6.67$). After Bunditkul & Yang (1979)

From their calculations they found that the dimensionless quantity B_f , defined as:

$$B_f = (Re \cdot d_H / l)^{1/3} \cdot \sigma^{1/4} \quad (2.3.2.4.d)$$

described the hydrodynamic effects of the flow constriction. Figure 2.3.2.4.h describes how B_f varies with d_H/l and σ for different Reynolds numbers.

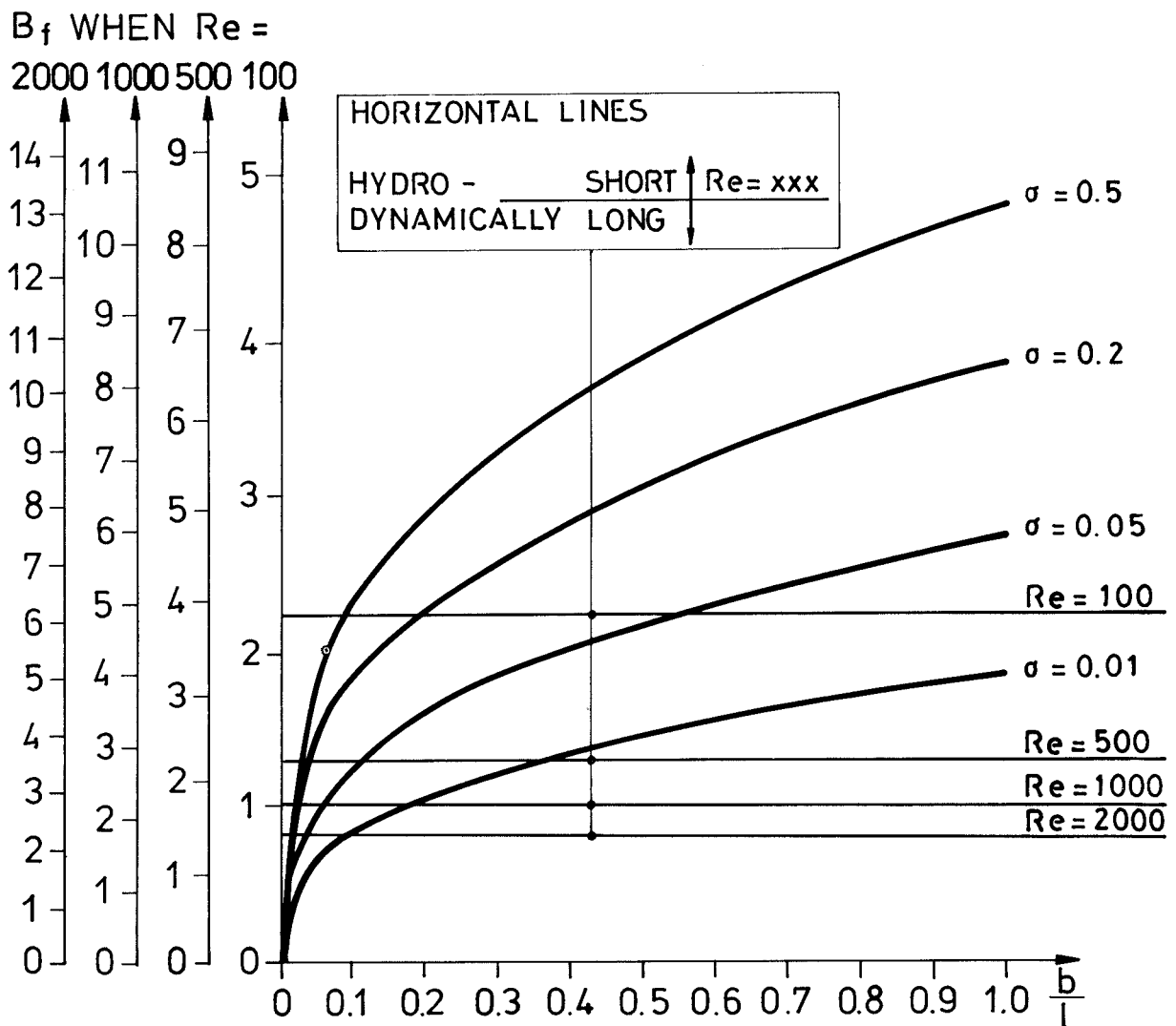


FIG. 2.3.2.4.h. B_f , according to Bunditkul (1979), vs. d_H/l for different ratios of constriction area to frontal area (σ) and Re . Over the horizontal lines with $Re = 100, \dots, 2000$ i.e. when $B_f > 2.25$ the constriction is considered to be hydrodynamically short.

$$\begin{aligned}
 K_c^* &= C_c \cdot K_c \\
 K_e^* &= C_e \cdot K_e \\
 \lambda^* &= C_f \cdot \lambda
 \end{aligned}
 \tag{2.3.2.4.e}$$

K_c and K_e are factors defined above with values according to figure 2.3.2.4.b for long tubes. λ is the friction factor ($\frac{96}{Re}$) for parallel plates. The correction factors C_c , C_e and C_f , derived from numerical computations, are plotted against B_f in figure 2.3.2.4.i. They are unity when $B_f \leq 2.25$ - the criterion for a construction to be hydrodynamically long. Hence:

$$\begin{aligned}
 C &= a B_f + b; & B_f > 2.25 \\
 C &= 1; & B_f \leq 2.25
 \end{aligned}
 \tag{2.3.2.4.f}$$

where

$a = -0.304, 0.792, 0.122$ and

$b = 1.684, -0.782, 0.725$ for

C_c, C_e, C_f respectively.

To make the reader familiar with what is meant by a hydrodynamically short channel the following example is given as a demonstration.

Duct width: 0.001 m (0.002) m

$\sigma = 0.05$

Hydrodynamically short if:

1 <	when Re =
0.002 (0.004)	100
0.01 (0.02)	500
0.02 (0.04)	1000
0.03 (0.07)	2000

This means that only at high Reynolds number, and when relatively wide cracks or ducts are concerned, the critical length is of the same order as the width of building constructions, i.e. walls, windows etc.

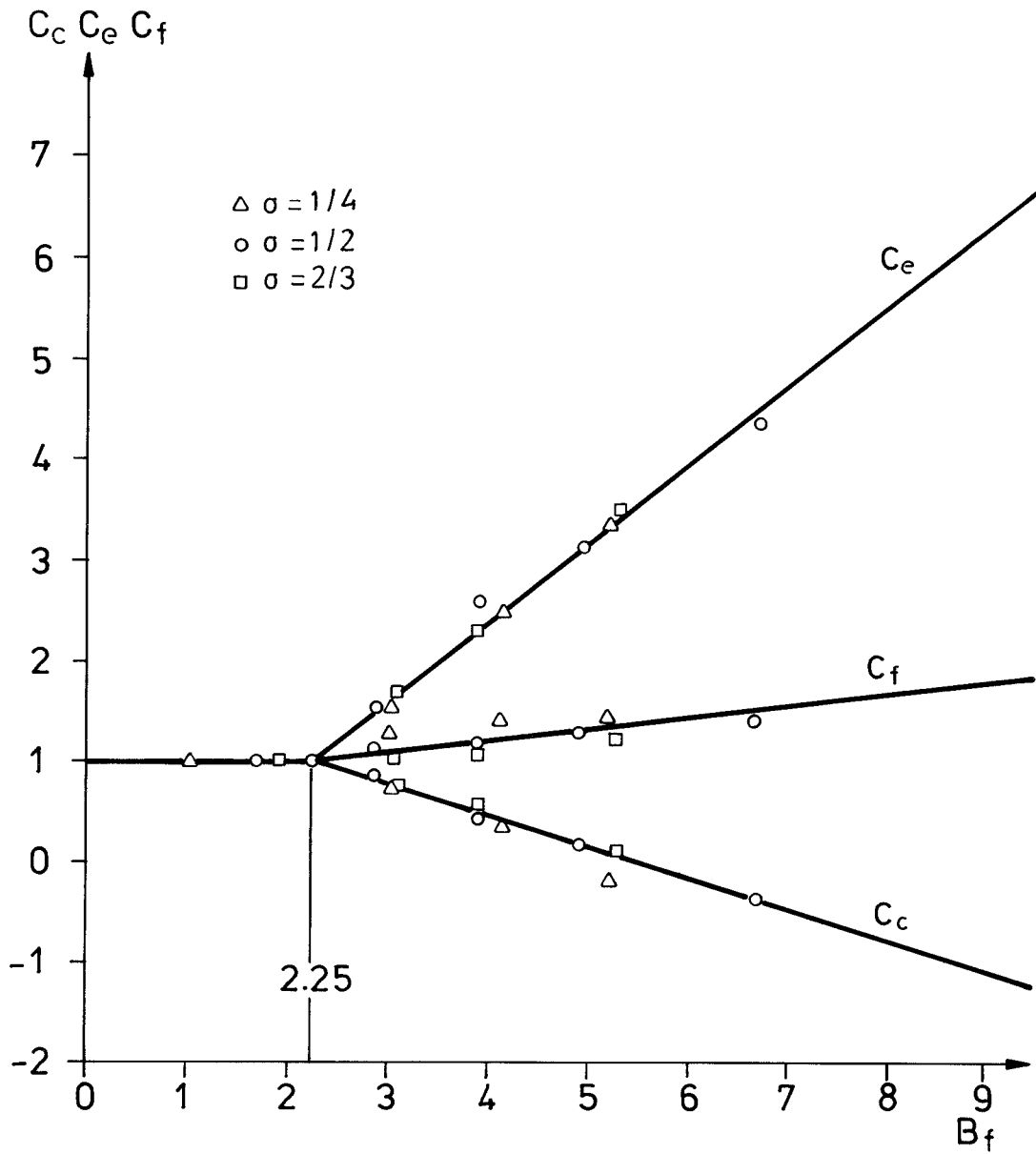


FIG. 2.3.2.4.i. Correction factors for loss factors and friction factor for flow in parallel channels with a short flow construction. After Bunditkul & Yang (1979).

Excess pressure losses due to abrupt changes in flow direction have been investigated only slightly as far as can be seen in the literature. Most hydraulic handbooks present values of loss factors for different types of bends for pipes of circular cross section. Loss factor values of bends in rectangular channels are rare in the literature. However, Idelchik (1960) gives a detailed procedure, including a lot of relevant parameters, for sharp elbows of rectangular section with converging or diverging exit section. Figure 2.3.2.4.k.

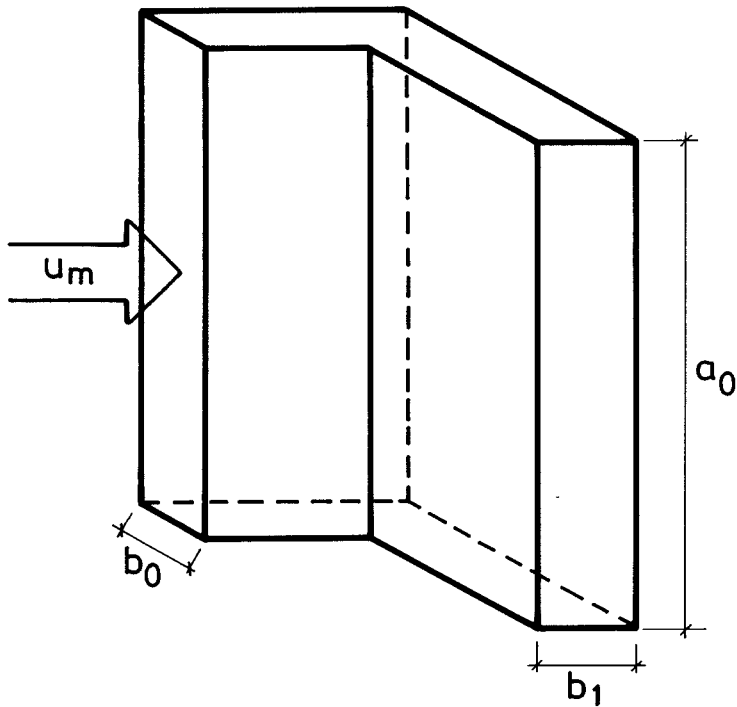


FIG. 2.3.2.4.k. Sharp elbow. Symbols.

The bend loss factor, ξ_b , is defined as

$$\Delta p_b = \xi_b \cdot \frac{\rho u_m^2}{2} \quad (2.3.2.4.g)$$

where Δp_b is the excess pressure loss due to the bend. ξ_b is written:

$$\xi_b = k_{\varepsilon/d_H} \cdot k_{Re} \cdot \xi \quad (2.3.2.4.h)$$

where k_{ε/d_H} and k_{Re} are factors depending on the relative roughness and the friction factor in the inlet channel. They are taken from table 2.3.2.4.a.

ξ is a loss factor according to figure 2.3.2.4.1.

ε/d_h	$3000 < Re < 40\ 000$		$Re > 40\ 000$	
	k_{Re}	k_{ε/d_H}	k_{Re}	k_{ε/d_H}
0	45λ	1.0	1.1	1.0
0 - 0.001	45λ	1.0	1.0	$1 + 0.5 \cdot 10^3 \cdot \varepsilon/d_H$
> 0.001	45λ	1.0	1.0	1.5

Table 2.3.2.4.a. Factors k_{ε/d_H} and k_{Re} to be used in eq. 2.3.2.4.h. After Idelchik (1960).

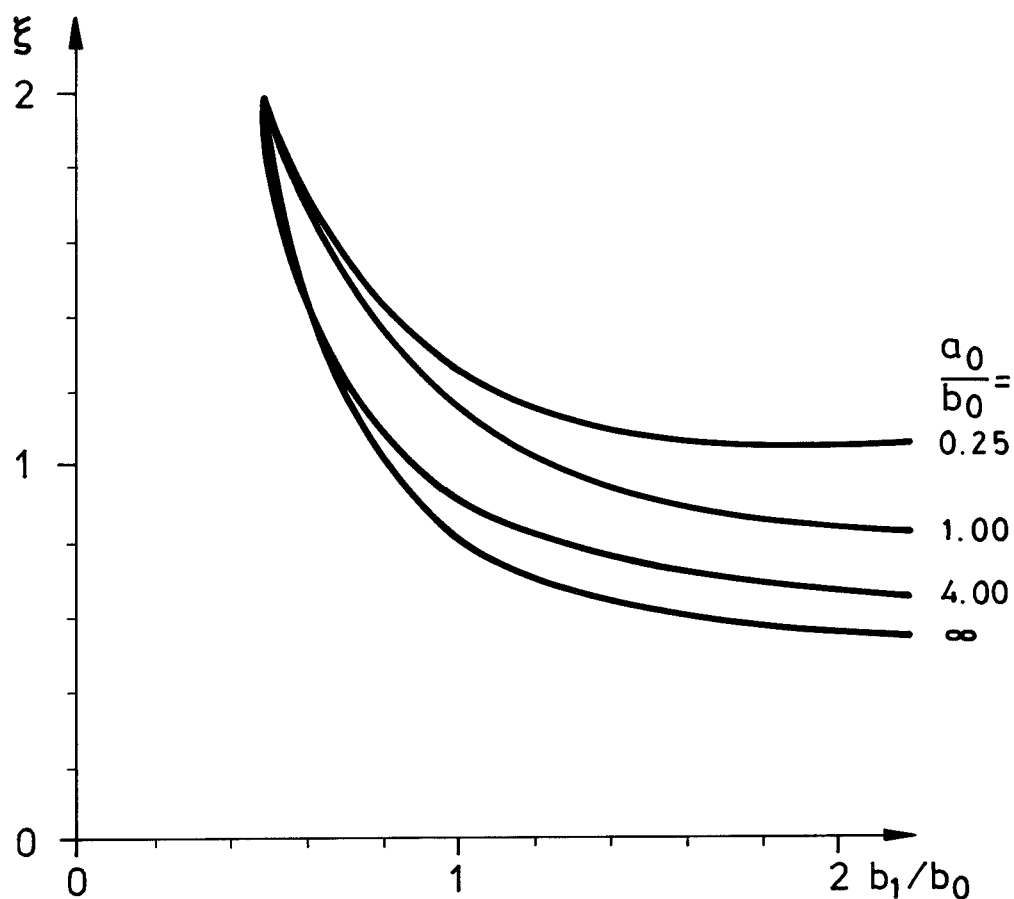


FIG. 2.3.2.4.1. Loss factor ξ to be used in eq. 2.3.2.4.h for different aspect ratios, a_0/b_0 , and degree of area change, b_1/b_0 . After Idelchik (1960).

Two or more bends after each other in the flow direction can also be treated. According to Idelchik (1960) the total loss factor will be close to the sum of the loss factors for each bend, provided that the relative distance, l/b_0 , between the bends is long enough - approximately 4 or more. For shorter distances the total resistance will be somewhat less than the sum of the individual bend losses. No numerical values for this reduction are given in the literature, however.

In addition to these pressure loss factors there are others for more specific flow cases such as tees and crosses. To find such loss factors, see for example Idelchik (1960).

2.3.3 Flow through holes and slots

From an engineering point of view much attention has been paid to fluid flow through holes (orifice flow) and slots. It is obvious from Bernoulli's Law that if a fluid flows through an opening, having the bulk mean velocity u_m , from a vessel with static pressure p_1 to another with static pressure p_2 , then

$$p_1 = p_2 + \frac{\rho u_m^2}{2} \quad \text{and}$$

$$\Delta p = \frac{\rho u_m^2}{2} \quad \text{or} \quad u_m = \sqrt{\frac{2 \cdot \Delta p}{\rho}} \quad (2.3.3.a)$$

In practice, however, the flow rate is reduced due to flow contraction so:

$$u_m = C_d \sqrt{\frac{2 \cdot \Delta p}{\rho}} \quad (2.3.3.b)$$

where, as already Kirchoff found in the middle of the 19th century

$$C_d = \frac{\pi}{\pi + 2} \cong 0.611 \quad (2.3.3.c)$$

If the wall is thin and the edges of the opening are sharp an energy-loss factor of around 0.97 should be applied too. The coefficient of discharge, C_d , can be denoted C_d^* if energy losses are included and

$$C_d^* = 0.97 \cdot C_d \cong 0.593 \quad (2.3.3.d)$$

These C_d and C_d^* are valid for both sharp edged holes and slots in a thin wall. Reorganizing eq. (2.3.3.b) yields the familiar form of:

$$\Delta p = \frac{1}{C_d^{*2}} \cdot \frac{\rho u_m^2}{2} \quad (2.3.3.e)$$

where $1/C_d^{*2}$ could be interpreted as a pressure loss factor, ξ_{opening} with the numerical value

$$\xi_{\text{opening}} = \frac{1}{0.599^2} = 2.85 \quad (2.3.3.f)$$

For walls that are not thin, flow length = 1, pressure loss factors for circular cross section are given for $Re \geq 10\,000$ by Idelchik (1960) from which figure 2.3.3.a is taken. The friction loss factor $\lambda \cdot \frac{1}{d_H}$ should be added as usual.

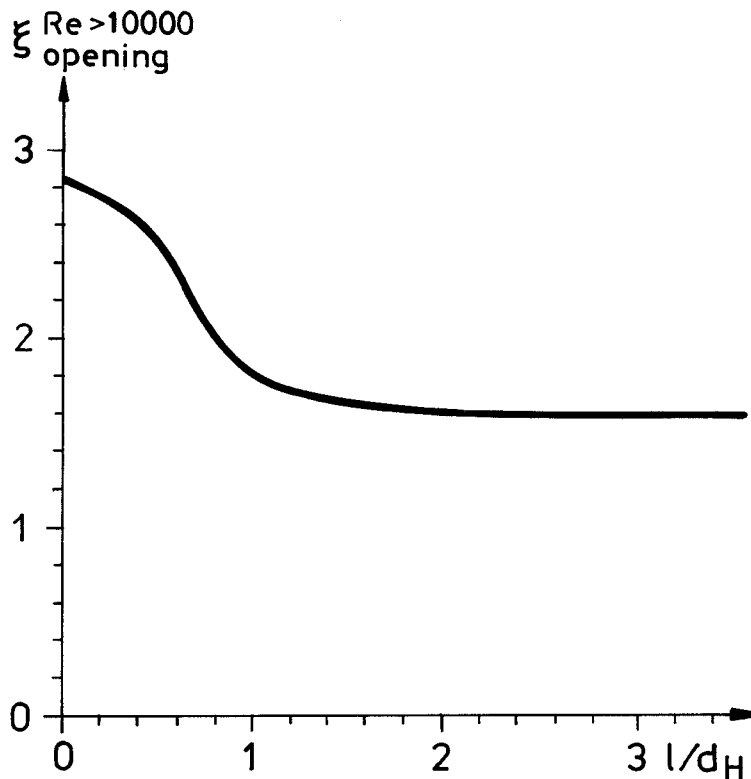


FIG. 2.3.3.a. Pressure loss factors for flow through a circular hole, flow length = 1, in a large wall. $Re \geq 10\,000$. After Idelchik (1960).

For $Re < 10\,000$ Idelchik states:

$$\xi_{\text{opening}}^{Re < 10\,000} = \xi_0(Re) + 0.342 e_0(Re) \cdot \xi_{\text{opening}}^{Re > 10\,000} \quad (2.3.3.g)$$

and gives the following diagram for determining ξ_0 and e_0 .

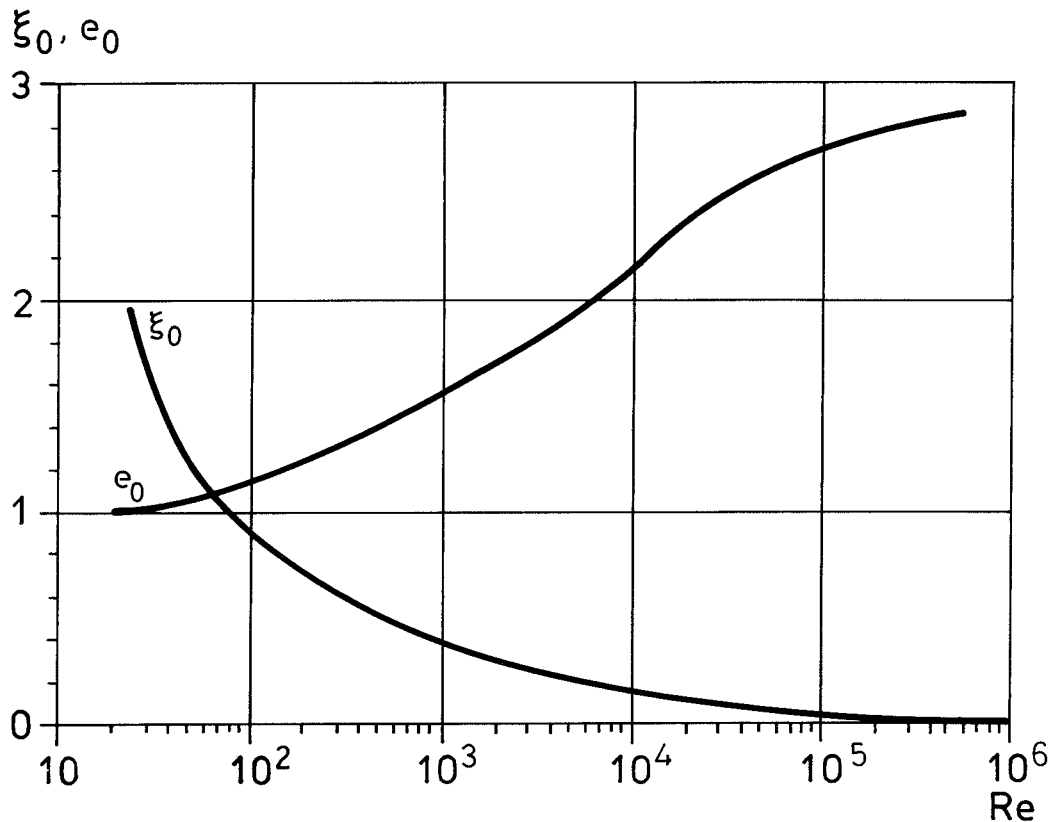


FIG. 2.3.3.b. Factors $\xi_0(Re)$ and $e_0(Re)$ for flow through a circular hole, in a large wall. $Re < 10\,000$. After Idelchik (1960).

For flow through a circular hole, with radius = r , in a thin wall at very low Reynolds number, so-called creeping flow, figure 2.3.3.c, (experimentally found to be < 6.4 if the diameter is the characteristic length), Sampson (1891) gives the analytically found expression

$$\Delta p = \frac{3 q_v \cdot \eta}{r^3} = \frac{12 \pi}{Re} \cdot \frac{\rho u_m^2}{2} \quad (2.3.3.h)$$

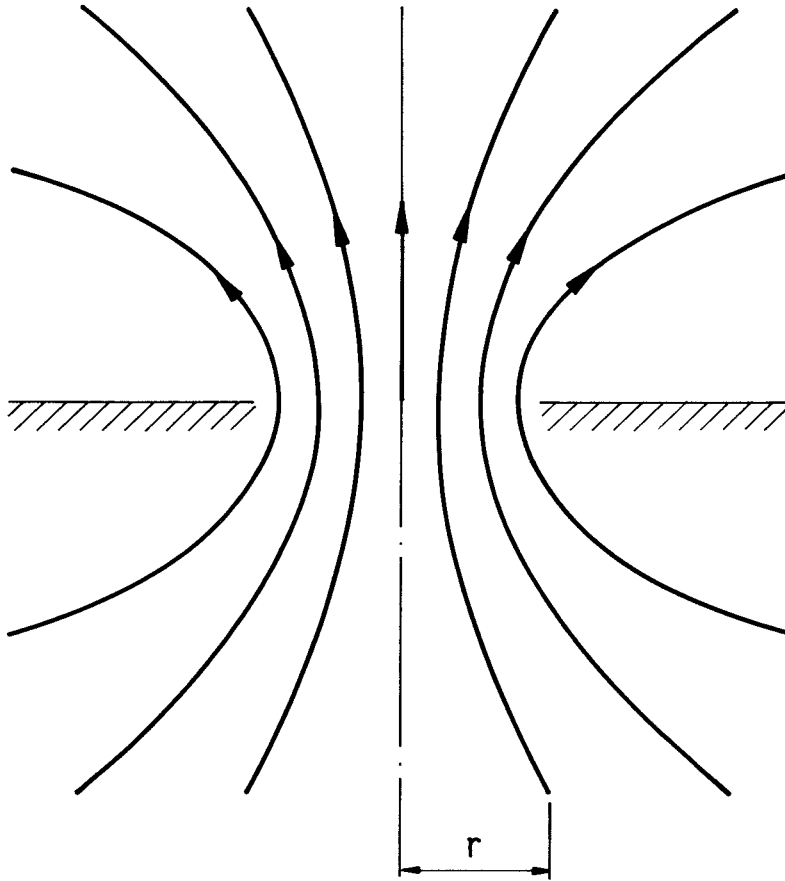


FIG. 2.3.3.c. Flow through a circular hole. Creeping flow.
After Happel & Brenner (1965)

3. EXPERIMENTAL INVESTIGATIONS

3.1 SURFACE ROUGHNESS

As was pointed out in part 2.3.2.3 the property of surface roughness is of significant importance in turbulent flow and it also determines the conditions of transition in many flow cases. Figure 3.1.a illustrates how the friction factor, λ , depends on the relative roughness, ϵ/d_H , for different Re numbers. It can be noted that the values of λ rise very rapidly as ϵ/d_H passes say 0.001.

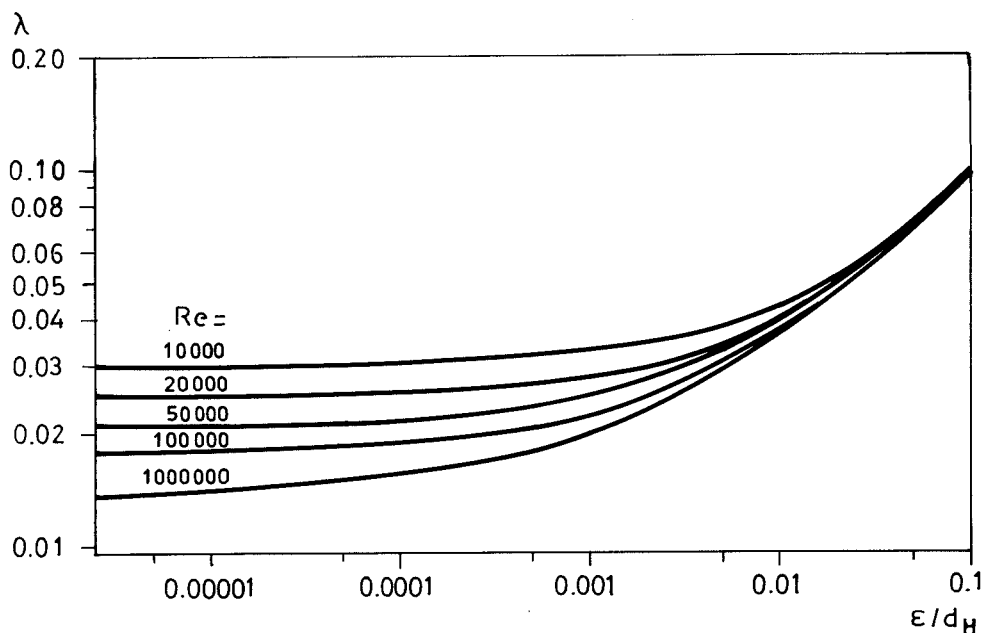


FIG. 3.1.a. Friction factor, λ , versus relative roughness, ϵ/d_H , for different Re numbers.

Most numerical values of the surface roughness factor given in the literature refer of course to wall materials, common for pipes for different purposes - in most cases transportation of liquids. Thus the literature gives numerous ϵ -values for iron and steel pipes, with and without rust, concrete pipes, new and used, etc. but surface roughness factors for ordinary building materials are almost completely lacking.

For this reason a measurement equipment for determining ϵ -values for different building materials was built up at the division of Building Technology at Lund Institute of Technology.

3.1.1 Laboratory test equipment

The test equipment was designed to make it possible to determine surface roughness factors for flat test specimens instead of pipes which normally has been the case.

To make this possible an air flow was led through a gap between walls of the material to be tested. The resulting pressure drop per unit length, as well as the average velocity, was measured at a number of locations of the plates. For every location ϵ was determined by use of the Colebrook & White equation (eq. 2.3.2.2.h).

The test equipment is shown in figure 3.1.1.a and 3.1.1.b.

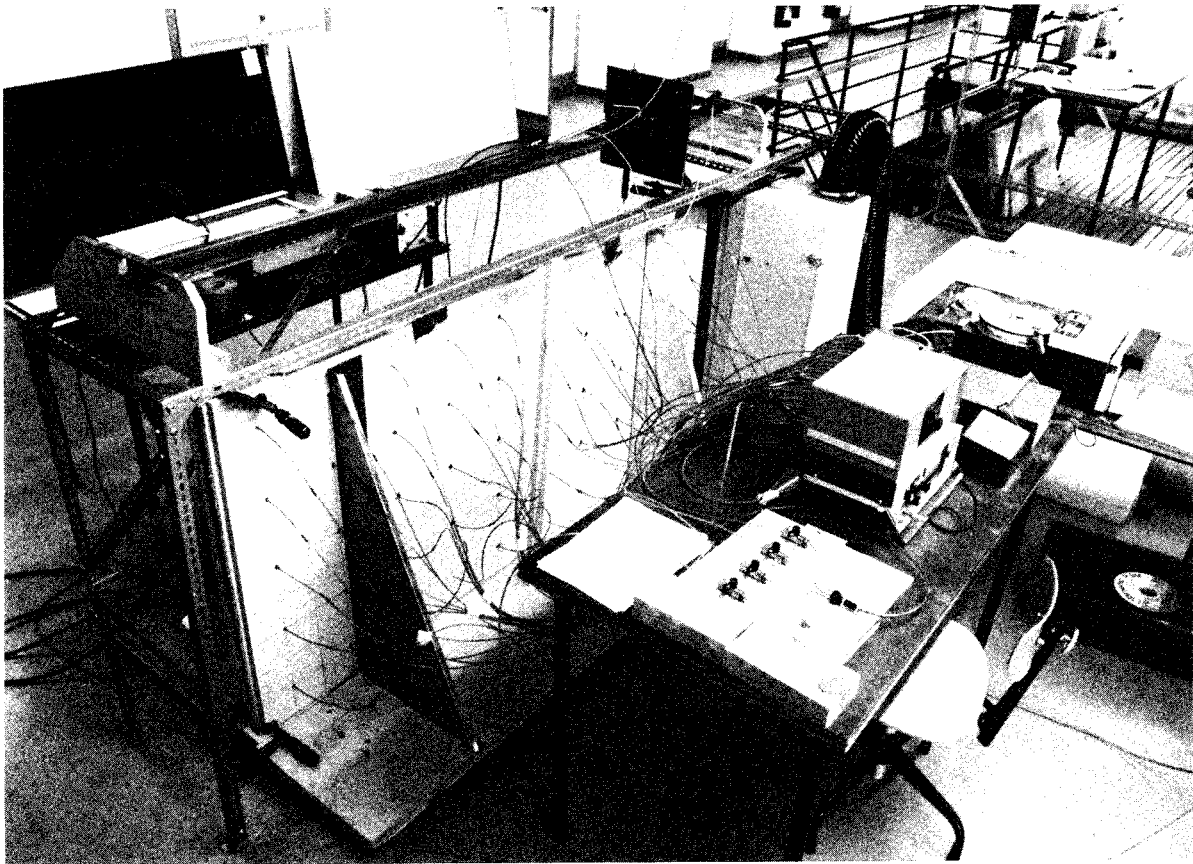


FIG. 3.1.1.a. The test equipment.

The air flow in the gap between the plates was produced by means of a centrifugal blower, (Bahco NAB), with a capacity of $0.35 \text{ m}^3/\text{s}$ in free blowing mode. Between the blower and the plates was placed a "pressure box" whose function was to produce an even suction in the exit section of the gap.

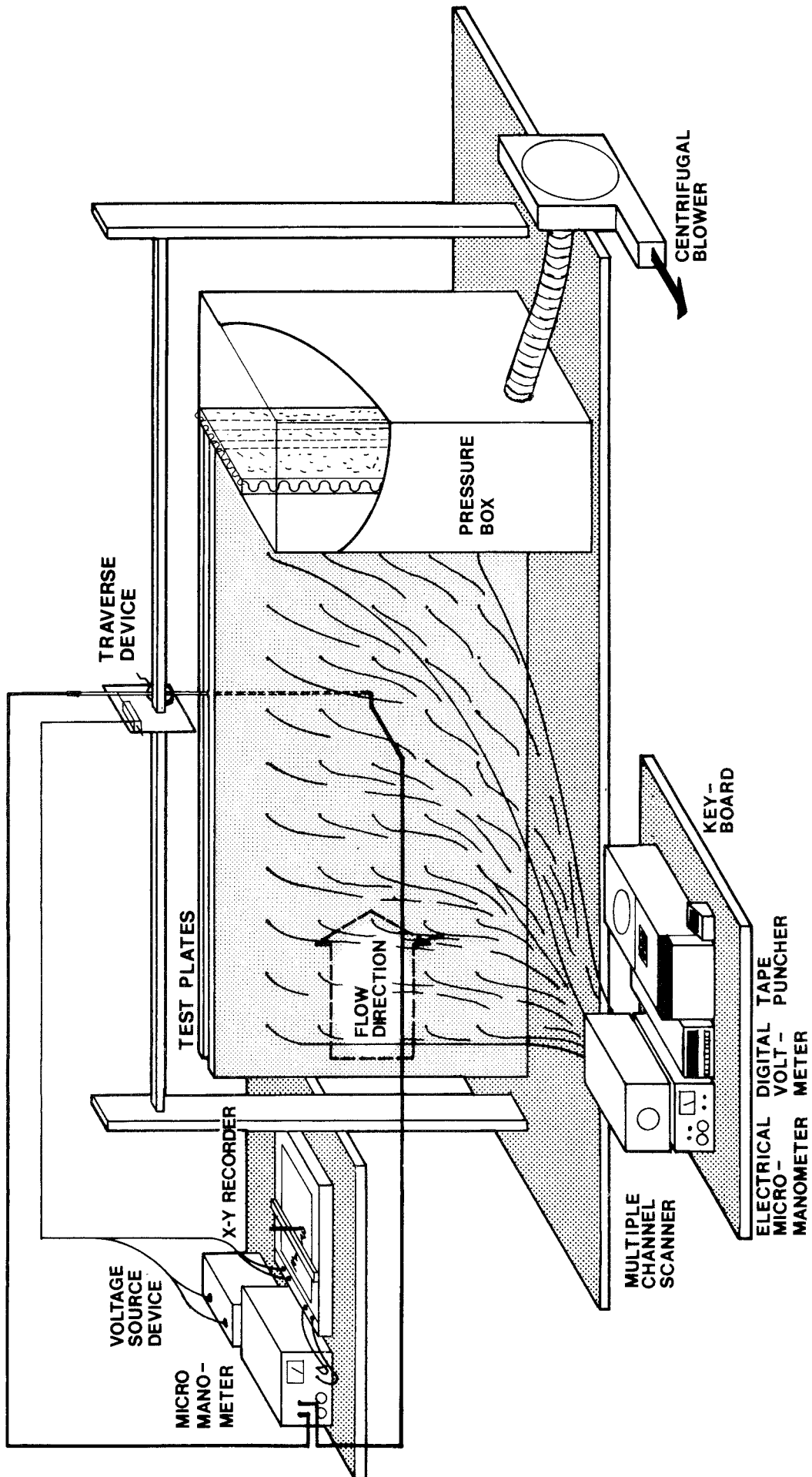


FIG. 3.1.1.b. The test equipment. Type sketch.

The area of the test specimens was 2.0 x 1.0 m. The nominal gap width was 50 mm. In one of the two plates of each material tested, 50 holes for sensing the local static pressure (ϕ 4 mm) were drilled through the plate. The holes were placed at equal distances (0.20 m) in both directions. The connections between the plates and the sill, and between the plates and the pressure box, as well as between the plates at the top of the plates, were sealed with a heavy duty tape, (tesa 5210, Beiersdorf). A plastic tube was connected to each hole and all the 50 tubes were connected to a multiple channel scanner (Scannivalve). The pressure difference between the atmosphere pressure and the pressure at the end of the connected tube sensing the local static pressure at the orifice of a hole in the wall was read on an electrical micromanometer (Furness Controls Ltd.) with different scales (0 - 10, 0 - 30 and 0 - 100 Pa).

The readings were transformed to punchings of the measurement values on paper tape by means of a digital volt-meter, a key-board and a tape puncher, (FACIT).

The local average velocities were calculated from readings of the velocity profiles. They were measured with a simple pitot tube connected to a traverse device making it possible to move the tube end from the surface of one plate to the other. As the other end of the pitot tube was connected to a high precision slide potential divider, it was also possible to read the distance between the plates in the measurement point. (Some simple calculations of uniformity had to be done too, of course). The traverse device is shown in detail in figure 3.1.1.c.

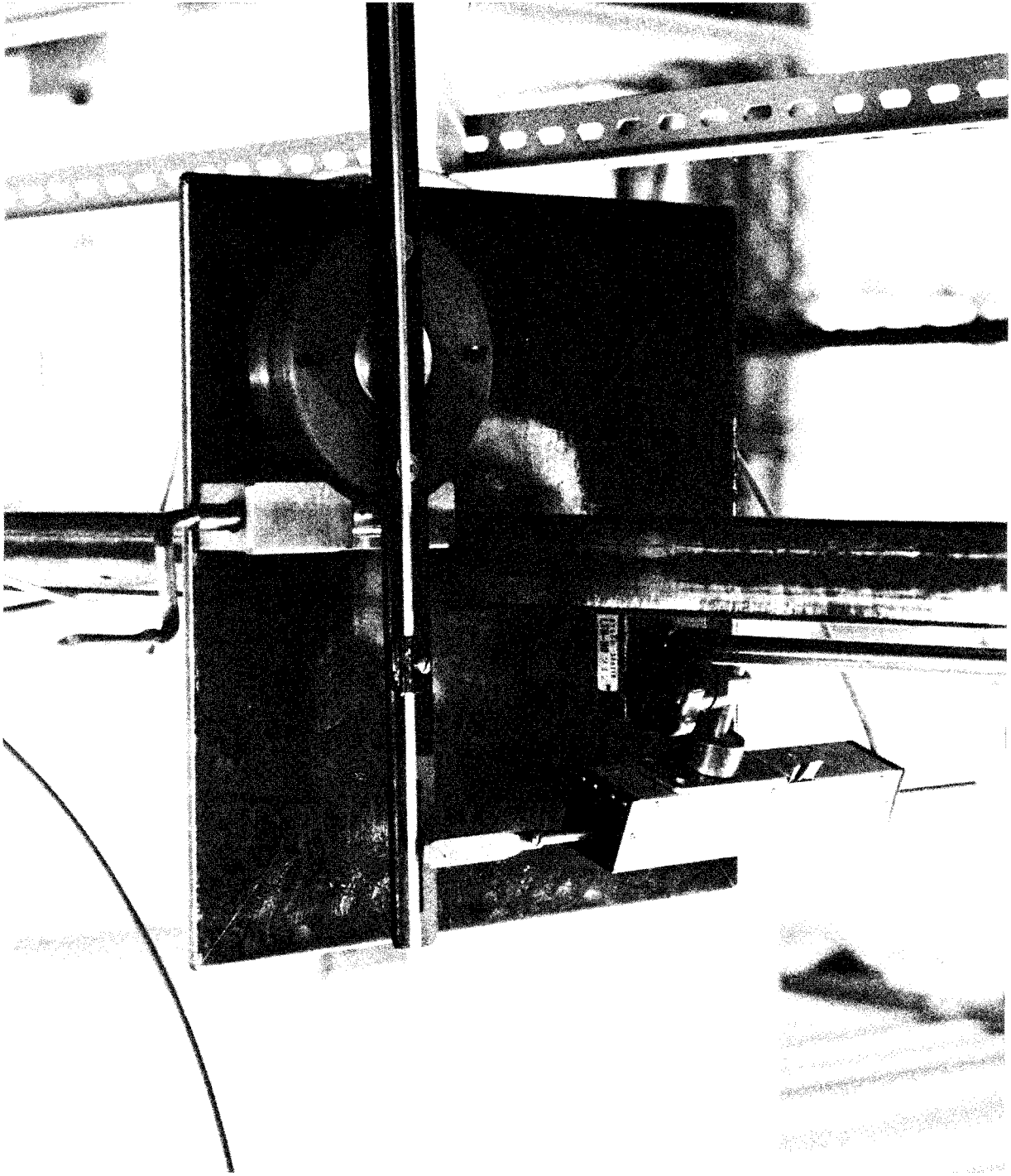


FIG. 3.1.1.c. The pitot tube traverse device.

The difference between the total pressure at the end of the pitot tube and the local static pressure measured at the wall - i.e. the dynamic pressure - was monitored with an electrical micromanometer similar to that described earlier. The distancemeter (slide potential divider) was supplied with a constant voltage from a voltage source device, and it produced a signal analogue to the location of the pitot tube end. The signals from the slide potential divider and electrical micromanometer

were eventually recorded by a x-y-recorder which produced a plot from which the velocity profile in the measurement location was calculated.

To sum up it can be stated that the measurement procedure produces measurement data concerning:

- o drop in static pressure per unit length in the flow direction
- o distance between the plates
- o velocity distribution between the plates

3.1.2 Data processing and analysis

The Colebrook-White equation states that in the complete turbulent zone (loc.cit.eq. 2.3.2.2.h):

$$\frac{1}{\sqrt{\lambda}} = -2 \log \left(\frac{\epsilon/d}{3.71} \right) \quad (3.1.2.a)$$

and the general friction formula, (loc. cit. eq. 2.3.1.b):

$$\frac{\Delta p}{l} = \frac{\lambda}{d_H} \frac{\rho u_m^2}{2} \quad (3.1.2.b)$$

Since the hydraulic diameter is approximately 2 b, where b is the duct width, ϵ could be written:

$$\epsilon = \frac{7.42 b}{e^{0.576} u_m \sqrt{\frac{\rho}{b \cdot \Delta p/l}}} \quad (3.1.2.c)$$

The temperature in the laboratory, in which the tests were performed, was approximately 20 °C during tests so the value of $\rho = 1.20 \text{ kg/m}^3$ was consequently used.

Hence, the calculation of ϵ involves determination of $\Delta p/l$, b and u_m . Cf. the concluding points of 3.1.1.

Determination of $\Delta p/l$

Static pressure wall taps were used to sense the static pressure at the wall of the plate. It is generally assumed that small square-edged holes installed normal to flow boundaries give the correct static pressure (Benedict (1977)). In practice, however, small perfectly square-edged holes are difficult to machine. Hence, it might be interesting to know the influence of imperfections in this respect. Rayle (1959) has investigated effects of orifice edge forms on static pressure measurements. Figure 3.1.2.a.

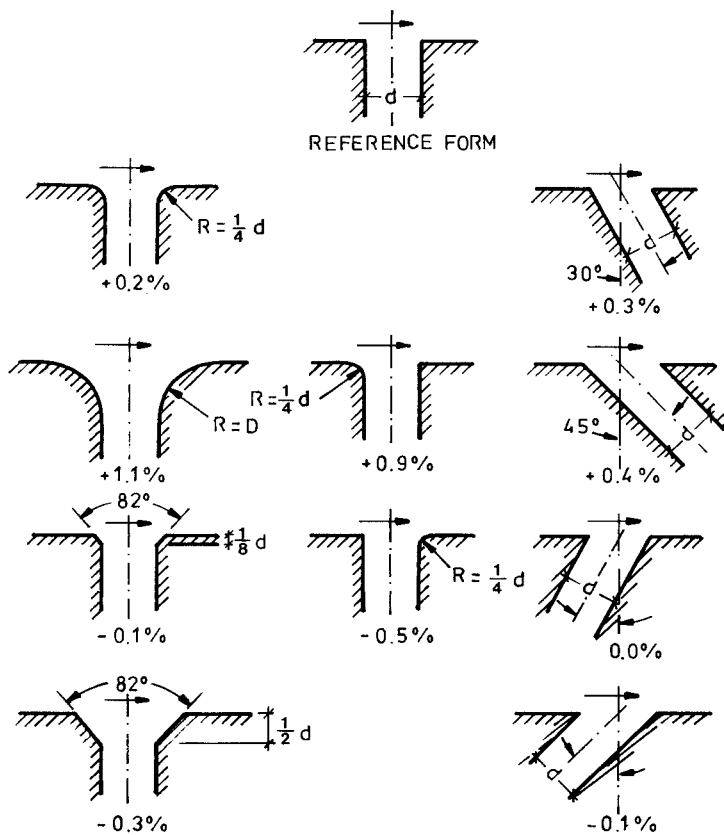


FIG. 3.1.2.a. Effect of orifice edge form on static pressure measurement. Variation in percentage of dynamic pressure. After Rayle (1959).

As can be seen in the figure the edge form does not at all play such an important part as one may believe, so even though some of the holes drilled in the test specimens have non-perfect sharp edges, only a minor error is introduced thereby.

The readings of the static pressures relative atmosphere pressure was punched on paper tape. The processing of these data included print out of the pressure readings, the pressure differences, and a simple isobar plot performed by the ordinary line-printer.

Determination of b

The distance between the plates was determined at each measurement point. The end of the pitot tube (the sensing part) was moved slowly from close to one wall to the other by means of the slow revolving of the circular plate of the traverse device arising from the rotating of the crank and its shaft. As the horizontal movement x of the pitot tube at a distance m from the centre of the circular plate - the reading of the slide potential divider - and the length of the tube from centre to end, n , are known the horizontal distance between the plates can be simply determined. Hence, due to conformity (Figure 3.1.2.b)

$$b = x \cdot \frac{n}{m} \quad (3.1.2.d)$$

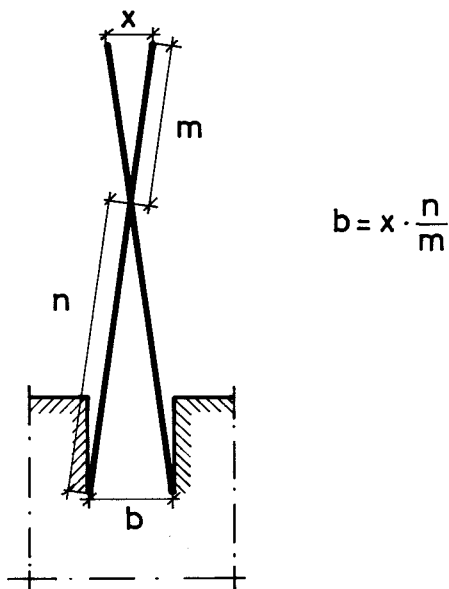


FIG. 3.1.2.b. Determination of duct width from known data of x , n , and m .

Since the radius of the pitot tube used was 2 mm, the value of b measured in this way should be increased by 2×2 mm to give the proper distance. This has been done in the experiments.

Determination of u_m

The velocity distribution between the plates was recorded on the x-y-recorder, figure 3.1.2.g. Then a smooth profile was drawn to fit the measured profile well. This was done by means of visual inspection of one half of the duct width at a time. For every 5 mm, then, the velocity was read (on the smooth line) and the points read were fitted to an analytical expression of the type $y = ax^b$ using least square curve fit. Having done that the average velocity, u_m , for each half was easily calculated as

$$u_m = \frac{1}{b/2} \int_0^{b/2} u(x) dx = \frac{2}{b} \int_0^{b/2} ax^b dx = \frac{2a}{b(b+1)} \left[x^{b+1} \right]_0^{b/2} \quad (3.1.2.e)$$

In cases of velocity distributions non-symmetrical around half the distance the upper integral limit differs from $b/2$ and instead the actual distance between the wall and the symmetry line was inserted.

The proceeding calculation of ϵ is performed for one half of the distance each and the resulting value is taken to be the mean of these two values.

Error analysis

It might be interesting to examine the resulting probable error in the determination of ϵ in a point.

The statistical concept for doing this is formulated in the general rule for error propagation which - with signs applicable to this problem - states; (See for example Beers (1962) or Cramér (1945)):

$$\begin{aligned}
s_{\epsilon} = & \sqrt{\left(\frac{\partial \epsilon}{\partial b}\right)^2 \cdot s_b^2 + \left(\frac{\partial \epsilon}{\partial u_m}\right)^2 \cdot s_{u_m}^2 + \left(\frac{\partial \epsilon}{\partial \left(\frac{\Delta p}{T}\right)}\right)^2 \cdot s_{\Delta p/T}^2 +} \\
& \frac{+ 2\rho_{b u_m} \left(\frac{\partial \epsilon}{\partial b}\right) \left(\frac{\partial \epsilon}{\partial u_m}\right) \cdot s_b \cdot s_{u_m} +}{+ 2\rho_{\frac{\Delta p}{T} b} \left(\frac{\partial \epsilon}{\partial \left(\frac{\Delta p}{T}\right)}\right) \left(\frac{\partial \epsilon}{\partial b}\right) \cdot s_{\frac{\Delta p}{T}} \cdot s_b +} \\
& \frac{+ 2\rho_{\frac{\Delta p}{T} u_m} \left(\frac{\partial \epsilon}{\partial \left(\frac{\Delta p}{T}\right)}\right) \left(\frac{\partial \epsilon}{\partial u_m}\right) \cdot s_{\frac{\Delta p}{T}} \cdot s_{u_m}}{\quad} \quad (3.1.2.f)
\end{aligned}$$

where s stands for standard deviation. The first three terms under the root sign are always applicable. The remaining terms are to be taken into account if some of the parameters b , u_m or $\Delta p/T$ are statistically dependent on each other. If so, ρ is the correlation coefficient for the two parameters.

If the parameters are statistically non-dependent on each other the analysis is limited to the first three terms.

$$\epsilon = 7.42 \cdot b \cdot e^{-0.576 \cdot u_m} \cdot \frac{\Delta p}{T}^{-\frac{1}{2}} \cdot \rho^{\frac{1}{2}} \cdot b^{-\frac{1}{2}} \quad (3.1.2.g)$$

$$\begin{aligned}
\frac{\partial \epsilon}{\partial b} = & 7.42 \left(e^{-0.576 \cdot u_m} \cdot \frac{\Delta p}{T}^{-\frac{1}{2}} \cdot \rho^{\frac{1}{2}} \cdot b^{-\frac{1}{2}} + \right. \\
& \left. + b \cdot e^{-0.576 \cdot u_m} \cdot \frac{\Delta p}{T}^{-\frac{1}{2}} \cdot \rho^{\frac{1}{2}} \cdot b^{-\frac{1}{2}} \cdot 0.576 \cdot \frac{\Delta p}{T}^{-\frac{1}{2}} \cdot \rho^{\frac{1}{2}} \cdot \frac{1}{2} \cdot b^{-\frac{3}{2}} \right) \quad (3.1.2.h)
\end{aligned}$$

$$\frac{\partial \epsilon}{\partial u_m} = \epsilon \left(-0.576 \cdot \frac{\Delta p}{T}^{-\frac{1}{2}} \cdot \rho^{\frac{1}{2}} \cdot b^{-\frac{1}{2}} \right) \quad (3.1.2.i)$$

$$\frac{\partial \epsilon}{\partial \left(\frac{\Delta p}{T}\right)} = \epsilon \left(0.576 \cdot u_m \cdot \frac{\Delta p}{T}^{-\frac{1}{2}} \cdot \rho^{\frac{1}{2}} \cdot b^{-\frac{1}{2}} \cdot \frac{1}{2} \cdot \left(\frac{\Delta p}{T}\right)^{-\frac{3}{2}} \right) \quad (3.1.2.k)$$

For realistic values of b , u_m , $\Delta p/l$, and ρ ($=0.05$ m, 4 m/s, 8 Pa/m, 1.20 kg/m³)

$$\frac{\partial \varepsilon}{\partial b} = 0.197$$

$$\frac{\partial \varepsilon}{\partial u_m} = -9.27 \cdot 10^{-3}$$

$$\frac{\partial \varepsilon}{\partial (\frac{\Delta p}{l})} = 5.30 \cdot 10^{-4}$$

and

$$s_\varepsilon = \sqrt{38.8 \cdot 10^{-3} \cdot s_b^2 + 85.9 \cdot 10^{-6} \cdot s_{u_m}^2 + 0.281 \cdot 10^{-6} \cdot s_{\frac{\Delta p}{l}}^2}$$

Typical values from the measurement which were carried out are:

$$\begin{aligned} s_b &= 0.001 \text{ m} \\ s_{u_m} &= 0.08 \text{ m/s} \\ s_{\frac{\Delta p}{l}} &= 0.3 \text{ Pa/m} \end{aligned}$$

This leads to an estimated value of s_ε equal to:

$$s_\varepsilon = 0.78 \cdot 10^{-3} \text{ m}$$

The total probable error is less than that if determinations are repeated. If n measurements are undertaken the resulting probable error, $s_{\varepsilon, \text{res}}$ will be

$$s_{\varepsilon, \text{res}} = \frac{s_\varepsilon}{\sqrt{n}} \quad (3.1.2.1)$$

If, for example, $n = 10$ then $s_{\varepsilon, \text{res}}$, according to the typical values given above, will be $0.78 \cdot 10^{-3} / \sqrt{10} = 0.25 \cdot 10^{-3}$ m.

If the statistical distribution of ϵ is Gaussian a confidence interval, I , corresponding to

$$P(\epsilon_{res} \in I) = 1 - \alpha \equiv \phi(\lambda_\alpha) \quad (3.1.2.m)$$

where

ϵ_{res} is the mean of all measured ϵ -values

$$I = \epsilon_{res} \pm \lambda_{\alpha/2} \cdot s_{\epsilon, res} \quad (3.1.2.n)$$

If a confidence degree of 90% is wished the value of $\lambda_{\alpha/2} \equiv \lambda_{0.05}$ is 1.64.

Criteria for accepting or alternatively rejecting data

Measurement values from a single point were accepted for further analysis only if both the following criteria were met:

- o the exponent, b , in the expression for the velocity profile, $u(y) = a \cdot y^b$ was within a range of 0.14 ± 0.035 (i.e. $\pm 25\%$)
- o the isobars in the vicinity of the point should be approximately vertical

The first criterion should give a certain assurance of the velocity profile to be developed. The figure 0.14 corresponds to one seventh, a value given by, among others, Prandtl (1927) in the so-called "Potenz-gesetz" for a simplified description of the nature of the velocity profile at fully developed turbulent flow.

The other criterion should ensure the flow direction to be (locally) horizontal.

3.1.3 Measurement results

The measurement results are summarized in table 3.1.3.a.

TABLE 3.1.3.a Surface roughness $\epsilon(m)$.

WALL MATERIAL	SURFACE ROUGHNESS $\times 10^3$, μ 90% CONFIDENCE INTERVAL
Concrete	
poured on boarding (tongued and grooved)	1.0 - 1.8
poured on plywood	1.3 - 2.1
poured on steel plate	0.5 - 1.3
screeded surface	3.2 - 5.9
Asphalt impregnated porous	
wood fibre board plate	1.8 - 3.4
Chipboard	0.2 - 0.6
Glass fibre board	2.8 - 4.5
Gypsum board	0.2 - 0.7

3.2 DUCT FLOW

Equations for air flow in ducts with walls parallel to each other are used throughout this work. In addition to friction losses the effects of losses due to entrance flow, exit flow and directional changes are sometimes substantial. In order to check the pressure drop along different well defined flow paths some experiments were carried out at the division of Building Technology, Lund Institute of Technology. Similar experiments have been reported earlier by Esdorn & Rheinländer (1978), Etheridge (1977) and Honma (1975) for example, but they all report the total pressure drop from one side to another only.

In this investigation entrance, exit, and bend losses are studied more in detail.

3.2.1 Experimental design

The experiments were made as laboratory tests. Air was led through ducts of different shapes made up of aluminum profiles from the room having atmospheric air pressure to a suction box. The inner dimensions of the box were 1 x 1 x 0,5 m and the test duct was placed in the middle of the square surface. The flow rate of the air, evacuated from the box by means of a fan was measured with a vortex flowmeter. This flow rate was corrected for the box own leakage and the corrected value represented the flow rate of the air passing through the duct. The pressure difference between the box and the room was measured with a micromanometer (Furness Controls Ltd.).

The static pressure along the flow path was sensed with pressure wall taps in the duct wall. The taps were connected with plastic tubes to a multiple channel scanner (Scannivalve). The pressure difference between atmosphere pressure and the pressure at the end of the connected tube, sensing the local static pressure at the orifice of a hole in the duct wall, was read on an electrical micromanometer of the same kind as that one mentioned above. The readings were transformed to punchings of the measurement values on paper tape by means of a digital volt-meter, a keyboard and a tape puncher, (FACIT).

Different duct widths could be created by inserting pieces of metal wire with known diameter between the aluminum profiles.

The experimental arrangement is shown in figure 3.2.1.a.

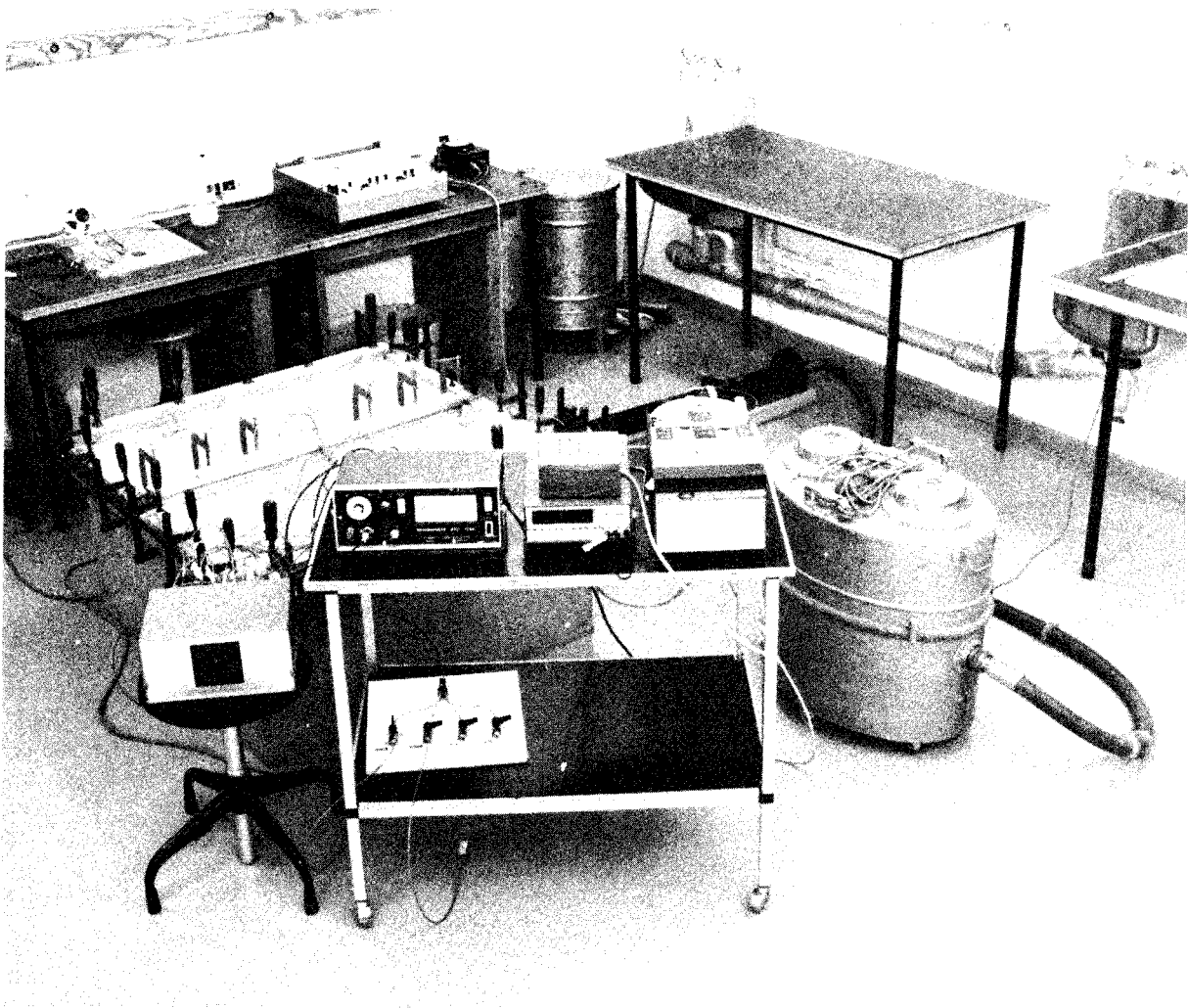


FIG. 3.2.1.a. Experimental arrangement for investigations of duct flow.

3.2.2 Data processing and analysis

For every geometrical configuration and duct width some ten readings of

o air flow rate

o pressure difference across the duct

o static pressures within the duct

were performed. The average values were then used for the further calculations.

The average velocity, u_m , in the duct was calculated in order to make it possible to relate the pressure readings to the quantity $\rho \cdot u_m^2/2$ thus making the pressure values dimensionless. Besides, the entrance, exit, and bend losses could be described in terms of loss factors once their magnitudes are identified from the measurement results.

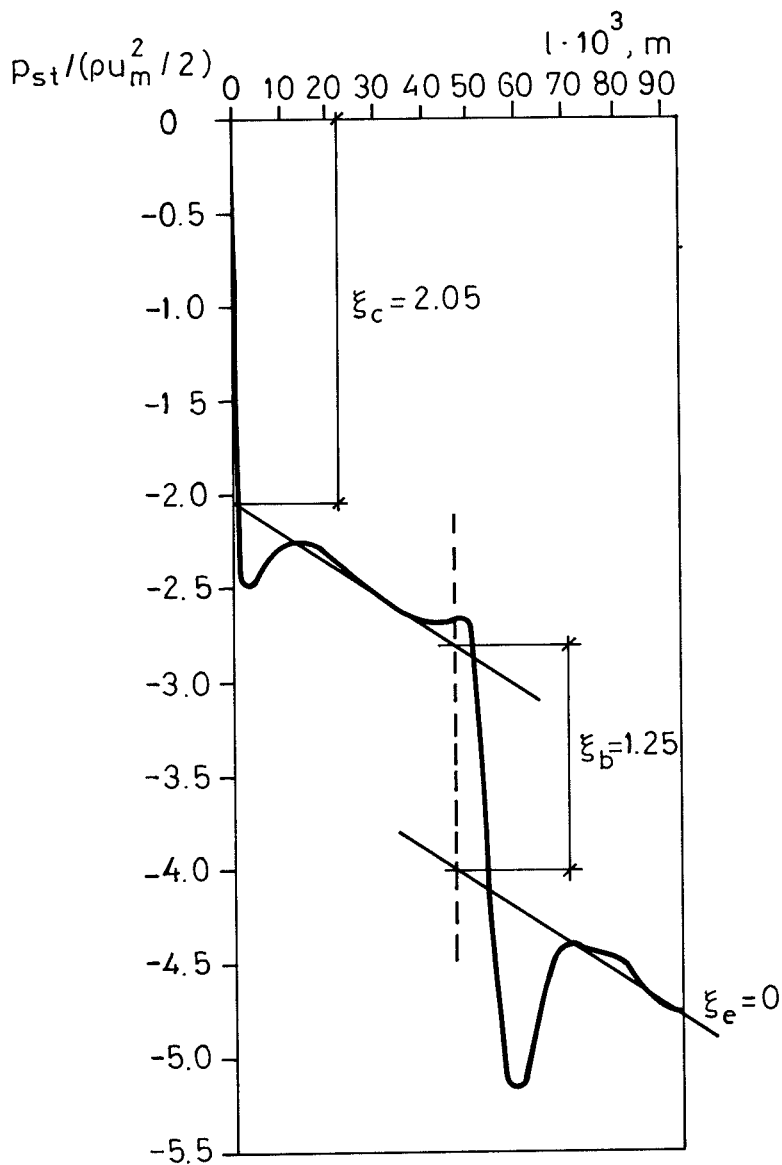


FIG. 3.2.2.a. Variation of static pressure along the flow path of a 2 mm wide duct with one 90° bend. Flow length = 94 mm and $Re = 1507$.

Figure 3.2.2.a shows a typical measurement result. It was obtained at $Re = 1507$ with a duct with one 90° bend having the width of 2.0 mm and the total length in flow direction of 94 mm. To make it possible to study the influence of the entrance and the exit the pressure drop corresponding to undisturbed flow is outlined in the figure. The general friction formula:

$$\Delta p = \lambda \cdot \frac{l}{d_H} \cdot \frac{\rho u_m^2}{2}$$

could be written

$$\frac{\Delta p}{\frac{\rho u_m^2}{2}} = \frac{\lambda}{d_H} \cdot l \quad (3.2.2.a)$$

Thus the quantity λ/d_H should equal the slope of the pressure drop line. In the case of laminar flow λ is dependent on Re only, while in the turbulent case the absolute roughness, ϵ , must be known too. ϵ for the aluminum profiles used were determined in a pilot experiment with flow through a 5 m long tube with rectangular cross-section. The value was determined to approximately 0.1 mm.

If the measurement result shown in figure 3.2.2.a is analysed in this way, two separate straight lines with the slope equal to $-\lambda/d_H$ ($= (96/1507)/(2 \cdot 0.002) = 15.9 \text{ m}^{-1}$) can be drawn, fitting the pressure loss curves before the bend and after the bend respectively. Resulting values of ξ_c and ξ_b are 2.05 and 1.25 respectively, which seem to be quite reasonable.

3.2.3 Measurement results

The different cases investigated in the experiments were analysed in a manner according to the example above. The results can be studied in detail in figure 3.2.3.a. - k.

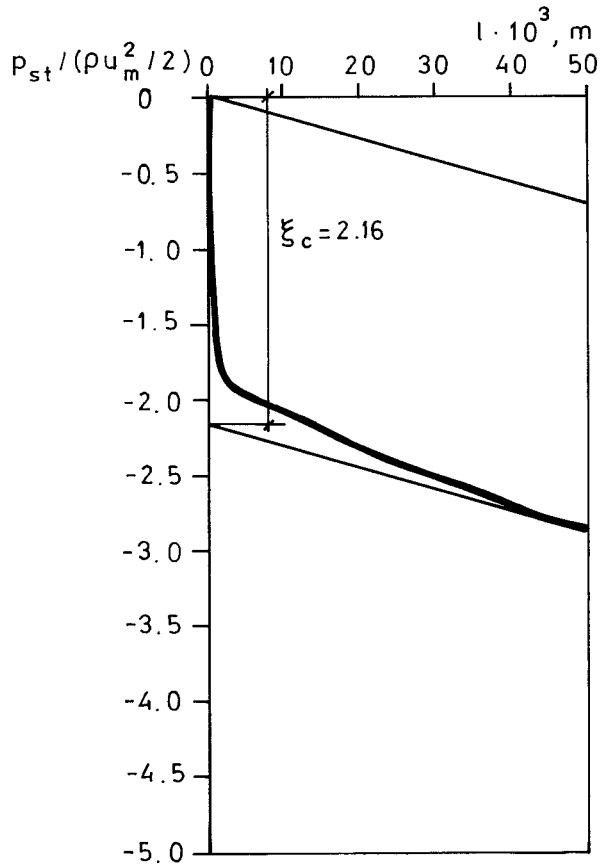


FIG. 3.2.3.a Straight duct.
width 2.0 mm, length 50 mm
Re = 1744

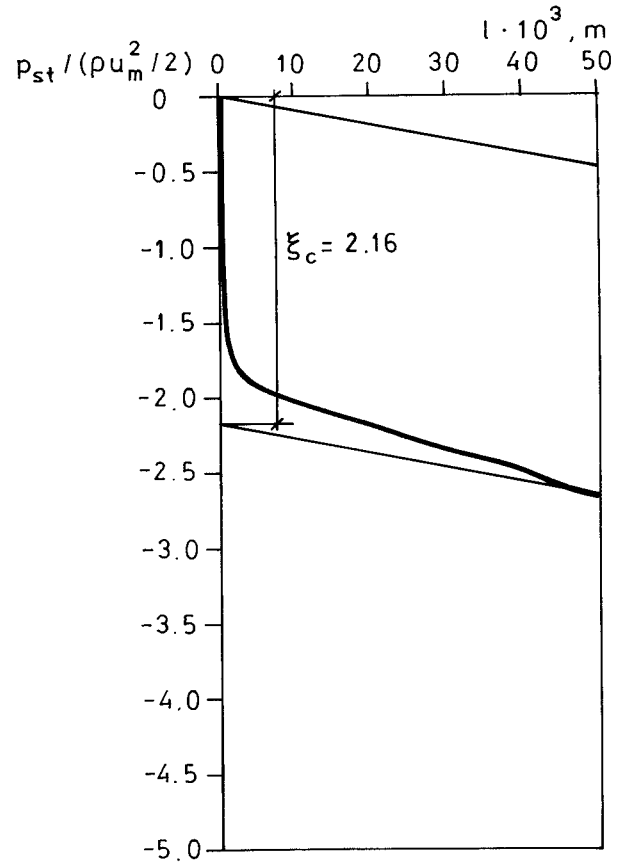


FIG. 3.2.3.b Straight duct
width 3.0 mm, length 50 mm
Re = 1717

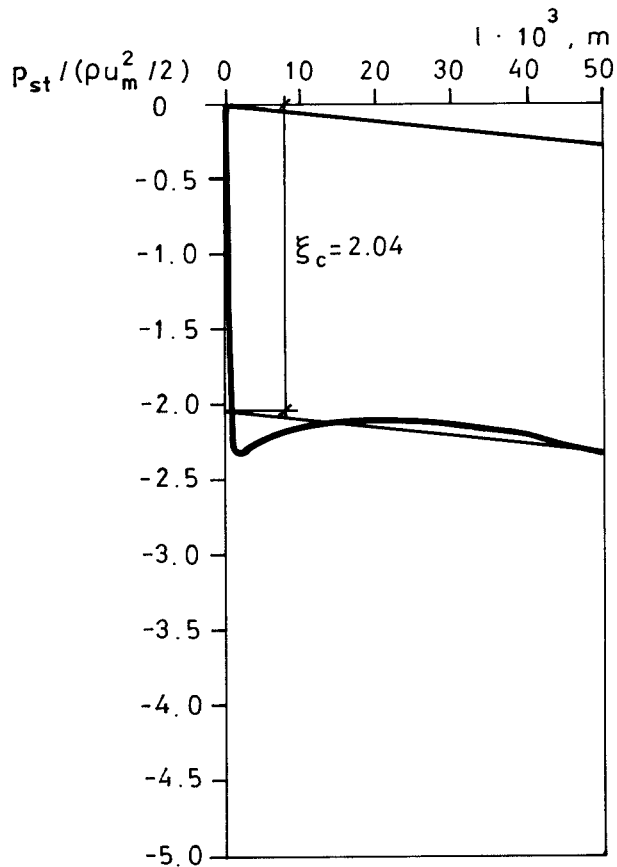


FIG. 3.2.3.c Straight duct
width 6.0 mm, length 50 mm

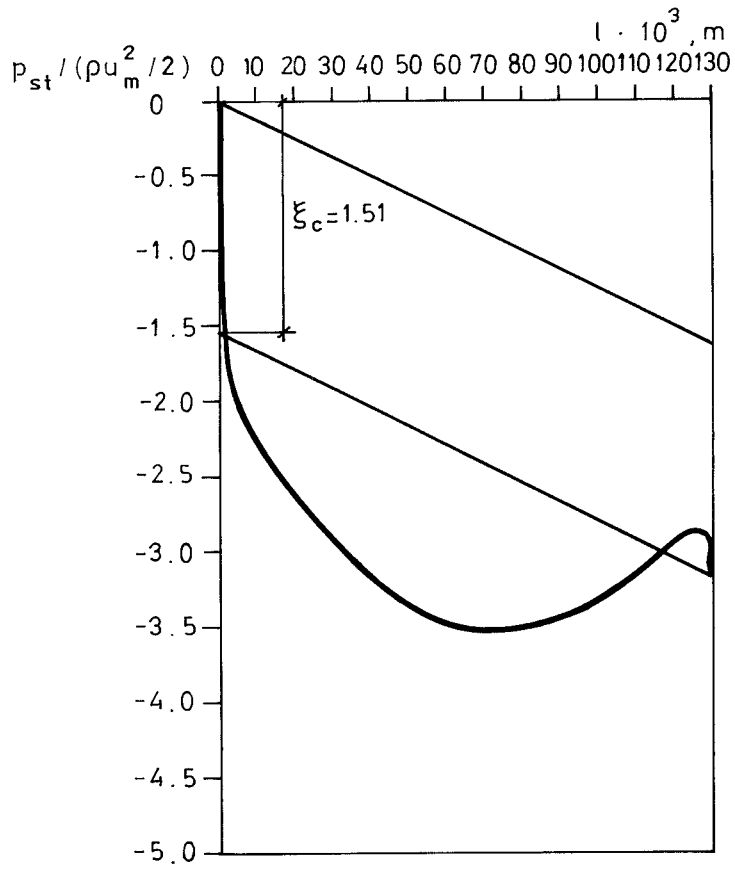


FIG. 3.2.3.d Straight duct.
width 2.0 mm, length 130 mm
Re = 1936

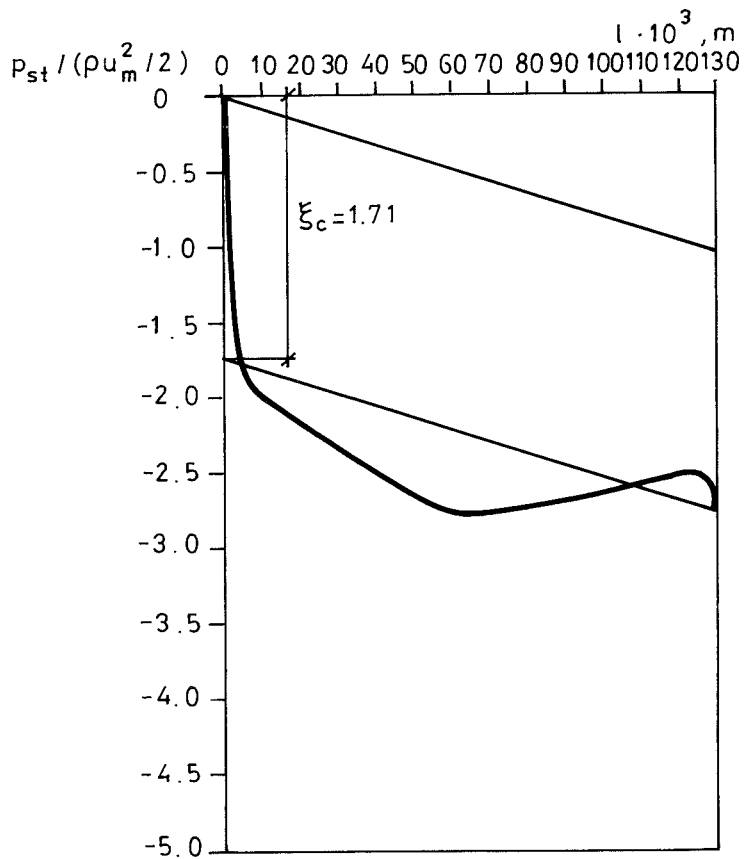


FIG. 3.2.3.e Straight duct.
width 3.0 mm, length 130 mm
Re = 1945

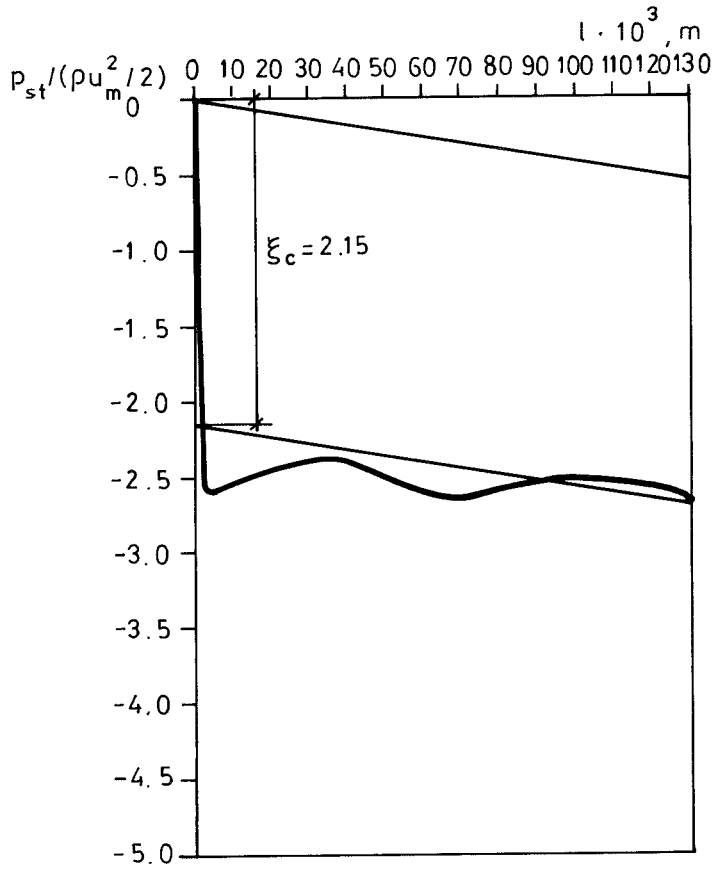


FIG. 3.2.3.f Straight duct.
width 6.0 mm, length 130 mm
Re = 1982

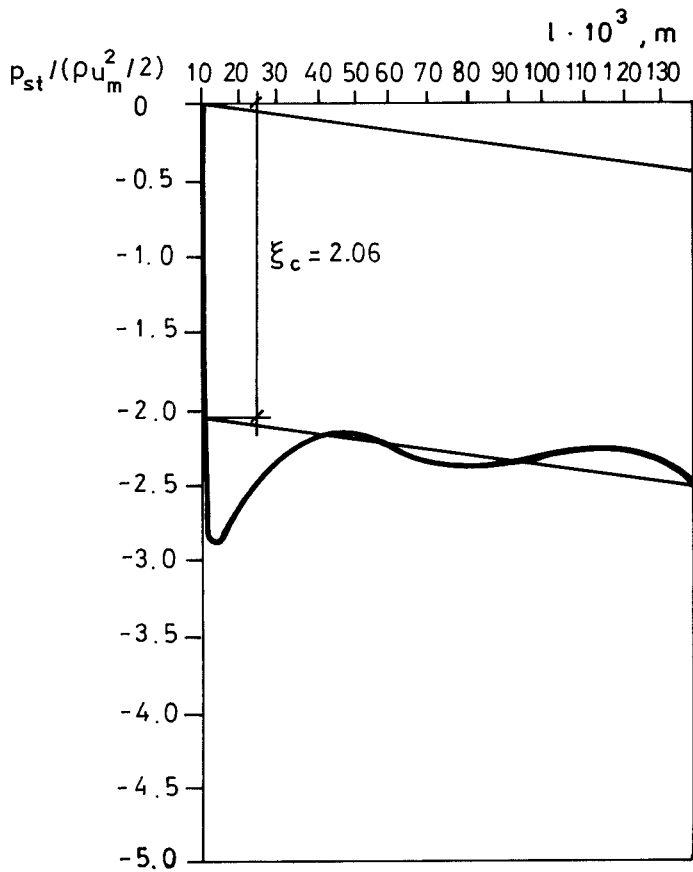


FIG. 3.2.3.g Straight duct.
width 6.0 mm, length 130 mm
Re = 4046

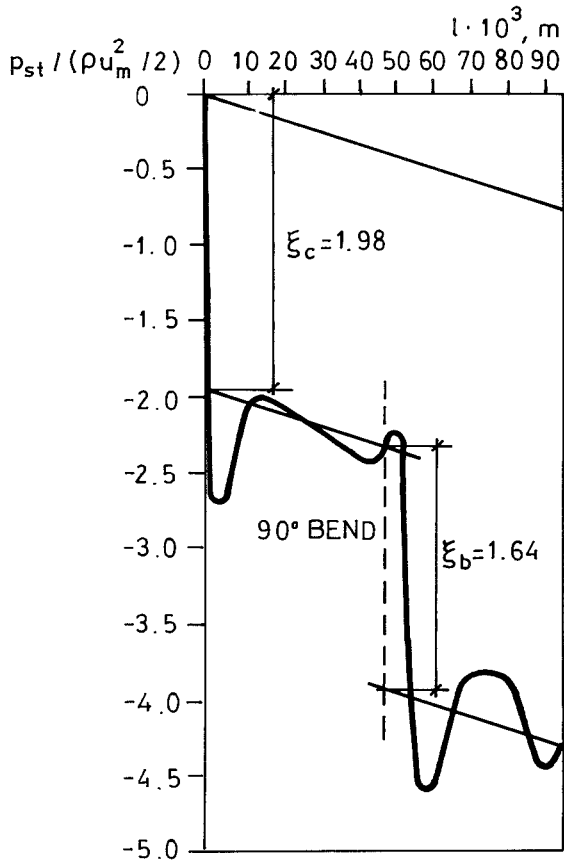


FIG. 3.2.3.h Duct with one 90° -bend. width 3.0 mm, length 94 mm, $Re = 2055$

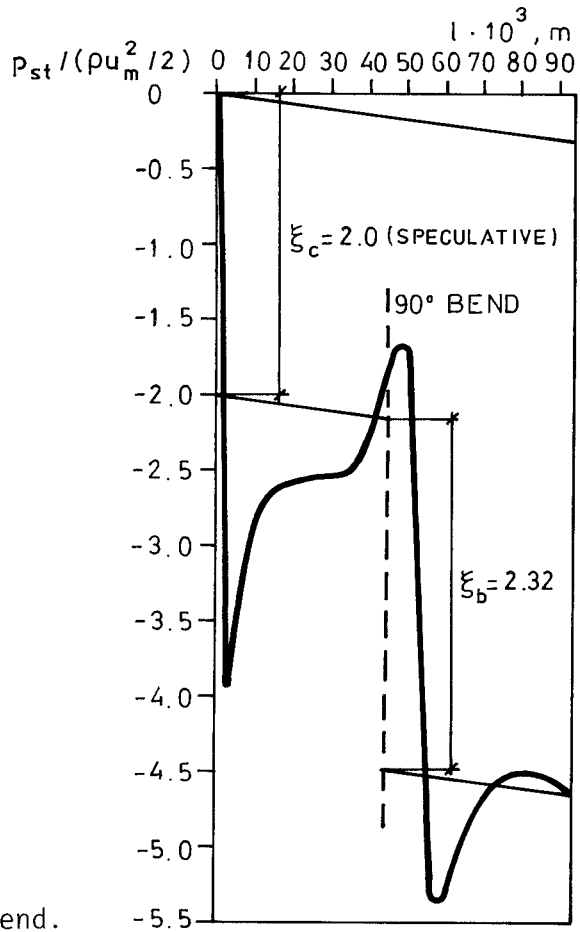


FIG. 3.2.3.k Duct with one 90° -bend. width 6.1 mm, length 94 mm, $Re = 3726$

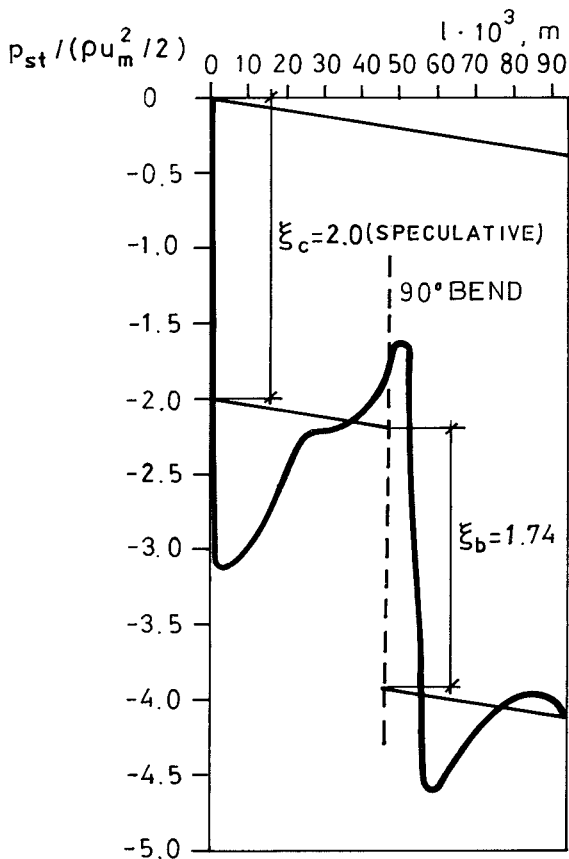


FIG. 3.2.3.i Duct with one 90° -bend. width 6.1 mm, length 94 mm, $Re = 2073$

Since the ratio of constricted to frontal area is zero, approximately the exit loss factor, ξ_e , is likely to equal zero. This value has been assumed throughout the analysis of the measurement results.

The results are summarized in table 3.2.3.a.

TABLE 3.2.3.a. Duct flow. Measurement results.

CONTRACTION (ENTRANCE, $\sigma = 0$)					
Flow length mm	Duct width mm	Re	ξ_C measured	K_C measured	K_C acc. to fig. 2.3.2.4.c
50	2.0	1744	2.16	1.16	0.52
	3.0	1717	2.16	1.16	0.52
	5.9	1973	2.04	1.04	0.52
130	2.0	1936	1.51	0.51	0.52
	3.0	1945	1.71	0.71	0.52
	6.0	1982	2.15	1.15	0.52
	6.0	4046	2.06	1.06	0.51
94 (incl. one 90° bend)	3.0	2055	1.98	0.98	0.52
	6.1	2073	2.00	1.00	0.52
	6.1	3726	2.00	1.00	0.51

ONE 90° BEND				
Flow length mm	Duct width mm	Re	ξ_b measured	ξ_b acc. to fig. 2.3.2.4.1
94	3.0	2055	1.64	1.70
	6.1	2073	1.74	1.69
	6.1	3726	2.32	1.46

The loss factors measured are generally high compared to the values originating from the literature. However, the result shows that the influence of contractions and bends on the pressure drop is substantial and that their influence by no means should be neglected in most calculations of air flow through ducts.

4 CALCULATING PRESSURE DISTRIBUTION AND AIR FLOWS IN BUILDING COMPONENTS

In chapter 2 the tools available for treating pressure distribution and air flow calculation problems have been reviewed. Most of the concept is based on flow through permeable material and pipe flow. Problems of air flow in or through building components are seldom so uncomplicated that it is possible to solve them directly in one single operation. Instead, a significant flow problem that may arise for a designer leads to a complicated network of flows through small openings, flows in ducts or interstices, flows in permeable materials etc. These circumstances implicate the need for methods to model the flow problem in a proper way thus making it possible to solve it as far as possible by means of a general calculation procedure. This means that the procedure does not have to be redesigned for the calculation of every new flow problem.

4.1 GENERAL REMARKS ON MODEL DESIGN

Extremely simple flow problems can be solved directly just by putting in actual figures in one single equation. Examples of such procedures are the calculation of the rate of air flow between infinite parallel plates for a certain pressure drop per unit length, or the calculation of the flow rate per square meter perpendicular to the flow direction through a permeable material with a certain pressure drop across the material sample. One of the main reasons why these problems are easy to solve lies in the fact that they are linear in character. This means that the flow rate is proportional to the pressure drop giving rise to the flow. Even somewhat more complicated flow situations are easily calculated by hand as long as the linearity remains.

Fluid flow in general is nothing but mass transfer caused by potential (i.e. pressure) differences and/or flow sources/sinks. This is something fluid flow has in common with many other physical transport phenomena such as heat transfer or currents in electrical circuits. However, both in heat transfer and electrical circuit theory non-linear relationships between potential difference and flow rate are rare. In heat transfer one could say that it simply does not occur. The thermal conductivity may be

dependent on the temperature level, for example, (e.g. constructions exposed to fire) but the thermal conductivity of solids is not influenced by the heat flow rate. The difference is illustrated in figure 4.1.a.

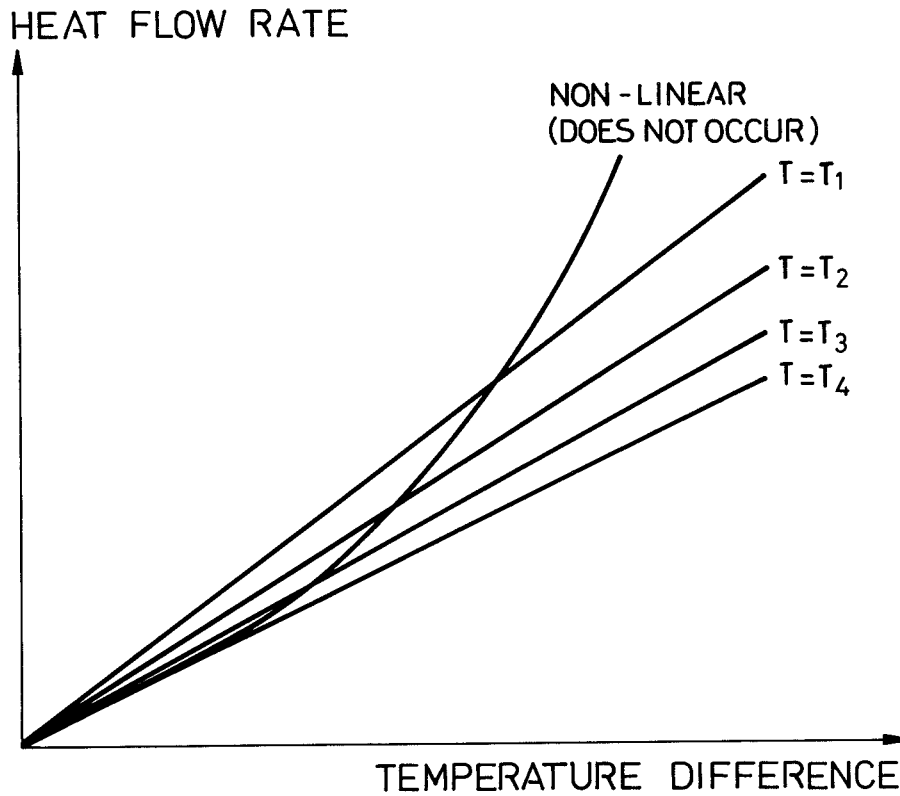
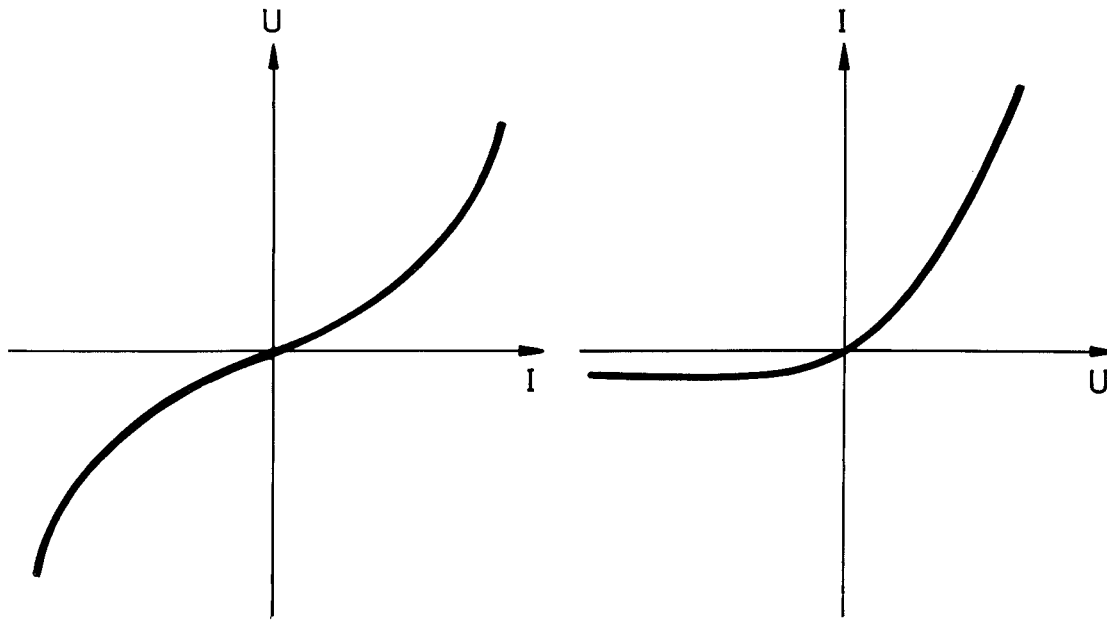


FIG. 4.1.a. Heat flow rate vs. temperature difference acting across a heat conducting specimen.

However, in electrical circuit theory there exist electrical components having non-linear characteristics. Figure 4.1.b.



INCANDESCENT LAMP

SEMICONDUCTOR DIODE

FIG. 4.1.b. Characteristics of non-linear components. After Smith (1976).

The difficulties in treating non-linear components in large networks are strongly emphasized by Huelsman (1972), Cornetet & Battocletti (1975), Smith (1976) and Anderson (1978) for example. The methods of analysis in the case of non-linearity suggested are:

- o analytical solution
- o piecewise linearization
- o graphical solution

What about the circumstances of fluid flow then? As was mentioned above, linear relationships between pressure difference and flow rate are rare. The only exceptions are (slow) flow in permeable material and developed laminar flow in closed conduits. In all other cases such as flow through constrictions, not fully developed flow, turbulent flow etc. the flow rate is not proportional to the acting pressure difference. This fact leads to more complicated calculation procedures than is the case for heat transfer in solids and other pure potential flow situations. The tackling of the non-linearity will be covered in part 4.3.

A difference that is important for the choice of a proper calculation model is whether the flow-path(s) in the building component is/are possible to predetermine (at least to a certain degree) or cannot be predetermined at all. In the first case a network analysis similar to

that of electrical circuit analysis may be successful, while in the latter a calculation method for potential flow (e.g. relaxation method) modified for the non-linearity may be used. The two methods in fact meet in the case when every component in the circuit analysis corresponds to a similar cell in a relaxation mesh.

Both methods involve a separation of the geometry of the flow problem into several discrete elements. Pressure differences across all the elements and resulting flow rates are calculated iteratively until a certain convergence criterium is met.

4.2 THE ALGORITHMS

Along a specific flow path pressure losses may occur due to flow resistances. They may be either of::

- o resistances of permeable materials
- o resistances of ducts
- o single resistances (contraction and expansion losses etc.)

If the different kinds of resistances occur in series their total influence on the pressure loss may be summarized in the following way:

$$\Delta p_{\text{tot}} = \Delta p_{\text{mat}} + \Delta p_{\text{duct}} + \Delta p_{\text{single}} \quad (4.2.a)$$

with easily understandable denotations.

In the case of one-dimensional flow in permeable isotropic material (cf. eq. 2.2.1.a)

$$\Delta p_{\text{mat}} = u_m \cdot \frac{l}{B_0/\eta} \quad (4.2.b)$$

where l is the length of the element in the flow direction.

Duct pressure losses are described by (cf. eq. 2.3.1.b)

$$\Delta p_{\text{duct}} = \lambda \cdot \frac{l}{d_H} \cdot \frac{\rho u_m^2}{2} \quad (4.2.c)$$

Single resistances influence the pressure loss in the following way:

$$\Delta p_{\text{single}} = \xi \cdot \frac{\rho u_m^2}{2} \quad (4.2.d)$$

where ξ is the specific loss factor.

While the specific permeability coefficient B_0 for most materials is an easily found table value λ and to a certain degree ξ are strongly dependent of the flow situation. As was pointed out in chapter 2 the friction factor λ depends on the Reynolds number. Different algorithms for air flow in ducts with parallel walls used for calculations in this work are summarized in table 4.2.a.

TABLE 4.2.a. Algorithms for determination of the friction factor, λ , in parallel-sided ducts. The analytical expression for λ_T is according to Selander (1978).

Re	λ
< 2300	$96/Re$
$2300 \leq Re \leq 3500$	$\frac{(3500-Re) \frac{96}{2300} + \lambda_T \text{ Re} = 3500}{1200}$
> 3500	λ_T

where

$$\lambda_T = \left[2 \log \left(\frac{-4.793}{Re} \log \left(\frac{10}{Re} + \frac{0.1 \epsilon}{b} + 0.1349 \frac{\epsilon}{b} \right) \right) \right]^{-2}$$

In the algorithms in table 4.2.a the value $d_H = 2b$ is used. If the duct has a low aspect ratio, a/b , (cf. figure 2.3.1.b) the accuracy of the calculation will be increased by use of the concept of table 2.3.2.2.a.

A plot of the $Re - \lambda$ relationship according to table 4.2.a is given in figure 4.2.a.

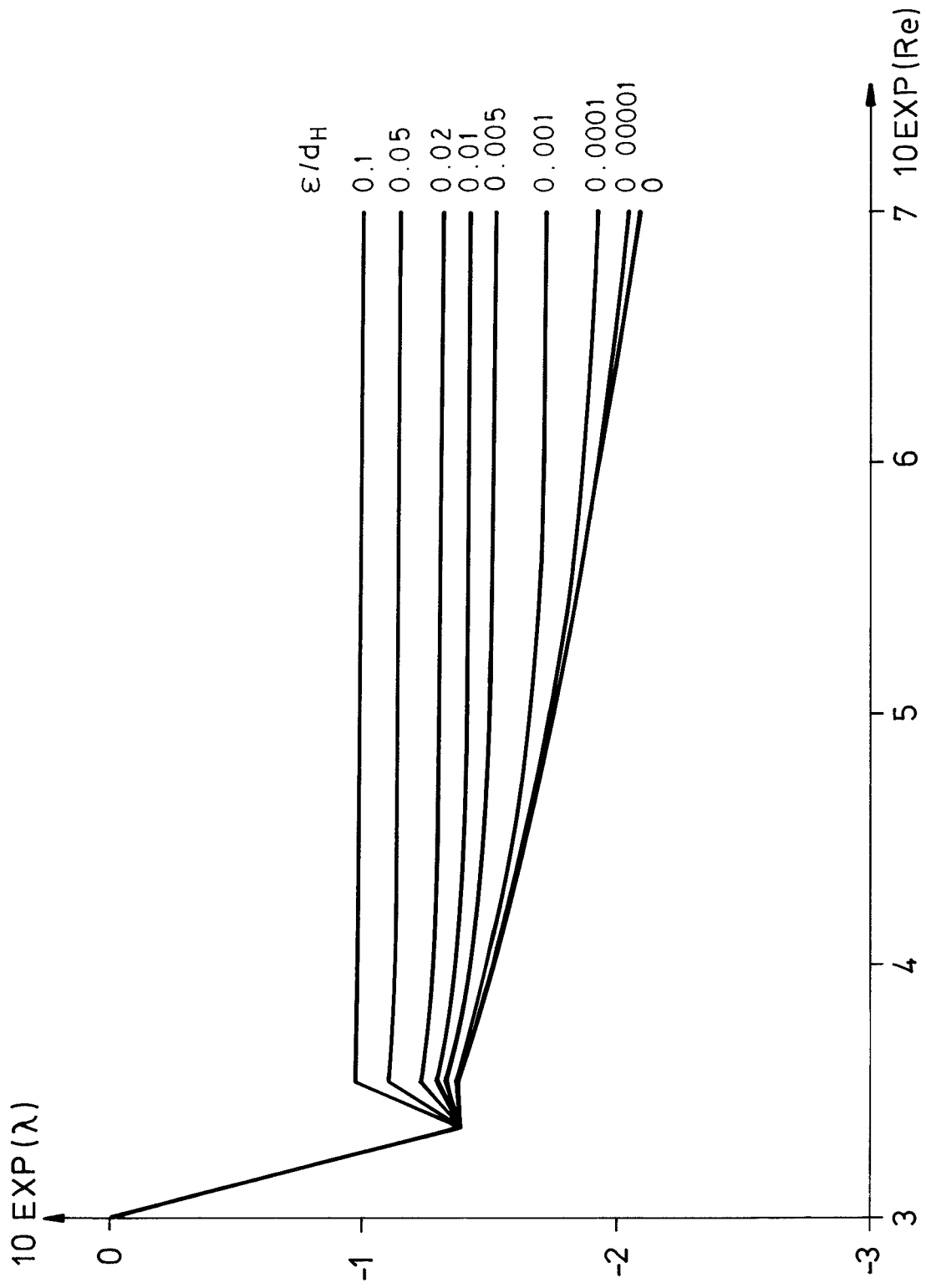


FIG. 4.2.a. Plot of the relationship between Re and λ for different values of ϵ/d_H ($\epsilon/2$ b)

Examples of single resistances are area changes, elbows, tees and crosses of ducts. Pressure losses due to area changes such as entrances and exits of ducts are frequent in problems of air flows in building components. The concept of part 2.3.2.4 is practically applicable to any calculation procedure.

4.3 CALCULATION PROCEDURES

4.3.1 Hand calculations

Apart from the most simple flow problems such as calculation of flow rate through a circular hole or a slot, or the rate of flow through a piece of permeable material, networks built up by flow resistances can be solved by hand unless they are too great and complicated.

Consider the following problem; (figure 4.3.1.a)!

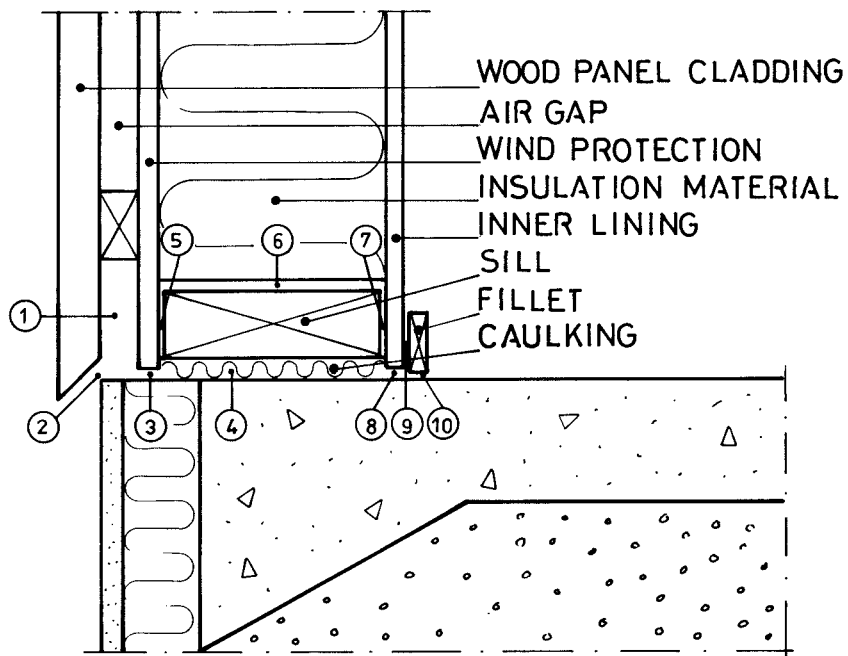


FIG. 4.3.1.a. Possible air flows around a sill of a timber-framed house.

At least ten possible flow paths may occur:

- 1: Air permeating the wood panel cladding.
- 2: Air flow between floor slab and panel.
- 3: Air flow between floor slab and wind protection.
- 4: Air permeating the caulking.
- 5: Air flow between wind protection and sill.
- 6: Air flow between insulation material and sill.
- 7: Air flow between inner lining and sill.
- 8: Air flow between inner lining and floor slab.
- 9: Air flow between fillet and inner lining.
- 10: Air flow between fillet and floor slab.

If every flow path is symbolized with the common resistance symbol used for electrical circuits the following resistance network may be outlined. (figure 4.3.1.b):

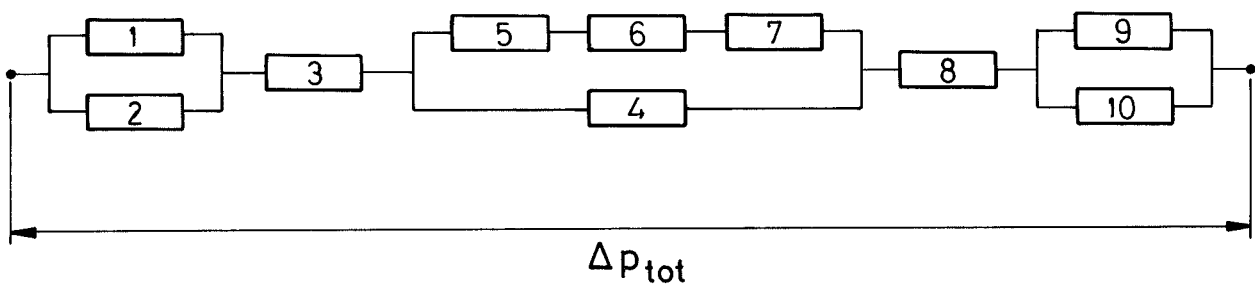


FIG. 4.3.1.b. Resistance network modelling the air flow problem of figure 4.3.1.a.

The modelling of the problem involves some assumptions. Thus the flow paths are predetermined and some of the building materials have been considered to be so airtight that no air permeate them (wood, wind protection and inner lining). Further, no air movement in the insulation layer of the wall is taken into account. Generally the validity and reasonableness of such assumptions must be carefully considered.

A complete straight-forward solution of the problem is not possible. However, a graphical solution is possible to obtain, which will be demonstrated here.

A solution procedure, based on the knowledge of the flow-pressure drop characteristic of each component, was once outlined by Nylund (1966).

If two components (denoted 1 and 2) constitute a branch with flow resistances in parallel the flow characteristics of them are written

$$q_1(\Delta p) = f_1(\Delta p) \quad (4.3.1.a)$$

and

$$q_2(\Delta p) = f_2(\Delta p) \quad (4.3.1.b)$$

and the flow characteristic of the total branch will be

$$q_{12}(\Delta p) = q_1(\Delta p) + q_2(\Delta p) \quad (4.3.1.c)$$

since the same pressure difference acts on the both resistances. This is demonstrated in figure 4.3.1.c.

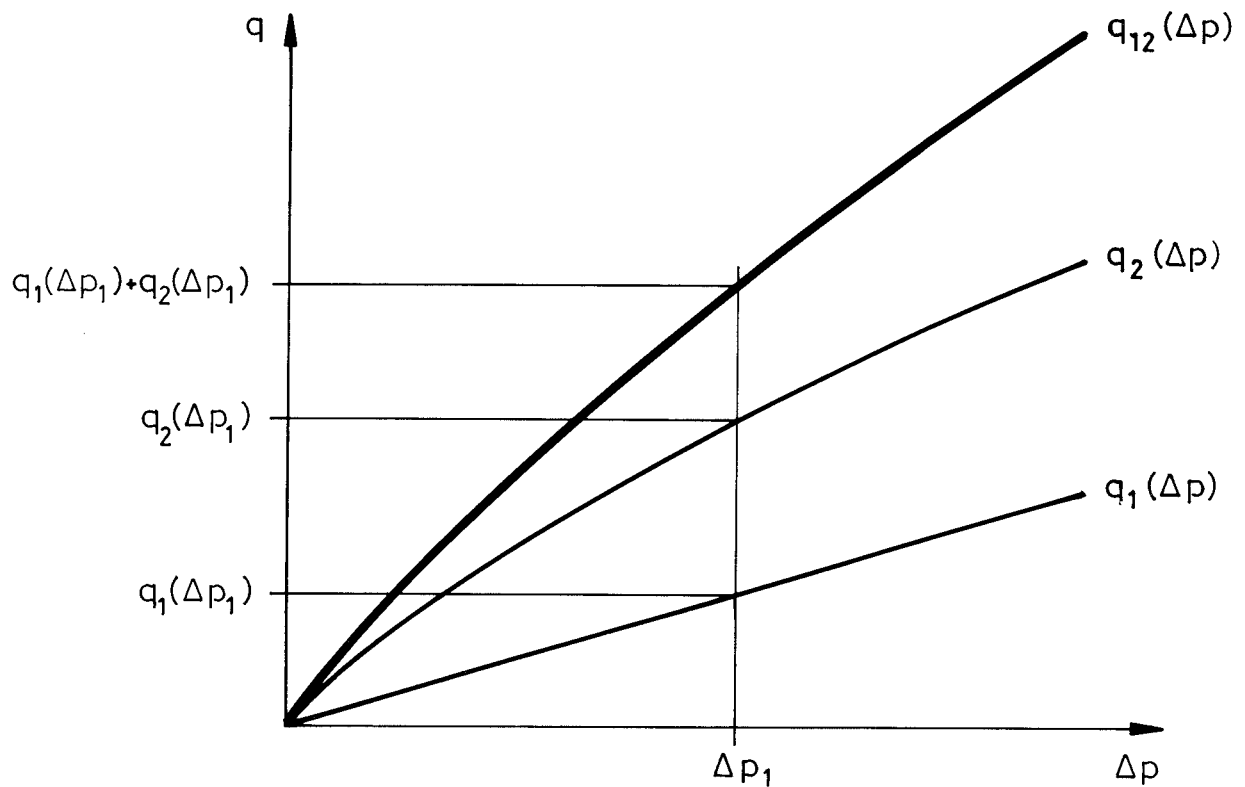


FIG. 4.3.1.c. Resulting flow characteristic. Flow resistances in parallel.

If two resistances (denoted 3 and 4) are connected to each other in series the flow rate is the same in each of the both components and the total system.

$$q_{12}(\Delta p) = q_1(\Delta p_1) = q_2(\Delta p_2) \quad (4.3.1.d)$$

$$\text{and } \Delta p(q_0) = \Delta p_1(q_0) + \Delta p_2(q_0)$$

See figure 4.3.1.d!

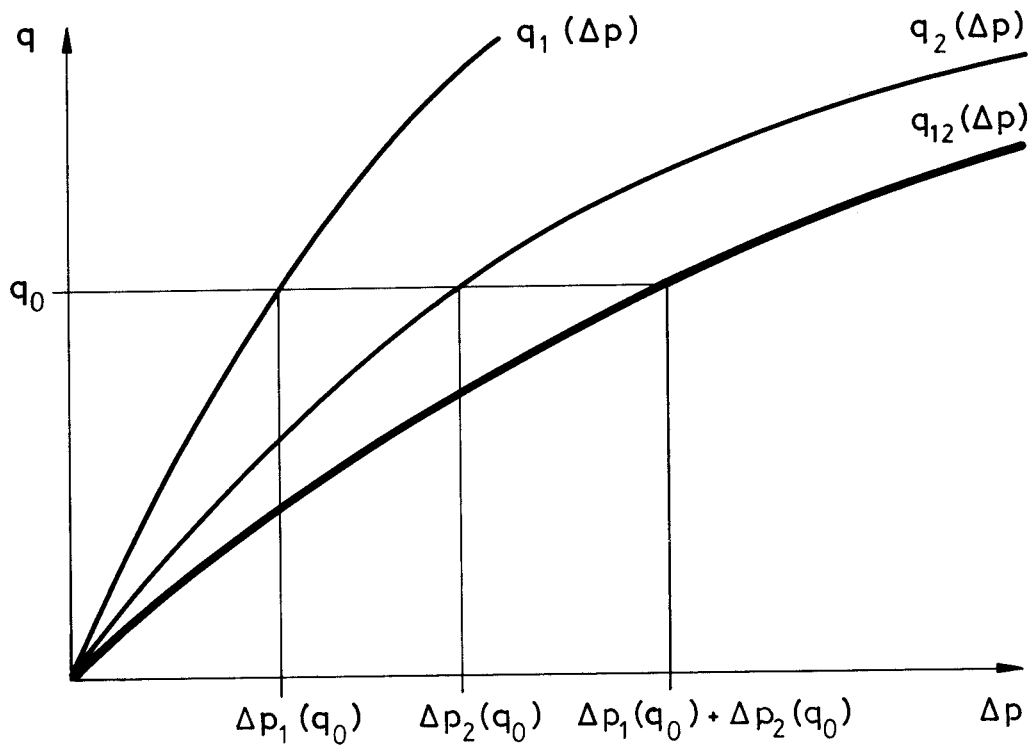


FIG. 4.3.1.d. Resulting flow characteristic. Flow resistances in series.

After finding out the flow characteristic of each component in the present problem, parallel resistance branches should be replaced by single components with a resulting flow characteristic. Hence the components 1, 2; 9, 10 and 5, 6, 7, 4 should be replaced by three components. How this is done graphically is shown in figure 4.3.1.e for the components 5, 6, 7, 4.

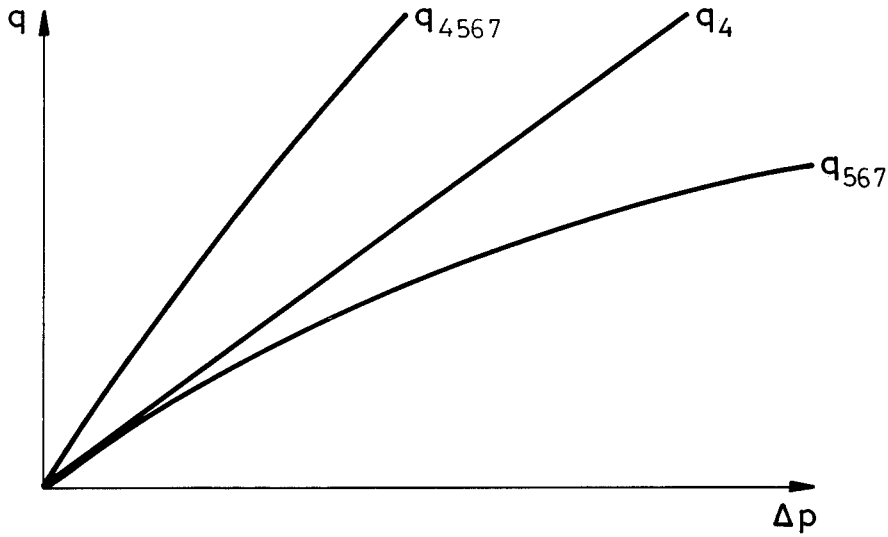
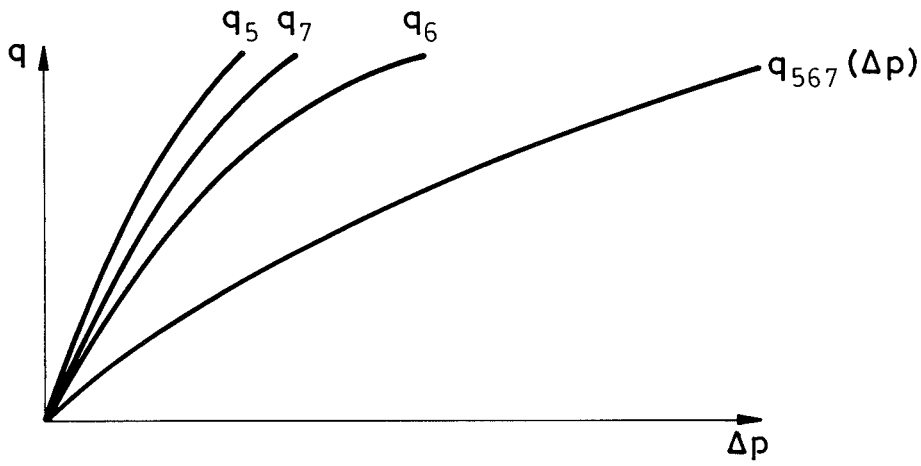


FIG. 4.3.1.e. Procedure to obtain the resulting flow characteristic of a branch with resistances in series and parallel.

Doing the same thing with the branches 1, 2 and 9, 10 yields a pure series network. See figure 4.3.1.f.

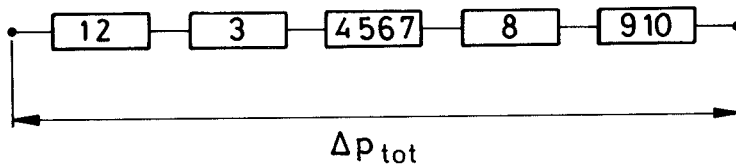


FIG. 4.3.1.f. Series network replacing the one in figure 4.3.1.b.

The remainder of the solution procedure is quite simple. If the flow rate is known the actual pressure drop Δp_{tot} is easily calculated simply by adding the pressure drops of each component to each other. If the total pressure drop is known the flow rate must be estimated and mostly re-estimated until the sum of the individual pressure drops equals Δp_{tot} .

4.3.2 Computer calculations

Reports on computer calculations of air flows in building components are extremely rare. In most cases the reported works have been limited to a certain flow problem and the calculation procedures have been designed exclusively for the problem in question. Hence the computer programs used normally are afflicted by severe lacks of universal applicability.

4.3.2.1 Computerized analysis of flow resistance networks.

Calculations of great complex networks of flow resistances are very time-consuming and sometimes impossible to perform by hand. A systematic computerized calculation procedure can be obtained by means of a proper computer program. Such a one, called JK-CIRCUS was written for this research project. Parts of the computer program originates from a program designed for analysis of electrical circuits; Anderson (1978). The solution procedure involves the following stages:

- o The flow problem geometry is split up into finite parts - components.
- o The admittance, defined below, of each component is calculated.
- o The computer calculates the potentials, $p(\text{Pa})$, in all nodes and flow rates, $q (\text{m}^3/\text{s})$, through all components.

In the case of (air) flow problems a component may be either of

- o a pressure difference between two nodes (active component)
- o a piece of permeable material (passive)
- o a piece (in the flow direction) of a duct (passive)
- o a single resistance (e.g. entrance, exit, bend loss), (passive).

Each component of a circuit with two connections is called a branch. Connection points are called nodes. Several branches can be connected to the same node.

The notation used for pieces of material or ducts is shown in figure 4.3.2.1.a.

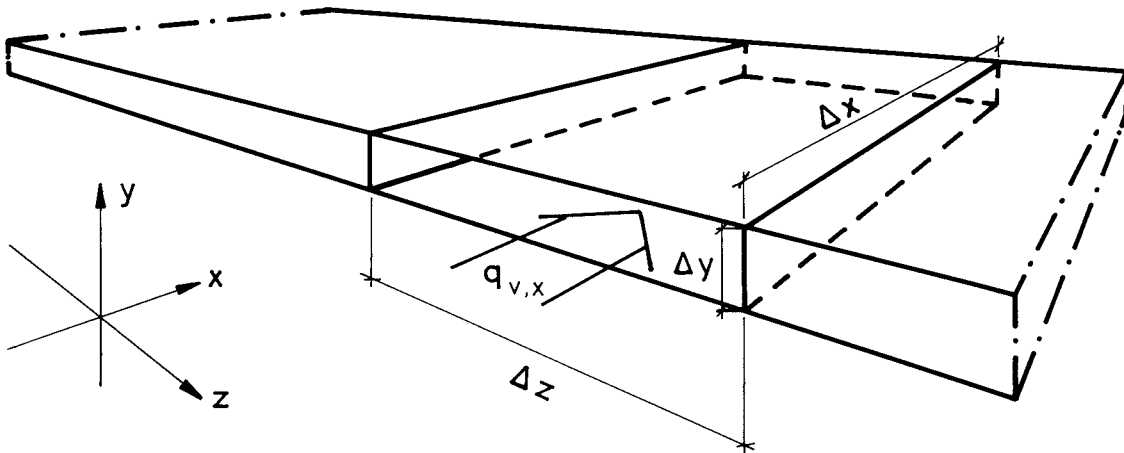


FIG. 4.3.2.1.a. Notation of geometrical properties of a component.

The computer program works with the concept of admittance. This property, A , is defined by:

$$q_{v, x} \left[\frac{\text{m}^3}{\text{s}} \right] = A_x \left[\frac{\text{m}^3}{\text{s} \cdot \text{Pa}} \right] \cdot \Delta p_x \left[\text{Pa} \right] \quad (4.3.2.1.a)$$

Hence the admittance, A, is a linear operator on the pressure difference, Δp , across a component returning the flow rate, q, Here an analogy with electricity is applied. The electrical admittance, Y, is defined by:

$$I \left[\text{A} \right] = Y \left[\frac{\text{A}}{\text{V}} \right] \cdot U \left[\text{V} \right] \quad (4.3.2.1.b)$$

It is obvious that the admittance is inverse to the resistance in both cases.

Now the algorithms for determining the admittance can be given: (cf. the notation given in figure 4.3.2.1.a)

Permeable material

$$A_x = \frac{B_0}{\eta} \cdot \frac{1}{\Delta x} \cdot \Delta y \cdot \Delta z \quad (4.3.2.1.c)$$

Ducts

$$A_x (q_v) = \frac{4 \cdot \Delta y^3 \cdot \Delta z^2}{\rho \cdot q_{v, x} \cdot \lambda \cdot \Delta x} \quad (4.3.2.1.d)$$

In general, the admittance of a duct depends on the flow rate, q, in the duct. In the laminar case, however, the friction factor, λ , is inversely proportional to the flow rate, $\lambda = 96/\text{Re} = 96 \cdot \Delta z \cdot \nu/2q$, so the admittance becomes constant.

Up to a certain Re-value the admittance of a pure duct component - i.e. without any end effects - is constant. If Re-values are greater than that the component behaves in a non-linear way, cf. figure 4.3.2.1.b.

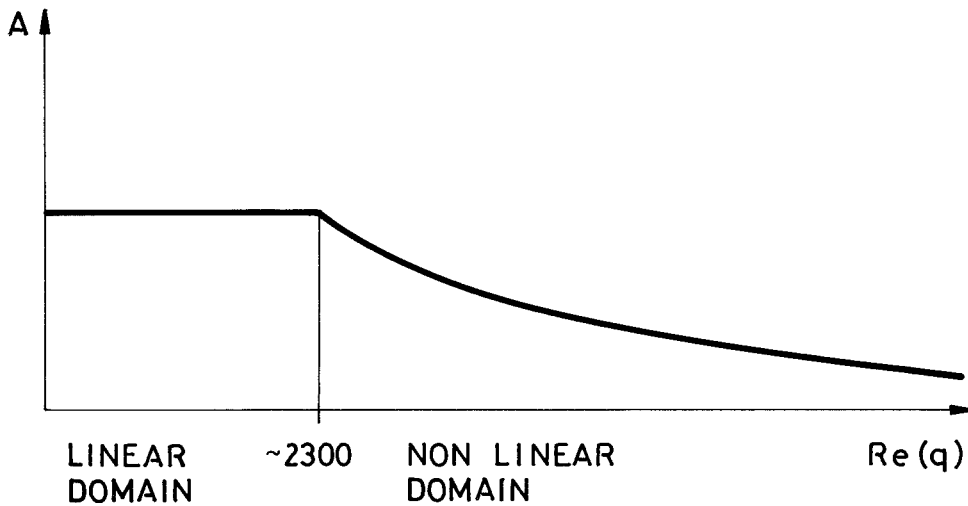


FIG. 4.3.2.1.b. Schematic picture showing how the admittance of a duct component varies with the Re-number.

Single resistances:

If the loss coefficient is denoted ξ then

$$A_x(q_v) = \frac{2 \cdot \Delta y^2 \cdot \Delta z^2}{\rho \cdot q_{v,x} \cdot \xi} \quad (4.3.2.1.e)$$

Unlike the duct the behaviour of a single resistance is non-linear for any Re-number.

The reference computer program mentioned above, Anderson (1978), was designed for linear electrical components only. Hence an extensive modification had to be undertaken to make the program applicable to flow problems including non-linear components.

A flow chart of the modified computer program is shown in figure 4.3.2.1.c.

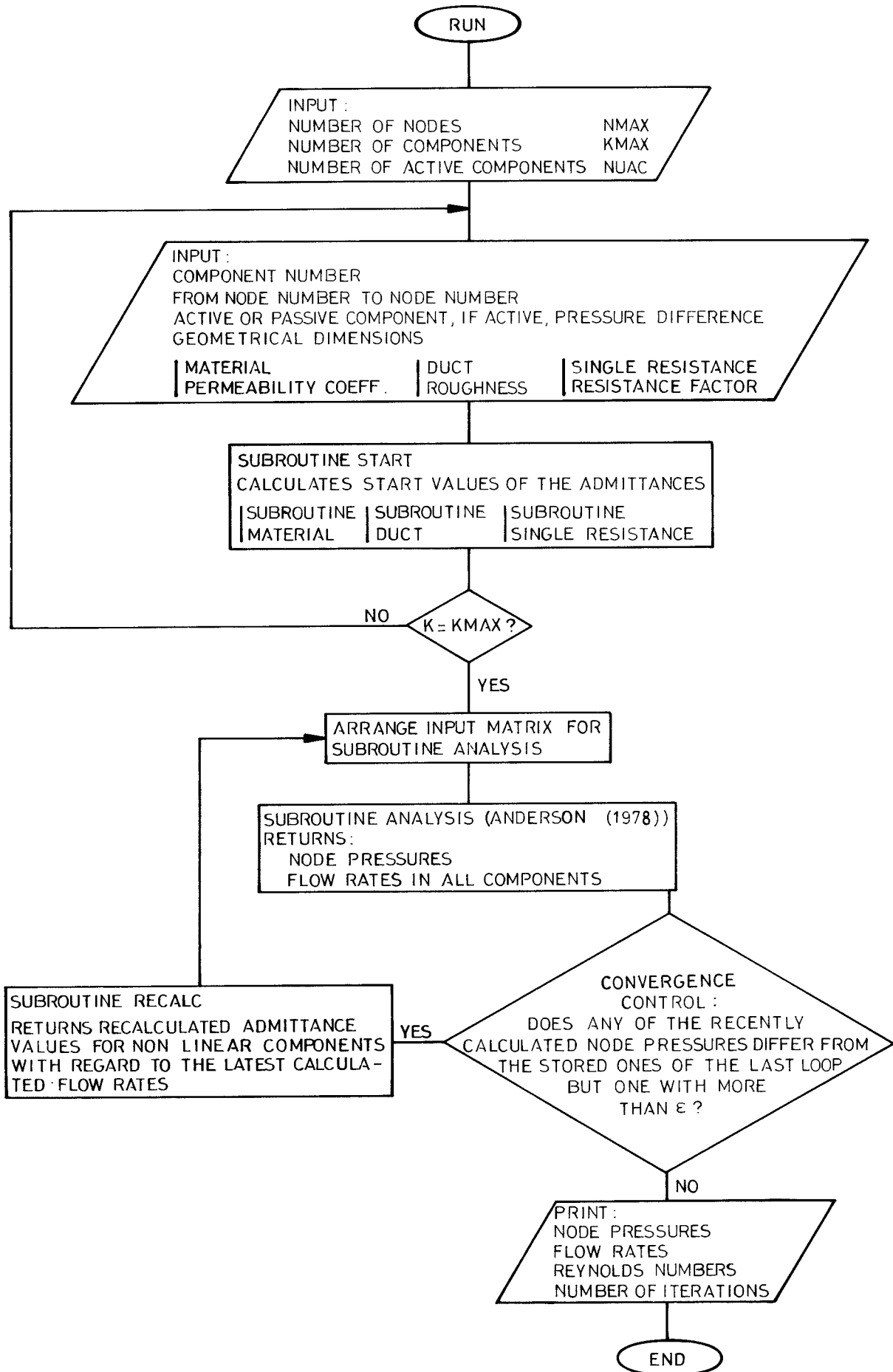


FIG. 4.3.2.1.c. Computer program JK-CIRCUS. Flow chart.

Some parts of the computer program need further explanation.

The subroutine START which calculates start values of the admittances have different internal subroutines for material, ducts and single resistances. The admittance of a permeable material is calculated straight ahead - eq. 4.3.2.1.c - and the calculated value is then used throughout the running of the program

For non-linear components, (turbulent duct flow and single resistances), the start admittance value is obtained by means of a linear approximation. First a test value of Δp is chosen equal to the greatest value possible with regard to the given pressure differences (Δp_{HIGH}). The corresponding q -value is q_{HIGH} . The slope of the secant from $(0, 0)$ to $(\Delta p_{\text{HIGH}}, q_{\text{HIGH}})$ is used as the linear approximation that constitutes the start admittance value. Figure 4.3.2.1.d.

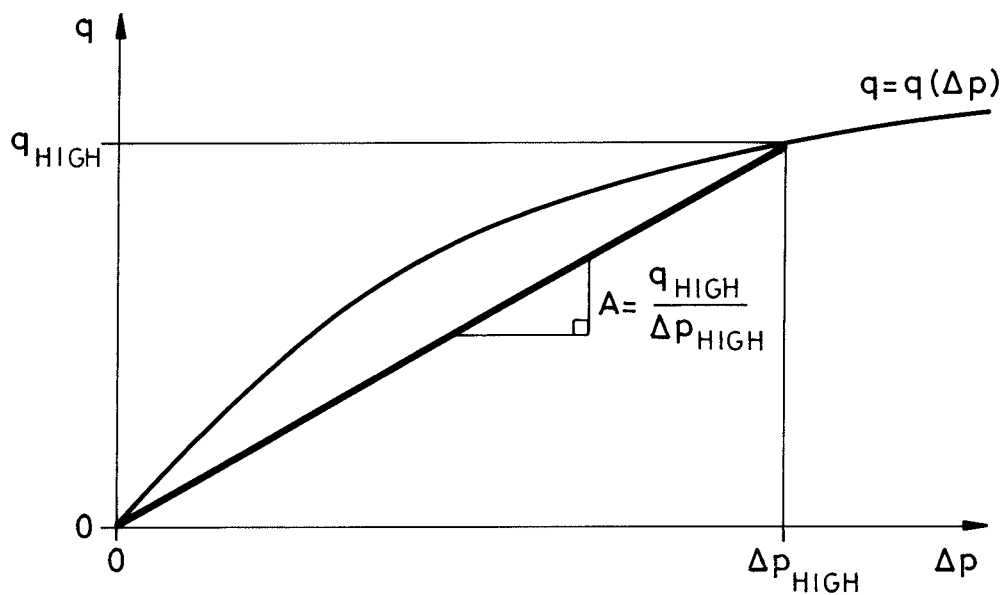


FIG. 4.3.2.1.d. Linear approximation of flow characteristic for a non-linear component returning start value of the admittance. Subroutine START.

If the flow rate q_{HIGH} is not great enough to produce turbulence in a duct ($Re < 2300$) then the secant is no approximation of course but gives

the proper admittance value.

The calculation procedure of the subroutine ANALYSIS follows that of electrical circuit analysis for which it was originally designed. An equation system - eq. 4.3.2.1.f - describes the flow problem.

$$\begin{bmatrix} A_{11} & A_{12} & A_{13} & \dots & A_{1NMAX} \\ A_{21} & A_{22} & A_{23} & \dots & A_{2NMAX} \\ A_{31} & A_{32} & A_{33} & \dots & A_{3NMAX} \\ \cdot & \cdot & \cdot & \dots & \cdot \\ \cdot & \cdot & \cdot & \dots & \cdot \\ \cdot & \cdot & \cdot & \dots & \cdot \\ A_{NMAX1} & A_{NMAX2} & A_{NMAX3} & \dots & A_{NMAXNMAX} \end{bmatrix} \cdot \begin{bmatrix} P_1 \\ P_2 \\ P_3 \\ \cdot \\ \cdot \\ \cdot \\ P_{NMAX} \end{bmatrix} = \begin{bmatrix} q_{v,1} \\ q_{v,2} \\ q_{v,3} \\ \cdot \\ \cdot \\ \cdot \\ q_{v,NMAX} \end{bmatrix} \quad (4.3.2.1.f)$$

The equation system is solved by Gaussian elimination technique.

In the calculation loops preceding the first one the admittances are recalculated with regard to the latest calculated flow rates in each component. This is done in the subroutine RECALC. For components with non-linear flow characteristics the admittance is determined by the slope of the secant from (0, 0) to $(\Delta p_1(q_1), q_1)$ - figure 4.3.2.1.e.

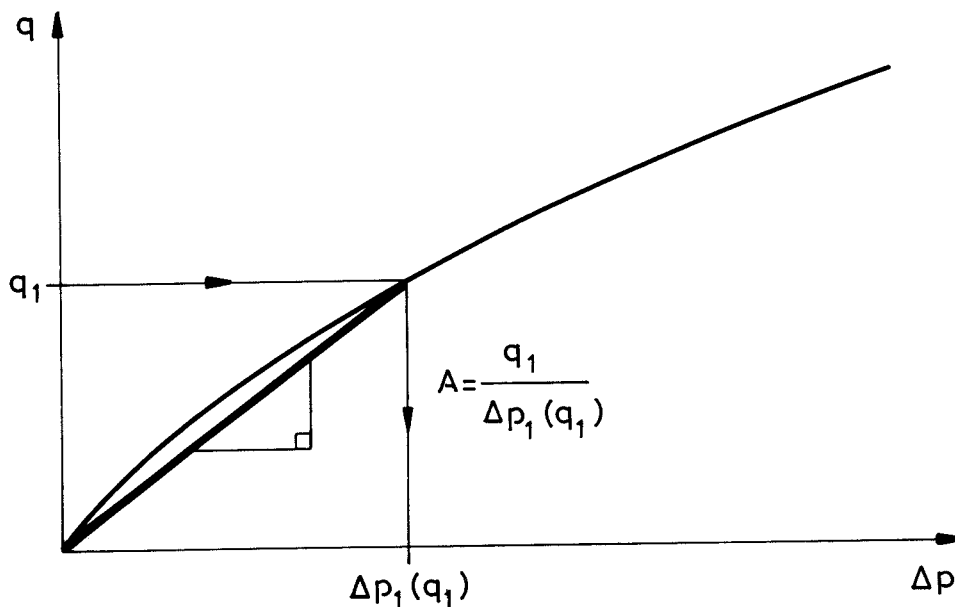


FIG. 4.3.2.1.e. Determination of admittance for a non-linear component in the iterations. Subroutine RECALC.

The convergence control involves checking of the differences between recently calculated node pressures and node pressures calculated in the last loop but one. In most cases, presented in this work, the criterion of necessity of doing a new calculation loop has been

$$\frac{P_{\text{LOOP NO.S}} - P_{\text{LOOP NO.S-1}}}{P_{\text{HIGH}}} > 0.005$$

The computer program was written in BASIC. A format for input data is presented in the appendix.

4.3.2.2 Computer calculation by means of relaxation

Relaxation is a frequently used calculation procedure for a variety of potential flow problems. The relaxation procedure starts with an estimated potential distribution. By means of iteration the distribution is modified until a stable one is obtained. In the case of heat conduction in solids with complicated geometry and boundary conditions, it is perhaps the most commonly used technique to determine the temperature distribution in the solid. See for example Holman (1963). Hence a number of computer programs exist for this kind of problem. Such a program - developed at the division of Building Technology at Lund Institute of Technology - was modified to make it possible to solve problems of air flow in building components too, Andersson (1980). A flow chart of the program is shown in figure 4.3.2.2.a.

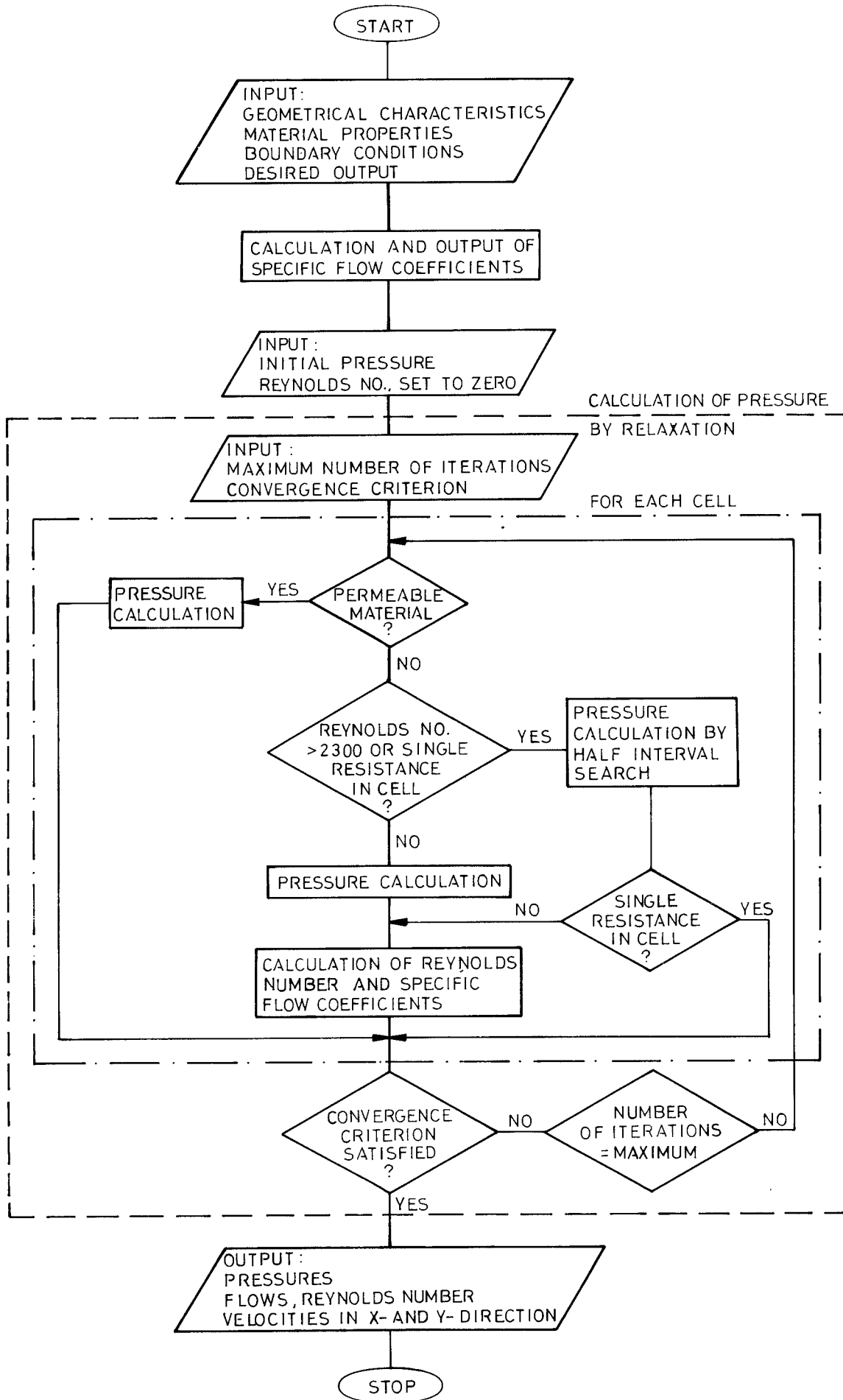


FIG. 4.3.2.2.a. Relaxation program. Flow chart. After Andersson (1980 B).

4.4 EXAMPLES

4.4.1 Hand calculations

Flow through a straight crack, duct etc.

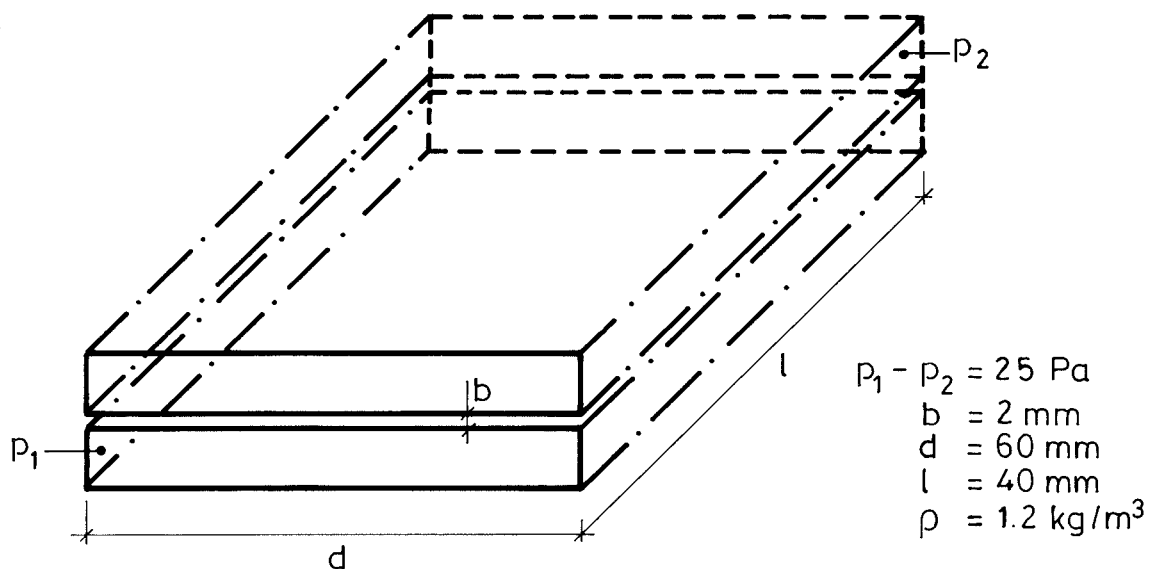
This is perhaps the most common flow problem in air flow calculations in building physics. Typical applications are

- o air flow in an air gap in a building component for removal of moist air
- o air infiltration through cracks and interstices of the building envelope
- o air flow in ventilation ducts.

Being very common the calculation procedure has in many cases been made much too simple. Thus many authors of works in building physics simply use the Hagen - Poiseuille equation without any attempt to take turbulence, end effects or roughness into account, for example.

Example 01:

Calculate the air flow rate through a crack with dimensions according to the figure below.



The algorithm for the calculation procedure is:

$$p_1 - p_2 = \left(\xi_{\text{ent}} + \lambda \cdot \frac{1}{d_H} + \xi_{\text{ex}} \right) \cdot \frac{\rho u_m^2}{2}$$

where

$$\begin{aligned}\xi_{\text{ent}} &= (1 - \sigma)^2 + K_c \quad \text{and} \\ \xi_{\text{ex}} &= -((1 - \sigma)^2 - K_e)\end{aligned}$$

Friction factor, λ :

Since d/b is quite high ($=30$) the hydraulic diameter, d_H , can be set equal to $2b$. (See figure 2.3.1.b). For the same reason $\lambda = 96/Re$ in the laminar case.

Entrance and exit losses:

ξ_{ent} and ξ_{ex} are dependent of the ratio of constriction to frontal area, σ , the Reynolds number, Re ; (see figures 2.3.2.4.c - d) and maybe of the flow length, l .

Solution:

First, make an estimate of the Re -number.

$$Re = 1000 \Rightarrow u_m = \frac{Re \cdot \nu}{2b} = \frac{10^3 \cdot 14.6 \cdot 10^{-6}}{2 \cdot 2 \cdot 10^{-3}} = 3.65 \text{ m/s}$$

Since $\frac{b}{T}$ is small ($=0.05$) the flow length is hydrodynamically long (figure 2.3.2.4.h) and no correction for short flow length has to be applied.

$$\text{Right membrum} = \left(1.78 + \underbrace{\frac{96}{1000} \cdot \frac{0.04}{2 \cdot 0.002}}_{0.96}\right) \cdot \frac{1.2 \cdot 3.65^2}{2} = 21.90 \text{ Pa} <$$

< left membrum ($=25$)

$$Re = 1100 \Rightarrow u_m = \underline{4.02 \text{ m/s}}$$

$$\text{Right membrum} = (1.69 + 0.87) \cdot \frac{1.2 \cdot 4.02^2}{2} = 24.8 \text{ Pa}$$

\approx left membrum.

For a hand calculation this value could be close enough.

Cf. a straight on calculation with the Hagen - Poiseuille equation (eq. 2.3.2.1.e) neglecting entrance and exit losses.

$$u_m = \frac{\Delta p \cdot b^2}{12 \cdot \eta \cdot l} = \frac{25 \cdot 2.0 \cdot 10^{-6}}{12 \cdot 17.5 \cdot 10^{-6} \cdot 0.04} = 5.95 \text{ m/s}$$

i.e. an overestimation of the velocity by around 50%.

Example 02:

In the first example the walls in the crack were considered to be relatively smooth. However, if for example a fracture crack of a building material is concerned, this assumption is a bit dubious.

Say that the crack width, b , stands for the distance between the mean levels of the crack wall surfaces and σ the standard deviations of the local deviations from the mean levels. If $\sigma = 1 \text{ mm}$ and $b = 2 \text{ mm}$ then $b/\sigma = 2$ and the flow factor $\phi = 0.70$ (fig. 2.3.2.3.e) if the surface roughness is isotropic ($\gamma = 1$). If this is included in the calculation one obtains:

$$p_1 - p_2 = \left(\xi_{\text{ent}} + \frac{1}{\phi} \cdot \lambda \cdot \frac{l}{d_H} + \xi_{\text{ex}} \right) \cdot \frac{\rho u_m^2}{2}$$

The flow resistance will be larger and after some estimations the solution

$$u_m = 3.64 \text{ m/s}$$

is obtained.

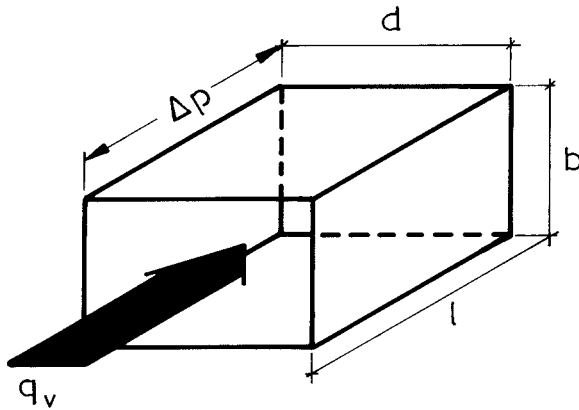
A greater value of σ , say 2 mm , yields $\phi = 0.49$ and this would give the result:

$$u_m = 3.28 \text{ m/s}$$

i.e. just around half of the value obtained by an unsuspecting use of the Hagen - Poiseuille equation.

Example 03:

Consider a duct with the following dimensions:



$$\begin{aligned} b &= 20 \text{ mm} \\ d &= 30 \text{ mm} \\ l &= 30 \text{ mm} \end{aligned}$$

Calculate the pressure difference, Δp , when $Re = 2000$. $b/l = 2/3$.
If σ is put at 0.01 the flow length is hydrodynamically short -
figure 2.3.2.4.h. Eq. (2.3.2.4.d) yields:

$$B_f = (Re \cdot d_H/l)^{1/3} \cdot \sigma^{1/4} \quad \Rightarrow$$

$$d_H = 4 \cdot b \cdot d / 2(b + d) = 0.024 \text{ m}$$

$$B_f = (2000 \cdot 0.024/0.03)^{1/3} \cdot 0.01^{1/4} = 3.70$$

Eq. (2.3.2.4.f):

$$C_c = -0.304 \cdot 3.70 + 1.684 = 0.560$$

$$C_e = 0.792 \cdot 3.70 - 0.782 = 2.148$$

$$C_f = 0.122 \cdot 3.70 + 0.725 = 1.176$$

$$\Delta p = \left[(1 - \sigma)^2 + C_c \cdot K_c + C_f \cdot \lambda \cdot \frac{1}{d_H} - ((1 - \sigma)^2 - C_e \cdot K_e) \right] \cdot \frac{\rho u_m^2}{2}$$

$$b/d = 2/3 \text{ so } d_H^* = 1.08 d_H \text{ (figure 2.3.2.1.b)}$$

$$d_H^* = 1.08 \cdot 0.024 = 0.025$$

$$u_m = \frac{Re \cdot \nu}{d_H} = \frac{2000 \cdot 14.6 \cdot 10^{-6}}{25 \cdot 10^{-3}} = 1.35 \text{ m/s}$$

$$K_c = 0.62, K_e = 1.0 \text{ (Figure 2.3.2.4.c and d)}$$

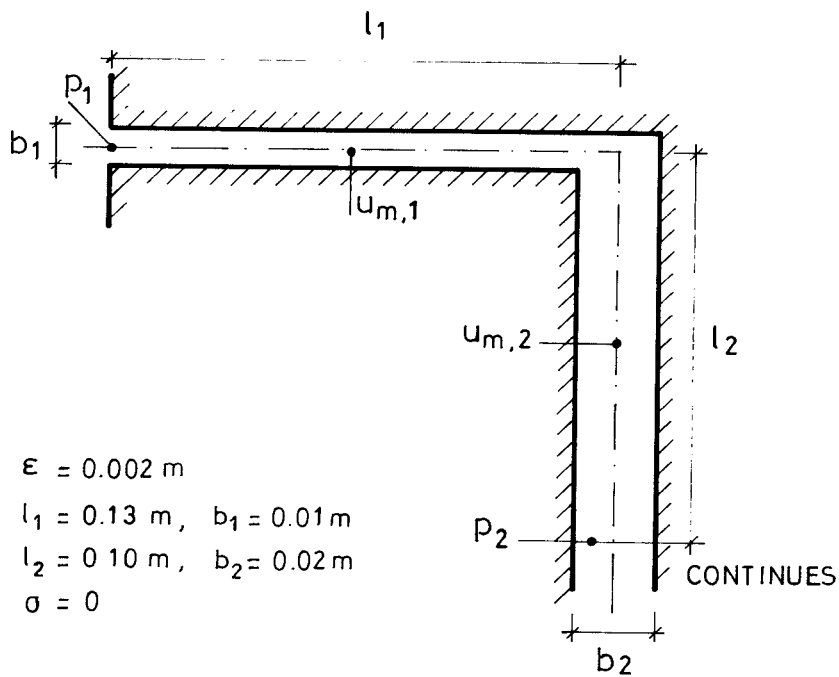
$$\Delta p = (0.56 \cdot 0.62 + 1.176 \cdot \frac{64}{1.08 \cdot 2000} \cdot \frac{0.03}{0.026} + 1.0) \frac{1.2 \cdot 1.35^2}{2} =$$

$$= 1.52 \text{ Pa}$$

Other examples

Example 04:

Flow through a bend. Dimensions etc:



Calculate the pressure loss when $Re = 1000$

Bend loss factor ξ_b :

$$\xi_b = k_{\epsilon/d_H} \cdot k_{Re} \cdot \xi \text{ (eq. 2.3.2.4.h)}$$

$$\xi_b = 45 \lambda \cdot \xi$$

$$a_0/b_0 = \infty, b_1/b_0 = 2 \Rightarrow (\text{figure 2.3.2.4.1}) \xi = 0.57$$

$$\xi_b = 45 \lambda \cdot 0.57 = 25.7 \lambda$$

$$\Delta p = \left((1 - \sigma)^2 + K_C + \lambda \cdot \frac{l_1}{2 \cdot b_1} + \xi_b \right) \frac{\rho u_{m,1}^2}{2} + \lambda \frac{l_2}{2 \cdot b_2} \cdot \frac{\rho u_{m,2}^2}{2}$$

$$\text{Re} = 1000 \Rightarrow K_C = 0.78, \lambda = 96/1000,$$

$$\xi_b = 25.7 \cdot 96 \cdot 10^{-3} = 2.47, u_{m,1} = \frac{1000 \cdot 14.6 \cdot 10^{-6}}{2 \cdot 10 \cdot 10^{-3}} =$$

$$= 0.875 \text{ m/s}$$

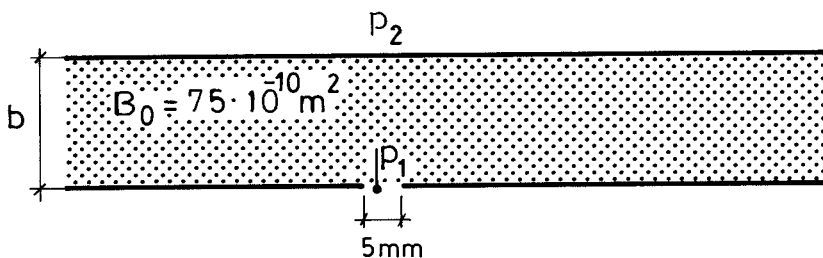
$$u_{m,2} = \frac{1}{2} \cdot 0.875 = 0.438 \text{ m/s}$$

$$p_1 - p_2 = \left(1.0 + 0.78 + 9.6 \cdot 10^{-2} \frac{0.13}{2 \cdot 10^{-2}} + 2.47 \right) \frac{1.2 \cdot 0.875^2}{2} +$$

$$9.6 \cdot 10^{-2} \cdot \frac{0.1}{2 \cdot 2 \cdot 10^{-2}} \cdot \frac{1.2 \cdot 0.438^2}{2} = 5.75 \text{ Pa}$$

Example 05:

Flow through a slot in contact with a permeable material.



An approximate solution can be obtained by use of eq. 2.2.2.f if the width of the slot ($=5 \text{ mm}$) is put equal to the diameter of the cylinder ($=2r$).

$$\frac{q_v}{l} = \frac{(p_1 - p_2) \cdot B_0 \cdot 2 \pi}{\eta \cdot \cosh^{-1} \frac{d}{r}}$$

$$b = 100 \text{ mm} \Rightarrow$$

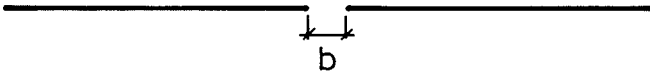
$$\frac{q_v/l}{p_1 - p_2} = \frac{75 \cdot 10^{-10} \cdot 2 \cdot \pi}{17.5 \cdot 10^{-6} \cdot \cosh^{-1} \frac{0.1}{2.5 \cdot 10^{-3}}} = 6.10 \cdot 10^{-4} \frac{\text{m}^3}{\text{m} \cdot \text{s} \cdot \text{Pa}}$$

$$b = 200 \text{ mm} \Rightarrow$$

$$\frac{q_v/l}{p_1 - p_2} = \frac{75 \cdot 10^{-10} \cdot 2 \cdot \pi}{17.5 \cdot 10^{-6} \cdot \cosh^{-1} \frac{0.2}{2.5 \cdot 10^{-3}}} = 5.30 \cdot 10^{-4} \frac{\text{m}^3}{\text{m} \cdot \text{s} \cdot \text{Pa}}$$

Example 06:

Flow through a slot in a thin wall



$$u_m = \frac{q}{l \cdot b} = C_d \cdot \sqrt{\frac{2 \cdot \Delta p}{\rho}} \quad (\text{eq. 2.3.3.b and d})$$

$$\Delta p = 10 \text{ Pa} \Rightarrow$$

$$\frac{q}{l \cdot b} = 0.593 \sqrt{\frac{2 \cdot 10}{1.2}} = 2.42 \text{ m/s}$$

If $b = 5.0 \cdot 10^{-3} \text{ m}$ then

$$\frac{q}{l} = 2.42 \cdot 5 \cdot 10^{-3} = 12.1 \cdot 10^{-3} \text{ m}^3/(\text{s} \cdot \text{m})$$

Example 07:

Flow through a "key-hole".

Diameter, $d = 8 \text{ mm}$

Flow length, $l = 30 \text{ mm}$

Roughness, $\epsilon = 0.5 \text{ mm}$

$Re = 5000$

$$\Delta p = \left(\xi_{\text{opening}} + \lambda \cdot \frac{l}{d} \right) \frac{\rho u_m^2}{2}$$

$$\xi_{\text{opening}} = \xi_0 (Re) + 0.342 e_0 (Re) \cdot \xi_{\text{opening}} \quad \text{for } Re \geq 10\,000 \quad (\text{eq. 2.3.3.g})$$

where

$$\xi_0 (Re) = 0.25$$

$$e_0 (Re) = 1.90$$

according to figure 2.3.3.b and

$$\xi_{\text{opening}} = 1.6 \quad \text{for } Re \geq 10\,000$$

according to figure 2.3.3.a

since $l/d = 3.75$

so:

$$\xi_{\text{opening}} = 0.25 + 0.342 \cdot 1.90 \cdot 1.6 = 2.05$$

$$\lambda = 0.038 \quad (\text{figure 4.2.a})$$

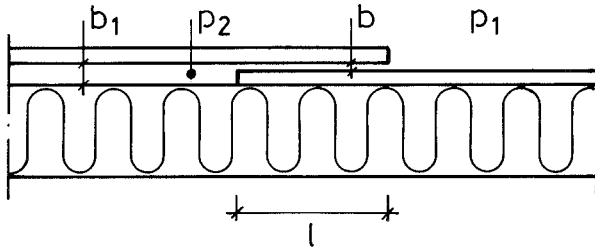
$$u_m = \frac{Re \cdot \nu}{d} = \frac{5000 \cdot 14.6 \cdot 10^{-6}}{8 \cdot 10^{-3}} = 9.125 \text{ m/s}$$

$$\Delta p = (2.05 + 0.038 \cdot 3.75) \cdot \frac{1.2 \cdot 9.125^2}{2} = 110 \text{ Pa}$$

$$q = u_m \cdot A = 9.125 \cdot \pi \cdot 4^2 \cdot 10^{-6} \text{ m}^3/\text{s} = 4.58 \cdot 10^{-4} \text{ m}^3/\text{s}$$

Example 08:

Overlap joint between airtight plates



$b = 0.001 \text{ m}$ $l = 0.05, 0.10 \text{ and } 0.20 \text{ m}$ respectively.

$b_1 = 0.014 \text{ m}$

$$u_m = \frac{Re \cdot \nu}{d_H}; \quad Re = 500 \Rightarrow u_m = \frac{500 \cdot 14.6 \cdot 10^{-6}}{2 \cdot 10^{-3}} = 3.65 \text{ m/s}$$

$$p_1 - p_2 = \left((1 - \sigma)^2 + K_c + \lambda \cdot \frac{l}{2b} - \left((1 - \sigma)^2 - K_e \right) \right) \cdot \frac{\rho u_m^2}{2} =$$

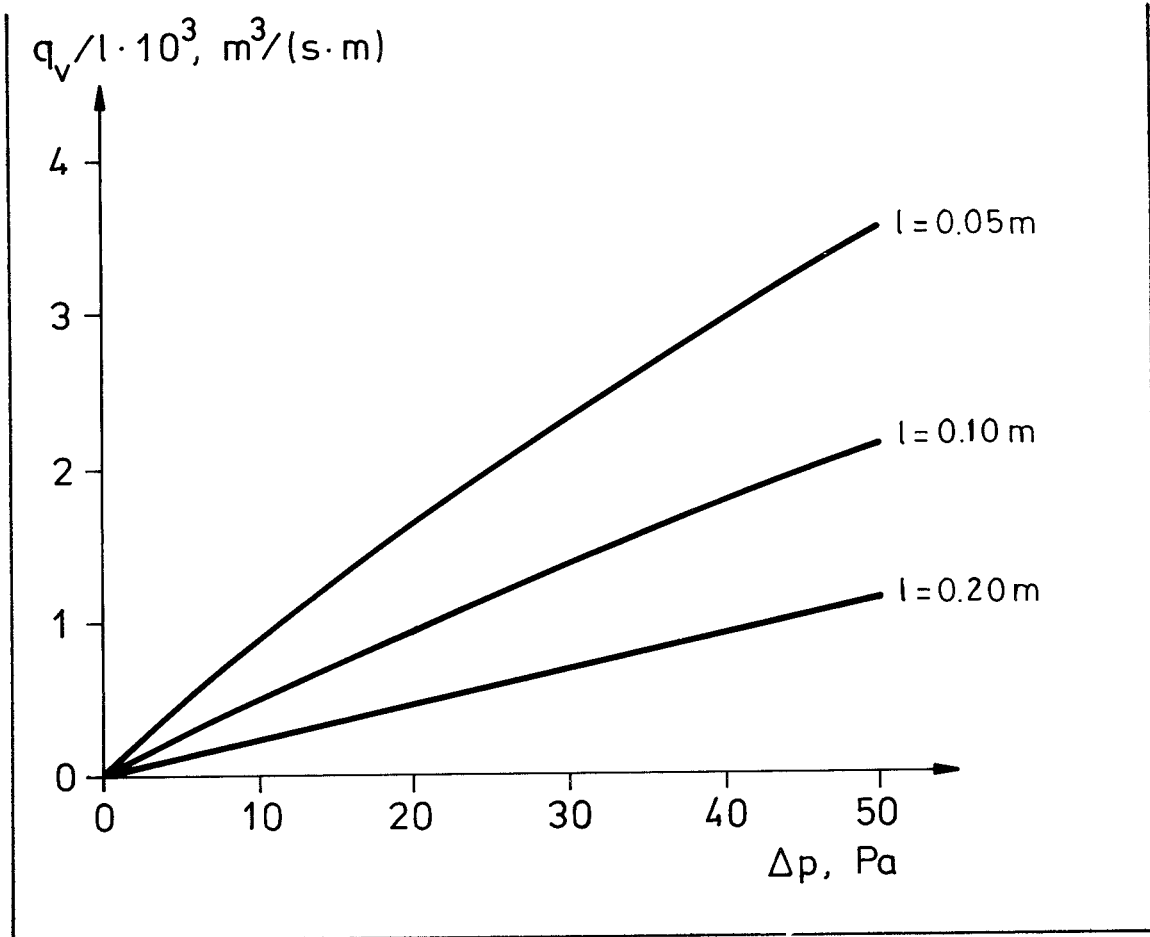
$$\underbrace{(1.0 + 0.81)}_{1.81} + \underbrace{\frac{96}{500} \cdot \frac{0.05}{2 \cdot 10^{-3}}}_{4.80} - \underbrace{\left(\left(1 - \frac{0.001}{0.014} \right)^2 - 1.0 \right)}_{0.14} \cdot \underbrace{\frac{1.2 \cdot 3.65^2}{2}}_{8.50} =$$

$$= 52 \text{ Pa} \quad (l = 0.05)$$

Similar calculations yields:

$l \text{ (m)}$	$\Delta p \text{ (Pa)}$
0.10	90
0.20	167

The consequences on the flow rate per unit breadth are shown in the figure below.

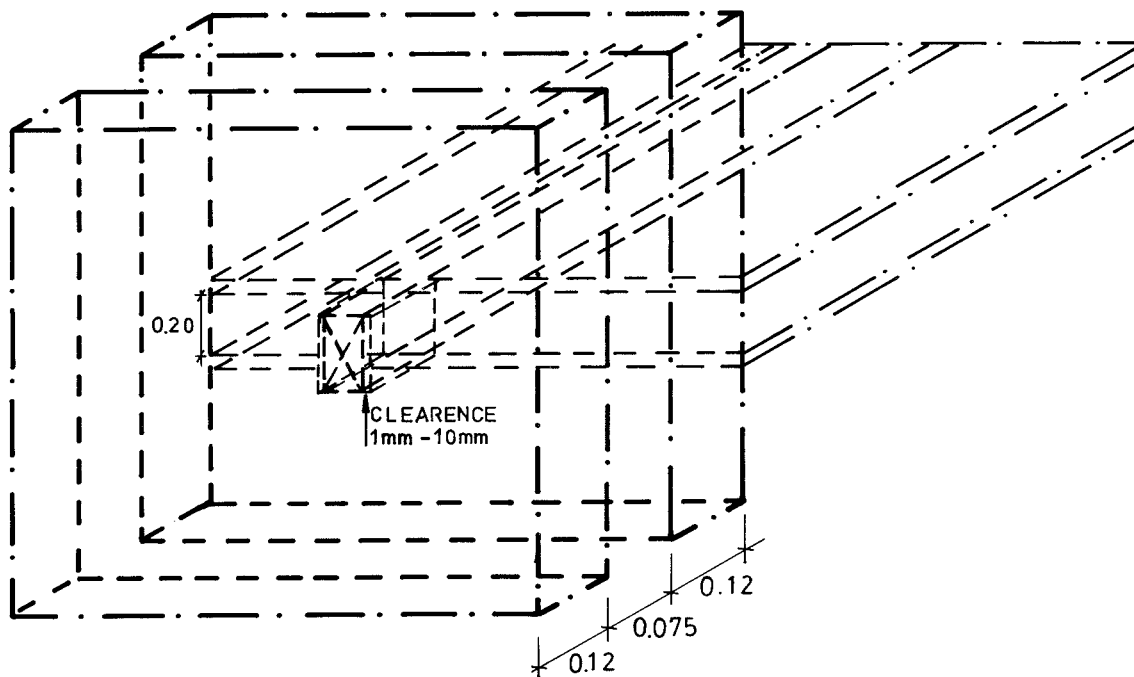


4.4.2 Computer calculations

4.4.2.1 Examples of computer calculations with flow resistance networks

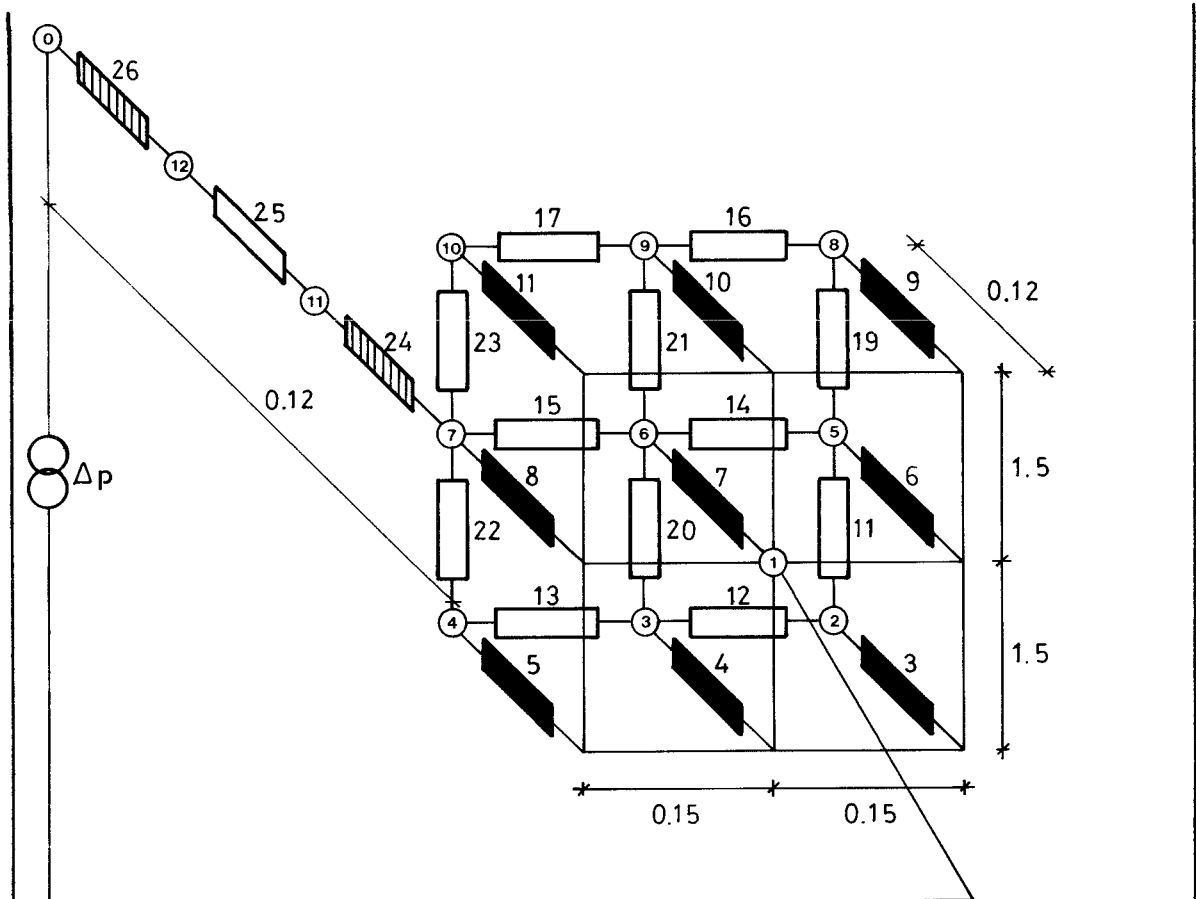
Example 11:

Cavity brick wall with beams penetrating the inner leaf.



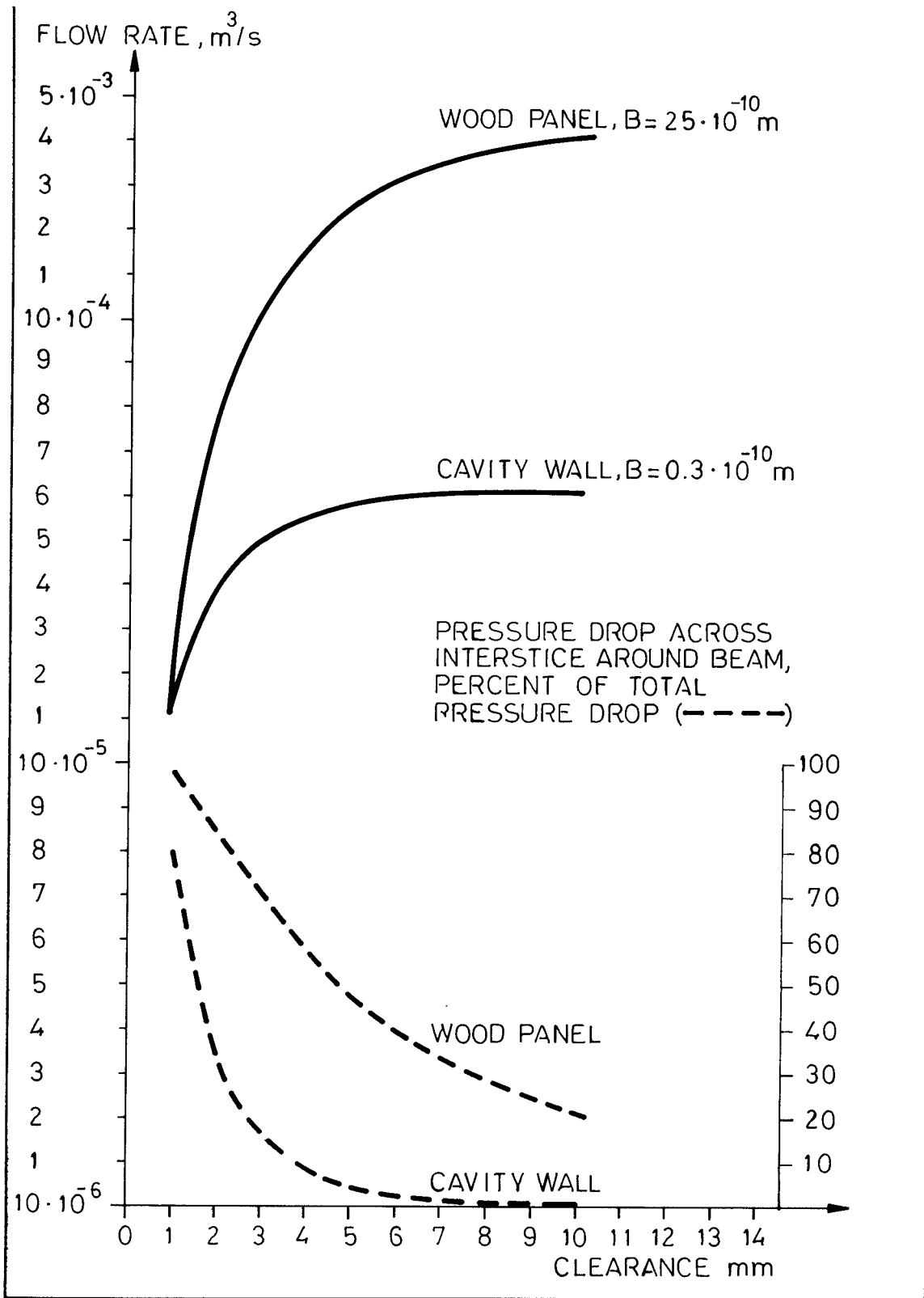
This is a typical design in many countries. If the cavity wall has a bad air tightness and the clearance around the beams is large there is a certain risk of discomfort in the house caused by movements of cold air in the intermediate floor.

A part of the wall (height 3.00 m, breadth 0.30 m) was chosen to represent the "flow area" of the wall corresponding to the clearance on one of the two long sides of the beam end. The back wall itself is assumed to be air tight. The network used for the analysis is outlined below.



The roughness, ϵ , was put at = 0.005 m in the cavity and 0.001 m in the interstice. Test pressure difference was 20 Pa.

The resulting flow rate through the interstice around the beam is shown in the following figure as well as the percentage of the pressure drop across the interstice compared to the total drop. An alternative wall material (wood panel) is added too as comparison.

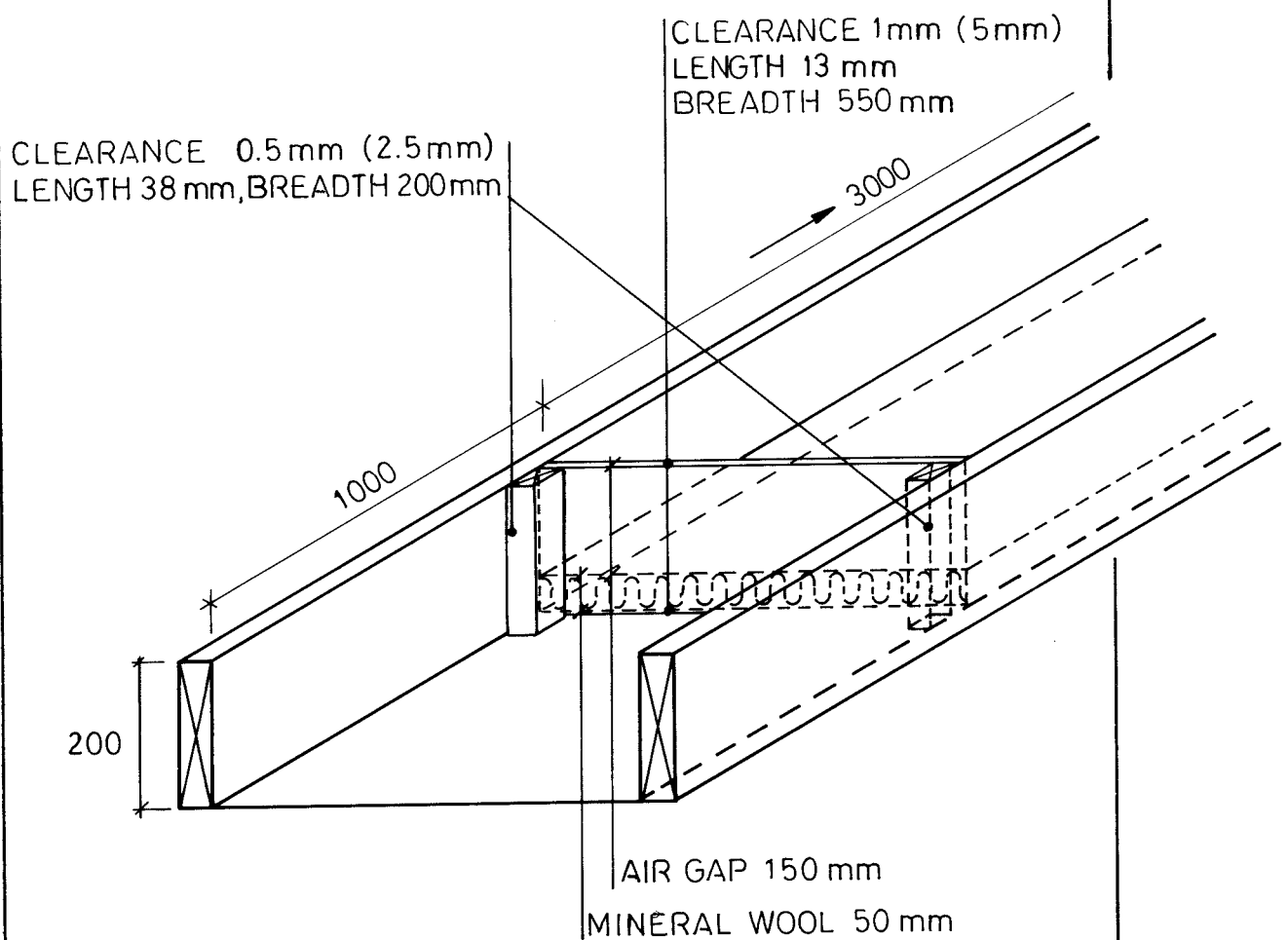


Example 12:

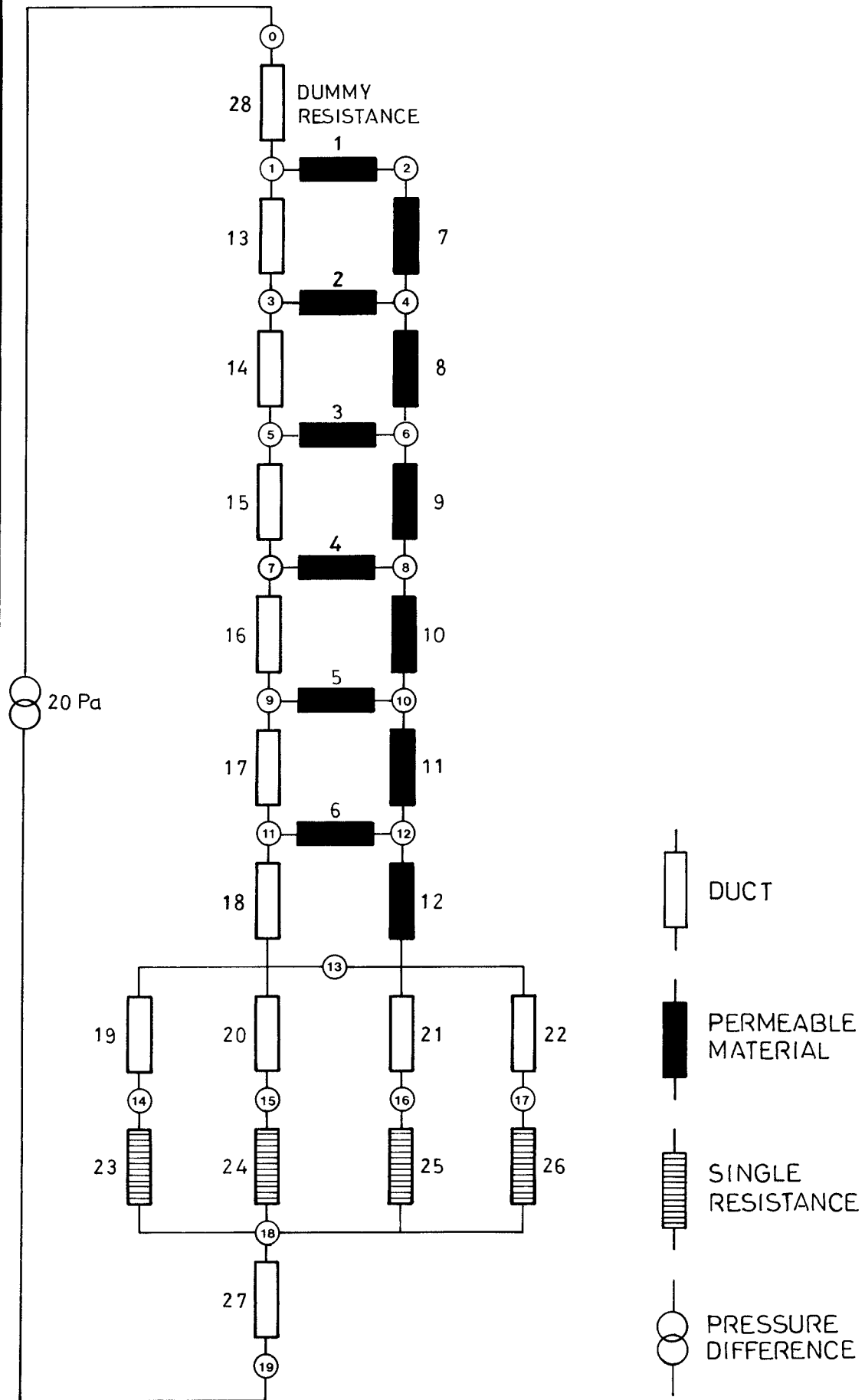
Air flow in the intermediate floor of a timber-framed house.

Many people living in 1½-storey timber-framed houses with intermediate floors of a wood structure complain about cold floors on the second floor. This example demonstrates the influence of different levels of accuracy in size for a wood fibre board plate meant to protect the floor from internal air movements.

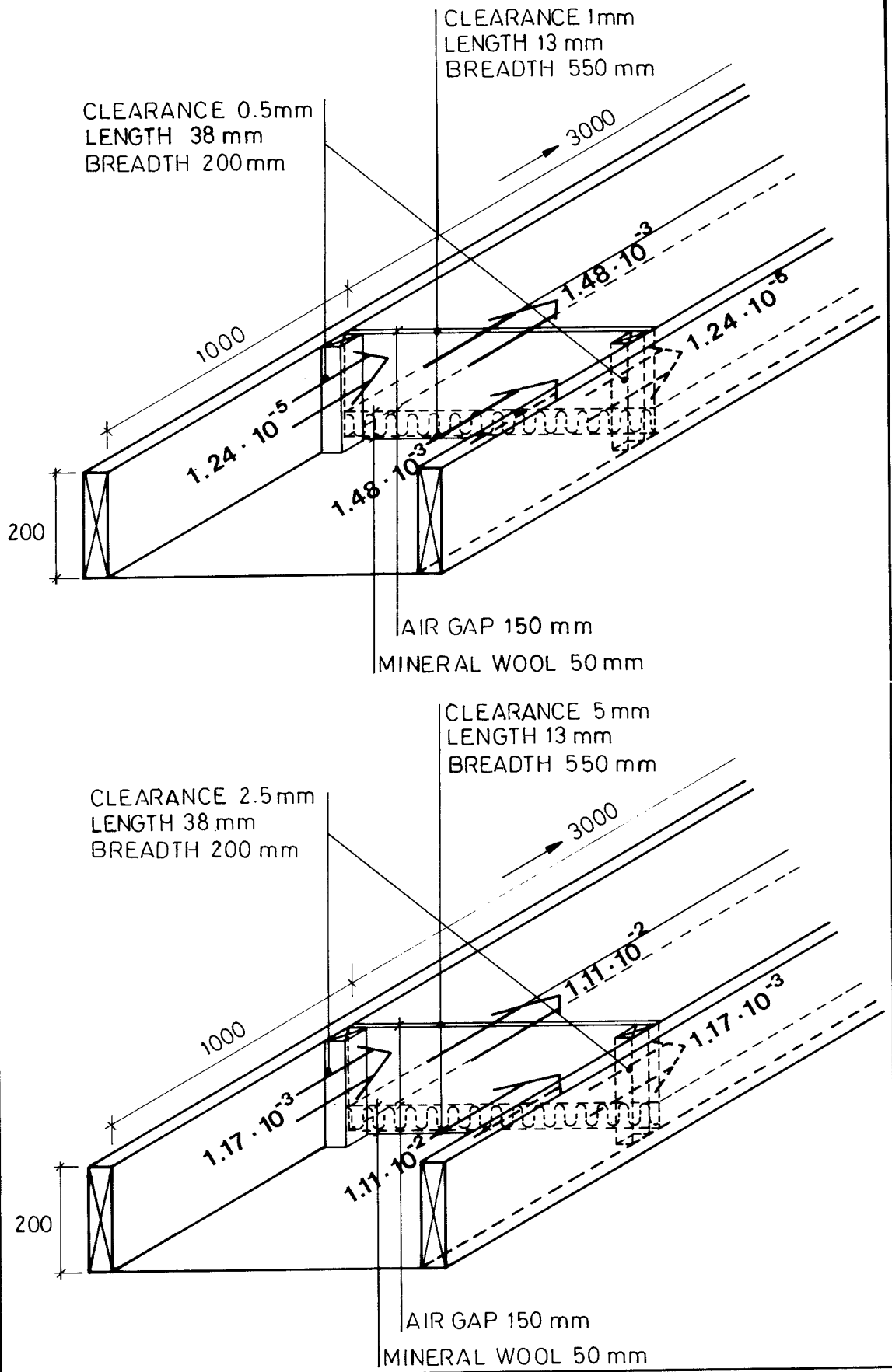
The design is outlined in the figure below.



Resistance network:



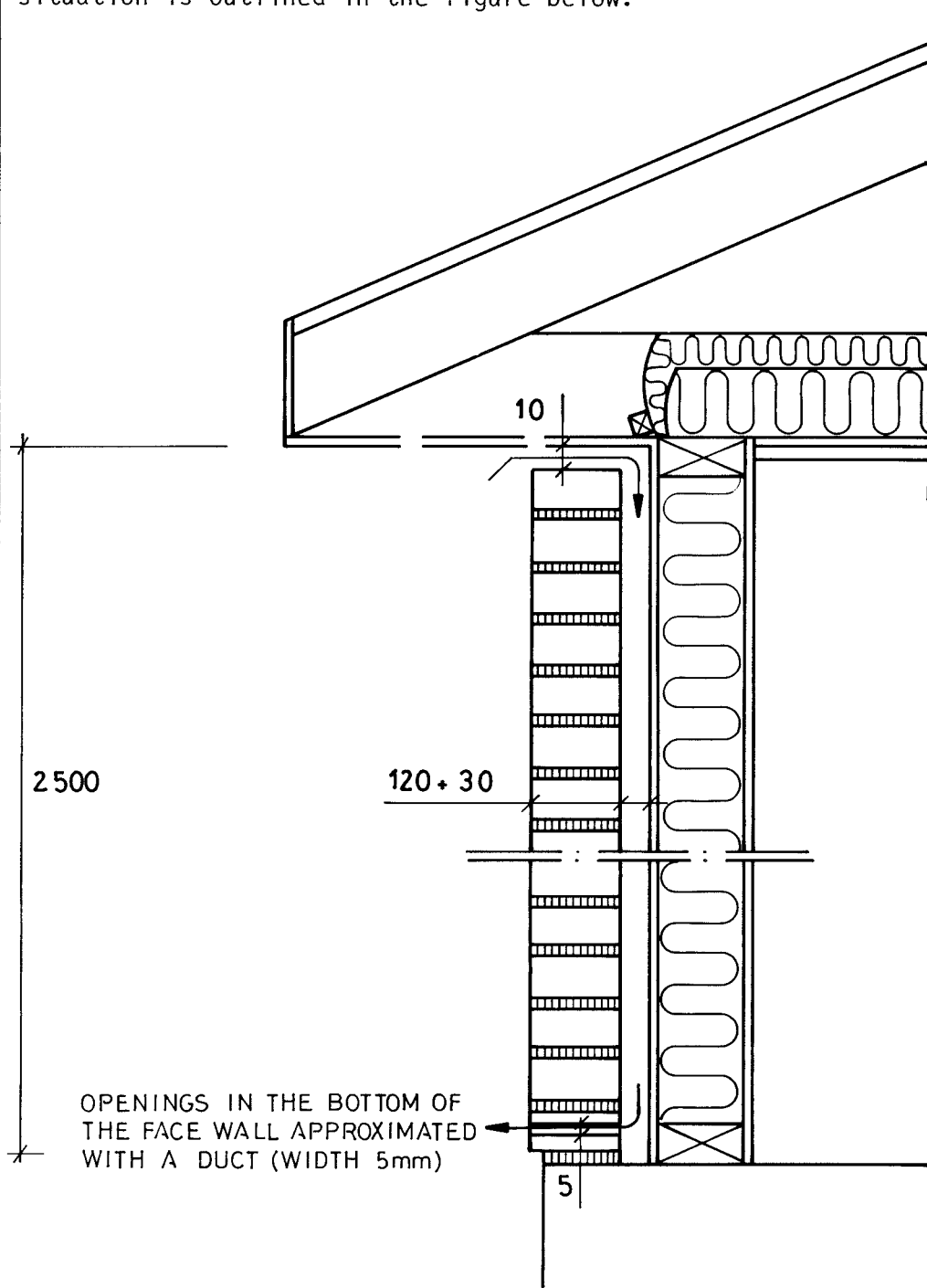
Resulting air flows (m^3/s)



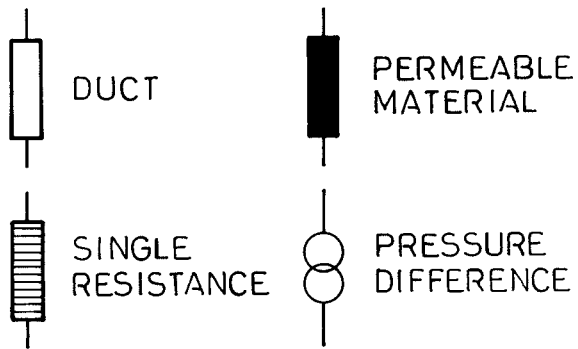
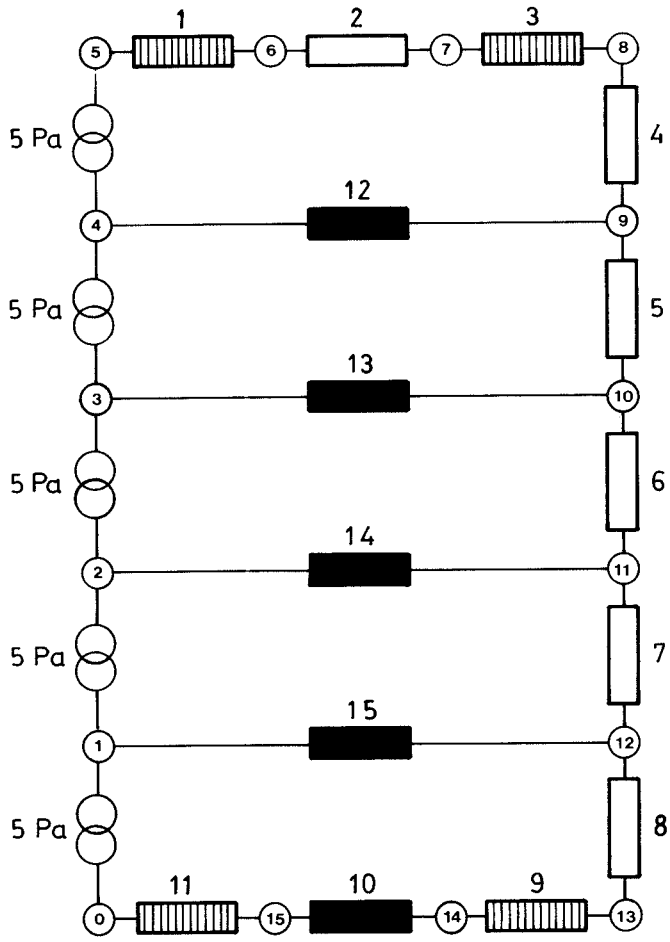
Example 13:

Stud wall with permeable face wall.

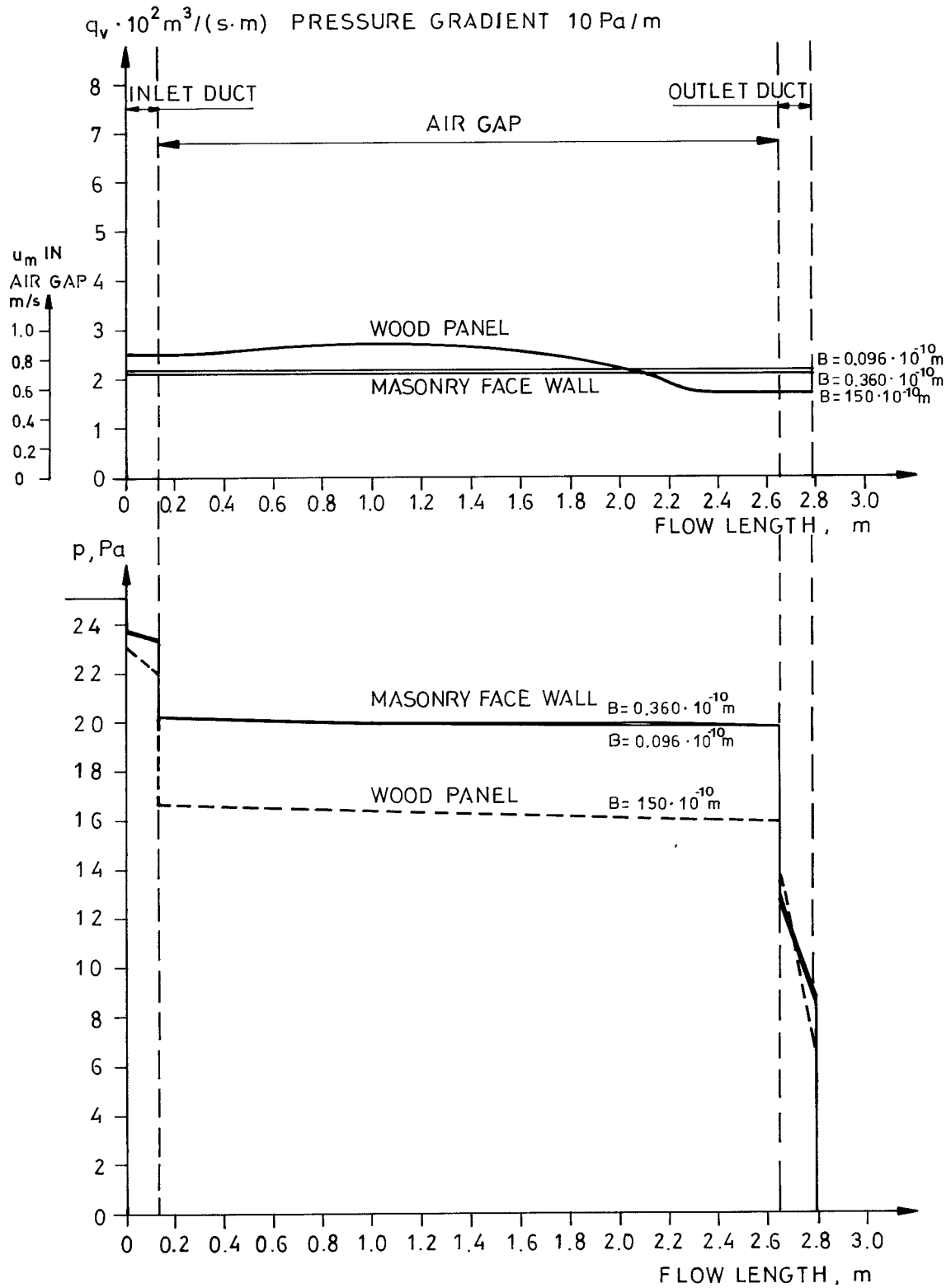
A great deal of effort has been spent on studies on air flows in stud walls of different designs and workmanships. Bankvall (1977). One interesting point among many others is the problem of determining the air velocity in an air gap between the stud wall and the permeable face wall under influence of a pressure gradient along the facade. The flow situation is outlined in the figure below.



Resistance network:



Results:

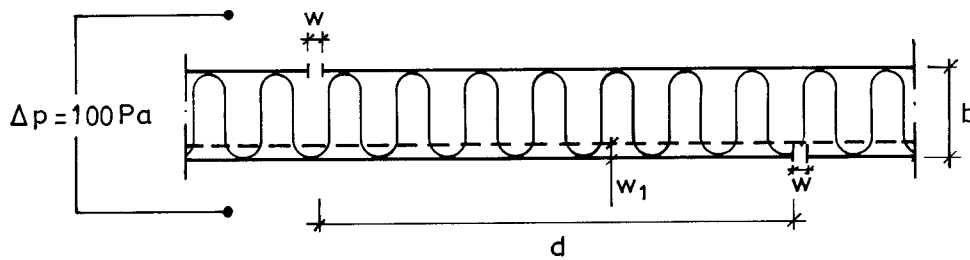


4.4.2.2 Examples of computer calculations by means of relaxation

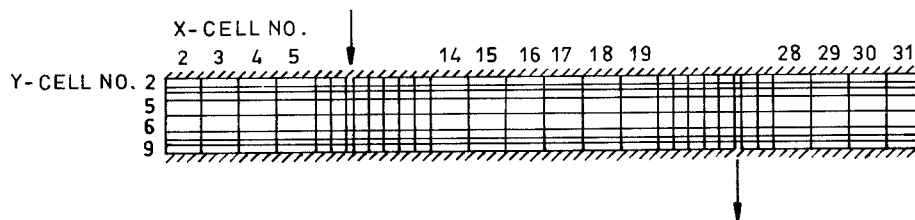
Example 21:

"Diagonal" flow in permeable material

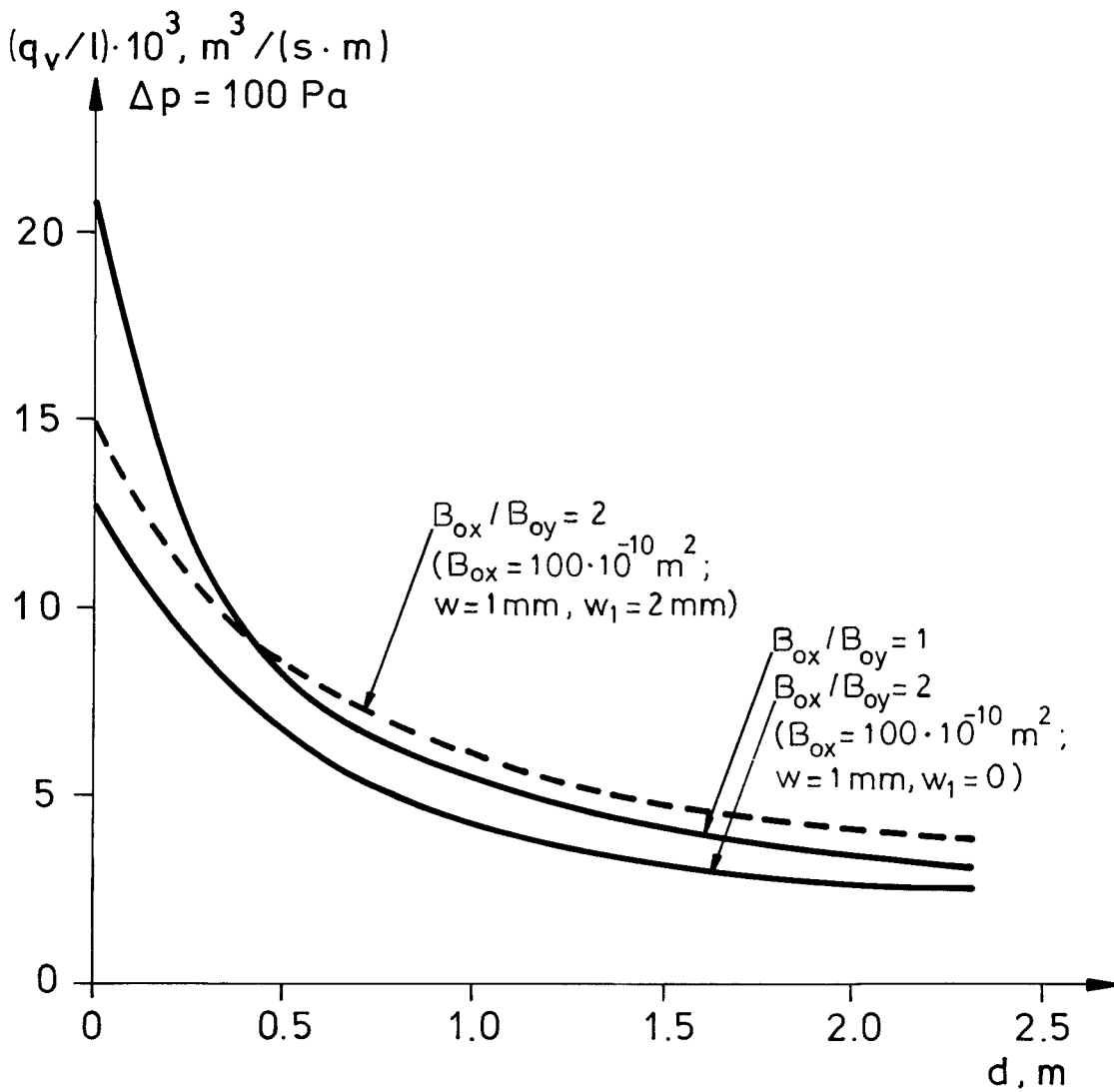
In many cases air flow perpendicular to the plane of a construction, e.g. a wall, is not the most relevant flow direction. Instead flow parallel or almost parallel to the sides may be of interest. Consider the following flow geometry!



For the computer calculation the geometry of the construction must be divided into small rectangular elements. The layout of the elements is called the mesh. One of the meshes used for this calculation is shown below.



RESULT:

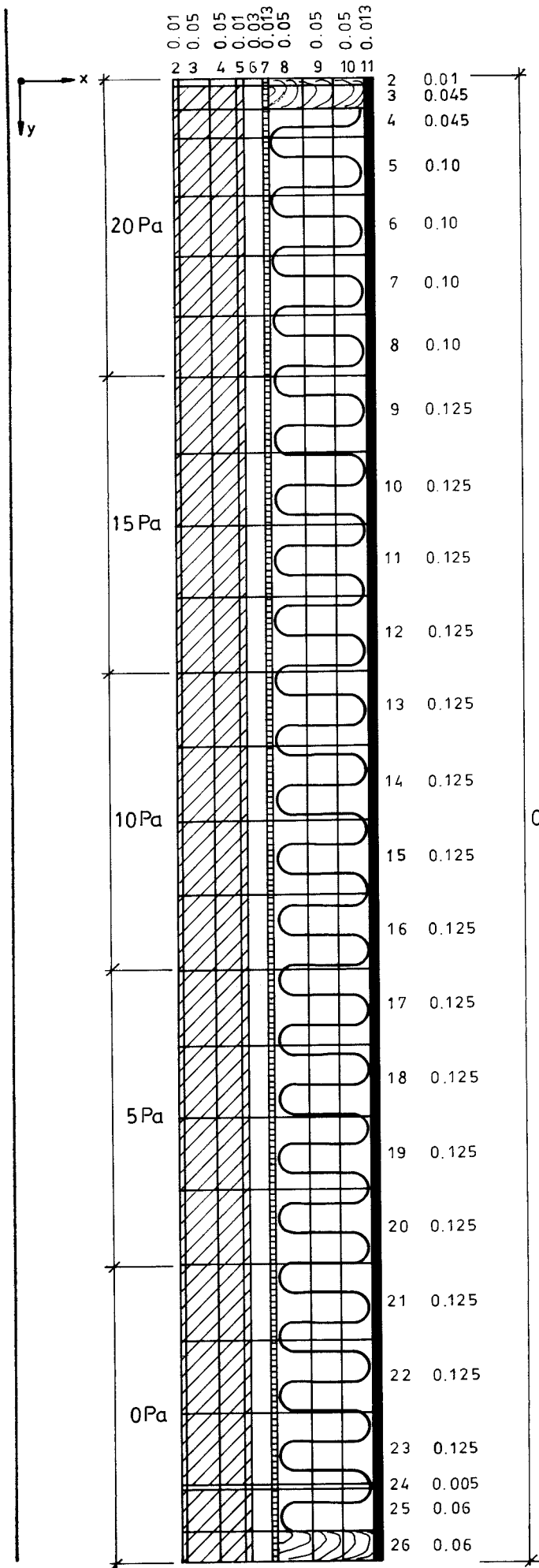



A calculation has also been done for a case with a small air gap between the insulation and one of the sides of the construction. The width (0.002 m) was studied and the result is given in the diagram (the dotted line). As can be expected, the flow rate gets larger than the corresponding case without any air gap.


Example 22:

Stud wall with permeable face wall

The construction is similar to that of example 13. The mesh, the materials and boundary conditions are shown below.




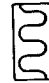
 MASONRY
 $B = 0.096 \cdot 10^{-10} \text{ m}^2, P$
 $0.36 \cdot 10^{-10} \text{ m}^2, O$


 WIND BARRIER
 ASPHALT IMPREGNATED
 WOOD FIBRE BOARD PLATE
 $B_0 = 0.0494 \cdot 10^{-10} \text{ m}^2 ; OA, PA$

GLASS FIBRE BOARD PLATE
 $B_{ox} = 1.3 \cdot 10^{-10} ; OB, PB$
 $B_{oy} = 2.6 \cdot 10^{-10} ; OB, PB$

ORDINARY MINERAL WOOL
 $B_0 = \text{SEE BELOW} ; OC, PC$

 WOOD
 $B_0 = 1.0 \cdot 10^{-15} \text{ m}^2$

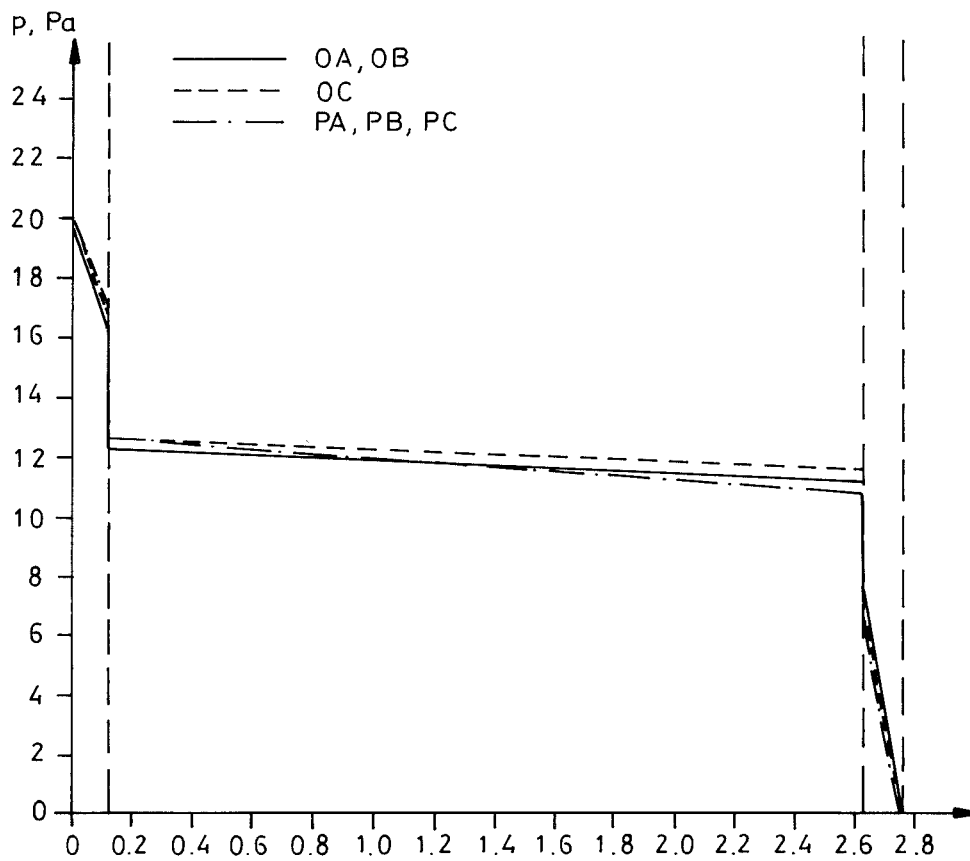
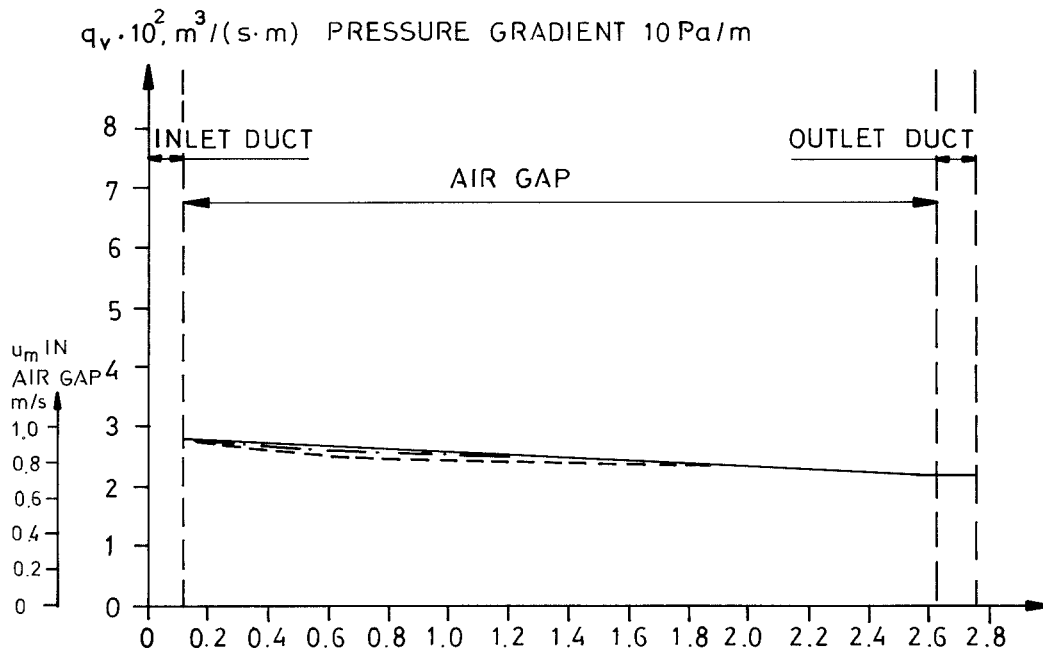
 MINERAL WOOL
 $B_{ox} = 50 \cdot 10^{-10} \text{ m}^2$
 $B_{oy} = 100 \cdot 10^{-10} \text{ m}^2$

 INNER LINING
 $B_0 = 37.7 \cdot 10^{-15}$

 AIR GAP

0 Pa

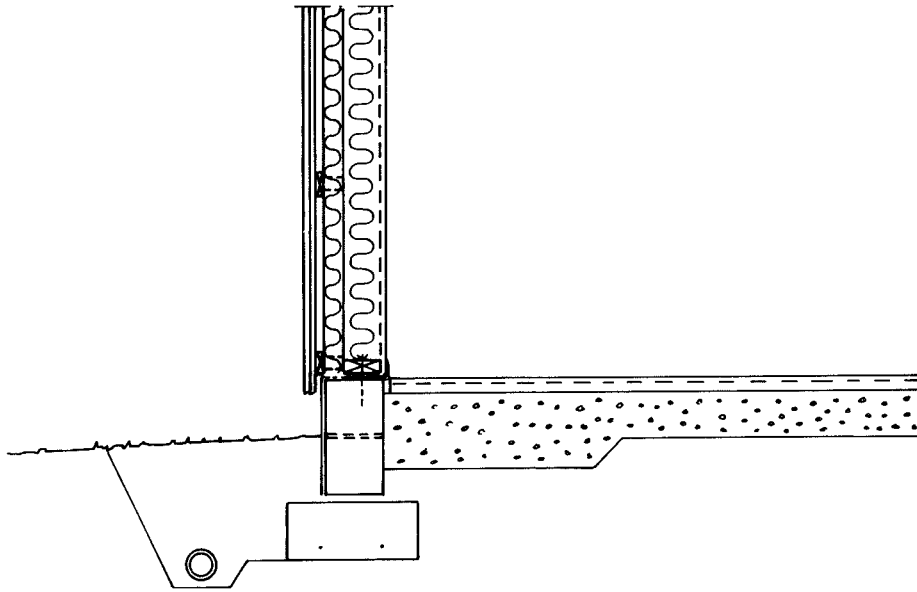
Result:



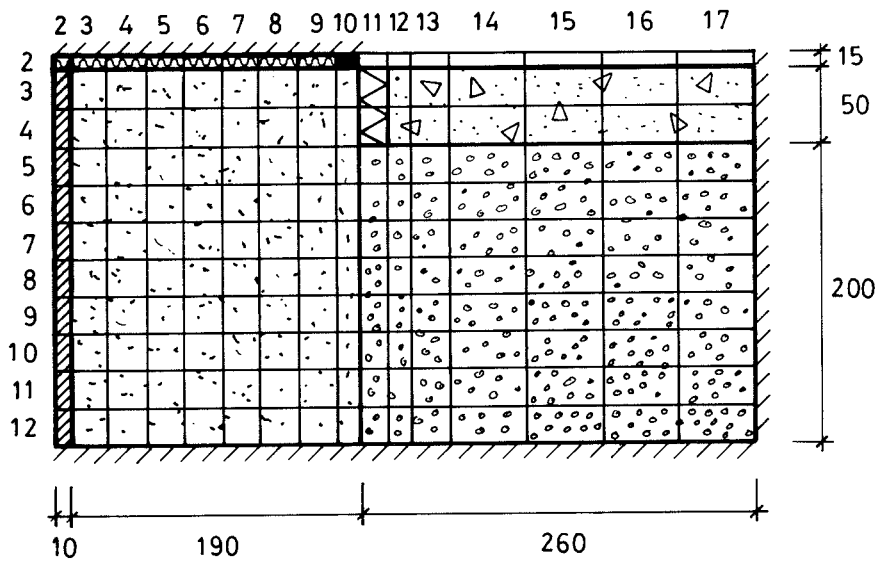
Example 23:








Edge beam of lightweight-aggregate concrete

Quite a common foundation type for houses is shown below.

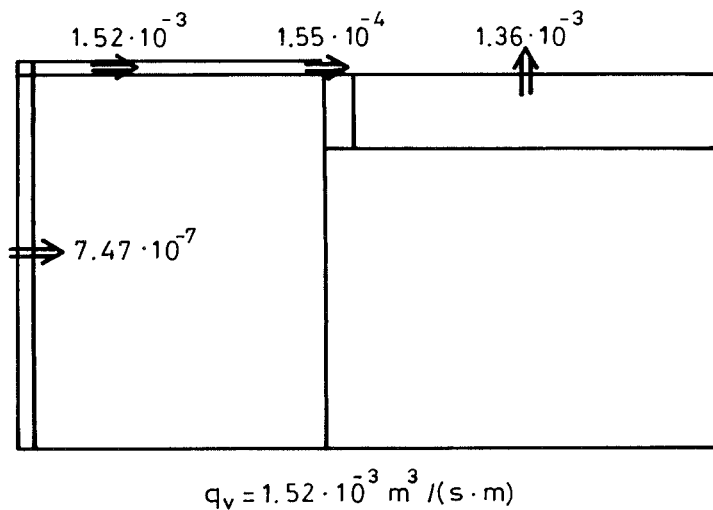


Mesh, dimensions, materials and material properties:

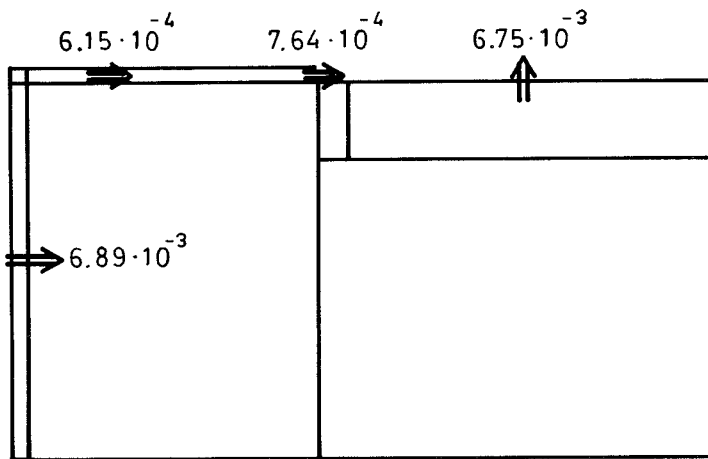


-  Building block of lightweight-aggregate concrete
 $B_0 = 60 \cdot 10^{-10} \text{ m}^2$
-  Rendering, lime cement mortar or alternatively no rendering.
 $B_0 = 6.0 \cdot 10^{-5} \text{ m}^2$
-  Caulking of compacted mineral wool
 $B_0 = 1.0 \cdot 10^{-10} \text{ m}^2$
-  Jointing mastic or alternatively caulking
 $B_0 = 1.0 \cdot 10^{-20} \text{ m}^2$
-  Polystyrene cellular plastic
 $B_0 = 50 \cdot 10^{-10} \text{ m}^2$
-  Concrete
 $B_0 = 1.0 \cdot 10^{-15} \text{ m}^2$
-  Shallow stabilized bed of haydite
 $B_0 = 800 \cdot 10^{-10} \text{ m}^2$

Resulting air flow rates at a pressure difference between inside and outside the house of 100 Pa:

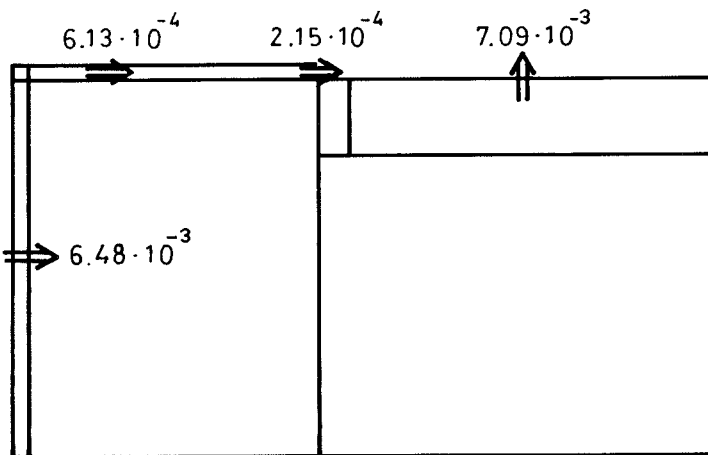


RENDERED



$$q_v = 7.51 \cdot 10^{-3} \text{ m}^3 / (\text{s} \cdot \text{m})$$

NO RENDERING



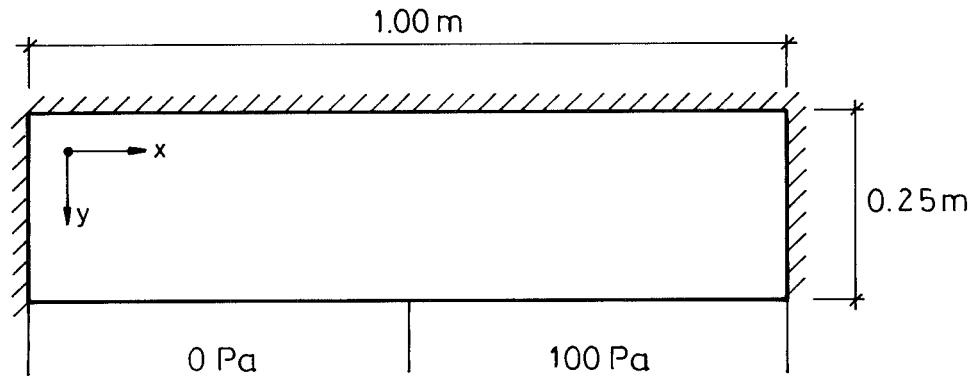
$$q_v = 7.09 \cdot 10^{-3} \text{ m}^3 / (\text{s} \cdot \text{m})$$

NO RENDERING, JOINTING MASTIC IN CELL (10, 2)

Example 24:

By-pass flow through air permeable material

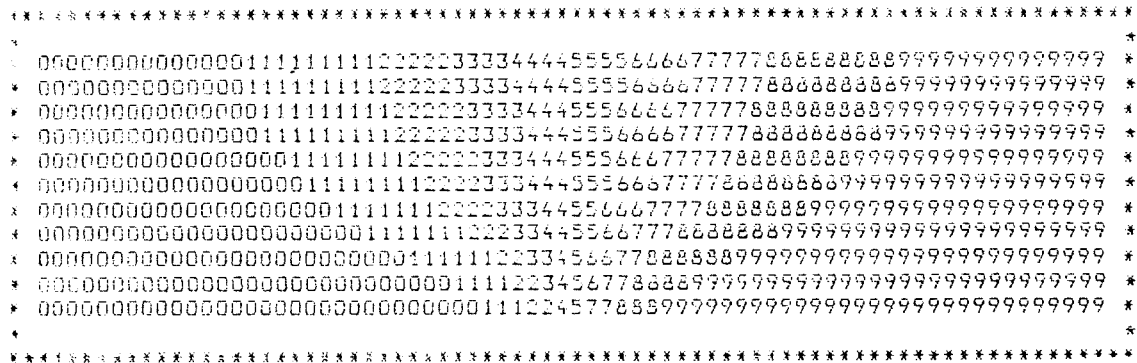
If two adjacent spaces have a wall in common, by-pass flow is likely to occur if the wall is made of an air-permeable material. The geometry and boundary conditions of the flow case investigated are shown below.



Three materials were investigated:

- Lightweight concrete $B_0 = 100 \cdot 10^{-15} \text{ m}^2$
- Wood wool slab $B_0 = 500 \cdot 10^{-10} \text{ m}^2$
- Mineral wool $B_{0x} = 100 \cdot 10^{-10} \text{ m}^2$
 $B_{0y} = 50 \cdot 10^{-10} \text{ m}^2$

Result:



Pressure distribution. Lightweight concrete. $q_{v,by-pass} = 6.29 \cdot 10^{-7} \text{ m}^3 / (\text{s} \cdot \text{m})$.

5 FLUCTUATING VS. STEADY STATE PRESSURE DIFFERENCES

The whole content of this work has hitherto been based on the assumption of steady state pressure differences causing the air flow. For most cases this is probably a proper assumption. However, if further investigations of the real nature of air infiltration, for example, is to be undertaken, unsteady state pressure differences are likely to be taken into account.

5.1 THE NATURE OF THE FLUCTUATIONS

There are principally three possible ways for pressure differences across a building component to occur. The pressure differences may be caused by:

- o wind
- o density differences between warm and cold air
- o the ventilation system

While the latter two create rather steady pressure differences, wind always implies fluctuating pressure differences.

The instantaneous value of the wind velocity is often written:

$$u(t) = \bar{u} + \delta u(t) \quad (5.1.a)$$

where

\bar{u} is the time average of the wind velocity and $\delta u(t)$ a randomly fluctuating component added to \bar{u} .

The standard deviation, σ_u , can be estimated by:

$$\sigma_u^2 = \frac{1}{t} \int_0^t (u(t) - \bar{u})^2 dt = \frac{1}{t} \int_0^t \delta u(t)^2 dt$$

where t is the time used for averaging. A commonly used value of t is 10 minutes, since this is the time used by meteorological stations to create the average value of the wind velocity.

The value of the average, \bar{u} , at a place near a building is affected by a number of different factors, such as:

- o geographical location
- o height above ground
- o atmospheric turbulence
- o turbulence caused by the surroundings and roughness of ground.

If the wind velocity at a place is studied, certain periodical elements may be observed. Hence, a so-called wind energy spectrum can be achieved. Perhaps the most commonly quoted one is that of van der Hoven - van der Hoven (1957). Figure 5.1.a.

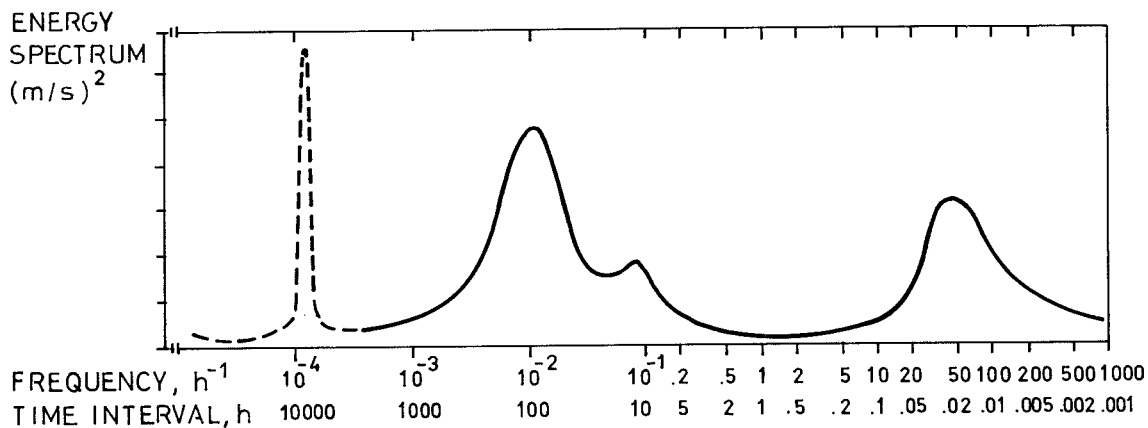


FIG. 5.1.a. Energy spectrum of the horizontal wind velocity component 100 m above ground at Brookhaven, N.Y., USA. After van der Hoven (1957).

From the figure it can be seen that there exists a number of peaks corresponding to different frequencies. Thus the first one is associated with one year variations, the second one corresponds to the passages of depressions with a time interval of approximately 4 days at this particular place. The third weak peak is related to wind velocity variation twice a day and the fourth to what is called turbulence. In this case the corresponding frequency lies around 40 h^{-1} i.e., as an average, one wind gust

every 1.5 minute. The frequency of what can be called the turbulence peak is not very stable but depends to quite a degree on the vertical temperature gradient. If this is strongly positive, which is the case on clear, cold nights the frequency can be as high as 0.1 s^{-1} , while on a hot day with negative temperature gradient the frequency will be $0.002 - 0.02 \text{ s}^{-1}$. Israelsson (1979), Lumley & Panofosky (1964). At frequencies above the peak the line in the energy spectrum decreases exponentially with an exponent of $-5/3$, Kolmogorov (1941), and no more peaks occur at higher frequencies - the fluctuations become exclusively random.

To study this, some studies were made of the wind pressure acting at the 3rd floor of a south facing wall of the laboratory building of the School of Civil Engineering, Lund Institute of Technology. The pressure difference was measured by means of an electrical micro manometer - Furness Control Ltd - and measurement values were sampled every 0.175 s. A total of 1024 samples were taken in each experiment and the measurement values were stored in the memory of a memory oscilloscope and eventually transferred on to paper tape by means of a tape puncher. The recorded time series of wind pressure data was analysed by means of a spectral analysis subroutine package - IDPAC - developed at the Department of Automatic Control at Lund Institute of Technology, Wieslander (1980).

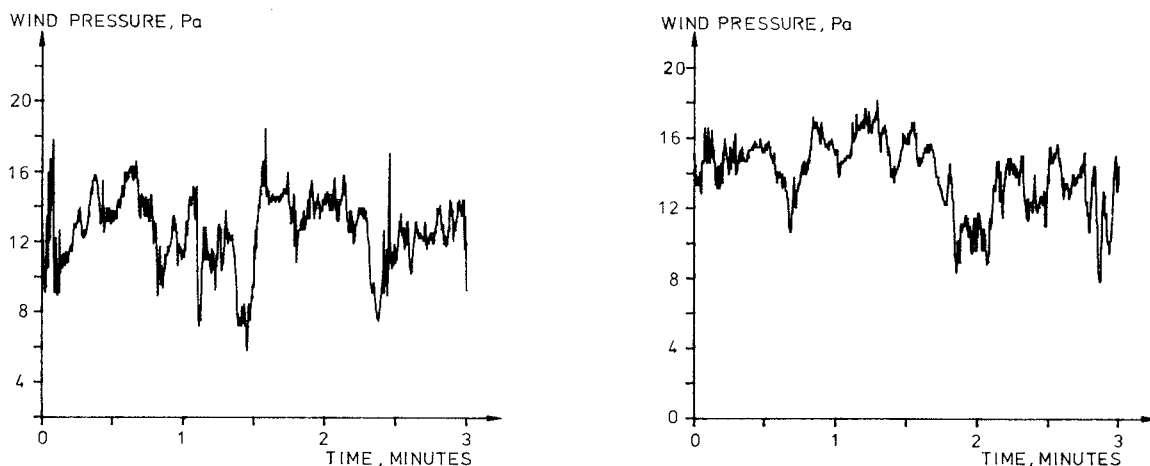


FIG. 5.1.b. Wind pressure vs. time.

	(a)	(b)
Mean	12.27	14.00
Standard deviation	2.47	1.91

Figure 5.1.b shows the realizations of the two monitored time series. In each of them a trend was found - figure 5.1.c - which was subtracted from the measurement values in the spectral analysis performed later on.

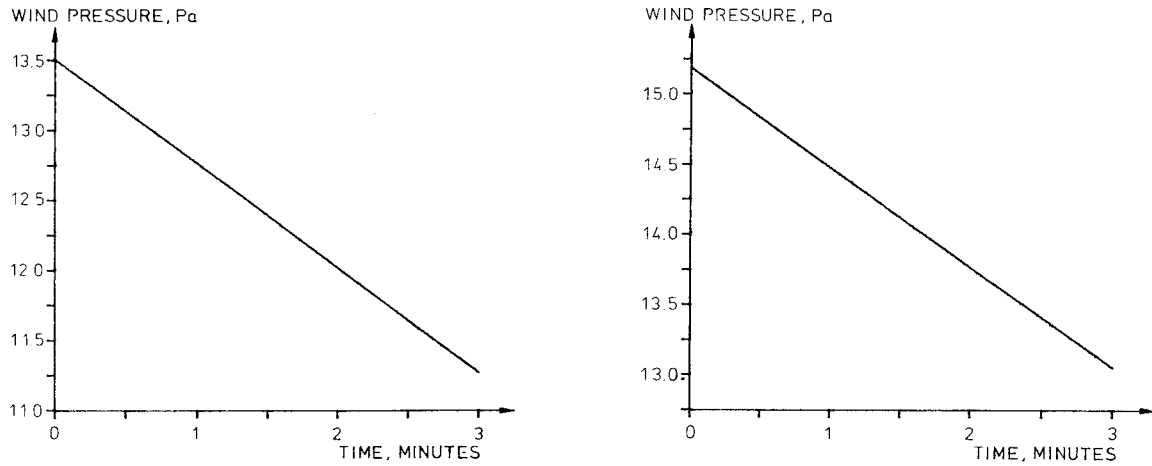


FIG. 5.1.c. The trends in the time series.

The spectral analysis was performed with so-called discrete Fourier transformation, and the results can be seen in figure 5.1.d, which shows the amplitude spectrum.

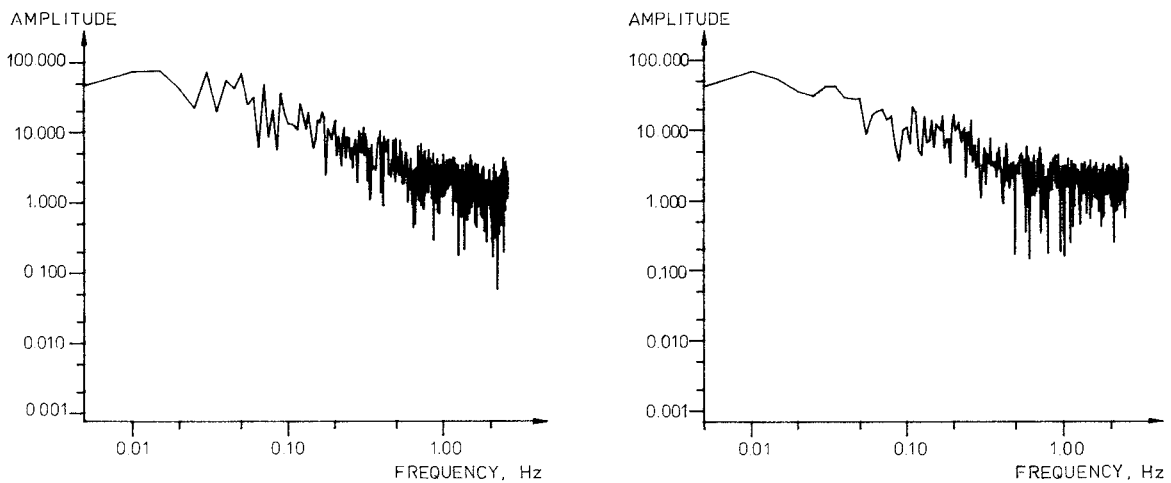


FIG. 5.1.d. Amplitude spectrum. Discrete Fourier Transform.

From the spectra it can be seen, at least in this experiment, that there obviously do not exist any peaks in the high frequency range. Hence, even as far as pressure fluctuations are concerned, the Kolmogorov assumption seems reasonable.

Apart from fluctuations in pressure caused by direct wind fluctuations there exist other pressure fluctuation phenomena too, which may cause air infiltration. These will not be discussed here, but it may not be out of place to mention for example the concept of air exchange by penetration of eddies, Malinowski, (1971) and that of turbulent diffusion, (Cockroft & Robertson (1976) and Warren (1977)). A good abstract of these matters is given in Handa et al (1979).

5.2 PRESSURE DISTRIBUTION UNDER FLUCTUATING PRESSURE CONDITIONS

In permeable material the same kind of physical behaviour concerning potentials and resulting potential flow is likely to occur as that of other potential flow situations. A differential equation, based on a formulation of Darcy's Law, and simplified in the way that

$$\rho \cong \rho_0 + \kappa_{\text{air}} \cdot \rho_0 (p - p_0) \quad (5.2.a)$$

where

ρ = density of the air, kg/m^3

ρ_0 = density when $p = p_0$, kg/m^3

κ_{air} = compressibility of the air, Pa^{-1}

p = pressure, Pa

p_0 = original pressure, Pa

and assuming that the permeable medium is elastic with compressibility κ_m is (Scheidegger (1963)):

$$a \frac{\partial^2 p}{\partial x^2} = \frac{\partial p}{\partial t} \quad (5.2.b)$$

where the "air diffusivity", a (m^2/s), is

$$a = \frac{B_0}{\eta (P \cdot \kappa_{\text{air}} + \kappa_m)} \quad (5.2.c)$$

where P is the porosity of the permeable material and κ_m is the compressibility of the material.

In analogy with heat conduction for example, certain combinations of a , l (length) and t (time) have a physical interpretation. Thus the length scale \tilde{l} of an unsteady state problem is described by:

$$\tilde{l} = \sqrt{a \cdot t} \quad (5.2.d)$$

and the time scale, \tilde{t} :

$$\tilde{t} = \frac{l^2}{a} \quad (5.2.e)$$

In the following some solutions of the governing differential equation will be penetrated.

One dimensional flow is studied. The limits are $x = 0$ and $x = L$.

A. Time domain solution

In this case the response of a step change is investigated. The step change is described by:

$$\begin{aligned} p &= p_0 \text{ for } x = 0 \text{ at all times} \\ p &= p_1 \text{ for } x = L \text{ at all times} \\ p &= p_0 \text{ everywhere for } t = 0 \end{aligned}$$

The solution of this problem can be shown to be:

$$p = p_0 - (p_0 - p_1) \frac{x}{L} + \frac{2}{\pi} (p_0 - p_1) \cdot \sum_{n=1}^{\infty} \frac{(-1)^{n-1}}{n} \cdot e^{-\frac{n^2 \pi^2 a}{L^2} t} \cdot \sin\left(\frac{n\pi}{L} \cdot x\right) \quad (5.2.f)$$

which can be verified by derivation.

In order to give a series of "standard" solutions, it is convenient to introduce the following dimensionless parameters:

$$\varepsilon = \frac{x}{L} \quad (\text{relative length}) \quad (5.2.g)$$

$$F = 2 \cdot \frac{a}{L^2} \cdot t \quad (\text{relative time}) \quad (5.2.h)$$

$$W = \frac{p_0 - p}{\varepsilon(p_0 - p_1)} \quad (\text{relative pressure}) \quad (5.2.i)$$

In this notation eq. (5.2.d) can be written:

$$W = 1 - \frac{2}{\varepsilon \cdot \pi} \sum_{n=1}^{\infty} \frac{(-1)^{n-1}}{n} \cdot e^{-\frac{n^2 \pi^2 \cdot F}{2}} \cdot \sin(n\pi\varepsilon) \quad (5.2.k)$$

In figure 5.2.a a series of solutions of eq. (5.2.h) are given.

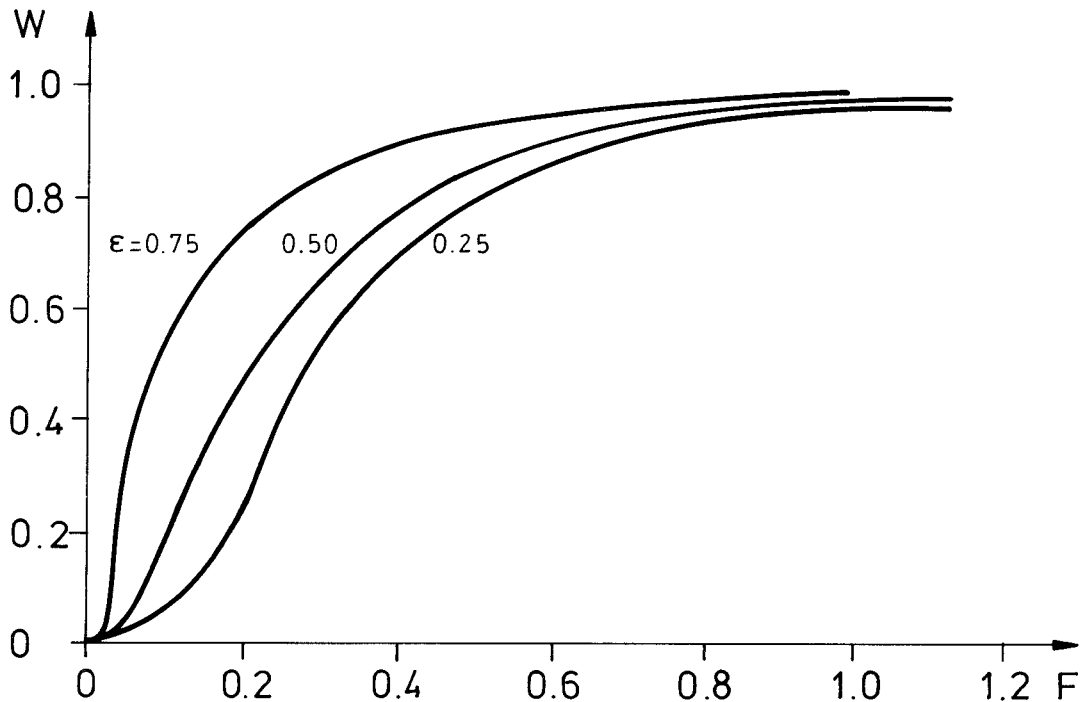


FIG. 5.2.a. A series of time domain solutions for linear unsteady state flow in porous media. After Shchelkachev (1946).

Example

Consider a plate of a porous material, 0.50 m thick. Let the pressure on one side ($x = L$) equal 100 Pa ($= p_1$) and let the initial pressure in the material and constant on the other side ($x = 0$) equal 0 Pa ($= p_0$). Study pressure vs. time in the middle of the specimen ($x/L = 0.5$)!

$$\frac{x}{L} = \epsilon = 0.5; \quad W = \frac{p_0 - p}{\epsilon(p_0 - p_1)} = \frac{-p}{0.5(-100)} = \frac{p}{50}$$

Mineral wool:

$$a = \frac{B_0}{\eta \cdot (P \cdot \kappa_{\text{air}} + \kappa_m)} = \frac{50 \cdot 10^{-10}}{17.5 \cdot 10^{-6} (0.99 \cdot 0.99 \cdot 10^{-5} + 0)} = 29.2 \text{ m}^2/\text{s}$$

$$t = 0.01 \text{ s} \Rightarrow$$

$$F = 2 \cdot \frac{a}{L^2} \cdot t = 2 \cdot \frac{29.2}{0.5^2} \cdot 0.01 = 2.33$$

From figure 5.2.a it can be seen that if $\epsilon = 0.5$ and $F = 2.33$ then $W = 1$ and $p = 50 \cdot W = 50 \text{ Pa} \Leftrightarrow$ equilibrium state. If $t = 0.001 \text{ s}$ then $F = 0.233$ and $W = 0.54 \Rightarrow p = 50 \cdot 0.54 = 27 \text{ Pa}$.

In the same way

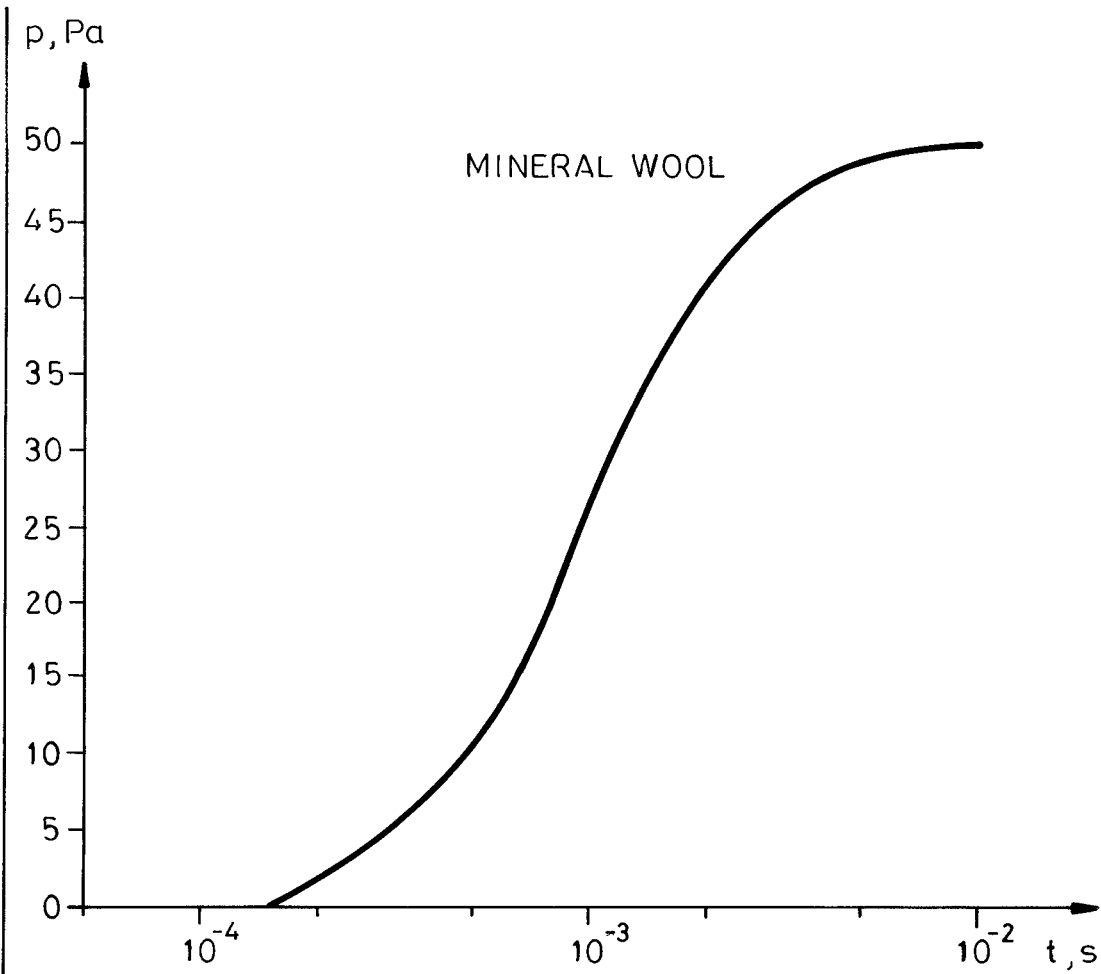
$$t = 0.002 \text{ s} \Rightarrow F = 0.466 \Rightarrow W = 0.83 \Rightarrow p = 41.5 \text{ Pa}$$

$$t = 0.0005 \text{ s} \Rightarrow F = 0.117 \Rightarrow W = 0.219 \Rightarrow p = 10.9 \text{ Pa}$$

$$t = 0.0002 \text{ s} \Rightarrow F = 0.047 \Rightarrow W = 0.039 \Rightarrow p = 1.95 \text{ Pa}$$

$$t = 0.004 \text{ s} \Rightarrow F = 0.932 \Rightarrow W = 0.969 \Rightarrow p = 48.4 \text{ Pa}$$

The figure below shows the pressure rise in the middle of the plate ($x = 0.25 \text{ m}$).

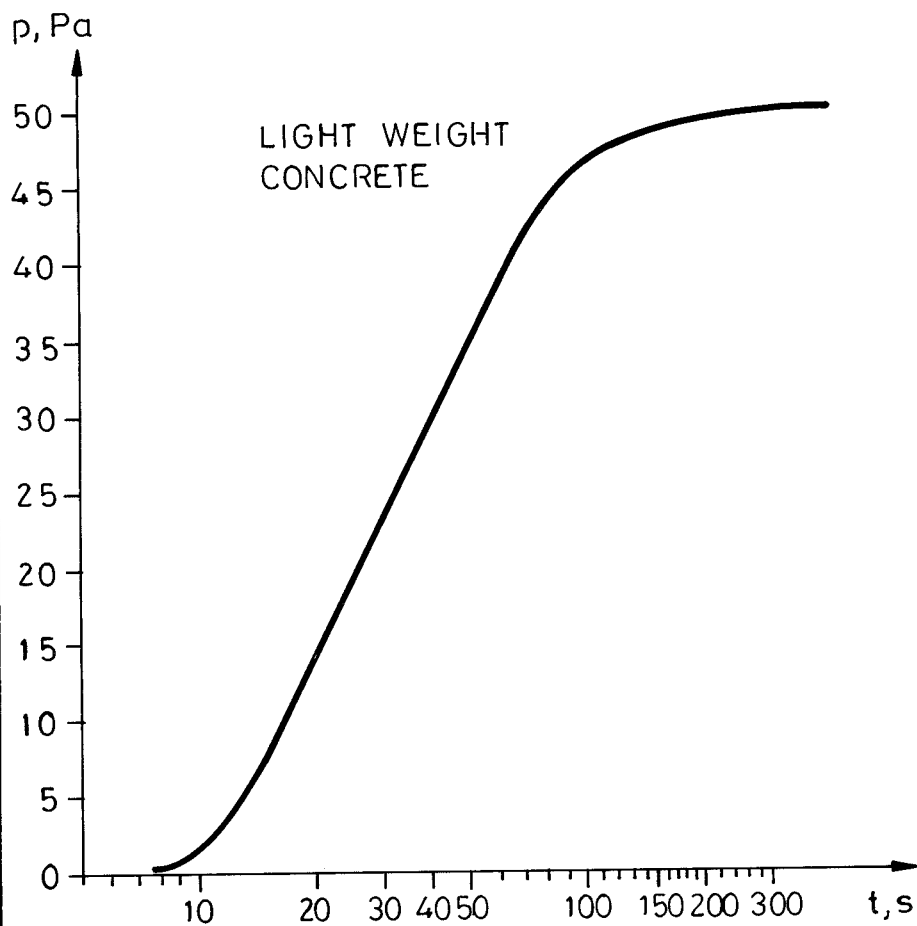


Lightweight concrete:

$$a = \frac{100 \cdot 10^{-15}}{17.5 \cdot 10^{-6} (0.70 \cdot 0.99 \cdot 10^{-5} + 0)} = 8.2 \cdot 10^{-4} \text{ m}^2/\text{s}$$

$$F = 2 \cdot \frac{8.2 \cdot 10^{-4}}{0.5^2} \cdot t = 6.56 \cdot 10^{-3} \cdot t$$

The resulting curve for this material is shown below.



In the case of laminar flow in a duct of width = b the specific permeability coefficient may be replaced by $b^2/12$; cf. eq. 2.3.2.1.d. $P = 1$ and $\kappa_{\text{mat}} = 0$. Thus:

$$a = \frac{b^2}{12 \eta \cdot \kappa_{\text{air}}} \quad (5.2.1)$$

The time for establishing equilibrium state is very short for ducts. For $b = 0.001$ m

$$a = \frac{10^{-6}}{12 \cdot 17.5 \cdot 10^{-6} \cdot 0.99 \cdot 10^{-5}} = 481 \text{ m}^2/\text{s}$$

If $l = 0.1$ m the time scale, $\tilde{t} = \frac{l^2}{a}$, indicates a time of only $0.01/481 = 2.1 \cdot 10^{-5}$ s to create equilibrium.

B. Frequency domain solution

Consider a case according to figure 5.2.b.

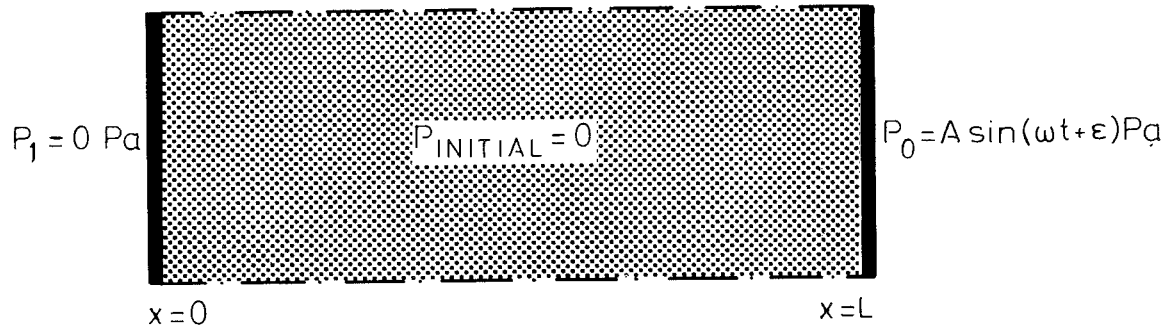


FIG. 5.2.b. Initial and boundary conditions. Frequency domain solution.

The analytical solution, using a complex number calculation procedure, is, Carslaw & Jaeger (1959):

$$p = A \sin(\omega t + \epsilon + \phi) + 4\pi a \sum_{n=0}^{\infty} \left(\frac{(-1)^n (2n+1) (4L^2 \omega \cos - a(2n+1)^2 \cdot \pi^2 \cdot \sin \epsilon)}{16L^4 \omega^2 + a^2 \pi^4 (2n+1)^4} \cdot e^{-a(2n+1)^2 \cdot \pi^2 t / 4l^2} \cdot \cos \frac{(2n+1)\pi x}{2l} \right) \quad (5.2.m)$$

where ϵ = initial phase angle lag,

$$A = \left(\frac{\cosh 2 kx + \cos 2 kx}{\cosh 2 kl + \cos 2 kl} \right)^{\frac{1}{2}} \quad (5.2.n)$$

$$\phi = \arg \left(\frac{\cosh kx (1 + i)}{\cosh kl (1 + i)} \right) \quad (5.2.o)$$

and

$$k = \left(\frac{\omega}{2a}\right)^{\frac{1}{2}} = \left(\frac{\pi f}{a}\right)^{\frac{1}{2}} \quad (5.2.p)$$

where ω = periphery velocity, rad/s and f = frequency, Hz.

The quantities A and ϕ which are the amplitude and phase of the pressure oscillations at the point x , are functions of the two dimensionless quantities x/L and $k \cdot L$. The variations of A and ϕ as functions of these two dimensionless quantities are shown in figure 5.2.2.c and figure 5.2.2.d.

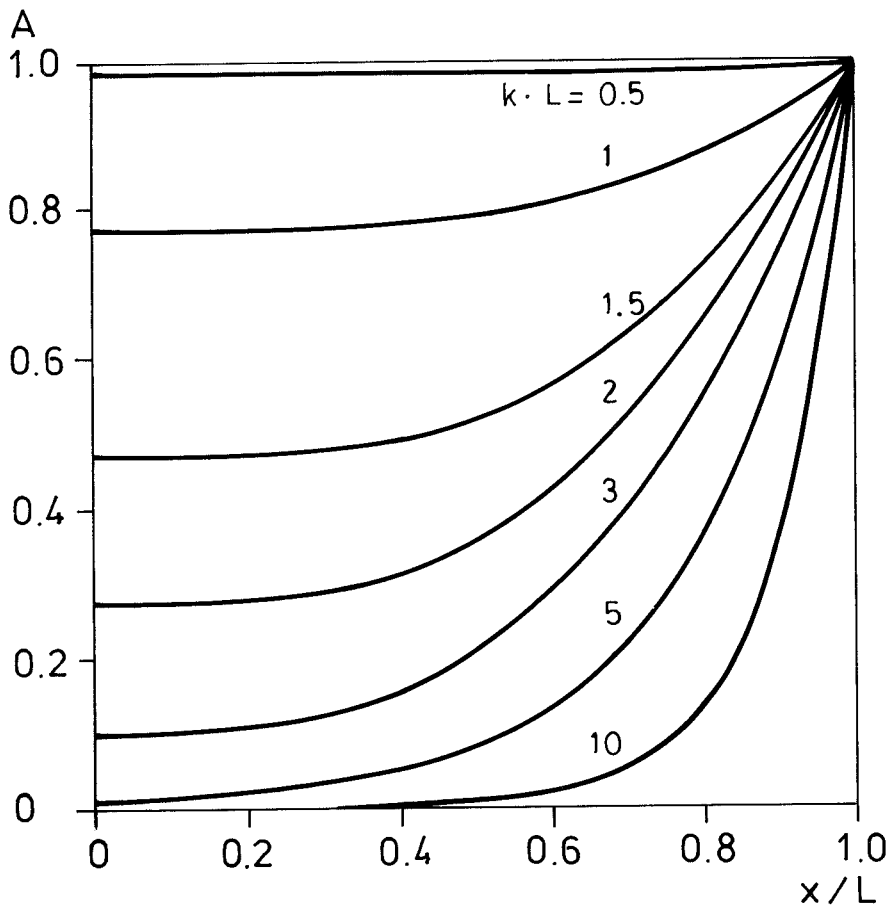


FIG. 5.2.c. Variation of amplitude of the steady oscillation of pressure in a slab caused by harmonic surface pressure.

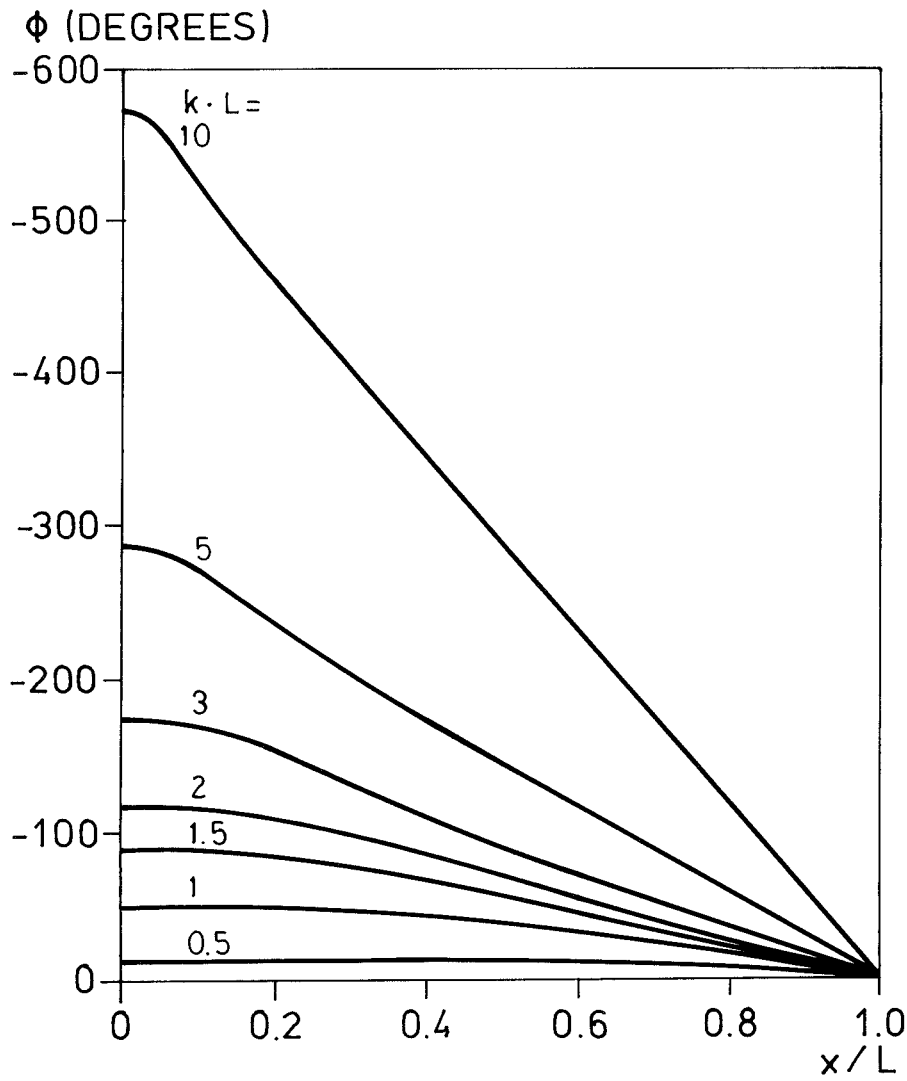


FIG. 5.2.d. Variation of phase of the steady oscillation of pressure in a slab caused by harmonic surface pressure.

To make the reader familiar with the magnitude of the parameter $k \cdot L$ figure 5.2.e shows how k varies for different frequencies and a -values.

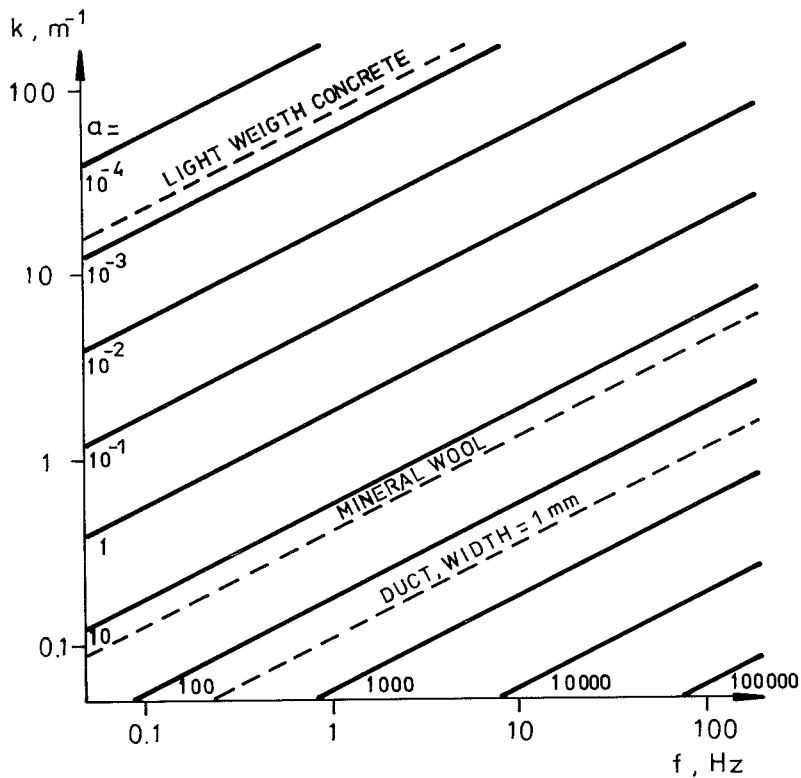


FIG. 5.2. e. k vs. f with α as a parameter.

5.3 AIR FLOW UNDER FLUCTUATING PRESSURE CONDITIONS

Suppose that for a certain flow passage the relationship between pressure differences, Δp , and flow rate, q_v , can be written

$$q_v = A \cdot \Delta p^B \quad (5.3.a)$$

where B is an exponent

$$0.5 \leq B \leq 1 \quad (5.3.b)$$

Now

$$\Delta p = p_0 - p_1 \quad (5.3.c)$$

where p_0 and p_1 are the pressures on the two ends of the flow passage.
Suppose $p_1 = 0$ and

$$p_0 = \bar{p}_0 + p_p \sin(\omega t) = \Delta p \quad (5.3.d)$$

i.e. the pressure difference is described by a harmonic pressure oscillation with the mean \bar{p}_0 and amplitude p_p .

Thus:

$$q_v = A (\bar{p}_0 + p_p \sin(\omega t))^B \quad (5.3.e)$$

We are interested in finding out how the time average of the flow rate, \bar{q}_v , depends on the exponent B and the amplitude p_p . It can be expected - figure 5.3.a - that \bar{q}_v gets smaller as the exponent varies from 1.0 towards 0.5. A high amplitude will be likely to work in the same direction i.e. lowering \bar{q}_v .

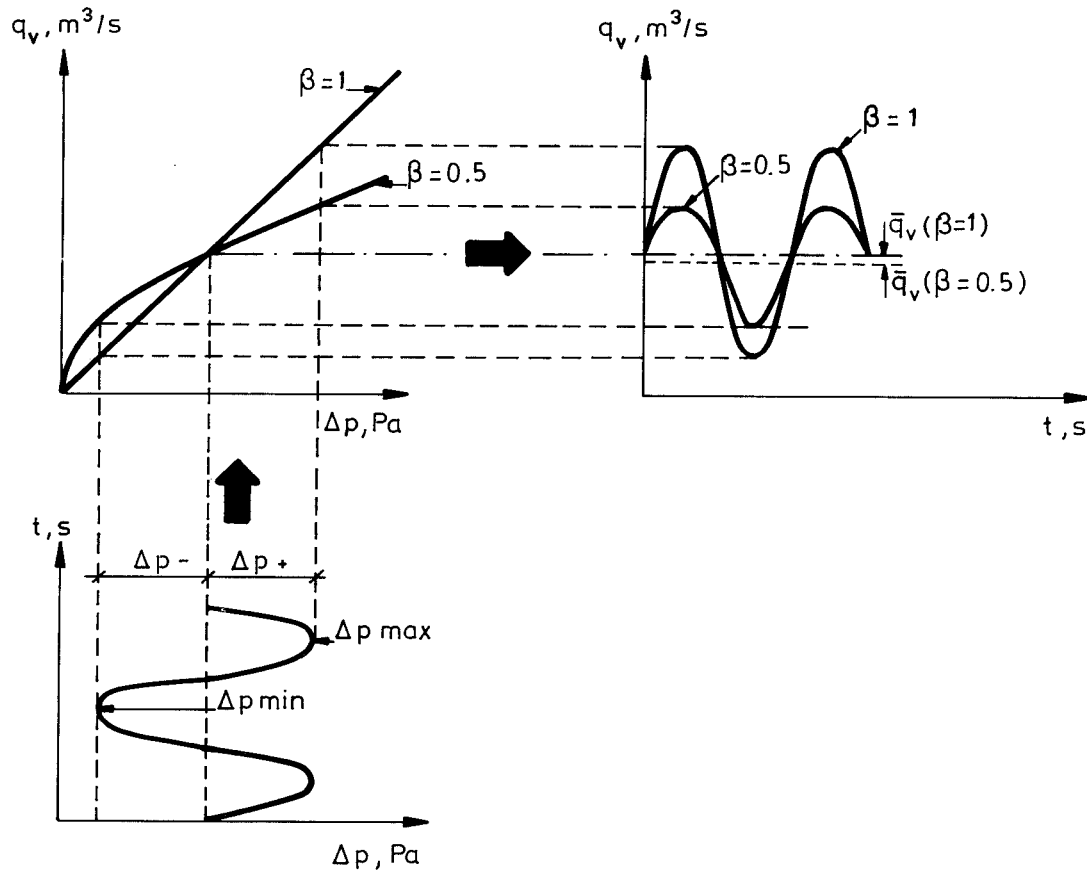


FIG. 5.3.a. The transfer procedure from fluctuating pressure difference to resulting air flow rate. Freely after Handa et al. (1979).

To be able to see the quantitative effects of non linear relationship between pressure difference and flow rate on the time averaged flow rate \bar{q}_V it is necessary in some way to integrate eq. 5.3.e over a period.

$$2\pi \cdot \bar{q}_V = \int_{t=0}^{2\pi/\omega} A (\bar{p}_0 + p_p \sin(\omega t))^B dt \quad (5.3.f)$$

This can hardly be done analytically, but it is a simple case to do it numerically. The result is shown in figure 5.2.3.b for a case with $\bar{p}_0 = 10 \text{ Pa}$ and \bar{q}_V at steady state $1.0 \cdot 10^{-3} \text{ m}^3/\text{s}$.

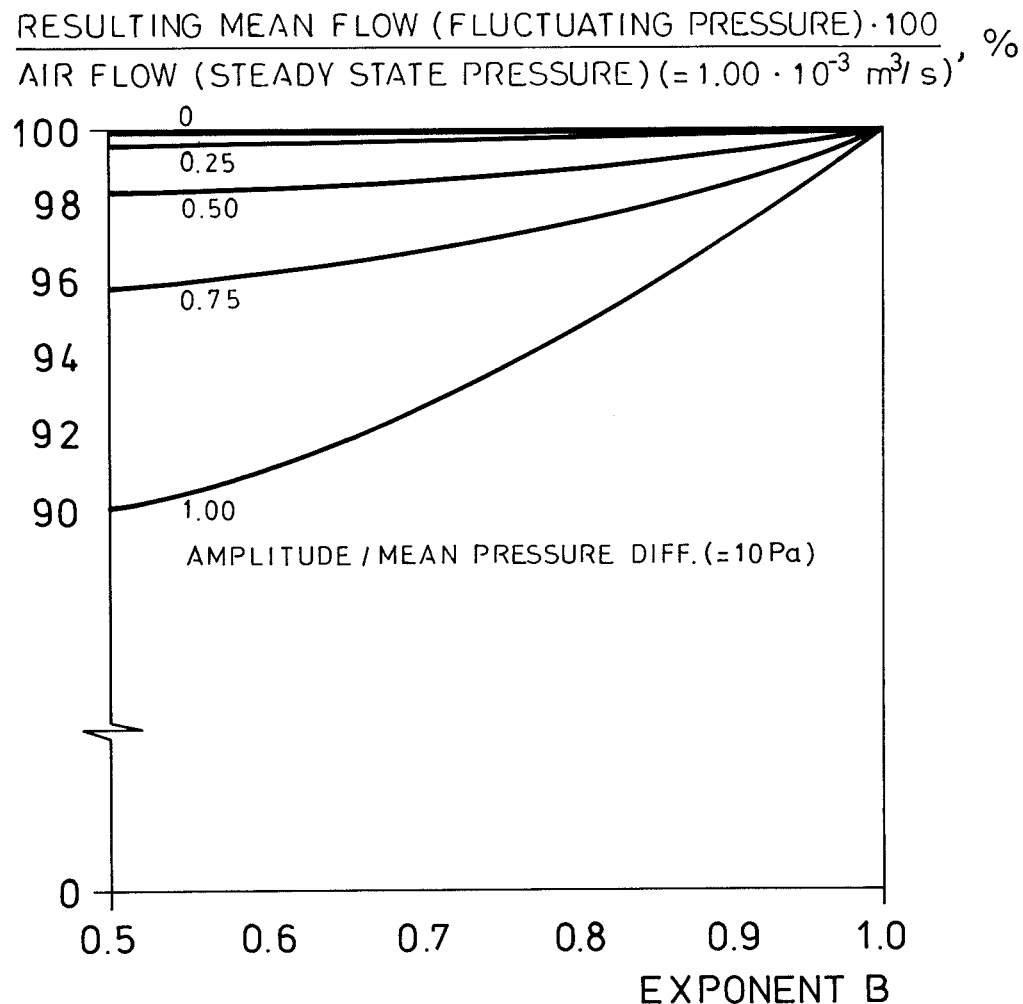


FIG. 5.3.b. Resulting mean flow at fluctuating pressure difference as a percentage of the air flow at steady state pressure difference for different exponents, B, and with the relative amplitude as a parameter.

From the analysis above it can be stated that rapid fluctuations influence the flow rate only little. If the fluctuations are slow it is possible to calculate the flow rate as if the problem was a steady state one, using time averaged values.

6 LEAKAGE CHARACTERISTICS OF SINGLE BUILDING COMPONENTS AND BUILDING ENVELOPES

6.1 BUILDING COMPONENTS

Air leakage characteristics of walls have now been investigated for some 6 decades. The earliest investigations concerned masonry walls. Several works may be mentioned e.g. Building Research Board (1921), Houghten & Ingels (1927), Raisch (1928), Larson et al. (1929), (1930 A), Raisch & Steger (1934), FKA (1943), Nevander (1949), (1958), (1961) and (1969). Presoly (1962) reports some experiments on lightweight concrete masonry walls.

A summing up of results from different Swedish investigations is given in table 6.1.a.

Figure 6.1.a gives examples of leakage curves for some of the tested walls in table 6.1.a.

It can thereby be noted that while wall No. 10 shows a linear characteristic, wall No. 12 behaves non-linearly. The result can probably be ascribed to the influence of different masonry quality. Wall No. 10 has the mark "good" and No. 12 "bad" workmanship. However, the absolute air tightness is about the same.

Wall No. 10 is rendered on one side. In the case of wall 12 there are likely to be separate flow paths in the form of holes or other larger openings penetrating the masonry in addition to the air permeating the material.

Rendering on masonry walls reduces the air leakage rate substantially. Thus the results above indicates a reduction with a factor of 40 - 60% for single sided and 75 - 85% for double sided rendering. Higher reductions still are presented in ASHRAE Handbook of Fundamentals (1968). Figure 6.1.b. The values originates from the foreign, early works presented above.

TABLE 6.1.a. Air leakage of masonry walls.
Abstract from Swedish measurements.

NO.	YEAR	THICK- NESS m	BRICK 1)	SORP- TION	WORK- MANSHIP 3)	JOINTING RENDERING 2)	NUMBER OF TEST OBJECTS	AIR LEAKAGE $m^3/(s \cdot m^2)$	NOTES
1	49	0.38	H	-	-	2 R	3	$3.1 \cdot 10^{-5}$	$\rho = 1100 \text{ kg/m}^3$
2		0.38	S	-	-	2 R	1	$3.9 \cdot 10^{-5}$	$\rho = 1600 \text{ kg/m}^3$
3		0.38	S	-	-	2 R	1	$4.7 \cdot 10^{-5}$	$\rho = 1400 \text{ kg/m}^3$
4		0.30	S	-	-	2 R	1	$5.0 \cdot 10^{-5}$	$\rho = 1200 \text{ kg/m}^3$
5		0.38	S/H	-	-	1 R + 1 P	3	$8.3 \cdot 10^{-5}$	$\rho = 1600 \text{ kg/m}^3$
6 a		0.38	S	-	-	0	2	$2.8 \cdot 10^{-4}$	$\rho = 1600 \text{ kg/m}^3$
6 b						1 R	2	$1.7 \cdot 10^{-4}$	
6 c						2 R	2	$6.9 \cdot 10^{-5}$	
7 a		0.25	S	-	-	0	3	$5.5 \cdot 10^{-4}$	$\rho = 1600 \text{ kg/m}^3$
7 b						1 R	3	$2.5 \cdot 10^{-4}$	
7 c						2 R	3	$8.9 \cdot 10^{-5}$	
8 a	58	0.12	H	HIGH	BAD	0 P	1	$8.3 \cdot 10^{-4}$	
8 b								$7.7 \cdot 10^{-4}$	Retested after 5 months
9 a		0.12	H	HIGH	BAD	1 Pa	1	$4.4 \cdot 10^{-4}$	
9 b								$5.5 \cdot 10^{-4}$	Retested after 5 months
10		0.12	H	HIGH	GOOD	1 Pb	1	$2.2 \cdot 10^{-4}$	
11 a		0.12	H	HIGH	GOOD	1 Pb	1	$1.4 \cdot 10^{-5}$	
11 b								$1.4 \cdot 10^{-4}$	Retested after 5 months
12 a		0.12	H	LOW	BAD	0 P	1	$3.3 \cdot 10^{-4}$	Non linear
12 b								$2.8 \cdot 10^{-4}$	Retested after 5 months
13 a		0.12	H	LOW	GOOD	1 Pb	1	$8.3 \cdot 10^{-5}$	
								$1.1 \cdot 10^{-4}$	Retested after 5 months
14	61	0.12+0.12	H	HIGH	NORMAL	1 Pb	1	$3.6 \cdot 10^{-4}$	Cavity wall. Floated back. Side leakage?
15 a		0.12+0.12	H	HIGH	NORMAL	1 Pb	1	$5.3 \cdot 10^{-4}$	Untightened sides
15 b								$4.4 \cdot 10^{-4}$	Tightened sides
16 a	69	0.12	H	LOW	P	1 Pa	3	$3.9 \cdot 10^{-4}$	
							3	$1.8 \cdot 10^{-4}$	One side treated with brick dust suspension
17 a		0.12	H	HIGH	P	1 Pa	3	$4.3 \cdot 10^{-4}$	
17 b							3	$8.3 \cdot 10^{-5}$	One side treated with brick dust suspension

1) H = hollow brick
S = solid brick

2) 0 = no rendering

1 R = rendering on one side

2 R = rendering on two sides

P = pointing of the joints

Pb = pointing of the joints at brick laying

Pa = pointing of the joints after brick laying

3) perforated horizontal joints

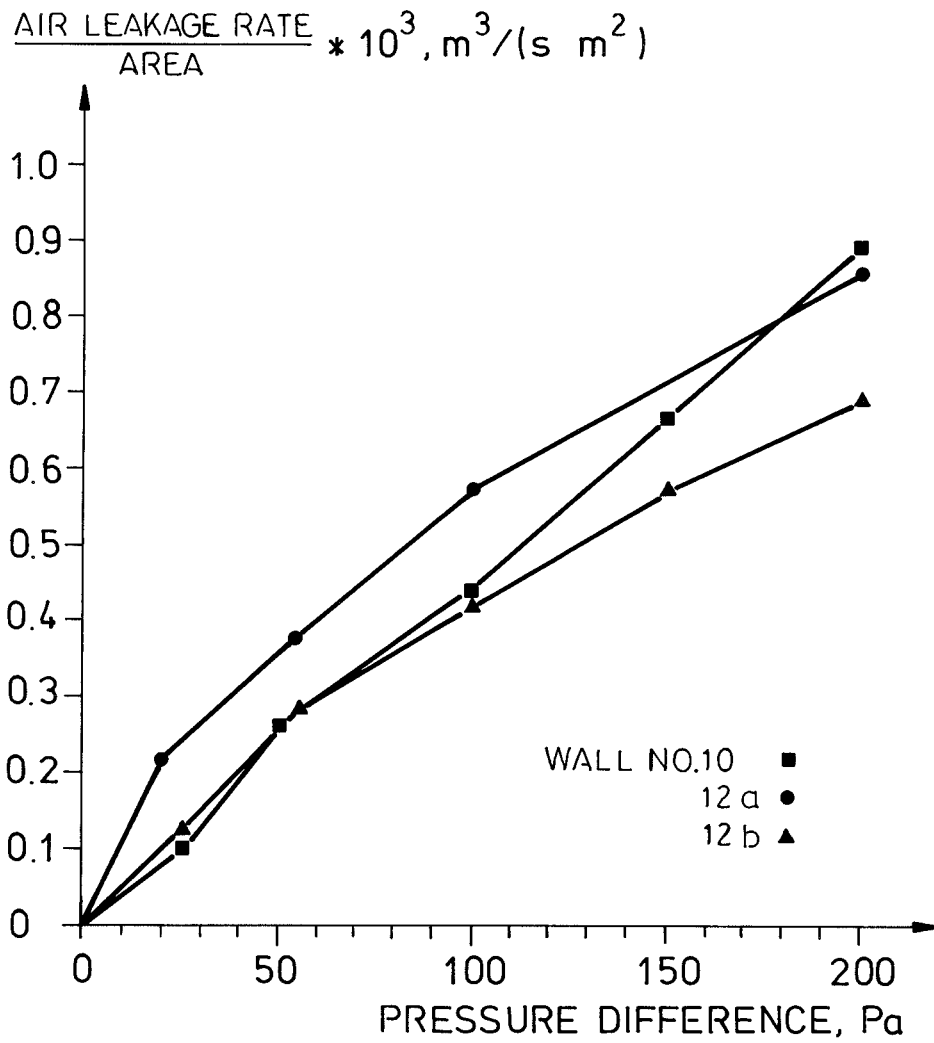


FIG. 6.1.a. Air leakage of masonry walls.
After Nevander (1958).

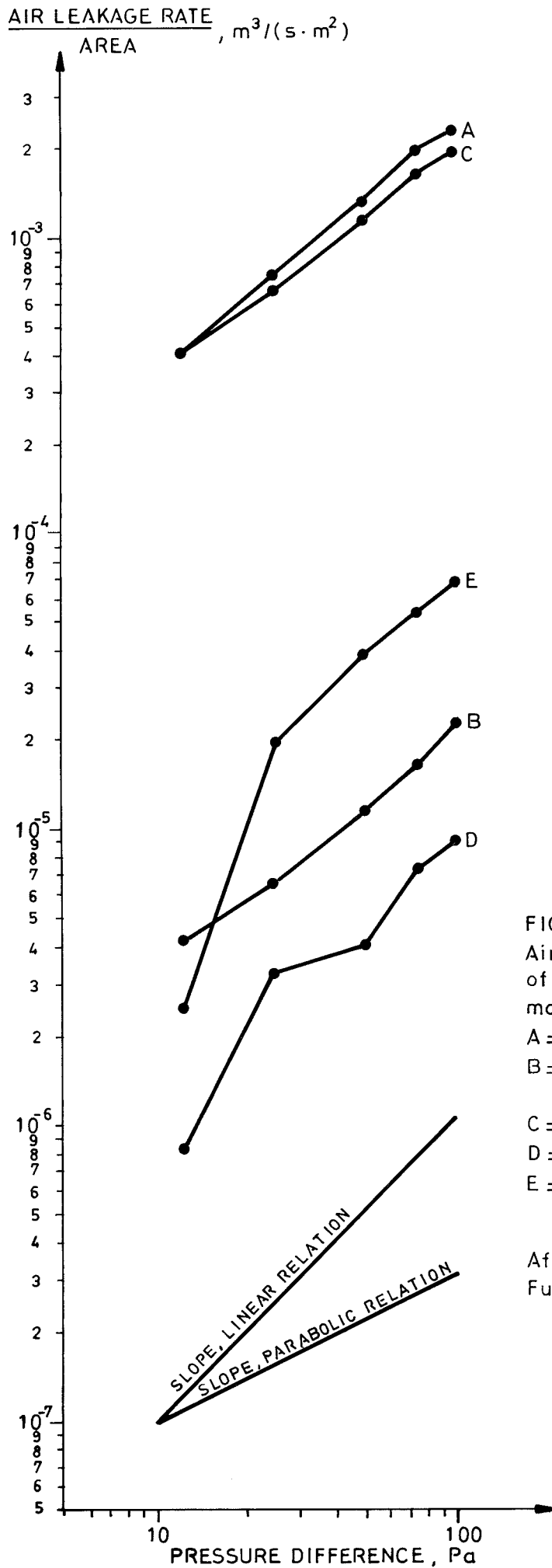


FIG. 6.1. b

Air leakage of brick walls constructed of porous brick and lime mortar – workmanship poor.

A = plain wall, 0.21 m (8 1/2 in.) thick,

B = A but rendered with two coats of prepared gypsum plaster,

C = plain wall, 0.33 m (13 in.) thick,

D = C but rendered like B

E = C but with furring, lath and two coats of prepared gypsum plaster

After ASHRAE Handbook of Fundamentals (1968)

The air tightness of wooden walls was studied in the United States in the late twenties, Larson et al. (1930 B). The tested wall construction was: bevel siding painted or cedar shingles, sheathing, building paper, wood lath and three coats of gypsum plaster. The average leakage rate is shown in figure 6.1.c.

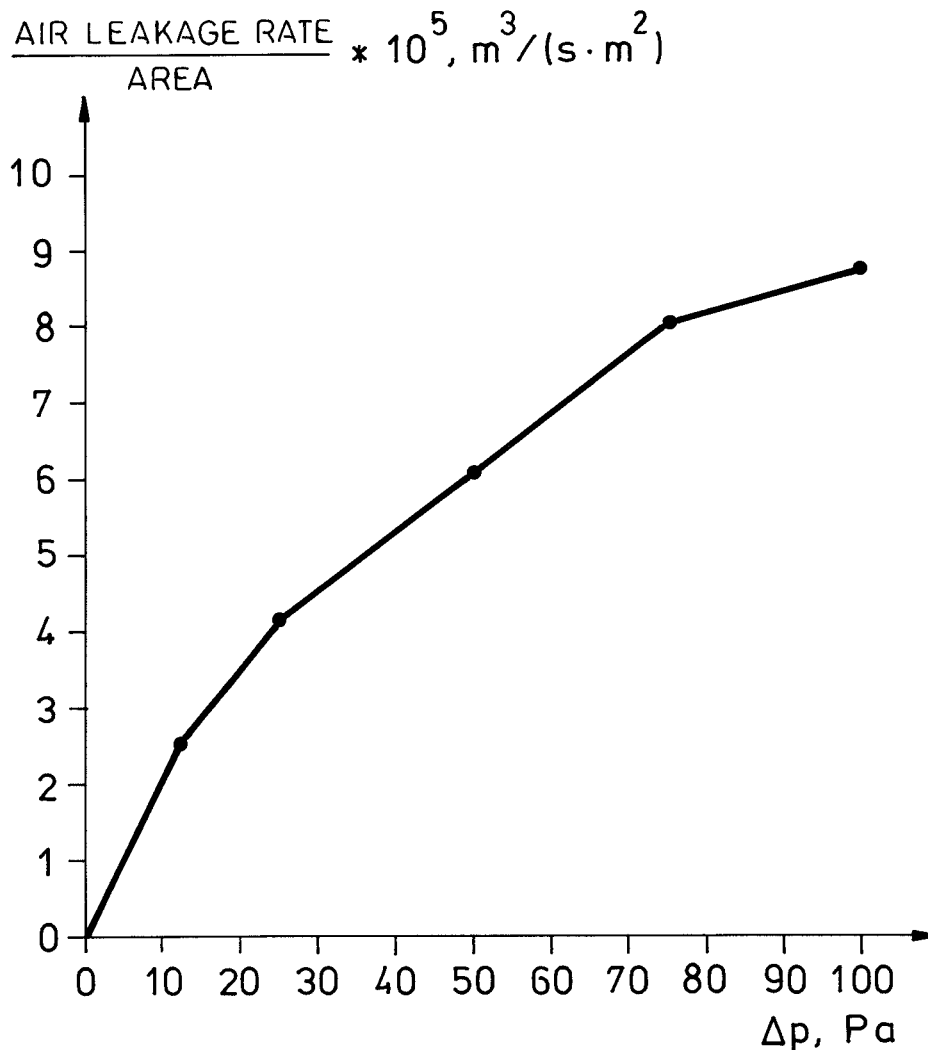


FIG. 6.1.c. Air leakage of wooden walls. After Larson et al. (1930 B).

Valuable contributions to the knowledge of how airtight stud walls are was given by Granum et al. (1954). The tests were carried out at pressure differences between 100 and 700 Pa and the successive pressure drop within the wall was also measured. It was shown that the air leakage rate varied considerably depending on the design and the quality of the workmanship. It was claimed that the exponent B in a relationship,

$q_v = A \cdot \Delta p^B$, in most cases lay around 0.7. The greater part of the total pressure drop across the walls took place in specific airtightening layers such as board plates, paper layers etc. The tightness of overlap joints was proved to be strongly dependent on the degree of compression of the overlap. It was also found that a good tightness requires an undamaged paper layer but a reasonable number of nail holes or small rips did not materially increase the leakage rate. Great leakages were reported where the floor joists seat in the wall, and between window frames and the wall.

The air tightness of different walls for factory buildings was investigated by Andersson (1978). The results indicates that it is possible to achieve a relatively high degree of airtightness of such walls (leakage rate of $\approx 1 \cdot 10^{-4} \text{ m}^3/(\text{s} \cdot \text{m}^2)$) provided that the problem spots of concentrated air leakage at joints in the walls and between the wall and windows/doors are thoroughly sealed. Certain elements of "traditional" technology and workmanship have to be abandoned to provide good airtightness. An example of this is "free" connection between the vapour barrier (polyethylene sheet) without any compression of the joint between the sheet and the tight construction.

The airtightness of different windows has been investigated to a certain degree. The results will not be reviewed here since the window types differ quite a lot from each other in the different investigations. However, it may not be out of place to mention some of the authors of more general works. Thomas & Dick (1953) carried out a pioneer work concerning air infiltration through gaps around windows. Birkeland & Wigen (1955) studied the influence of caulking of the gaps around windows. A classical investigation of the influence of gaskets in window joints (between casement and window frame) was made by Dalaker (1961). Later Swedish works on this matter are Höglund & Wånggren (1979) and Jergling (1979).

The knowledge of the airtightness behaviour of other building components and the connections between them is generally poor. However, a recently published work, Carlsson et al. (1980) describes very detailed building design solutions intended to achieve a high degree of airtightness of various building components in both the design stage and in the house production stage.

6.2 BUILDING ENVELOPES

The building envelope is here considered to consist of the total climatic shelter of a building. The knowledge of air leakage characteristics of building envelopes of different buildings has been extended substantially during the last few years. This is due to a high degree to the rapidly increasing use of the pressurization technique to test the airtightness of whole buildings. The pressurization procedure, as well as error analysis etc. of the method is described in Kronvall (1978) and (1980 A). The concept is nowadays rather familiar to many people. Thus, in this work, only the results from such tests will be discussed.

The pressurization procedure establishes a relationship between pressure difference across the building envelope and resulting leakage rate.

In most cases the result is given as a leakage curve - figure 6.2.a.

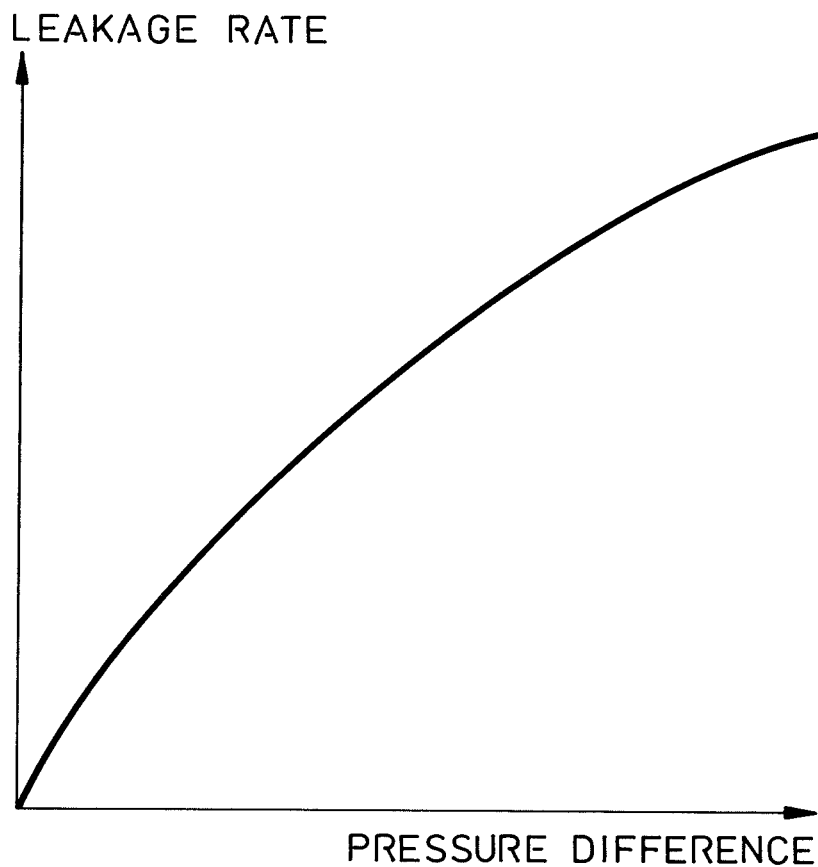


FIG. 6.2.a. Leakage curve from pressurization test.

The leakage rate at 50 Pa is often chosen as a kind of reference value and, in order to make comparisons between houses of different sizes possible, the leakage rate is often divided by the volume of the house or, sometimes, the area of the envelope.

From pressurization practice it can be observed that the shape of the leakage curve differs from house to house. The extremes of the shape are a parabolic curve on one hand and a straight line on the other. It is tempting to claim that this corresponds to complete turbulent flows in the flow paths of the envelope and complete laminar flow respectively. While the second statement is reasonable, the first one is quite dubious, since other phenomena than turbulence may cause the flow rate to be proportional to the square root of the pressure difference. Obviously, since single resistances like entrance, bend and exit losses operate on the square of the average velocity in the flow path, turbulence is not the only reason. This will be discussed more in detail below.

A versatile way of describing the relationship between leakage rate and pressure difference is to use a power function

$$q_{v, \text{tot}} = \alpha \cdot \Delta p^\beta \quad (6.2.a)$$

where

α is a flow rate coefficient, $\text{m}^3/(\text{s} \cdot \text{Pa}^\beta)$

β is a flow exponent, $0.5 \leq \beta \leq 1$

It is sometimes claimed that this expression is in conflict with a proper description of the physics of the flow. Of course, such an objection is correct and perhaps it would have been wiser to use a quadratic equation of the form

$$\Delta p = c_1 \cdot q_{v, \text{tot}} + c_2 \cdot q_{v, \text{tot}}^2 \quad (6.2.b)$$

where the relative contributions of laminar flow on the one hand and orifice and single resistances and turbulent flow on the other could be shown.

A third way of making the description, used especially in the Anglo-Saxon countries, is by using the concept of equivalent leakage area, A_{eq} , defined as follows - cf. eq. 2.3.3.b - i.e. an equation for turbulent flow through a sharp-edged opening in a thin wall.

$$A_{eq} = \frac{q_{v, tot}}{C_d \cdot \sqrt{\frac{2 \Delta p}{\rho}}} \quad (6.2.c)$$

Thus the leakage behaviour of the building envelope is described as an area, A_{eq} , producing a certain flow rate $q_{v, tot}$, at a certain pressure difference, Δp . The choice of Δp seems to be rather arbitrary. C_d is a coefficient of discharge usually given the value of 0.6. A_{eq} has a constant value in an interval of Δp only if the leakage flow is proportional to the square root of the pressure differences in the interval.

Some researchers use a leakage function, $f_l(\Delta p)$ defined as:

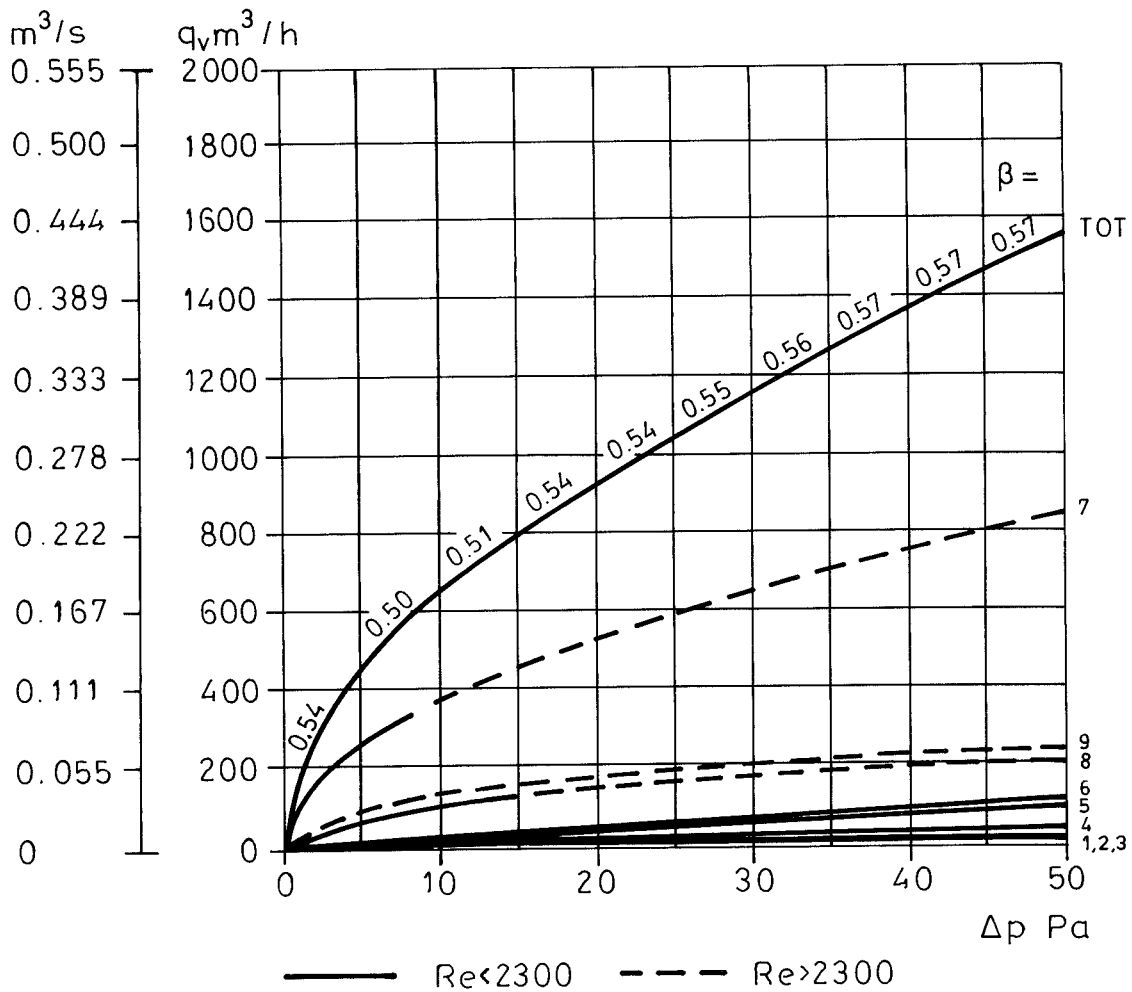
$$q_{v, tot} = f_l(\Delta p) \cdot \Delta p \quad (6.2.d)$$

The observant reader realizes of course immediately that this is nothing but an "overall" admittance of a building envelope - cf. eq. 4.3.2.1.a.

The leaky envelope of a building may be considered to consist of a rich variety of different flow paths from tiny cracks and airpermeable material to relatively large (hidden) openings. It is possible to simulate the air leakage characteristic of a house by assuming arbitrary combinations of different flow paths. For the case of pure crack/duct flow, an example of such a simulation is shown in figure 6.2.b.

Perhaps the most astonishing thing about this simulation lies in a comparison between the leakage rates of different leaks. Though quite long - 20 to 70 running-metres - the narrow cracks No. 1 - 6 with widths between 0.075 and 1 mm create only minor contributions to the total leakage. Wider cracks, (5 to 10 mm), however, have a substantial influence on the total leakage, even though their lengths are quite small (1 to 5 running-metres).

The total leakage curve of figure 6.2.b will be analysed in accordance with the four different ways of description reviewed above.



DESCRIPTION OF FLOW PATHS :

FLOW PATH NUMBER	1	2	3	4	5
LENGTH IN FLOW DIRECTION (m)	0.25	0.225	0.20	0.175	0.15
WIDTH (m)	0.000075	0.0001	0.00025	0.0005	0.00075
LENGTH (m)	70	60	50	40	30
ROUGHNESS (m)	0.0000075	0.00001	0.000025	0.00005	0.000075
FLOW PATH NUMBER	6	7	8	9	
LENGTH IN FLOW DIRECTION (m)	0.125	0.10	0.075	0.05	
WIDTH (m)	0.001	0.0075	0.005	0.01	
LENGTH (m)	20	5	2	1	
ROUGHNESS (m)	0.0001	0.00075	0.0005	0.001	

FIG. 6.2.b. Simulated leakage characteristic of a house assuming crack/duct flow only. $\Sigma \xi = 1.5$. After Kronvall (1980 B).

Power function approach

The result of a least squares curve fit to a power function was:

$$q_{v, \text{ tot}} = 0.047 \cdot \Delta p^{0.57} \text{ (m}^3/\text{s)}$$

In addition, for each 5 Pa-interval (except the first one - being 1-5 Pa) the exponent β is displayed in the figure.

The exponent, β , was calculated as

$$\beta = \frac{\ln\left(\frac{q_{v,1}}{q_{v,2}}\right)}{\ln\left(\frac{\Delta p_1}{\Delta p_2}\right)} \quad (6.2.e)$$

Thus the exponent of the potential expression seems to have a rather constant value for all pressure differences. Some authors have claimed that this is not the case; Nylund (1980) and Grimsrud et al. (1979), for example. Their opinion is that the exponent is close to 1.0 at lower and close to 0.5 at higher pressure differences across the envelope. However, it rather seems to be that high leakage rates are caused by quite few, large leaks. The dimensions of these are big enough to create either turbulent flow or flow with such high velocities that in and outlet effects become considerable. It is obvious that the duct width has a very great influence on the leakage rate. Once a leak of large dimension is introduced.

- o the total leakage rate increases strongly,
- o the exponent β of the total flow curve is altered,
- o the value of β - in the total flow curve - does not vary much in different pressure difference regimes.

Quadratic equation approach

The result of a least squares curve fit to a quadratic equation was:

$$\Delta p = 16.7 \cdot q_{v, \text{ tot}} + 238.1 \cdot q_{v, \text{ tot}}^2$$

which shows that the influence of the second term is considerable.

Equivalent leakage area approach

The equivalent leakage area can be written:

$$A_{\text{eq}} = \frac{1}{C_d \cdot \sqrt{\frac{2}{\rho}}} \cdot \frac{q_{v, \text{tot}}}{\sqrt{\Delta p}} \quad (6.2.e)$$

For $C_d = 0.6$ and $\rho = 1.25 \text{ kg/m}^3$ the equivalent leakage area was calculated for different pressure differences. The result is shown in figure 6.2.c.

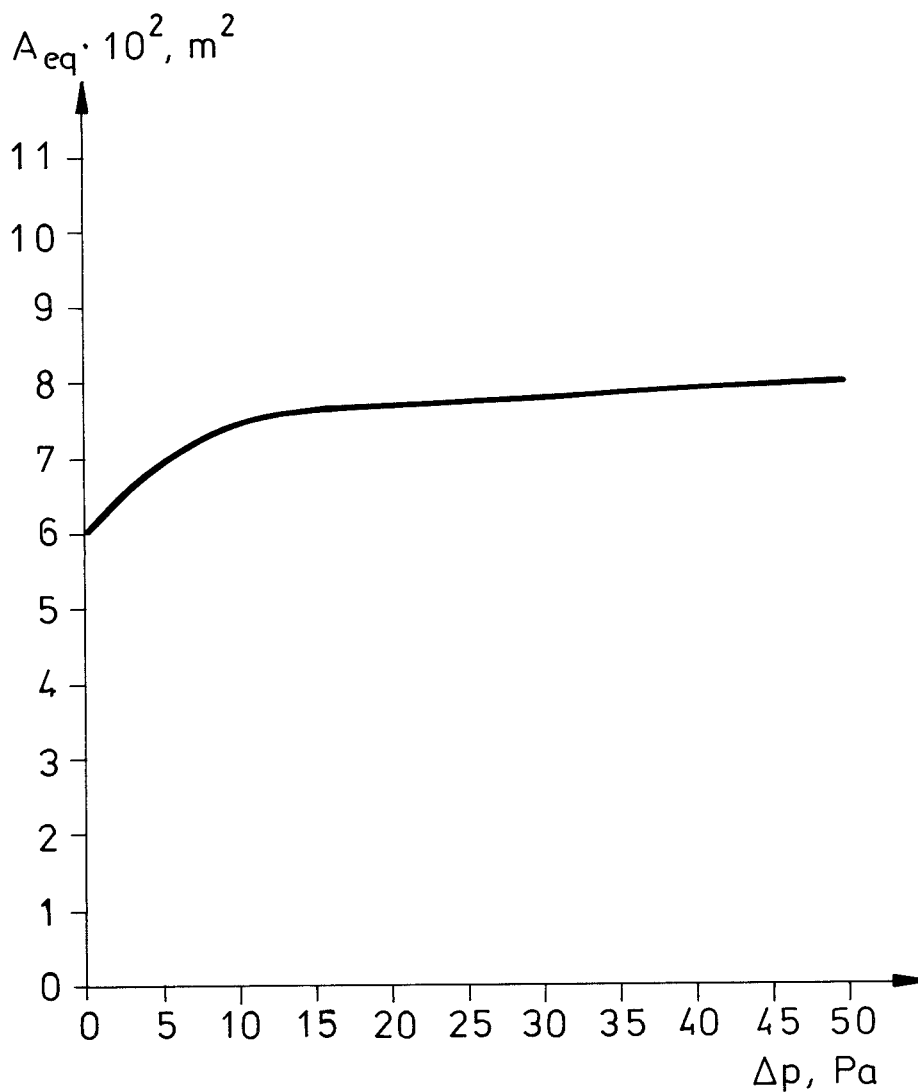


FIG. 6.2.c. Equivalent leakage area for house envelope leakage in accordance with figure 6.2.b.

From the figure it can be seen that at low pressure differences the equivalent leakage area decreases strongly. The value of A_{eq} at 1 Pa differs from that of 50 Pa by around 25%. This is the case even though the exponent formula in the power expression approach was found to be quite close to 0.5. If $\beta \equiv 0.5$ the A_{eq} -value must be constant by definition. For narrow cracks the deviations from a constant A_{eq} value are likely to be larger still, of course.

Leakage function approach

According to definition the leakage function $f_l(\Delta p)$ simply equals the ratio between leakage rate and corresponding pressure difference. The resulting curve for the present example is shown in figure 6.2.c.

Obviously the leakage function varies within a large interval, and it seems to be rather high at small pressure differences. This behaviour was also found in field studies reported from the Lawrence Berkeley Laboratories, Grimsrud et al. (1979), from which figure 6.2.e is taken.

Grimsrud et al. were using a method of testing the leakage behaviour at small pressure differences by means of a device creating fluctuating pressure difference - the AC method. They were, however, not able to explain the rise in the leakage function at low pressure differences. Instead they expected a linear relationship between pressure difference and flow - i.e. constant leakage function - to occur in the low pressure domain.

The results may be explained if different basic duct/crack flow cases are studied. The figures 6.2.f - h are based on calculations of flow rate through ducts of different widths and with different values of total single resistance loss factors.

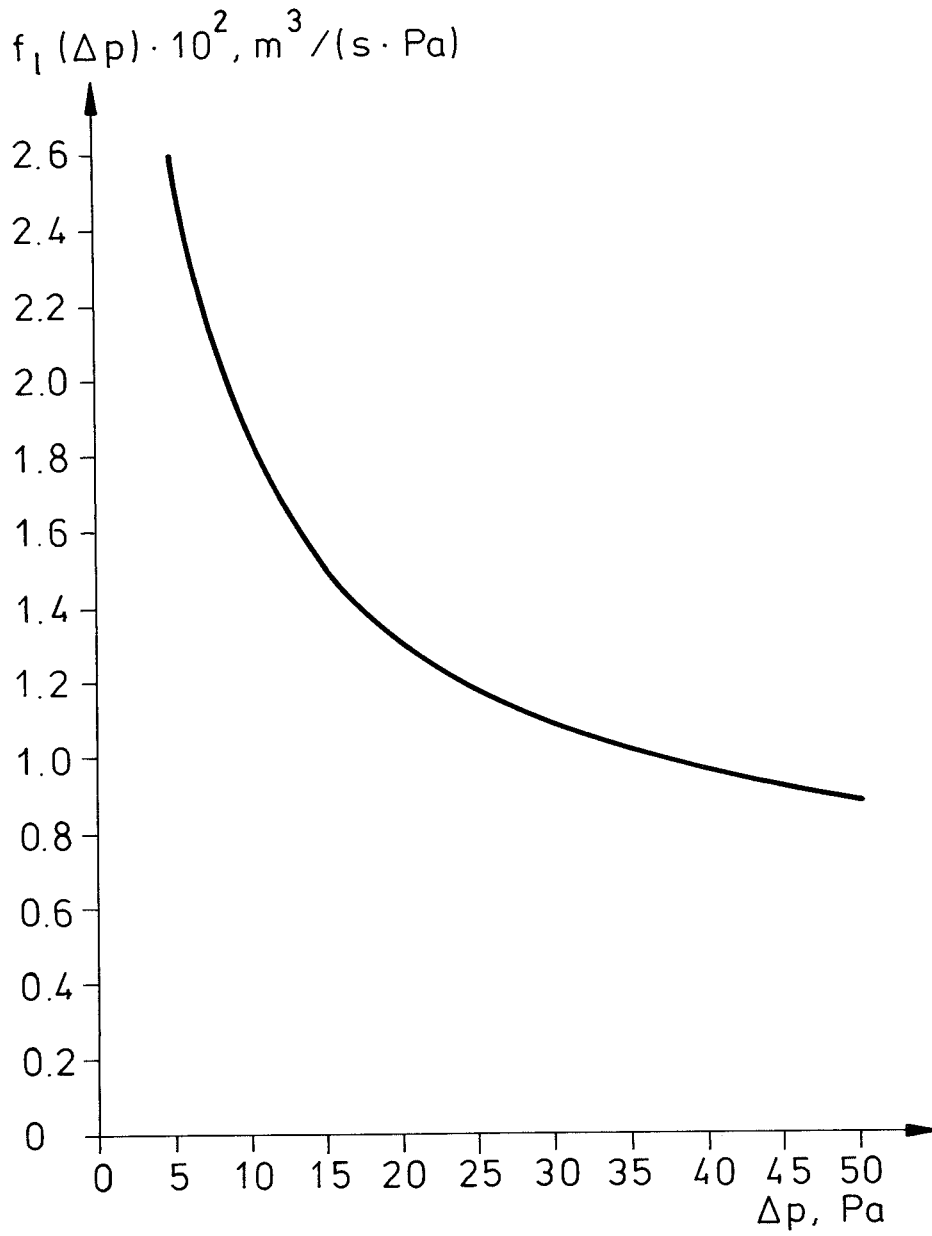


FIG. 6.2.d. Leakage function for house envelope leakage in accordance with figure 6.2.b.

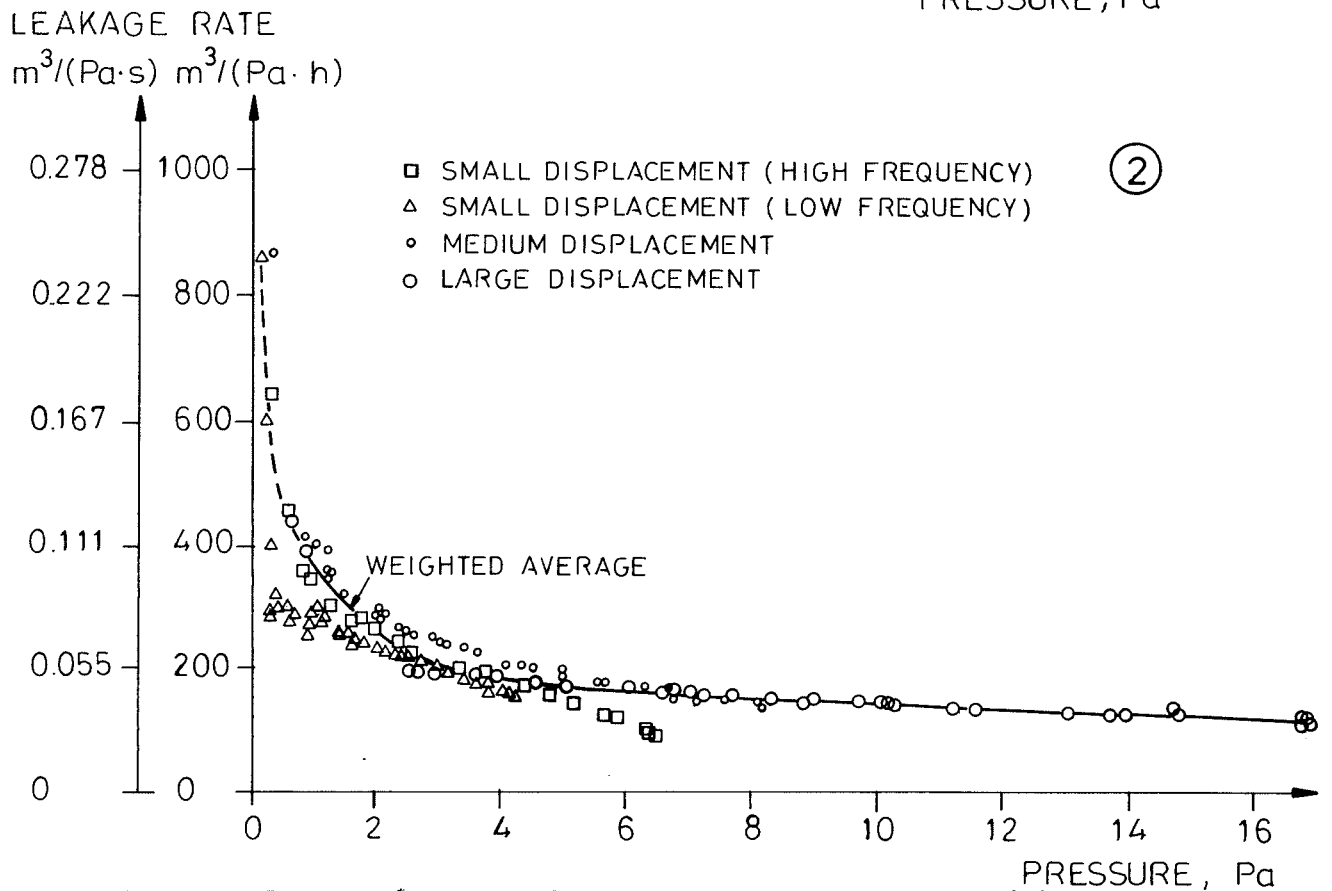
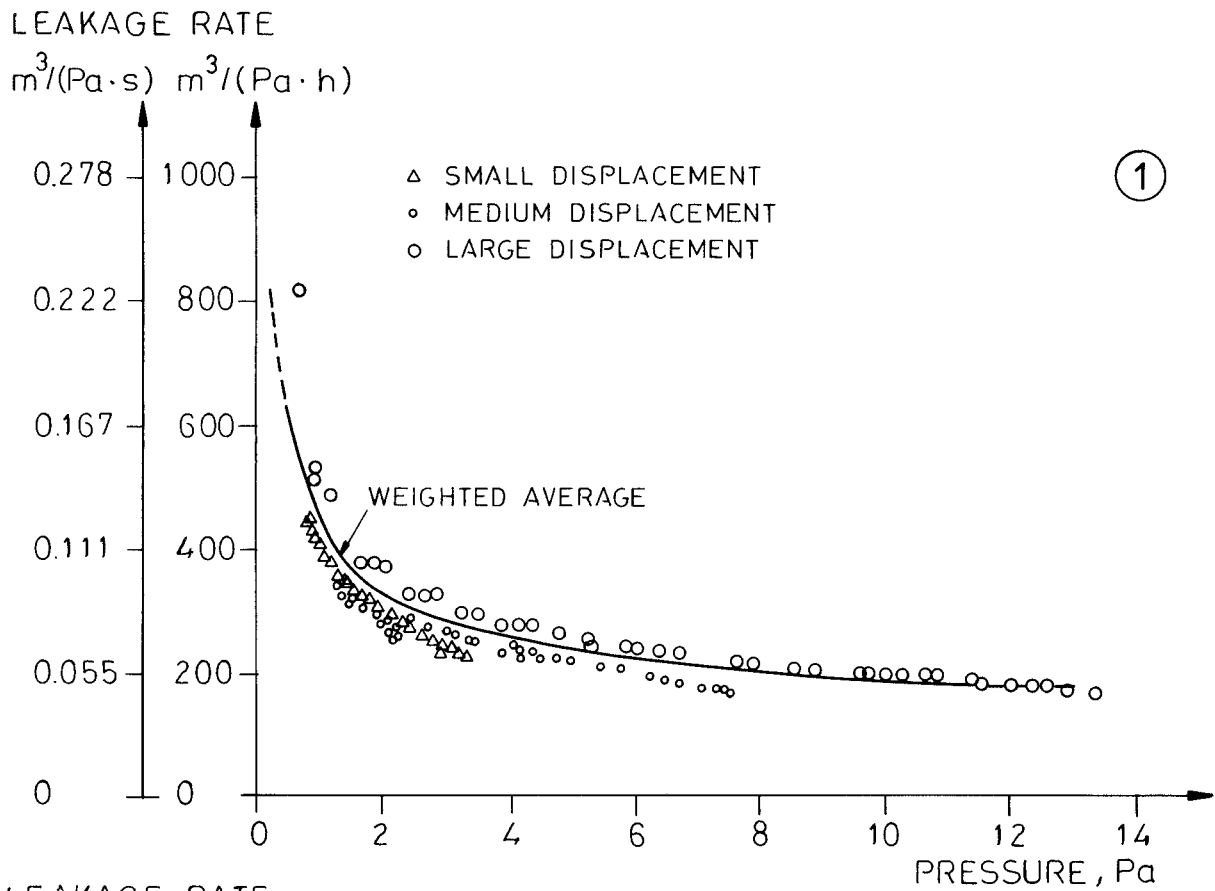


FIG. 6.2.e. The leakage function of the structure in the loose (1) and tight (2) configurations vs. the applied pressure. Each point represents a one-minute average reading at a particular frequency and displacement. Points of the same displacement have the same symbol. The curves are the weighted averages of all of the data points. After Grimsrud et al. (1979).

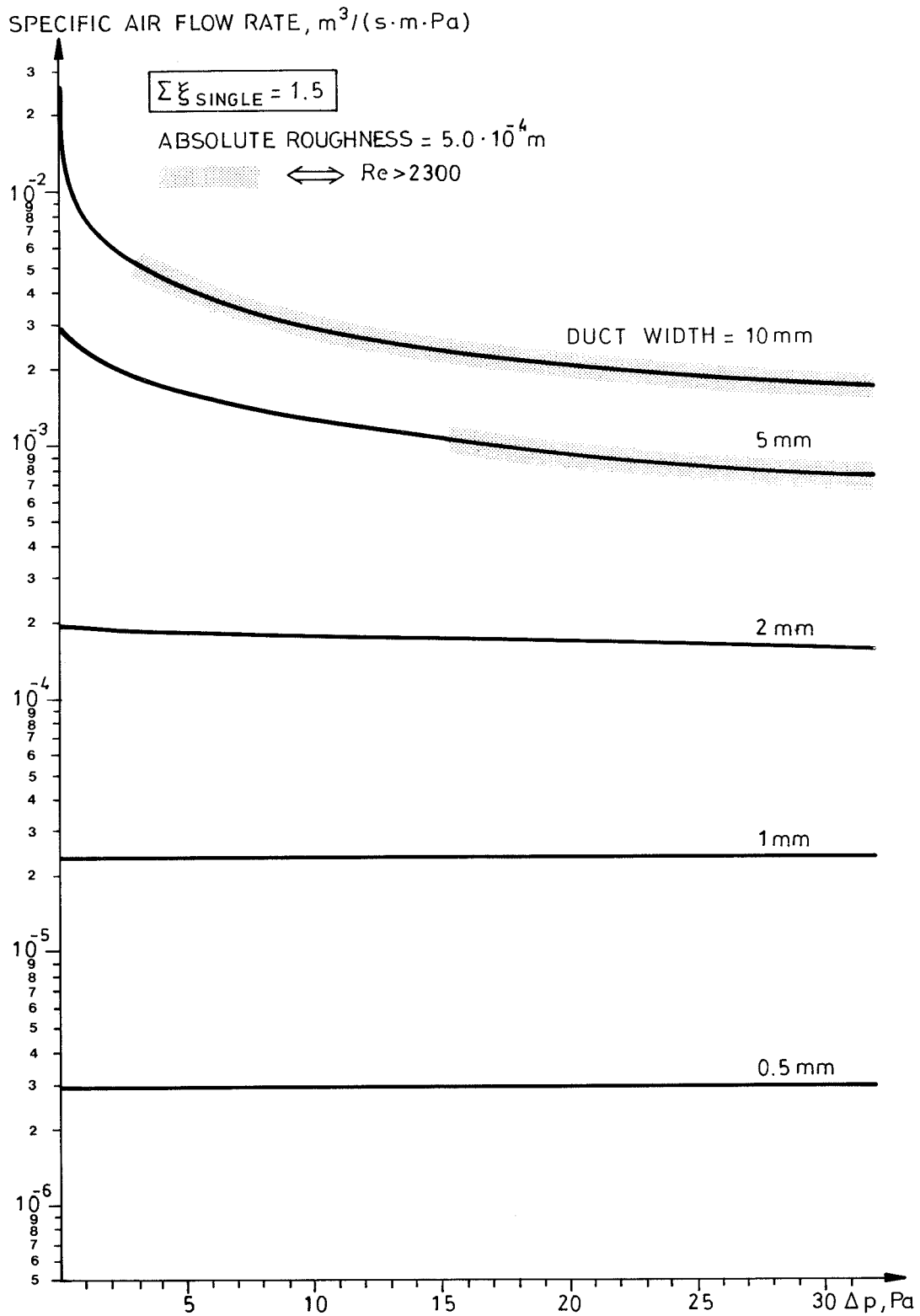


FIG. 6.2.f. Air flow through ducts of different widths with length 0.2 m in flow direction. $\Sigma \xi_{\text{single}} = 1.5$.

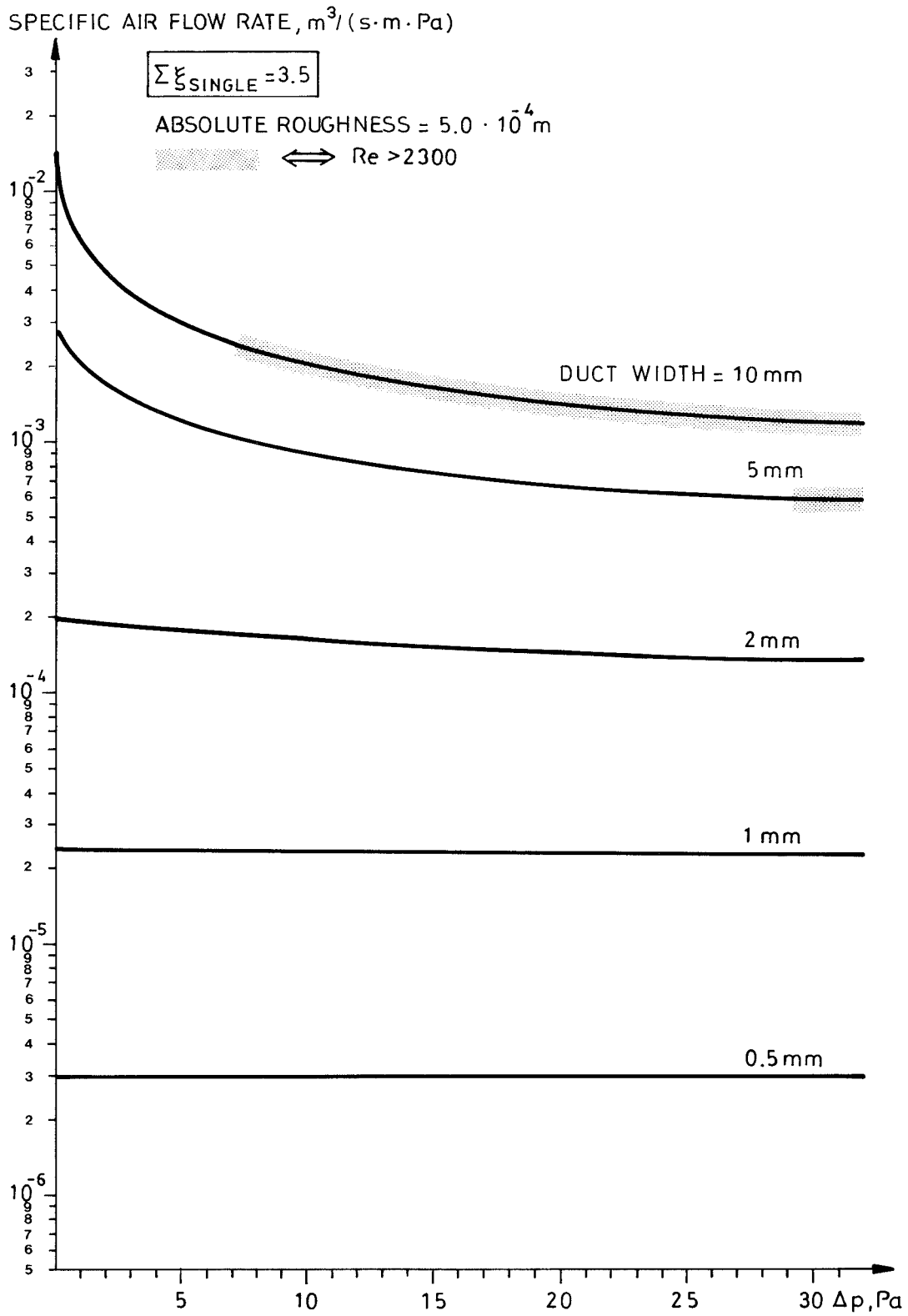


FIG. 6.2.g. Air flow through ducts of different widths with length 0.2 m in flow direction. $\Sigma \xi_{\text{single}} = 3.5$.

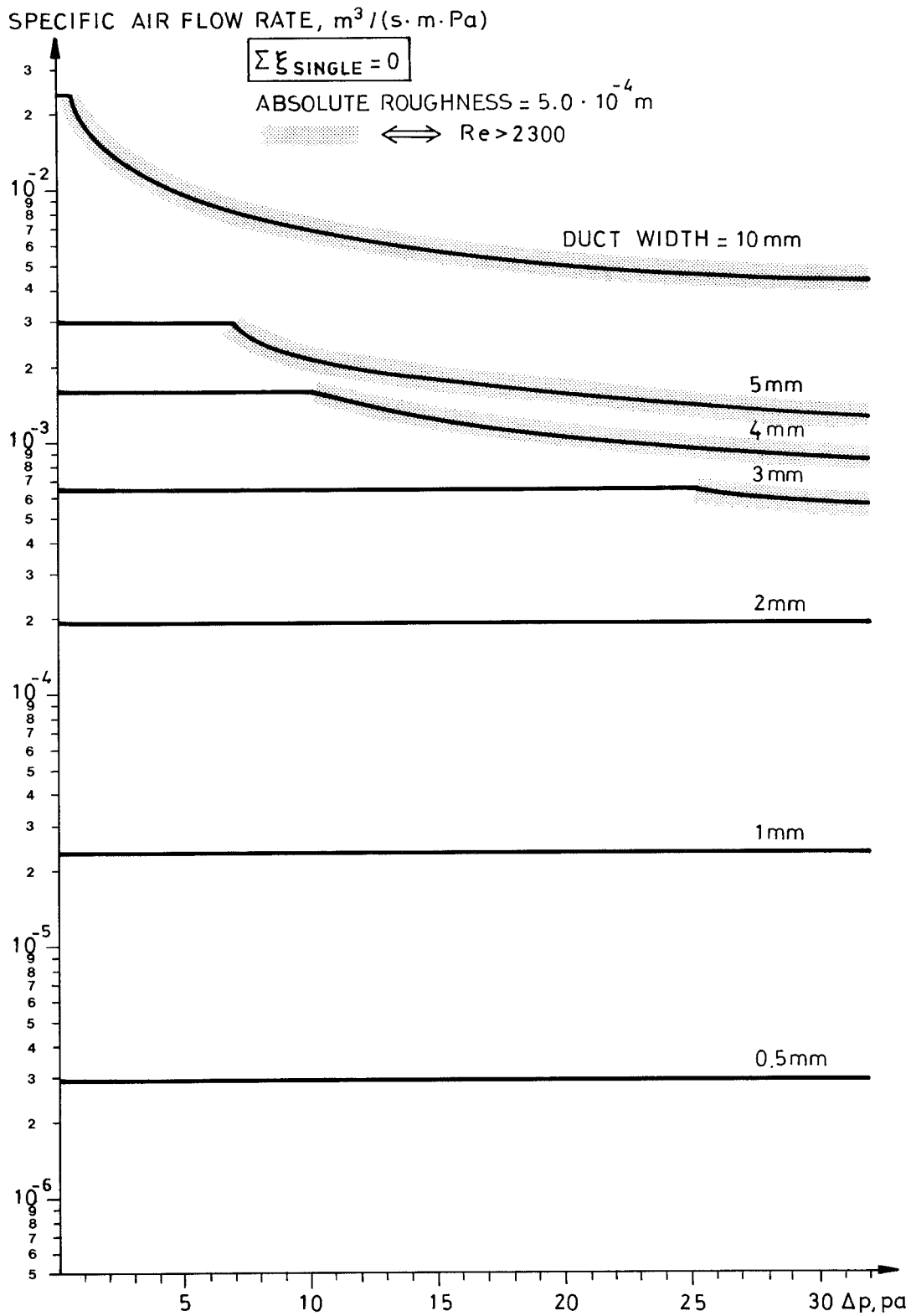


FIG. 6.2.h Air flow through ducts of different widths with length 0.2 m in flow direction. $\Sigma \xi_{\text{single}} = 0$, i.e. pure Poiseuille flow.

The figures show distinctly the influence of single resistances such as entrance, bend and exit losses. From figure 6.2.h in which $\Sigma\xi_{\text{single}} = 0$ it is obvious that the leakage function has a constant value until the flow turns over from laminar flow at $Re > 2300$. This will not happen at all at low pressures provided the ducts are not too large (< 10 mm). Perhaps this pure Poiseuille flow case is in people's mind when "linear relationships are expected". However, real ducts/cracks in fact have entrances and exits and the flow direction may be changed too. Thus the assumption of $\Sigma\xi_{\text{single}} = 0$ cannot hold in practice.

The figures 6.2.f and 6.2.g show how different magnitudes of $\Sigma\xi_{\text{single}}$ influence the shape of the leakage function curves. Introducing single resistances implies that:

- o the value of the leakage function for a specific crack width decreases
- o the leakage function can become non-linear and non-constant even though $Re < 2300$
- o the maximum value of the leakage function occurs at $\Delta p = 0$ and equals the value corresponding to the case when $\Sigma\xi_{\text{single}} = 0$.

General remarks

The analysis above show that there is a relationship between leak dimensions and degree of discrepancy from linear flow characteristic. Hitherto this has not been taken into account as far as pressurization test practice is concerned. Instead of concentrating the effort on giving a leakage rate value at 50 Pa only, it would be worthwhile to investigate the shape of the leakage characteristic too. If considerable deviations from linearity is observed when the pressurization test is performed, a short time spent on looking around in the house in order to detect some few leak paths with large dimensions could in many cases probably be very profitable.

7 APPENDICES

7.1 SURFACE ROUGHNESS OF SOME BUILDING MATERIALS

Material	Surface roughness $\times 10^3, \text{m}$	Reference
<u>Metals</u>		
"Smooth" metal (steel, brass, copper etc)	<0.01	Bretting (1960)
Slightly corroded	0.4	Idelchik (1960)
Corroded	0.15 - 1	Idelchik (1960)
	0.4	Dubbel (1970)
Extremely corroded	<3	Dubbel (1970)
<u>Concrete etc.</u>		
Poured on boarding (tongued and grooved)	1.0 - 1.8	This work, part 3.1
Poured on plywood	0.7 - 2.0	Bretting (1960)
Poured on plywood	1.3 - 2.0	This work, part 3.1
Poured on steel plate	0.5 - 1.3	This work, part 3.1
Screeded surface	3.2 - 5.9	This work, part 3.1
	4 - 7	Bretting (1960)
Steel trowelled surface	0.15- 0.6	Bretting (1960)
	0.5	Idelchik (1960)
	0.15	Eck (1978)
Cement rendering	0.5 - 1.5	Bretting (1960)
	0.5	Idelchik (1960)
<u>Masonry</u>		
Brick masonry, well jointed	1 - 3	Bretting (1960)
<u>Wood</u>		
Planed timber	0.15- 1.5	Bretting (1960)
	0.18-0.9	Bjørnø (1972)
Sawn timber	0.7 - 2.5	Bretting (1960)
Boarding	0.9 - 3	Bretting (1960)
	0.2 - 1	Eck (1978)
	0.2 - 3	Rouse (1950)
<u>Glass</u>	0.0010-0.0015	Idelchik (1960)

Material	Surface roughness $\times 10^3, \mu\text{m}$	Reference
<u>Different boards</u>		
Porous wood fibre board	0.25- 0.38	Lentz & Nakano (1971)
Asphalt impregnated wood fibre board	1.8 - 3.4	This work, part 3.1
Chip board	0.2 - 0.6	This work, part 3.1
Plywood	0.05- 0.08	Lentz & Nakano (1971)
	0.03- 0.12	Idelchik (1960)
Glass fibre board	2.8 - 4.5	This work, part 3.1
Asbestos-cement board	0.05- 0.60	Idelchik (1960)
	0.1	Dubbel (1970)
	0.1	Eck (1978)
Gypsum board	0.2 - 0.7	This work, part 3.1
Cork board	2.5 - 3.8	Lentz & Nakano (1971)
Plastic board (foamed)	0.5 - 0.9	Lentz & Nakano (1971)

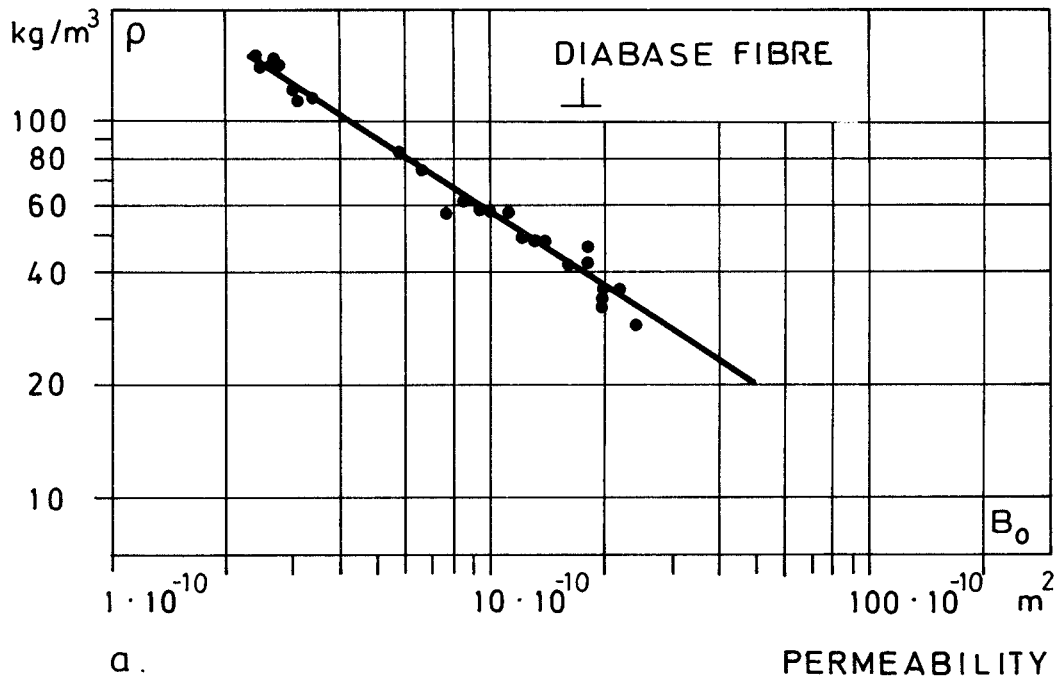
7.2 PERMEABILITY DATA

7.2.1 Fluid permeability coefficients of some building materials

Material	Density kg/m ³	B ₀ m ²	Reference	
<u>Brick, concrete etc.</u>				
Brick	1470	0.1-1.0·10 ⁻¹²	5	
	1720	68·10 ⁻¹⁵	1	
	1840	18·10 ⁻¹⁵	1	
Lightweight concrete	500	0.3-1.5·10 ⁻¹⁵	5	
	460	1.8·10 ⁻¹²	1	
	510	0.41·10 ⁻¹²	1	
Concrete, 300 kg cement/m ³ , W/C = 0.6, slump 50 mm	2100	4.4·10 ⁻¹⁵	1	
Lime-sandstone	2120	28·10 ⁻¹⁵	1	
Mortar L:S = 100/880	1860	35·10 ⁻¹⁵	1	
	L:C:S = 50/50/610	1990	7.3·10 ⁻¹⁵	1
	L:C:S = 20/80/440	1930	9.7·10 ⁻¹⁵	1
	L:C:S = 35/65/520	2000	4.4·10 ⁻¹⁵	1
	C:S = 100/330	2060	2.6·10 ⁻¹⁵	1
Lightweight aggregate concrete	600	6.0·10 ⁻⁹	6	
<u>Wood and wood products</u>				
Balsa	125	0.27·10 ⁻¹⁵	1	
Abachi	370	0.58·10 ⁻¹⁵	1	
Spruce ⊥ fibres	410	0.22·10 ⁻¹⁵	1	
	// fibres	450	97·10 ⁻¹⁵	1
Pine	530	0.12·10 ⁻¹⁵	1	
Teak	600	0.49·10 ⁻¹⁵	1	
Doussie	660	0.22·10 ⁻¹⁵	1	
Chipboard	560	0.44·10 ⁻¹²	1	
	-	0.64·10 ⁻¹⁵	3, 4	
<u>Wood fibre board plates</u>				
Hard	870	3.4·10 ⁻¹⁵	1	
	960	5.1·10 ⁻¹⁵	1	
	-	1.5·10 ⁻¹⁵	3, 4	
Semi-hard	610	0.16·10 ⁻¹²	1	
		80·10 ⁻¹⁵	3, 4	

Material	Density kg/m ³	B ₀ m ²	Reference
Porous	215	6.7·10 ⁻¹²	1
	260	3.7·10 ⁻¹²	2, 5
Asphalt impregnated	280	3.2·10 ⁻¹²	1
		4.7·10 ⁻¹²	2
		2.1·10 ⁻¹²	3, 4
Plywood		7.9·10 ⁻¹⁵	3
		31·10 ⁻¹⁵	4
<u>Heat insulation material</u>			
Mineral wool			
Glass fibre wool see figure 7.2.1.a - d			
Polystyrene cellular plastic	17.2	2.9·10 ⁻¹⁵	1
	15-20	1.0-10.0·10 ⁻⁹	5
Polyester foam	55.2	19·10 ⁻¹²	1
Urea formaldehyde foam	14.3	11·10 ⁻¹²	1
Polyether foam	26.6	0.46·10 ⁻⁹	1
Granulates:			
Polystyrene pellets, ø 2-8 mm	13.1	17·10 ⁻⁹	7
Haydite, ø 8-16 mm		80·10 ⁻⁹	8
Granulated mineral wool	35	7.5·10 ⁻⁹	8
<u>Different boards</u>			
Glass fibre board	150	0.13·10 ⁻⁹	2
	150	0.16·10 ⁻⁹	3, 4
Mineral wool board	175	2.1·10 ⁻¹²	1
	400	34·10 ⁻¹²	1
Asbestos cement board	775	0.87·10 ⁻¹⁵	1
Cellulose cement board	1600	2.7·10 ⁻¹⁵	1
Linoleum	1235	1.2·10 ⁻¹⁵	1

DENSITY



DENSITY

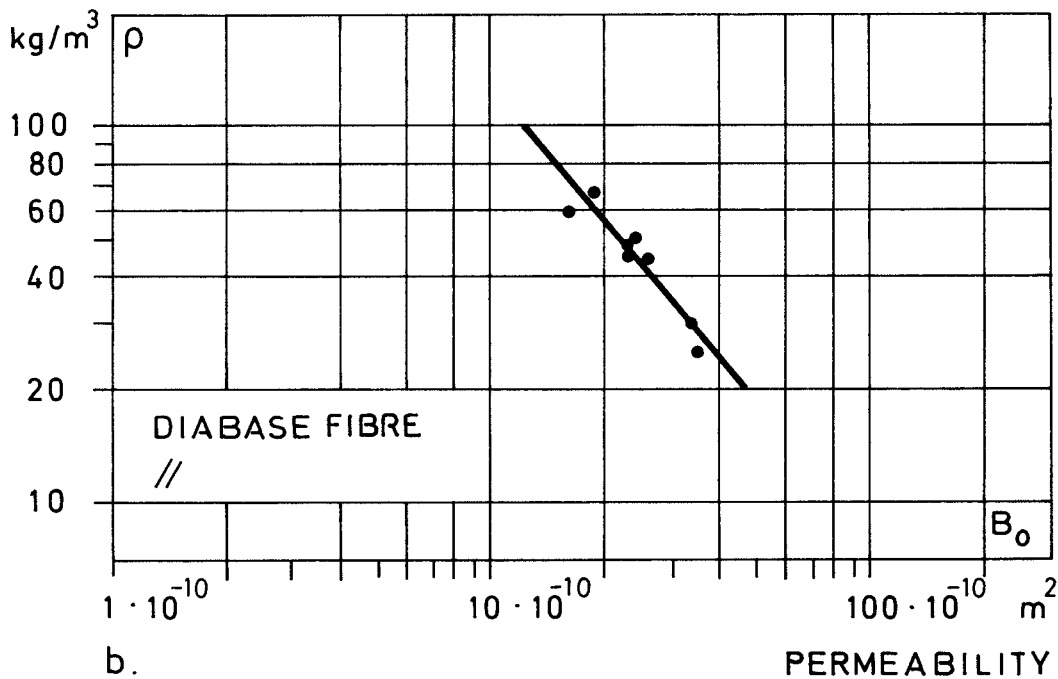


FIG. 7.2.1.a - 7.2.1.b. Experimental permeability coefficient values.
After Bankvall (1972).

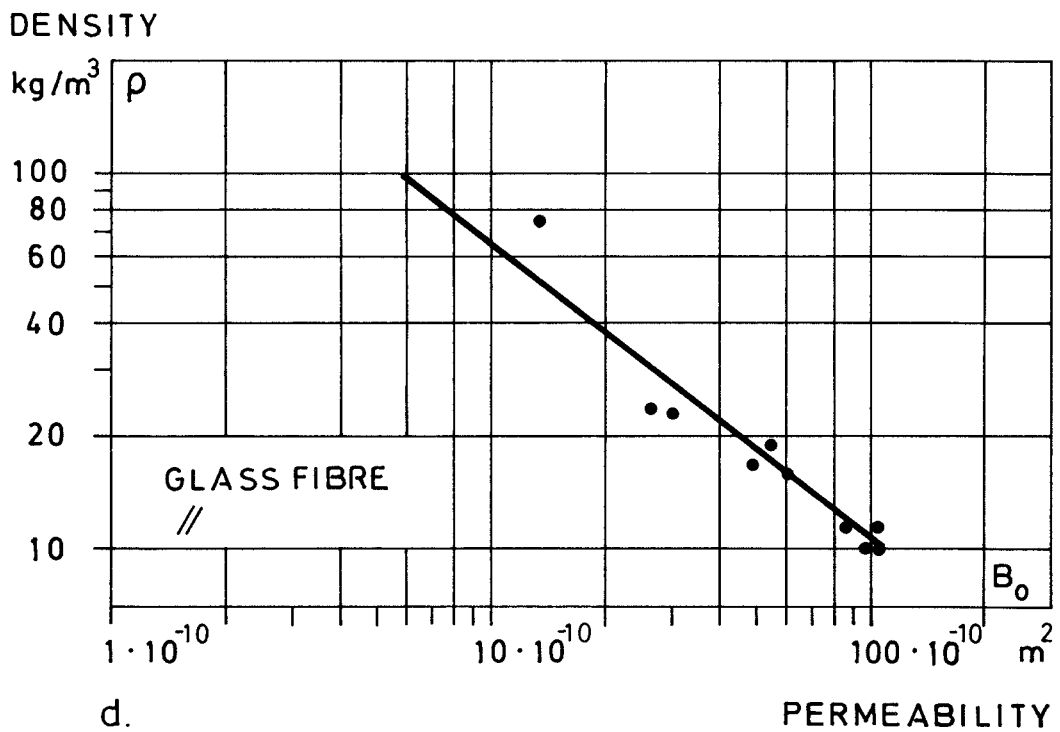
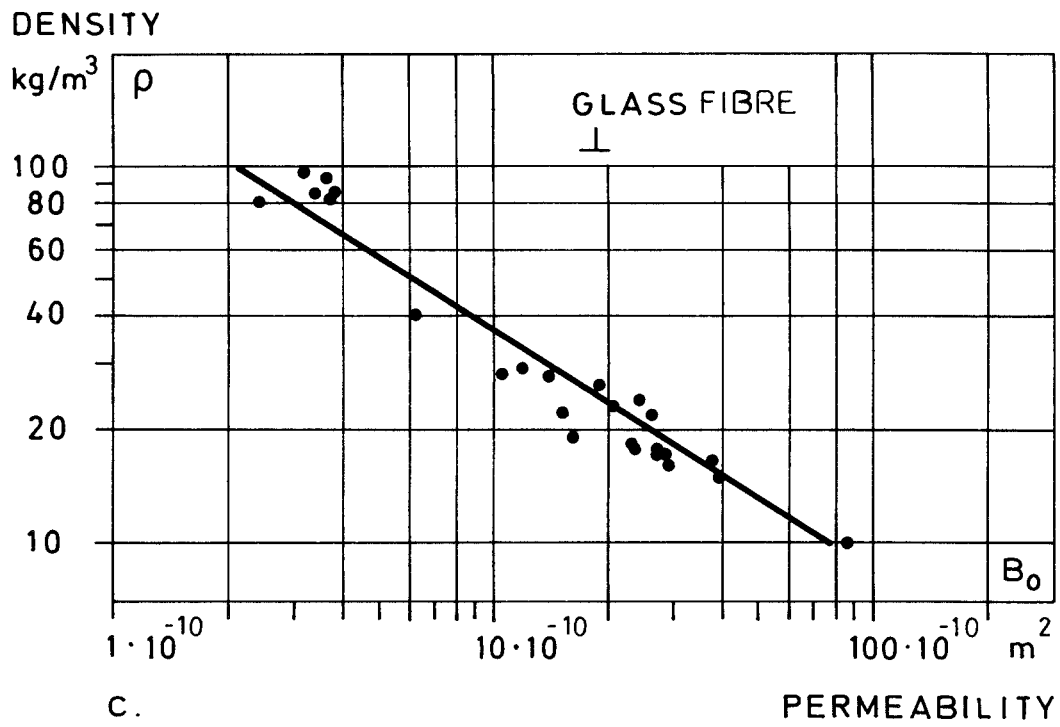


FIG. 7.2.1.c - 7.2.1.d. Experimental permeability coefficient values.
After Bankvall (1972).

7.2.2 Fluid permeance coefficients

In some cases, e.g. thin or built up specimens it may be more convenient to speak of a permeability quantity describing the material layer. This can be done using the quantity fluid permeance. The fluid permeance coefficient, B , is defined:

$$B = \frac{q_v \cdot \eta}{A \Delta p} = B_0 \cdot l \quad (7.2.2.a)$$

Material	Thickness mm	Weight kg/m ²	B m	Reference
Gypsum board	13		$2.9 \cdot 10^{-12}$	3
	9		$2.9 \cdot 10^{-12}$	3, 4
	9.8	7.2	$0.25 \cdot 10^{-12}$	1
Cellulose building paper	0.35	0.3	$51 \cdot 10^{-12}$	1
	0.50	0.3	$1.0 \cdot 10^{-12}$	1
		0.2	$0.28 \cdot 10^{-9}$	5
Rag building felt	1.00	0.5	$0.31 \cdot 10^{-9}$	1
" asphalt impregnated	0.65	0.6	$2.0 \cdot 10^{-12}$	1
			$0.75 \cdot 10^{-12}$	5
Asphalt impregnated cellulose paper (wind protection)		0.2	$13.0 \cdot 10^{-9}$	7
Polyethylene foil	0.10		$0.15 \cdot 10^{-12}$	7

REFERENCES USED IN 7.2.1 AND 7.2.2.

- 1 Tveit (1966)
- 2 Bankvall (1977)
- 3 Swedish plywood ass. (1978), unpublished
- 4 Nyström et al. (1977)
- 5 Nevander & Samuelson (1978)
- 6 Folders etc.
- 7 Mainly for internal use, not published
- 8 Bankvall (1980)

7.3 POROSITY OF SOME BUILDING MATERIALS

Material	Density kg/m ³	Porosity %
Brick	1400	47
	1600	40
	1800	32
Mortar, Lime	1850	30
Mortar, Lime-Cement	2000	25
Mortar, Cement	2100	20
Lime sandstone	1700	37
	2000	26
Lightweight concrete	400	85
	500	80
	650	75
Concrete	2250	15 - 18
Wood; pine, spruce	500	70
oak, beech	700 - 900	55 - 45
Polystyrene cellular plastic	20	98

7.4 SOME PROPERTIES OF AIR

Density, ρ

The table below gives the density of moist air, ρ (kg/m^3), at different temperatures and relative humidities, ϕ .

ϕ , %	-20 °C	-10 °C	0 °C	10 °C	20 °C	30 °C
0	1.395	1.342	1.293	1.247	1.203	1.163
10	1.395	1.342	1.293	1.246	1.202	1.161
20	1.395	1.342	1.292	1.246	1.201	1.159
30	1.395	1.342	1.292	1.245	1.200	1.157
40	1.395	1.341	1.292	1.245	1.199	1.156
50	1.395	1.341	1.291	1.244	1.198	1.154
60	1.395	1.341	1.291	1.244	1.197	1.152
70	1.395	1.341	1.291	1.243	1.196	1.150
80	1.395	1.341	1.290	1.242	1.195	1.148
90	1.395	1.341	1.290	1.242	1.194	1.146
100	1.394	1.341	1.290	1.241	1.193	1.145

Viscosity, η and ν

The dynamic viscosity, η , (Ns/m^2), at different temperatures is shown in the table below.

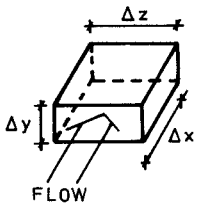
Temperature °C	η	<u>Kinematic viscosity, ν, (m^2/s):</u>
-10	$16.5 \cdot 10^{-6}$	$\nu = \eta/\rho$
0	$17.0 \cdot 10^{-6}$	
10	$17.5 \cdot 10^{-6}$	
20	$18.0 \cdot 10^{-6}$	
30	$18.5 \cdot 10^{-6}$	

Compressibility, κ

$$\kappa = \frac{c_p}{c_v} \cdot \frac{1}{p_{\text{atm}}} \quad (\text{Pa}^{-1})$$

where $c_p/c_v = 1.40$ for air

7.5 INPUT FORMAT FOR COMPUTER PROGRAM JK-CIRCUS

IDENTIFICATION	1	2	3	4	5	6	7	8
NUMBER OF NODES :								
COMPONENTS :								
ACTIVE COMPONENTS:								
	ACTIVE COMPONENTS :							
	FROM NODE NO.	TO NODE NO.	1	PRESSURE DIFFERENCE				
	PASSIVE COMPONENTS :							
	FROM NODE NO.	TO NODE NO.	0	MATERIAL 1	PERMEABILITY B_0	LENGTH Δx	HEIGHT Δy	BREADTH Δz
	FROM NODE NO.	TO NODE NO.	0	DUCT 2	LENGTH Δx	WIDTH Δy	BREADTH Δz	ROUGHNESS ϵ
	FROM NODE NO.	TO NODE NO.	0	SINGLE RES. 3	LOSS FACTOR ξ	WIDTH Δy	BREADTH Δz	
FROM NODE NO.	TO NODE NO.	0	KNOWN 4	ADMITTANCE A				

LIST OF REFERENCES

Anderson, L H. Linear circuit analysis. Byte, Oct 1978, p 100 - 118. 1978.

Andersson, A C. (1980 A). Stationära temperatur- och fuktförhållanden i tak med ventilerad isolering. (In Swedish). CODEN: LUTVDG/(TVBH-7057)/1-9 (1980). Div of Building Technology, Lund Institute of Technology, Lund, Sweden, 1980.

Andersson A C. (1980 B). ACA-LUFT. Two dimensional pressure distribution in building components with permeable materials and ducts. Computer program. Not published. Div of Building Technology, Lund Institute of Technology, Lund, Sweden, 1980.

Andersson L I E. Ofrivillig ventilation. Industriväggars täthet. (In Swedish), Report R99:1978, The National Swedish Board for Building Research, Stockholm, 1978.

ASHRAE HANDBOOK OF FUNDAMENTALS. 1st Edition, American Society of Heating, Refrigerating and Air-conditioning Engineers, Inc. New York, 1968.

Astarita G & Greco G. Excess pressure drop in laminar flow through sudden contraction. I & EC Fundamentals, Vol 7, No 1. Washington, 1968.

Bankvall C G. Natural convective heat transfer in insulated structures. Report 38, Div of Building Technology, Lund Institute of Technology, Lund, Sweden, 1972.

Bankvall C G. Påtvingad konvektion. Praktisk värmeisoleringsförmåga under inverkan av vind och arbetsutförande. In Swedish (Forced convection. Practical heat insulation capacity influenced by wind and workmanship. With an English summary). The National Swedish Testing Institute, Report 1977:21. Borås, Sweden, 1977.

Bankvall C G. Värmeisoleringsförmågan påverkad av luftrörelser och arbetsutförande. (In Swedish). To be published. The National Swedish Testing Institute, Borås, Sweden, 1980.

Beers Y. Introduction to the theory of error. Addison - Wesley Publishing Co. Inc. 2nd Ed. Reading, Ma., USA, 1962.

Benedict R P et al. Flow losses in abrupt enlargements and contractions. Journal of Engineering for Power. Vol 88, Jan 1966, p 73 - 81. New York 1966.

Benedict R P. Fundamentals of temperature, pressure and flow measurements, 2nd Ed. John Wiley & Sons, New York 1977.

Birkeland Ø & Wigen R. Fuge mellom karm og vegg. (In Norwegian). Norwegian Building Research Institute. Report No 15, Oslo 1955.

Bjørnø L. Strømningslaere. (In Danish). Polyteknisk forlag. Lyngby, Danmark 1972.

Bodoia J R & Osterle J F. Finite difference analysis of plane Poiseuille and Couette flow developments. Applied Scientific Research, Vol A 10, p 265 - 276, Hague 1961.

Boussinesq J. Title unknown. Comptes Rendus, Vol 110, p 1160 & 1238, 1890.

Boussinesq J. Comptes Rendus, Vol 113, p 9 - 15 and 49 - 51, 1891. Sur la maniere dont la vitesse, dans un tube cylindrique de section circulaire, évasé a son entrée, se distribuent depuis cette entrée jusqu'aux endroits on se trouve établi un regime uniforme.

Bretting A E. Hydraulik, stationaere strömninger. (In Danish), Teknisk forlag, Copenhagen 1960.

Brundrett E. Modified hydraulic diameter for turbulent flow. Proceedings from a conference on turbulent forced convection in channels and bundles in Istanbul 1978. Eds. Kakac C & Spalding D B. Published by Hemisphere Publ. Corp. (Nato adv. study inst. book). Washington D.C. and Mc Graw-Hill Inst. book Co, New York, 1978.

Building Research Board. The transmission of heat and gases through, and the condensation of moisture on the surface of wall materials. Report No 4. Dept of Scientific and Industrial Research. Building Research Board, London, 1921.

Bunditkul S & Yang W. Laminar transport phenomena in constricted parallel ducts. Letters in heat and mass transfer, Vol 4, p 249 - 260, London 1977.

Bunditkul S & Yang W. Laminar transport phenomena in parallel channels with a short flow constriction. Journal of Heat Transfer, Vol 101, p 217 - 221. New York 1979.

Campbell W D & Slattery J C. Flow in the entrance region of a tube. Journal of basic engineering. Vol 85, p 41 - 44. New York 1963.

Carlsson B et al. Air tightness and thermal insulation - building design solutions. National Swedish Board for Building Research, Report D37:1980. Stockholm 1980.

Carslaw H S & Jaeger J C. Conduction of heat in solids, 2nd edition, Oxford University press. Oxford 1959.

Chen N H. An explicit equation for friction factor in pipe. Ind. Eng. Chem. Fundam, Vol 18, No 3, p 296 - 297, 1979.

Chetwynd D G. The digitization of surface profiles. Wear, Vol 57, p 137 - 145. Lausanne, 1979.

Chivers T C & Mitchell L A. On the limiting velocity through parallel bore tubes. Journal of Physics D, Applied physics, Vol 4, 1971, p 1069 - 1076. London 1971.

Christiansen E B et al. Laminar tube flow through an abrupt contraction. Journal of the American Institute of Chemical Engineers, Vol 18 No 2, p 372 - 380. New York 1972.

Christoffel. Sul problema della temperature stazionarie. Annales di matematica, pura ed applicata Vol 1, p 89. Bologna 1867.

Churchill S W. Title unknown. Chemical Engineering, p 91. Nov 7, 1977.

Cockroft J P & Robertson P. Ventilation of an enclosure through a single opening. Building and Environment, Vol 11, No 1, p 29 - 35, Pergamon press. Oxford 1976.

Colebrook C F. Turbulent flow in pipes, with particular reference to the transition region between the smooth and rough pipe laws. Journal of the Institution of Civil Engineers Vol 11, p 133 - 156. London 1938.

Collins M & Schowalter W R. Title unknown. Physics of fluids, Vol 5, p 1122. New York 1962.

Cornet W H Jr & Battocletti F E. Electronic circuits by system and computer analysis, Mc Graw-Hill. New York 1975.

Cornish R J. Flow in a pipe of rectangular cross section. Proceedings of the Royal Society, 120 (A), p 691 - 700. London 1928.

Cramér H. Mathematical methods of statistics. Almqvist & Wiksell, Uppsala 1945.

Dalaker M. Tettelister for vinduer. (In Norwegian). Byggemesteren No 10. Oslo 1961.

Darcy H. Les fontaines publique de la ville de Dijon. Libraire des corps imperiaux des ponts et chaussées et des mines. Paris 1856.

Deissler R G & Taylor M F. Analysis of turbulent flow and heat transfer in non-circular passages. NASA, TR R-31. 1958.

Drew T B et al. The friction factor for clean round pipes. Transactions from the American Institute of Chemical Engineers, Vol 28. New York, 1932.

Dubbel S. Taschenbuch für den Maschinenbau. (In German), Vol 1. 13th ed. Berlin 1970.

Eck B. Technische Strömungslehre, Vol 1, 8th ed. (In German). Springer Verlag, Berlin. Heidelberg 1978.

Esdorn H & Rheinländer J. Zur rechnerischen Ermittlung von Fugendurchlasskoeffizienten und Druckexponenten für Bauteilfugen. (In German). Heizung-, Luft- und Haustechnik, HLH, Vol 29, No 3, p 101 - 108. Berlin 1978.

ESDU (1978). Pressure losses in flow through a sudden contraction of duct area. Engineering Sciences Data Item No 78007, publ by Engineering Science Data Unit, London 1978.

Etheridge D W. Crack flow equations and scale effect. Building and Environment, Vol 12, p 181 - 189. London 1977.

FKA. Rapport över täthetsförsök med byggnadsmaterial för gastäta skyddsrum. (In Swedish), Försvarsväsendets Kemiska Anstalt. Stockholm 1943.

Fromm K. Strömungswiderstand in rauhen Röhren, Zeitschrift für angewandten Mathematik und Mechanik, Vol 3, p 339, Berlin 1923.

Goldstein S. Modern developments in fluid dynamics. Vol I & II. Dover books on engineering and engineering physics. Dover publ.inc. New York 1965.

Grimsrud D T et al. Infiltration - pressurization correlations: Detailed measurements on a California house. Lawrence Berkeley Lab. Dept of Energy, Report LBL - 7824. Presented at the ASHRAE-symposium on air infiltration in Philadelphia, PA in Jan 1979. Berkeley 1979.

Hagen G H L. Über die Bewegung des Wassers in engen zylindrischen Röhren. Poggendorff's Annalen der Physik, Vol 46. 1839.

Hahnemann H & Ehret L. Der Druckverlust der laminaren Strömung in der Anlaufsstrecke von geraden, ebenen Spalten. Jahrbuch der Deutschen Luftfahrtforschung, p I 21 - I 32. Berlin 1941.

Hahnemann H & Ehret L. Der Strömungswiderstand im geraden ebenen Spalt unter Berücksichtigung der Einlaufverluste. Jahrbuch der deutschen Luftfahrtforschung, p I 186 - I 207. Berlin 1942.

Han L S. Hydrodynamic entrance lengths for incompressible laminar flow in rectangular ducts. Journal of applied mechanics. Sept 1960. p 403 - 409. New York 1960.

Handa K et al. Mikroklimat och luftväxling. (In Swedish). Report T3:1979. The National Swedish Board for Building Research. Stockholm 1979.

Happel J & Brenner H. Low Reynolds number hydrodynamics with special applications to particulate media. Prentice Hall Inc. Englewood Cliffs, N.J. 1965.

Holman J P. Heat transfer, 2nd ed. Mc Graw-Hill Book Co. New York 1963.

Honma H. Ventilation of dwellings and its disturbances. Report 63, Dept. of Heating and Ventilation Technology at The Royal Institute of Technology Stockholm 1975.

Hopf L. Die Messung der hydraulischen Rauigkeit. Zeitschrift für angewandten Mathematik und Mechanik, Vol 3, p 329. Berlin 1923.

Houghten F C & Ingels M. Infiltration through plastered and unplastered brick walls ASHVE Transactions, Vol 33, p 377. New York 1927.

van der Hoven I. Power spectrum of horizontal wind speed in the frequency range from 0.0007 to 900 cycles per hour. Journal of meteorology, Vol 14, p 160. London 1957.

Huelsman L P. Basic circuit theory with digital computers. Prentice-Hall Series in computer applications in electrical engineering. Englewood Cliffs, N.J. 1972.

Höglund I & Wånggren B. Funktionsstudier av tätninglistor för fönster och dörrar. (In Swedish). National Swedish Board for Building Research. Report T7:1979. Stockholm 1979.

Idelchik I E. Spravochnik po gidravlicheskim soprotivlniyam. Koeffitsienty mestnykh soprotivlenii isoprotivleniya treniya. Gosudarstvennoe Energeticheskoe Izdatelstvo, Moskva-Leningrad, 1960. Translated: Handbook of hydraulic resistance. Coefficients of local resistance and of friction. Israel program for scientific translations, Jerusalem, 1966. Available from the US Dept of Commerce. Clearingshouse for Federal Scientific and Technical Information, Springfield. Va 22151.

Israelsson S. Ljudutbredning i de marknära luftskikten. The Meteorological Institution of Uppsala University. Uppsala, Sweden 1979.

Jergling A. Fogar mellan byggnadskomponenter i ytterväggar. Luftläckning genom fasadfogar med tätningslister. (In Swedish). National Swedish Board for Building Research. Report R132:1979. Stockholm 1979.

Johnson W E & Hughes R V. Title unknown. Producers monthly. Vol 13. No 1, p 17. 1948.

Jones O C. An improvement in the calculation of turbulent friction in rectangular ducts. Journal of Fluids Engineering, Transactions of ASME, June 1976, p 173 - 181.

Karev V N. Poteri napora pri vuezapuom suzhenii truboprovada i vliyanie mestnykh soprotivelinii na narusheniya potoka. (In Russian). Head losses at sudden contraction of a pipe and influence of local resistance on the stream disturbance. Neftyanoe khozyaistvo, No 8, 1953.

Kaye S E & Rosen S L. The dependence of laminar entrance loss coefficients on contraction ratio for Newtonian fluids. AIChE Journal, Vol 17, No 5, p 1269 - 1270. New York 1971.

Kays W M. Loss coefficients for abrupt changes in flow cross section with low Reynolds number flow in single and multiple-tube systems. Trans. ASME Vol 72, p 1067 - 1074. New York 1950.

Kays W M. An investigation of losses of flow stream mechanical energy at abrupt changes in flow cross section. Technical Report No 1. Navy Contract N6-ONR-251, Task order VI (Nr -035-104). Dept of Mechanical Engineering, Stanford University. Stanford 1948.

Knibbs G H. Title unknown. Proceedings of the Royal Society of New South Wales, Vol 30, p 186. 1897.

Kolmogorov A N. Die lokale Struktur der Turbulenz in einer inkompressiblen zähen Flüssigkeit bei sehr grossen Reynold'schen Zahlen. Sammenband zur Statistischen Theori der Turbulenz. Akademie-Verlag. Berlin 1941.

Kreith F & Eisenstadt R. Pressure drop and flow characteristics of short capillary tubes at low Reynolds number. Transactions of the ASME, Vol 79, p 1070 - 1078, paper No 56-SA-15. New York 1957.

Kronvall J. Testing of houses for air leakage using a pressure method. ASHRAE transactions No 2473. New York 1978.

Kronvall J (1980 A). Airtightness - measurement and measurement methods. National Swedish Board for Building Research. Report D8:1980. Stockholm 1980.

Kronvall J (1980 B). Correlating pressurization and infiltration rate data - test of a heuristic model. Report TVBH-7055. Div of Building Technology. Lund Institute of Technology. Lund Sweden 1980. Presented at the 1st AIC-conference in Windsor, UK, 6th - 8th October 1980.

Kronvall J (1980 C). Effects of air movements in heat insulation materials. Report TVBH-7058. Div of Building Technology, Lund Institute of Technology. Lund, Sweden 1980.

Kutateladze S S & Borishanskii V M. A concise encyclopedia of heat transfer. Pergamon press. Oxford 1966.

Künzli A. Das Messen und Prüfen der Rauheit an technischen Oberflächen. Schweizer Archiv, Juni 1964, p 179 - 190. Solothurn 1964.

Langhaar H L. Steady flow in the transition region of a straight pipe. Journal of applied Mechanics, Vol 9, p 55 - 58. New York 1942.

Larson G L et al. Air infiltration through various types of brick wall constructions, ASHVE Transactions, Vol 35, p 183. New York 1929.

Larson G L et al. (1930 A). Air infiltration through various types of brick wall constructions. ASHVE Transactions, Vol 36, p 99. New York 1930.

Larson G L et al. (1930 B). Air infiltration through various types of wood frame constructions. ASHVE Transactions, Vol 36. New York 1930.

Leibenzon L S. Dvizhenie prirodnykh zhidkosti i gasow v poristoi srede. Gosudarstv.izdat.tekh.teoret.lit.Moskow and Leningrad 1947

Lentz C P & Nakano V. Predicting air friction pressure loss in shallow ducts. ASHRAE Journal, February 1961, p 82 - 85, 122. New York 1961.

Lin C C. The theory of hydrodynamic stability. Cambridge University Press. Cambridge 1955.

Lumley J L & Panofsky H A. The structure of atmospheric turbulence. Interscience Publishers, J Wiley & Sons. New York 1964.

Lundgren S Å. Das Bendtsen - Prüfgerät für Holzfaser-Hartplatten. Holz als Roh- und Werkstoff, Vol 17, No 3, p 98 - 102. Berlin 1959.

Lundgren T S. Pressure drop due to the entrance region in ducts of arbitrary cross section. Journal of Basic Engineering, Vol 86, p 620 - 626. New York 1964.

Malinowski H K. Wind effect on air movements inside buildings. International conference on wind effects on buildings and structures. Tokyo 1971.

Melsom & Booth. Title unknown. Journal of the institution of Electrical Engineers, Vol 52, p 779. London 1915.

Mikoláz M & Bardoc Z. On a generalization of the Hagen-Poiseuille Law and its technical applications. Zeitschrift für angewandten Mathematik und Mechanik, Vol 59. No 5. p 120 - 121. Berlin 1979.

Mohanty A K & Asthana S B L. Laminar flow in the entrance region of a smooth pipe. Journal of fluid mechanics, Vol 90, p 433 - 447. London 1978.

Moody L F. Friction factors for pipe flow. American Society of Mechanical Engineers. Transactions, Vol 66. New York 1944.

Nevander L E. Luftgenomsläplighet hos tegelväggar. (Air tightness of masonry walls) (In Swedish). Tegel No 3. Stockholm 1949.

Nevander L E. Investigations of different physical properties of masonry walls. The Swedish Brick Industry Association. Not published. 1958.

Nevander L E. Tekniska egenskaper hos isolerade hålmurar av tegel. (Technical properties of heat insulated cavity walls of brick masonry) (In Swedish). Report No 23. Div of Building Technology, Royal Institute of Technology. Stockholm 1961.

Nevander L E & Samuelson I. Elementär byggnadsfysik (In Swedish). Div. of Building Technology, Lund Institute of Technology. Lund, Sweden 1978.

Nevander L E & Wennerström N. Tätning av vattenläckage i fasadtegelmurverk. (How to increase the rain-tightness of masonry walls) (In Swedish). Tegel No 4. Stockholm 1969.

Nikuradse J. Untersuchungen über die Geschwindigkeitsverteilung in turbulenten Strömungen. Forsch.-Arb. Ing. Wes., Vol 281. Berlin 1926.

Nikuradse J. Strömungswiderstand in rauhen Rohren. Zeitschrift für angewandte Mathematik und Mechanik, Vol 11. p 409. Berlin 1931.

Nikuradse J. Widerstandsgesetz und Geschwindigkeitsverteilung von turbulenten Wasserströmungen in glatten und ranken Rohren. Verh. d. 3 intern. Kongr. f. techn. Mechanik in Stockholm 1930, Vol 1, p 239 ff. Stockholm 1931.

Nikuradse J. Gesetzmässigkeiten der turbulenten Strömung in glatten Rohren. VDI-Forschungsheft 356. Berlin 1932.

Nikuradse J. Strömungsgesetze in rauhen Rohren. VDI-Forschungsheft 361. Berlin 1933.

Nir Z. Partition lines in Moody's diagram. International Water Power & Dam Construction, Vol 31, No 3, March 1979 p 29 - 34.

Nylund P O. Vindtäthet hos flerskiktsväggar. (In Swedish). Byggmästaren No 11. Stockholm 1966.

- Nylund P O. Infiltration and ventilation. Report D22:1980. National Swedish Board for Building Research. Stockholm 1980.
- Nyström P et al. Täta hus. (In Swedish). Träinformation. Stockholm 1977.
- Paivanas J A. Laminar steady flow of a fluid in the entrance region of a flow passage. State University of New York at Buffalo, School of Engineering, Dept of Mechanical Engineering, Project report No 6. Buffalo 1962.
- Patir N & Cheng H S. Air average flow model for determining effects of three-dimensional roughness on partial hydrodynamic lubrication. Journal of Lubrication Technology, Vol 100, p 12 - 17. New York 1978.
- Peklenik J. New Developments in surface characterization and measurement by means of random process analysis. Proceedings of the Institution of Mechanical Engineers, Vol 182, Part 3 K, p 108 ff. London 1967-68.
- Poiseuille J L. Recherches expérimentelles sur le mouvement des liquides dans les tubes de très petits diamètres. Comptes Rendus, Vol 11, 1840 and Vol 12 1841.
- Poiseuille J L. Title unknown. Mémoires Savants Etrangers, Vol 9, p 433, 1846.
- Prandtl L. Verhandlungen den 2. internationalen Kongress für technische Mechanik, p 70 - 74. Zürich 1926.
- Prandtl L. Ergebnisse der Aerodynamischen Versuchsanstalt Göttingen. Vol 3, p 1. Göttingen 1927.
- Prandtl L. Strömungslehre. Friedrich Vieweg & Sohn. Braunschweig 1965.
- Presoly E. Blåser det genom stavväggen?(In Swedish). Lättbetong Vol 4, No 4. Stockholm 1962.

- Raisch E. Die Luftdurchlässigkeit von Baustoffen und Baukonstruktions-
teilen. Gesundheits-Ingenieur, p 485. Berlin 1928.
- Raisch E & Steger H. Die Luftdurchlässigkeit von Bau- und Wärmeschutz-
stoffen. Gesundheits-Ingenieur, p 553. Berlin 1934.
- Rau N & Leonhardt K. Bestimmen der Oberflächenrauheit im Granulations-
muster. Industrie-Anzeigen, Vol 28, No 103/104, p 52 - 53. Essen 1979.
- Rayle R E. Influence of orifice geometry on static pressure measurements.
ASME-paper 59-A-234, Dec. 1959. (See also M.I.T. Master's thesis, 1949).
- Reynolds O. An experimental investigation of the circumstances which
determine whether the motion of water shall be direct or sinuous and the
law of resistance in parallel channels. Phil. Trans. Roy. Soc. Ser. A,
174:935. London 1883.
- Roidt M & Cess R D. An approximate analysis of laminar magnetohydrodynam-
ic flow in the entrance region of a flat duct. Journal of appl. mech.
Vol 29. p 181. New York 1962.
- Rouse H. Evaluation of boundary roughness. Proceedings Second hydraulic
conference, July 1942, University of Iowa. Bulletin No 27, 1943.
- Rouse H (ed). Engineering hydraulics. John Wiley & Sons Inc. New York
1950.
- Sampson R A. Phil. Trans. Roy Soc. A 182, p 449 ff. London 1891.
- SCAN-P 21:67. Ytråhet hos papper och papp, bestämd med Bendtsen-apparat.
(In Swedish), Svensk Papperstidning, Vol 70, No 20, p 683 - 685, 1967.
- Scheidegger A E. Title unknown. Geofis. Pura Appl. Vol 28, p 75, 1954.
- Scheidegger A E. The physics of flow through porous media. University
of Toronto Press. London 1963.
- Schiller L. Die Entwicklung der laminaren Geschwindigkeitsverteilung und
ihre Bedeutung für Zähigkeitsmessungen. Zeitschrift für angewandte Mathe-
matik und Mechanik, Vol 2, p 96 - 106. Berlin 1922.

Schlichting H. Laminare Kanaleinlaufströmung. Zeitschrift für angewandten Mathematik und Mechanik, Vol 14, p 368 - 373. Berlin 1934.

Schwartz. Title unknown. Crelle, Vol 70, p 105, 1869.

Selander W N. Explicit formulas for the computation of friction factors in turbulent pipe flow. Atomic Energy of Canada Ltd. Report AECL-6354. Chalk River, Nuclear Laboratories. Chalk River, Ontario 1978.

Shchelkachev V N. C. R. Acad. Sci. URSS, Vol 52, p 203. Moscow 1946.

Smith R J. Circuits, devices and systems, 3 ed, Wiley International Edition, John Wiley & Sons Inc. New York 1976.

Sparrow E M & Lin S H. Title unknown. Physics of fluids, Vol 7, p 338. New York 1964.

Stephan K. Wärmeübergang und Druckabfall laminarer Strömungen im Einlauf von Rohren und ebenen Spalten. Ph.D.-thesis. Faculty of Mechanical Engineering, Karlsruhe Institute of Technology. Karlsruhe 1959.

Thomas D A & Dick J R. Air infiltration through gaps around windows. Journal of the Institution of Heating and Ventilating Engineers, June 1953, p 85 - 97. London 1953.

Tveit A. Measurements of moisture sorption and moisture permeability of porous materials. Report 45, Norwegian Building Research Institute. Oslo 1966.

Verma S H. Solve pipe flow problems directly. Hydrocarbon processing, Vol 58, No 8. Houston, Texas 1979.

Wadmark T. Implicit friktion kan skrivas explicit. (In Swedish), VVS No 1, p 14. Stockholm 1978.

Warren P R. Ventilation through opening on one wall only. International Conference on Heat and Mass Transfer in Buildings, Aug 29 - Sept 3 1977. Also available as paper PD94/77 from Building Research Establishment, Garston, Watford, UK.

Waschull H. Rauheitsmessungen mit einem Auflichtmikroskop. Feingeräte-technik, Vol 28, No 7, p 316 - 318. Berlin 1979.

Weisbach J. Theoretical Mechanics with an introduction to the calculus. D van Nostrand. New York 1878.

Welty J R. Engineering heat transfer. John Wiley & Sons Ltd. New York 1974.

Wieslander J. Idpac Commands - User's Guide. Dept of Automatic Control, Lund Institute of Technology. CODEN: LUTFD2/(TFRT-3157)/1-108/(1980). Lund Sweden 1980.

Wood D J. Title unknown. p 60 - 61. Civil Engineering. Dec. 1966.